This version of the manuscript has been peer reviewed and was accepted for publication in Ore Geology Reviews on 2 November 2021. A journal pre-proof version was published online on 9 November 2021 (https://doi.org/10.1016/j.oregeorev.2021.104569). However, please note that the version here on EarthArXiv (complete with all figures, Appendices and Supplementary Information) differs from the OGR online pre-proof version. Subsequent versions of this manuscript may have slightly different content. The published version of this manuscript is available via the 'Peer reviewed Publication DOI' link on the right-hand side of this webpage. Please feel free to contact the author; feedback is welcomed.

Iron oxide copper-gold (IOCG) deposits – A review (part 1): settings, mineralogy, ore geochemistry and classification

Roger G. Skirrow[1]

Geoscience Australia, GPO Box 378, Canberra, ACT Australia 2601

Abstract

Characteristics of ten of the world's metallogenic provinces hosting iron oxide Cu-Au (IOCG) deposits have been critically assessed, including their geological and tectonothermal evolution, alteration-mineralisation parageneses, and ore geochemistry. A new classification framework is proposed in which IOCG deposits form the major part of a family of deposits within Cu-Au-Fe (CGI) mineral systems. Other family members include Fe-sulfide Cu-Au (ISCG) deposits lacking significant iron oxides. The classification combines three criteria: geological and tectonic settings, oxide-sulfide mineralogy, and ore geochemical characteristics. These criteria form the basis for defining deposit subtypes, and also distinguish deposits in CGI mineral systems from porphyry Cu (-Au), skarn Fe-Cu (-Au) and iron oxide-apatite (IOA) deposits, although there are some shared features.

CGI mineral systems with IOCG deposits occur in three geological and tectonic settings. Two settings are closely linked and are termed orogenic and post-orogenic settings. Syn-deformational IOCG and related deposits in orogenic settings formed during regional tectonothermal events at mid- to shallow-crustal levels at generally brittle-ductile conditions. Available data are consistent with a model in which provinces hosting orogenic IOCG deposits experienced tectonic switching from compression to extension, which was also commonly marked by regional bimodal magmatism. This review shows that many of world's IOCG provinces are hosted in such orogenic settings. The rarer post-orogenic extensional setting, often previously described as 'anorogenic', hosts the super-giant Olympic Dam deposit. Andean-type continental margin magmatic arcs undergoing extension comprise the third important setting of IOCG provinces. All major IOCG metallogenic provinces are characterised by the coincidence in space and time between pre-IOCG sedimentary ± volcanic basins and syn-IOCG intrusive ± volcanic regional magmatism.

IOCG and ISCG deposits in CGI mineral systems are characterised by an association of Cu and Au with highly elevated Fe (e.g. 15-60 wt % Fe) in the form of abundant Fe oxides and/or Fe sulfides and/or Fe-rich silicates, and with sufficient Cu-Au to be classed as a resource. Deposits in CGI

[1] *Formerly Geoscience Australia; current contact: roger.skirrow@gmail.com*

mineral systems exhibit distinctive enrichments of elements in the chalcophile-siderophile suite (Co, Ni, Bi, Se, Te) and/or elements in the LILE-HFSE suite (REE, U, F, Ba, Mo), the ratios of which vary greatly between deposits and define a continuum. A key finding is the correlation of these geochemical variations with the range of oxidation-reduction (redox) characteristics of the ore-related hydrothermal minerals, and also with the three geological-tectonic settings. The causes of these variations are likely fundamental in the formation of IOCG and related deposits.

CGI mineral systems are characterised by paragenetically early Na ± Ca-rich hydrothermal alteration (generally in regional-scale zones), followed by combinations of Fe-, Ca- and K-rich minerals that preceded or accompanied Cu-Au mineralisation. This review has shown that volatile-bearing minerals (e.g. carbonate (CO_2), apatite (P), fluorite (F), barite (SO_4), tourmaline (B)) were deposited with the Cu-Au mineralisation in almost all IOCG provinces, albeit less abundantly in the continental arc-hosted deposits.

It is argued that the special combinations of basinal-derived and magmatic/igneous-derived inputs to ore formation produces the distinctive range of characteristics of IOCG and related deposits in CGI mineral systems.

1. Introduction

The diverse group of iron oxide copper-gold (IOCG) deposits has been one of the most contentious classes of ore deposits since its recognition as a new type in the mid 1980s to early 1990s. Central to the debates have been the issues of definition, classification, the roles of magmatic versus and non-magmatic sources of fluids and metals, and tectonic settings. Early studies (e.g. Meyer, 1988) noted similarities between the giant Olympic Dam Cu-U-Au deposit, discovered in 1975 in South Australia, and iron oxide-apatite-rich deposits of the southeast Missouri and Kiruna areas (USA, Sweden), and the Bayan Obo magnetite-REE deposit in China. Hitzman et al. (1992) included a number of other iron oxide-rich deposits in first defining the 'Proterozoic iron oxide (Cu-U-Au-REE)' class of ore deposits, and proposed a preliminary model involving extensional tectonic settings. Subsequently, a large number of highly diverse deposits, some newly discovered and others re-classified, have been included within an expanding group of IOCG deposits.

Despite major efforts to clarify and tighten the definition of IOCG deposits and to understand their settings (e.g. reviews by Sillitoe, 2003; Williams et al., 2005; Corriveau, 2007; Groves et al., 2010; Barton, 2013), there remain many unresolved first-order problems of definition and classification. Some of these issues stem from the IOCG name itself, which describes the mineralogy (iron oxide) associated with the principal ore metals (copper, gold) in the deposits.

This terminology contrasts with many other well known deposit types such as porphyry Cu, volcanic-hosted massive sulfide Zn-Pb-Cu, orogenic Au, epithermal Au, etc, which include their principal ore metals and an aspect of either their mode of origin or the ore depositional environment. As a consequence of the wide-embracing IOCG name, deposits of likely fundamentally different origins (e.g. magmatic-hydrothermal versus non-magmatic fluid or metal sources) have been included by some workers in the IOCG group of deposits.

Also problematic has been the variance in the definitions of the required grades of copper and gold to qualify as IOCG deposits. Several workers have proposed broad definitions of IOCG deposits such that some iron oxide-rich deposits with little or no copper or gold are considered part of the IOCG 'family' as possible 'end-members' or as 'affiliated' deposits (e.g. Hitzman et al., 1992; Williams et al., 2005; Corriveau, 2007; Barton, 2013). For example, Barton (2013) included a range of iron oxide-rich deposits lacking, or with sub-economic levels of, Cu-Au-REE-P-Ag-U-Co as part of an 'iron oxide (-Cu-Au-REE-P-Ag-U-Co) clan'. Groves et al. (2010) addressed this and other problems relating to the extreme diversity of deposits previously classified as IOCG deposits by defining a sub-group of 'IOCG sensu stricto' containing >100 Mt of economic Cu and Au ore, within a broader group of 'iron oxide-associated' deposits. Their broader group included some alkaline intrusion- and carbonatite-related deposits such as Palabora (Cu) and Vergenoeg (magnetite-fluorite), considered to be end-members of the 'iron oxide-associated deposits'. The definition of IOCG deposits by Williams et al. (2005) was revised by Groves et al. (2010) as follows: (1) Cu + Au as economic metals, (2) hydrothermal characteristics and structural controls, commonly with breccias, (3) abundant low-Ti Fe oxides (magnetite, hematite) and/or Fe silicates (grunerite, Fe actinolite, fayalite), (4) LREE enrichment and low-S sulfides, including chalcopyrite-bornite-chalcocite and pyrrhotite, (5) lack of abundant syn-sulfide quartz veins and alteration that commonly includes a decreased SiO_2 content of wall rocks, and (6) a temporal relationship with magmatism, yet no close spatial association with causative intrusions.

While consistent with the definition of IOCG deposits of Williams et al. (2005), the classification scheme of Williams (2010) included 'hematite-group' and 'magnetite-group' IOCG deposits, and differentiated these from several types of 'affiliated deposits' (low-Fe-oxide Cu-Au; Co-As±Au±Ag±U ± Fe-oxide deposits with low Cu; and Fe oxide-U deposits with low Cu). Iron oxide-apatite (IOA) deposits of the Kiruna type were excluded from the 'IOCG and affiliated deposits' grouping of Williams (2010), as were several types of 'orthomagmatic/magmatic-hydrothermal iron oxide ± apatite ± Cu ± Au ± rare metal deposits' such as Palabora (Cu), Bayan Obo (Fe, REE), magnetite-rich porphyry-related Cu-Au deposits such as Ertsberg-Grasberg, and the Vergenoeg magnetite-fluorite deposit. Following Groves et al. (2010), yet another grouping was proposed by Porter (2010) termed 'iron oxide associated-alkali altered (IOAA) mineralised systems', which

incorporate: IOCG sensu stricto deposits, IOA deposits, carbonatite and alkaline igneous-related iron oxide deposits, and a subgroup of 'miscellaneous deposits sharing characteristics of both iron oxide alkali-altered systems and another ore system'. Finally, Corriveau et al. (2010, 2016) refined the IOAA scheme of Porter (2010) and considered 'iron oxide and alkali-calcic alteration ore systems' as including IOCG deposits (with economic Cu ± Au, Ag, REE, U) and five other deposit subtypes (iron oxide ± apatite ± REE deposits; albitite-hosted U or Au; skarn-hosted + K-skarn ± Fe oxides with base and precious metals; low-Cu IOCG variants with Au, Co, As, Bi, Ag; and 'skarn' alteration).

The foregoing overview of previous classifications of IOCG and 'affiliated' deposits highlights the challenges in defining and categorising the highly diverse deposits of Cu-Au associated with iron oxides and/or iron sulfides. As noted by Groves et al. (2010) the "IOCG group of deposits . . . has progressively become too-embracing . . . ", and "consideration of this broad group as a whole obscures the critical features of the IOCG sensu stricto deposits . . .". This appears still to be the case. The aim of this two-part review is to critically re-examine IOCG deposits from a fresh perspective using newly available data so as to identify the diagnostic geological and geochemical characteristics and ore-forming processes of deposits previously included in the IOCG class. Ultimately, it is intended to clarify the issues of 'what is an IOCG deposit' and 'what controls where they occur' based on an improved understanding of the fundamental processes of ore formation, using a mineral systems framework. A mineral system is defined as 'all geological factors that control the generation and preservation of mineral deposits' (Wyborn et al., 1994). The 'essential ingredients' in a mineral system are the sources of ore metals, transport of those metals, and their deposition in a mineral deposit. The scales of these geological components and processes range from crustal and regional to deposit and micro scales. A mineral system may generate a range of deposit types and subtypes that are genetically related to the same shared ore-forming processes and geological 'ingredients' of the system. Fossil mineral systems can be mapped by identifying (1) the energy sources or 'drivers' of the mineral system, (2) the sources of the ore metals, fluids and sulfur, (3) the architecture or structure of the fluid flow pathways, and (4) the physico-chemical gradients of ore deposition. The present contribution addresses aspects of components (1), (3) and (4) by focussing on the regional geological and tectonic settings of IOCG mineral systems, and the mineralogical and geochemical characteristics of the hydrothermal systems, so as to improve the mapping of mineral systems with IOCG deposits and the discovery of new resources. This builds on previous efforts to map the potential for IOCG mineral systems (Skirrow et al., 2019).

This contribution commences with a summary of the general features and definition of IOCG and related deposits and then describes CGI mineral systems containing IOCG deposits from the broad

(regional) scale geological context to the deposit- and micro-scale features. First, a synthesis of the geological characteristics and tectonic settings of IOCG deposits is presented, based on detailed descriptions of ten of the world's IOCG metallogenic provinces and geochronological constraints presented in the Supplementary Information. This is followed by descriptions of hydrothermal mineral assemblages and their paragenetic sequences, including proximal and regional alteration and zoning. The next section addresses the ore geochemistry of IOCG and related deposits using published data, and links this to the geotectonic settings and mineralogical variations. Finally, the findings are integrated within a new classification of the global family of IOCG and related deposits. An accompanying contribution reviews the sources of ore components and discusses the ore-forming processes and origins of these enigmatic deposits (Skirrow, in prep.).

2. General features and global distribution of IOCG deposits

2.1 General features

This review considers a group of Cu-Au-Fe-rich deposits that have been variously described as IOCG deposits as well as iron oxide-poor Cu-Au deposits occurring in the same metallogenic provinces. The latter deposits are commonly Fe-sulfide- rather than Fe-oxide-rich and were termed iron sulfide Cu-Au or ISCG deposits by Haynes (2000). In the current study IOCG and ISCG deposits have been grouped together to form a family of Cu-Au-Fe or CGI deposits with a specific set of characteristics that distinguish them from other well known Cu (-Au) and/or Fe ore deposit types such as porphyry Cu (-Au), skarn Fe and Cu, and IOA deposits. These characteristics, listed below, form a descriptive definition of IOCG and related ISCG deposits within CGI mineral systems. They are based on the current review of the geology and deposits in ten global provinces together with previous reviews (e.g. Hitzman et al., 1992; Haynes, 2000; Sillitoe, 2003; Williams et al., 2005; Corriveau, 2007; Barton, 2013).

- IOCG and ISCG deposits display a deposit- and orebody-scale spatial association of Cu-Au resources with Fe-rich rocks (e.g. 15-60 wt % Fe), with Fe hosted by low-Ti oxides (magnetite and/or hematite), and/or sulfides and/or other Fe-rich minerals; Fe-oxide/Fe-sulfide ratios vary greatly between and within deposits.
- Copper sulfides and Au are associated with moderate to strong enrichments of several of the following groups of elements which may attain ore grade in some deposits: Ag, Co, Ni, Bi, Se, Te, In and/or U, LREE, F, Ba, Mo; in most deposits there are little or no significant

enrichments in Zn, Pb, Cd, As, Sb, W, Sn, Ta, Nb or Li, although rare examples of outer/distal Zn-Pb-As-rich zones are known.

- Copper and Fe-sulfides and Au either post-dated, or were deposited synchronously with, the Fe-oxides and Fe-silicates; Fe-sulfides are pyrrhotite and/or pyrite, whereas the Cu-sulfides include chalcopyrite, bornite and chalcocite which are spatially zoned in some deposits; provinces with IOCG and related deposits may contain a wide range of oxide-sulfide assemblages and from reduced pyrrhotite ± magnetite to pyrite ± magnetite to oxidised hematite ± pyrite; IOCG deposits that lack Fe-sulfides are also known.
- Deposit- and orebody-scale hydrothermal alteration in higher temperature settings generally comprises variants of iron, potassic and calcic mineral assemblages including magnetite, biotite, Ca-amphibole (e.g. actinolite-tremolite), Ca- and/or Fe-carbonate, K-feldspar, and much less common Ca-Fe-rich clinopyroxene, garnet, and iron silicates.
- In lower temperature settings the proximal alteration with Fe-Cu-Au minerals comprises combinations of hematite, sericite/phengite, chlorite, and Ca- and/or Fe-carbonate.
- Some IOCG and related deposits contain hydrothermal barite, fluorite, apatite, allanite, molybdenite, tourmaline, and a range of U- and REE-bearing minerals accompanying Cu-Au mineralisation; anhydrite is rarely reported, and epidote is generally inconspicuous although allanite is a key host of REE in some deposits.
- Paragenetically early sodic alteration (albitic plagioclase, scapolite) is uncommon in most Cu-Au ore zones but is characteristic of distal and regional alteration zones where it may be accompanied by Ca-amphiboles, Ca-clinopyroxenes, and minor titanite and magnetite; breccias and brittle-ductile structures commonly control the sites of regional Na (-Ca) alteration; calcic-iron (Ca-Fe) and potassic-iron (K-Fe) alteration typically overprints sodic alteration.
- Hydrothermal quartz is generally not abundant with iron oxide-rich Cu-Au mineralisation but may be present within iron oxide-poor, iron sulfide-rich, Cu-Au zones of the same deposits or in separate ISCG deposits.
- The higher temperature deposits that formed in mid-crustal settings are commonly hosted by brittle-ductile shear zones and related deformation structures including breccias, whereas deposits in lower temperature shallow-crustal settings occur in brittle deformation structures such as faults, veins and breccia zones.
- Two (or more) fluids have been identified as related to Fe-rich alteration and Cu-Au mineralisation in many deposits, including hypersaline and lower salinity brines; CO_2-rich fluids are also commonly present; isotopic and geochemical evidence suggests contributions of water, halogens and sulfur from non-magmatic as well as magmatic or leached-igneous rock sources.

- Proximal intrusive igneous rocks contemporaneous with Cu-Au-Fe mineralisation are not present at many deposits or are volumetrically minor; however, in specific settings (e.g. Andean) there are close spatial and temporal relationships with intrusions of generally intermediate composition; in other IOCG provinces regional magmatism that was broadly coeval with Cu-Au mineralisation tends to be bimodal in composition.
- Almost all IOCG and related deposits occur within volcano-sedimentary basinal host rocks that have been metamorphosed at low to medium grades either before or during Cu-Au-Fe ore formation; local host rocks are highly variable and include metasedimentary, metavolcanic, and igneous rocks ranging from mafic to felsic in composition.

Any proposed holistic genetic and exploration model(s) for this group of IOCG and related deposits must account for all of the key features listed above. This review leads to the conclusion that there are two fundamentally different types of IOCG deposits that formed in separate geotectonic settings (orogenic to post-orogenic versus arc-hosted Andean-type), yet both types involved the coincidence in time and space between pre-IOCG basins and syn-mineralisation regional igneous activity. It is proposed here and in the companion paper that the great diversity of deposits in the CGI family is a result of these variations in geological settings and differing contributions of fluids and metals from the basinal and magmatic/igneous sources.

2.2 Global distribution

The major IOCG deposits occur widely in space and time, as previously recognised (e.g. Groves et al., 2010) and summarised in Figure 1. The ten IOCG metallogenic provinces and their mineral deposits considered in this review include (in age order from Archean to Mesozoic): Carajás province (northern Brazil); Guelb Moghrein deposit (Mauritania); Kiruna province (northern Sweden); Great Bear magmatic zone (northwest Canada); Tennant Creek province (northern Australia); Kangdian province (southwest China) and possible extension in Vietnam including the Sin Quyen deposit; eastern Gawler Craton and subjacent Curnamona Province (southern Australia); Cloncurry province (northeastern Australia); Khetri province (northwest India); and the Andean province (Chile and Peru). The background image in Figure 1 shows global seismic velocity (shear wave) anomalies at a depth of 165 km (Lu et al., 2019), which is a proxy for the present day boundaries of cratonic blocks at this depth. Although the spatial resolution is relatively low, it is strikingly evident that almost all of the major IOCG provinces occur close to the gradient (highlighted in white) between 'fast' and 'slow' velocity. This relationship is less evident for the Mesozoic IOCG provinces in South America and, arguably, the Kangdian province in southwest China. Groves et al. (2010) noted a similar relationship between craton margins and

the Precambrian IOCG 'sensu stricto' deposits defined in that study; the current investigation supports this proposal with additional provinces and data. Furthermore, in Australia this spatial relationship has been shown more precisely by Hoggard et al. (2020) who demonstrated that the large Cu-Au deposits of the eastern Gawler Craton and the Cloncurry provinces lie within ~100 km of the surface projection of the 170 km depth contour of the lithosphere-asthenosphere boundary (LAB). The same spatial association of the LAB with the IOCG and related deposits considered in the present review is evident globally (Czarnota, Hoggard, Skirrow, in prep.), as it is for sedimentary basin-hosted resources of Zn, Pb and Cu (Hoggard et al., 2020).

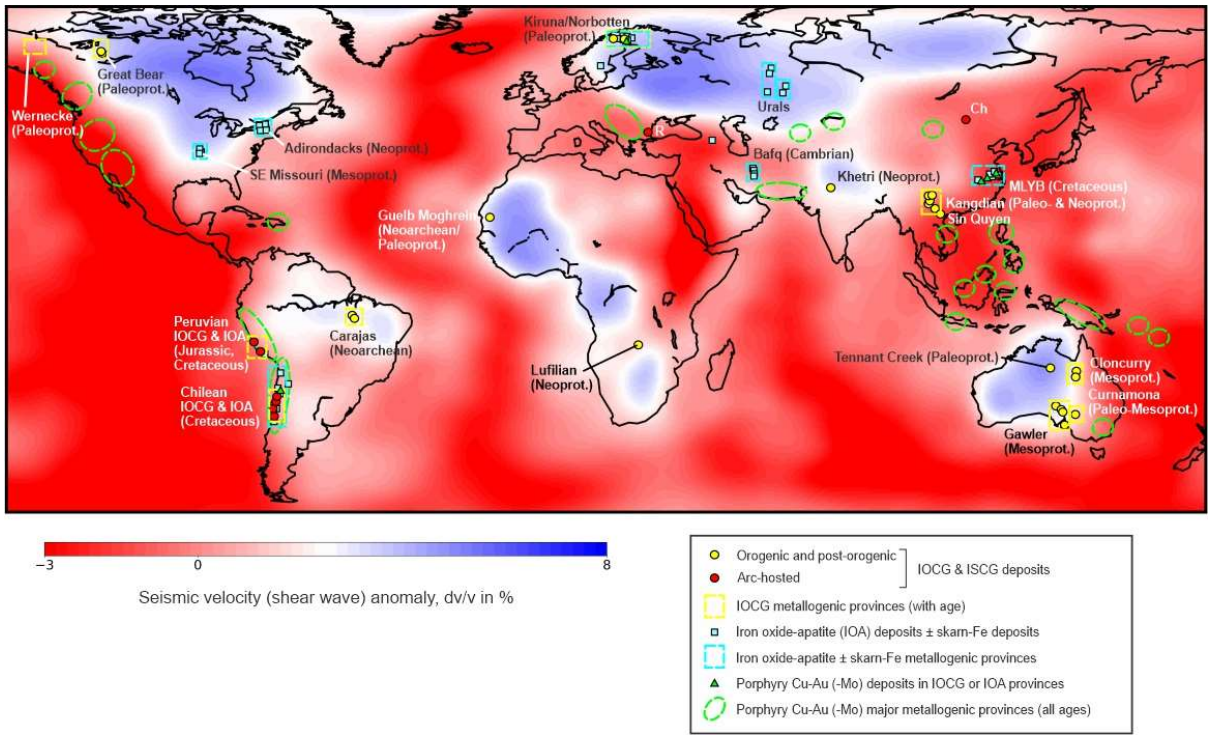

Figure 1. Locations of global major IOCG deposits and provinces, compared to iron oxide-apatite (IOA) and porphyry Cu-Au (-Mo) deposits and provinces, plotted on a background image of seismic velocity (shear wave) anomalies at 165 km depth relative to the ak135 reference model (from TX2019slab-S model of Lu et al., 2019). Blue areas represent anomalous fast seismic wave speeds representing depleted cratonic lithospheric mantle beneath Archean and Proterozoic cratons. Locations of deposits and metallogenic provinces based on references cited in the text and in the Supplementary Information, and Sillitoe (2010). Abbreviations: Ch – Chandmani Uul deposit (Oyunjargal et al., 2020), R – Rosen deposit (Sillitoe et al., 2020).

In contrast, the locations of major porphyry Cu (-Au) metallogenic provinces are almost all above global domains of relatively low seismic velocity at 165 km depth. The major IOA provinces range in age from Paleoproterozoic (e.g. Kiruna province) and Mesoproterozoic (e.g. southeast Missouri) through Paleozoic (e.g. Bafq, Iran) to Mesozoic (e.g. Chilean Andes, and Middle-Lower Yangtze Belt, China) and even Cenozoic (e.g. El Laco, Chile). Most are situated above relatively low velocity mantle but those in the Urals (Russia) are exceptions, and the IOA deposits of southeast Missouri and the Adirondacks (USA) are located, like the IOCG provinces, close to a cratonic margin.

3. Three regional and tectonic settings of IOCG provinces

The timing of regional geological events in relation to Cu-Au-Fe mineralisation is summarised in Figure 2 for six of the world's major IOCG metallogenic provinces. Detailed descriptions of regional and hydrothermal events in these provinces along with four others are presented in the Supplementary Information, and summary information is given in Table 1. Event time spans shown in Figure 2 represent the main bodies of available geochronological data for each event, with emphasis on ages determined with robust geochronometers such as U-Pb and U-Th-Pb isotope ages for zircon, titanite and monazite, and Re-Os isotope ages of molybdenite. Additional constraints from $^{40}Ar/^{39}Ar$ dating have been utilised for hydrothermal minerals in some provinces. Uncertainties on individual ages are given in the detailed compilations of geochronological data in the Supplementary Information. The timing and character of deformation/tectonic events have been largely taken from the literature, supplemented by further interpretation by the author in some provinces as described in the Supplementary Information.

This global review of ten IOCG metallogenic provinces has revealed three distinct lithostratigraphic-tectonothermal settings for the major IOCG and related deposits: two associated with major orogenic/tectonothermal events, and a third where continental margin arcs were undergoing extension (Andean type). The orogenic-related setting of IOCG and related deposits is subdivided into 'orogenic' and 'post-orogenic' settings. These settings are partly similar to the three tectonic settings proposed by Hitzman (2000), namely 'intra-continental orogenic basin collapse', 'intra-continental anorogenic magmatism' and 'extension along a subduction-related continental margin'. Groves et al. (2010) emphasised the latter two of these settings for their IOCG sensu-stricto deposits of Precambrian and Phanerozoic ages, respectively. However, the 'intra-continental anorogenic magmatism' setting of Hitzman (2000) and Groves et al. (2010) is considered in the present study to be a post-orogenic setting, typified by the eastern Gawler Craton. Moreover, the examples of IOCG provinces assigned to each setting differ between this and previous studies.

The three settings and possible hybrids are summarised below; for full referencing see the Supplementary Information.

Table 1. Summary of IOCG metallogenic provinces and their mineral deposits. Data sources are given in the Supplementary Information. Deposit type abbreviations: IOCG – iron oxide Cu-Au deposits, ISCG – iron sulfide Cu-Au deposits, IOA – iron oxide apatite deposits, PCD – porphyry Cu deposits, SSC – sediment-hosted stratiform Cu deposits.

Metallogenic province	**Basin rocks hosting CGI mineral systems**	**Magmatism syn-IOCG (name of suite)**	**Deposit types in province**	**Age of Cu-Au deposits**	**Setting of Cu-Au deposits (# of events)**
Carajás	siliciclastics, BIF, felsic & mafic volcanics	Bimodal, alkali-calcic (I-type) felsics & A-types (Planalto)	IOCG, Au-PGE, Ni, Fe (BIF) & late granite-related Cu-Au	Neoarchean & Paleoproterozoic	orogenic (2, Neoarchean); post-orogenic (1, Paleoprot.)
Guelb Moghrein	siliciclastics, BIF, carbonate-rich, mafic volcanics	none recognised	IOCG/ISCG	Neoarchean/early Paleoproterozoic,	orogenic (1)
Kiruna/Norbotten	Intermediate-mafic-felsic volcanic-rich, minor siliciclastics, carbonate & graphite	Calc-alkaline to alkaline, bimodal (Haparanda & Perthite-Monzonite)	IOCG, ISCG, IOA, PCD, VHMS, orogenic Au	Paleoproterozoic	orogenic (2)
Great Bear magmatic zone	Intermediate-mafic-felsic-volcanic-rich, minor siliciclastics	Calc-alkaline to alkaline I-type, and A-type (various GBMZ)	IOCG, IOA, skarn, albitite-U	Paleoproterozoic	orogenic to post-orogenic (1)
Tennant Creek	Siliciclastics, hematitic shale, minor felsic volcanics, minor carbonate	I-type, bimodal (Tennant Creek)	IOCG, ISCG	Paleoproterozoic	orogenic to post-orogenic (2)
Gawler-Curnamona	Siliciclastics, minor mafic & felsic volcanics, minor BIF, calc-silicates & scapolite	Bimodal, high-temperature I- and A-type; minor alkaline (Hiltaba-GRV)	IOCG, minor Mo & Au-Mo (orogenic Au or IRG & epithermal Ag to west; Pb-Zn-Ag to east)	Early Mesoproterozoic	Major deposits: post-orogenic (1)
Cloncurry	Siliciclastics, calcsilicates & scapolite, mafic & felsic volcanics, minor BIF; minor graphite	Bimodal, high-temperature I- and A-type (Williams-Naraku)	IOCG, ISCG, Mo, Pb-Zn-Ag (albitite-U, skarn-REE-U and orogenic? Au to west)	Early Paleoproterzoic	orogenic (2)
Kangdian	Siliciclastics, carbonate-rich, minor graphite	Mafic intrusive	IOCG, SSC, Fe	Paleo- to Neoproterozoic	?orogenic (2)
Khetri	Siliciclastics, calcsilicates & scapolite	Bimodal (Erinpura, timing unclear)	IOCG, SSC (Pb-Zn-Ag and albitite-U to south)	Neoproterozoic	?orogenic (1)
Chilean Iron Belt and south coastal Peru	Mafic-intermediate-felsic volcanic-rich, marine sediments	Calc-alkaline (Coastal Batholith)	IOCG, IOA, Fe-skarn, PCD, manto Cu-Ag	Cretaceous	Syn-extensional pre-orogenic to early-orogenic (1)

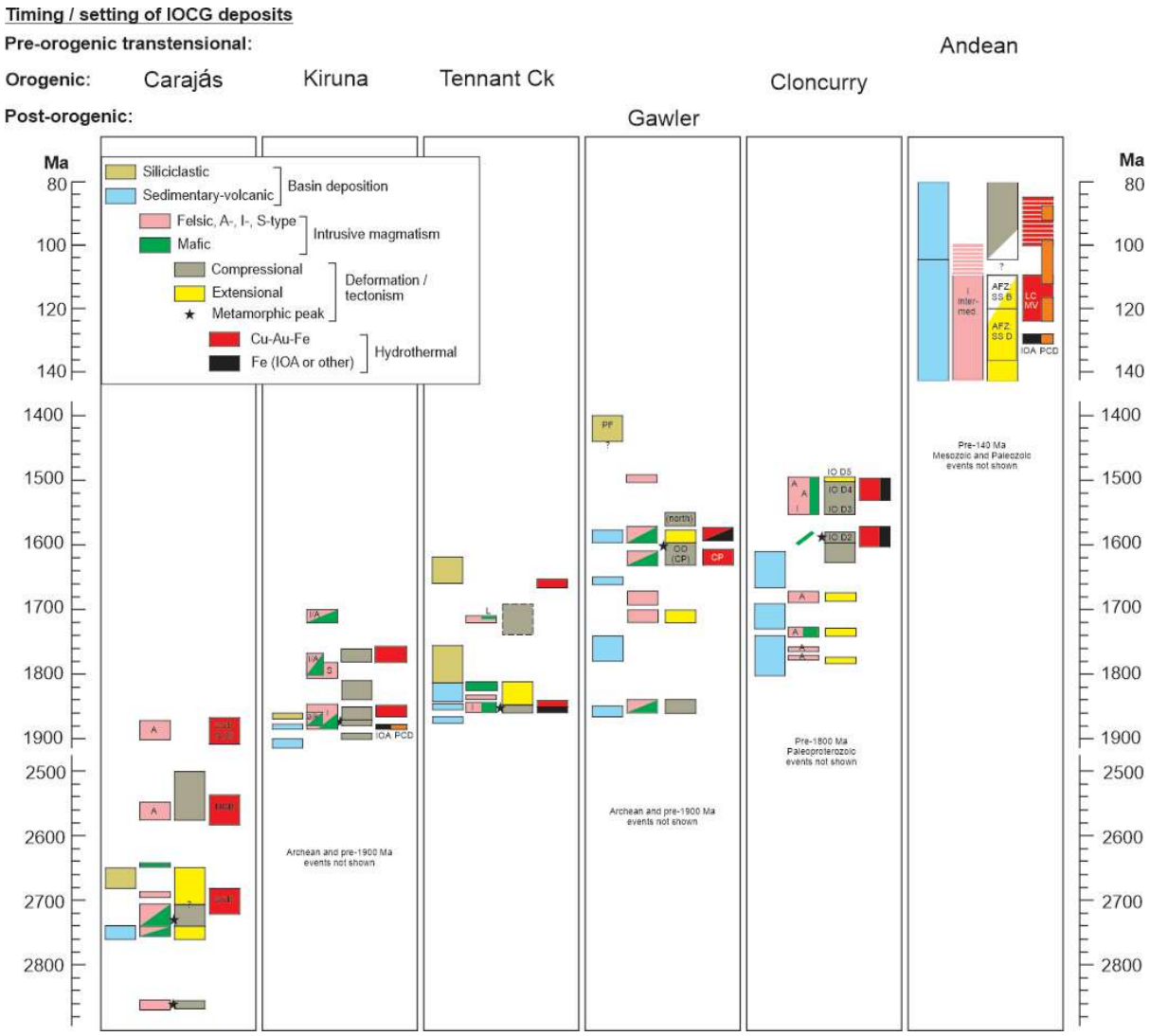

Figure 2. Synthesis of geochronological data for mineralisation, tectonic, magmatic and supracrustal depositional events in key provinces with IOCG deposits. The Kiruna and Mesozoic Andean provinces also contain well known IOA deposits and small-medium sized porphyry Cu (-Au) deposits. Note breaks in time scale. For sources of data and named rock units see the Supplementary Information. Abbreviations for intrusive magmatism: A – A-type felsic, I – I-type felsic, L – lamprophyre, S – S-type felsic, alk – alkaline. Other abbreviations: AFZ – Atacama Fault Zone, CP – Curnamona Province Cu-Au deposits, IO – Isan Orogeny, IOA – iron oxide apatite deposits, LC – La Candelaria Cu (-Au), MV – Mantoverde Cu (-Au) deposit, NCB – Northern Copper Belt, OO (CP) – Olarian Orogeny in Curnamona Province, PCD – porphyry Cu deposits, SCB – Southern Copper Belt, SS B – strike-slip brittle, SS D – strike-slip ductile.

3.1 Orogenic settings

The Cloncurry province was given by Hitzman (2000) as an example of an IOCG province with an 'orogenic basin collapse' setting, along with the Grenville province (with IOA deposits) and the Lufilian Orogen of southern Africa. In the past two decades many more IOCG deposits and provinces have been recognised worldwide, and it is suggested here that in fact many of the world's major IOCG provinces occur in orogenic tectonic settings. These include the Carajás, Guelb Mohgrein, Cloncurry, Sin Quyen, Tennant Creek and probably Kangdian and Khetri provinces. The term 'orogenic' is appropriate because the IOCG and related deposits in this setting are

interpreted to have formed during regional deformation and tectonothermal events at mid-upper-crustal, low to medium grade metamorphic, conditions within brittle-ductile structures such as shear zones. Where sufficient data are available it is evident in many cases that syn-tectonic IOCG and related deposits in this setting post-dated peak metamorphism by millions to tens of millions of years, and hence can be described as having 'late-orogenic' timing. Notwithstanding, until more comprehensive geochronological and structural data are available the broader term 'orogenic' is used herein for such settings.

Moreover, this review (as detailed in the Supplementary Information) indicates that the settings of the orogenic IOCG and related deposits in many cases exhibit similar and distinctive patterns of evolution. This involves: basin formation; then tectonic/orogenic processes leading to inversion of the basins and regional metamorphism of commonly high-temperature low-pressure style; and I- and/or A-type felsic and mafic bimodal magmatism that temporally overlaps with particularly the latter stages of the tectonic/orogenic events. A key hypothesis in the present review, building on an earlier proposal (Skirrow, 2010; Skirrow et al., 2018, 2019), is that CGI mineral systems in orogenic settings preferentially develop during a switch in tectonic style from early compressional to transpressional and thence in some cases to transtensional or extensional regimes. The fully extensional setting is described separately in the next section, as the post-orogenic setting. This switch in tectonic style can explain the apparent dilemma of bimodal magmatism associated with orogenic events, if such magmatism commenced late within the tectonic event, during the tectonic switching from compression to extension. This is consistent with the available geochronological data for the IOCG provinces in orogenic settings, although further testing of this hypothesis is required.

The sedimentary-volcanic basins hosting orogenic IOCG and related deposits typically are of continental to shallow marine rather than deep marine character, and commonly contain oxidised facies and strata with evidence of former evaporites, as well as Fe-rich lithologies such as mafic volcanics and banded iron formation (Barton, 2013; Haynes, 2000; Hitzman, 2000). Carbonaceous units are volumetrically minor or absent in the host sequences but may be locally present at some deposits (Haynes, 2000). The host volcanic-sedimentary-volcanic basins generally formed in extended continental margin including passive margin settings. Later basins that post-date the IOCG deposits in some provinces, such as the Águas Claras Formation in the Carajás province and Ooradidgee Group in the Tennant Creek province, tend to be sedimentary-siliciclastic in character or contain bimodal volcanic rocks (Fig. 2) and may be indicative of extensional tectonic regimes.

Regional magmatism was broadly coeval with the formation of most orogenic IOCG and related deposits although syn-mineralisation intrusions are rarely present within or subjacent to the Cu-Au mineralisation. A few examples of orogenic IOCG and related deposits appear to lack major syn-mineralisation magmatism (e.g. Osborne deposit, Cloncurry district; Guelb Moghrein, Mauritania). A- and/or high-temperature I-type felsic intrusive ± volcanic rocks are commonly coeval with less voluminous (at the exposed crustal level) mafic to ultramafic intrusive rocks that are weakly to moderately K-rich; calc-alkaline intermediate compositions are generally absent or minor, as are highly alkaline igneous compositions, within the syn-mineralisation igneous complexes. The Kangdian province is unusual in the apparent very low abundance of felsic as compared to mafic intrusive magmatism around the period(s) of IOCG deposit formation.

As noted above, syn-deformational Cu-Au mineralisation occurred synchronously with, and generally late within (e.g. post-peak-metamorphic), the associated orogenic event as demonstrated by the available radiometric ages (Supplementary Information) and by the structural controls described in the literature for IOCG and related deposits in each province. The author's field observations support such timing in the following provinces: Tennant Creek, Gawler Craton, Curnamona Province, Cloncurry, Kiruna, Kangdian and Khetri. For example, brittle-ductile shear zones and breccias associated with dilatant jogs in shear zones, as well as fold hinges at various scales, are common sites for syn-deformational hydrothermal alteration and Cu-Au mineralisation in the orogenic IOCG setting. Geochronological and geological data indicate that some provinces experienced multiple Cu-Au mineralising events 10s to 100s of millions of years apart as well as multiple tectonothermal events. This raises the possibility of 'remobilisation' of early Cu-Au mineralisation during later tectonothermal events, which may be difficult to distinguish from the introduction of 'new' Cu-Au during the later events. However, several lines of evidence based on descriptions in the literature and the author's observations support the proposal of syn-deformational, syn- to late-orogenic introduction of Cu-Au-Fe mineralisation in the orogenic setting. First, ore-related hydrothermal mineral assemblages are largely confined to zones of deformation such as shear zones, en-echelon and sigmoidal extension veins sets related to shearing, saddle reef-style infillings in fold hinges, attenuated fold limbs, breccias with clasts and hydrothermal matrix exhibiting a tectonic foliation, and hydrothermal veinlets and replacements along a tectonic foliation. Second, there is little or no evidence for extensive Cu-Au mineralisation outside of such syn-deformation features in the orogenic IOCG and ISCG deposits that could be described as pre-tectonic mineralisation (except in several provinces with possible SSC mineralisation; see below). Third, as discussed in later sections, the geochemical compositions of IOCG and ISCG deposits in orogenic settings are different to those in the post-orogenic and arc-hosted settings where the ores are not controlled by mid-crustal

brittle-ductile structures but by shallow-crustal generally brittle deformation structures. Therefore, if some/all deposits in orogenic settings were simply the deformed, metamorphosed, equivalents of the post-orogenic or arc-hosted deposits then their ore geochemistry may be expected to be similar, which they are not (although Sin Quyen is a possible exception). These arguments do not rule out the possibility of multiple Cu-Au-Fe mineralising events or some degree of 'remobilisation' of Cu-Au during second or later tectonothermal events.

Other deposit types that may or may not be present in the same metallogenic provinces as the orogenic IOCG deposits include: ISCG deposits, Davidson & Large, 1994; Haynes, 2000); sedimentary and/or hydrothermal Fe oxide deposits and Fe-oxide-rich alteration of various origins; and less common mafic-ultramafic intrusion-hosted Ni-Cu sulfide mineralisation (e.g. Carajás province). The ISCG mineralisation is represented variously as deposits separate from the IOCG deposits (e.g. Greenmount, Mt Dore in the Cloncurry province, Haynes, 2000) or as zones within deposits with otherwise abundant Fe oxides (e.g. Eloise, Osborne in Cloncurry province, Haynes, 2000; Cu-Au-Bi zones outside ironstones at the Orlando East and Gecko ironstone-hosted deposits, Tennant Creek province, Skirrow, 2000). The ISCG deposits show similar structural controls, relative timing, and alteration (notwithstanding differences in Fe-oxide/Fe-sulfide ratios and quartz abundances) to the IOCG deposits in the same metallogenic provinces. Several provinces with orogenic IOCG deposits also host sediment-hosted stratabound Cu deposits that are known as 'SSC' deposits in the Kangdian and Khetri provinces, and which contain no or minor Fe oxides (Chen & Zhou, 2012; Zhao et al., 2012; Mukhopadhyay et al., 2019). Some stratabound Cu (Co) and polymetallic mineralisation in the Olary Domain of the Curnamona Province also may be of SSC affinity (Cook & Ashley, 1992). In some provinces there is evidence for early, possibly syn-diagenetic, stratabound Cu mineralisation and Fe-sulfides overprinted by epigenetic, syn-deformational, Cu (-Au) of IOCG affinity (e.g. Khetri province, Sharma et al., 2020). Although this scenario also seems plausible in the Kangdian and Curnamona provinces (e.g. Bierlein et al., 1995; Skirrow et al., 2000; Teale & Fanning, 2000), other interpretations have been advanced (e.g. early stratabound IOCG mineralisation overprinted by deformation, Armistead et al., 2018). However, the relative importance of 'remobilised' mineralisation versus introduction of new Cu-Au during the syn-deformational stages is unclear in these provinces (e.g. Su et al., 2021). This is also a problem in some provinces with multiple stages of IOCG and/or ISCG mineralisation, and requires further careful textural and paragenetic work to resolve the timing of Cu-Au particularly in relation to deformation fabrics.

The Fe oxide deposits and Fe-oxide-rich alteration zones are important features of all of the IOCG provinces in orogenic settings, and variously occur as zones with little or no Cu-Au mineralisation within some IOCG deposits and as Fe-oxide accumulations spatially quite separate from the Cu-

Au mineralisation. For example, in the Carajás province giant Fe ore deposits related to sedimentary BIF formed prior to the IOCG deposits (Grainger et al., 2008), whereas massive magnetite deposits of hydrothermal origin occur in the Southern Copper Belt, separately from the large IOCG deposits and also in some cases occur within the deposits associated with albite-actinolite alteration (e.g. Sequeirinho orebody in the Sossego deposit, Monteiro et al., 2008). In most orogenic IOCG provinces hydrothermal Fe-oxide bodies with little or no Cu-Au represent alteration within IOCG mineral systems where physico-chemical conditions and/or availability of suitable fluids were unfavourable for significant Cu-Au deposition.

Although uranium is anomalous in some IOCG deposits in orogenic settings (e.g. Salobo deposit in Carajás province, de Melo et al., 2017; Ernest Henry, E1 and Monakoff deposits in Cloncurry province, Mark et al., 2006, Williams et al., 2015; Juno deposit in Tennant Creek province, Large, 1975), significant U enrichments in IOCG deposits in these settings are evidently quite rare. In the Mt Isa Inlier the Mary Kathleen U-REE deposit and albitite-hosted U deposits such as Valhalla occur in separate metallogenic provinces to the west of the Cloncurry IOCG province. Available geochronology suggests that uraninite mineralisation formed at 1550 ± 15 Ma at Mary Kathleen (Page, 1983), and between ~1555 Ma and ~1530 Ma at the Valhalla albitite-hosted U deposit (Polito et al., 2009). The youngest ages of this U mineralisation are within uncertainty of the oldest ages of the second major Cu-Au ore-forming event in the Cloncurry province at ~1530-1490 Ma (Perkins & Wyborn, 1998; Duncan et al., 2011). These relationships are permissive of a link between U in some of the IOCG deposits of the Cloncurry province and the late-stage U in deposits to the west in the Mount Isa Inlier, but more clarification is required. Albitite-hosted U mineralisation in the Great Bear magmatic zone may be a further example where U mineralisation formed coevally with IOCG deposits, in this case within the same iron oxide-alkali alteration systems according to Corriveau et al. (2010, 2016) and Montreuil et al. (2015).

3.2 Post-orogenic settings

The prime example of this setting is the eastern Gawler Craton hosting the giant Olympic Dam Cu-U-Au deposit; the subjacent Curnamona Province to the east, with minor known Cu-Au (± Fe-oxide) deposits, shared a similar evolution around the period of Cu-Au-Fe mineralisation in the early Mesoproterozoic. Whereas the eastern Gawler Craton and Curnamona Province experienced similar early (Paleoproterozoic) histories to those of the orogenic IOCG provinces (basin formation; inversion related to major orogenic events; temporally overlapping felsic and mafic magmatism; and syn-tectonic IOCG-related hydrothermal alteration) the eastern Gawler Craton and probably the Curnamona Province appear to have undergone a further stage of

geodynamic development. This involved a switch from a broadly compressional (orogenic) to an extensional tectonic regime, referred to here as post-orogenic and which was marked by voluminous felsic-dominated bimodal igneous activity. The major IOCG deposits such as Olympic Dam, Prominent Hill and Hillside are interpreted to have formed during this tectonic switching at ~1595-1575 Ma (Skirrow, 2010; Skirrow et al., 2018, 2019). Unlike the orogenic settings, volcanic and sedimentary rocks of roughly similar age to the deposits are preserved in the post-orogenic setting of the Gawler Craton IOCG deposits. The associated magmatism is characteristically A- and/or high-temperature I-type with weakly to moderately K-rich mafic to ultramafic intrusive and volcanic rocks, and there are few igneous rocks of intermediate composition (Budd, 2006). Broadly syn-mineralisation alkaline igneous rocks appear to be more abundant in post-orogenic compared to orogenic settings of IOCG and related deposits. For example the ultramafic dykes at the Olympic Dam deposit (Johnson & Cross, 1995) and picrite dykes at the Wirrda Well prospect (Huang et al., 2016) have affinities with alkaline magmatism, compared with less alkaline compositions of similar aged mafic igneous rocks in other parts of the Gawler Craton (Skirrow et al., 2018).

Other deposit types in the eastern Gawler Craton and Curnamona Province that formed within a few 10s of millions of years of the ~1595-1575 Ma period of IOCG mineralisation include: small low-Fe-oxide Cu-Au deposits in the Moonta-Wallaroo district, associated with quartz veins and K-feldspar-chlorite-sericite alteration; low-Fe-oxide Cu-Mo (-Au) stratabound mineralisation adjacent to Fe-oxide-rich alteration zones (e.g. Kalkaroo and Portia deposits, Curnamona Province); Au-Mo-bearing quartz veins (e.g. White Dam deposit, Curnamona Province) and Mo-greisen type mineralisation (Moonta-Wallaroo district); Ag- and Pb-rich epithermal-like quartz vein mineralisation and shear-hosted Au-quartz vein deposits in the central Gawler Craton to the west of the IOCG metallogenic province. In addition there are numerous Fe oxide bodies of hydrothermal origin in both the eastern Gawler Craton and western Curnamona Province, as well as BIF-related Fe ore deposits that pre-date the Cu-Au mineralisation (e.g. Middleback Ranges, Gawler Craton). Many of the hydrothermal Fe oxide bodies, which are largely barren of Cu-Au, appear to represent alteration within CGI mineral systems (Skirrow et al., 2002; Bastrakov et al., 2007). Finally, the giant Paleoproterozoic Broken Hill Pb-Zn-Ag deposit occurs in the eastern Curnamona Province. This spatial relationship between early basin-hosted Zn-Pb-Ag and later IOCG deposits is similar to that observed in the eastern Mt Isa Inlier where the Broken Hill-type Cannington and Pegmont Pb-Zn-Ag deposits occurs immediately to the east of the Cloncurry IOCG deposits.

Other possible examples of post-orogenic settings of CGI mineral systems include the paragenetically late stages of Cu-Au-Bi mineralisation in the Tennant Creek province which, like

the IOCG mineralisation in the Gawler Craton, is characterised by brittle deformation fabrics and a dominance of hematite-rich (rather than magnetite-rich) iron oxide alteration. Examples include: Gecko K44 upper zone of Au-rich Cu-Bi mineralisation, and the Au-Bi-Se-rich Eldorado deposit (Huston et al., 1993; Skirrow, 2000; Skirrow & Walshe, 2002). Also, the Cu-U- and hematite-magnetite-bearing breccias at the Sue-Dianne deposit in the Great Bear magmatic zone (Goad et al., 2000) may represent a post-orogenic overprint on an orogenic metallogenic belt (see also hybrid settings, below).

3.3 Continental margin arc (Andean type) settings

In contrast to the Neoarchean to Neoproterozoic orogenic settings, Cretaceous IOCG deposits in the Chilean and Peruvian Andes formed within a continental margin magmatic arc, either during extensional tectonism (Sillitoe, 2003) or during a switch from extension to inversion (Chen et al., 2013). Moreover, available geochronological data reviewed in the Supplementary Information indicate that the Cretaceous Andean IOCG deposits formed up to ~15 million years prior to the onset of a major inversion event, rather than during such an event as in the orogenic IOCG deposits or immediately following an orogenic event as in the post-orogenic setting of the eastern Gawler Craton deposits. Host rocks in the Cretaceous Andean settings are dominated by volcanic and intrusive rocks of mainly intermediate to felsic and minor mafic compositions and with relatively minor sedimentary or metamorphic components. The abundance of calc-alkaline intermediate compositions in this setting, and the close spatial-temporal relationships between intrusions and IOCG mineralisation (Sillitoe, 2003), differ from the settings of orogenic and post-orogenic IOCG deposits. The Cretaceous Andean metallogenic provinces containing the IOCG deposits also host small to medium size porphyry copper and skarn, large iron oxide-apatite (IOA), and 'manto' Cu-Ag deposits that comprise stratabound, epigenetic, Fe-oxide-poor mineralisation.

Based on the few available high-precision ages using robust geochronometers for the Cretaceous Fe and Cu deposits, most of the dated IOA deposits formed at ~131-127 Ma along with some porphyry Cu deposits. Importantly, the limited available geochronology indicates that the dated IOA deposits significantly predated the major IOCG deposits, which formed at ~122-110 Ma (e.g. Mantoverde, Candelaria, Raúl-Condestable, early alteration at Mina Justa). The few available dates for Cretaceous manto Cu (-Ag) deposits indicate alteration at ~106-101 Ma, based on K-feldspar ^{40}Ar-^{39}Ar dating (e.g. El Soldado deposit, Wilson et al., 2003). However, the significance of these K-feldspar ages, along with other ^{40}Ar-^{39}Ar ages of ~104-95 Ma for adularia associated with copper mineralisation at the Mina Justa IOCG deposit (Chen et al., 2010a), remains unclear

and they may represent cooling rather than formation ages. By comparison, at the latitudes of the Chilean Cretaceous IOCG deposits (e.g. 20°-33° S) the onset of inversion of the Jurassic arc and basin system hosting many of the IOCG deposits occurred at ~107-105 Ma, with a main phase of compression at ~100-95 Ma (Bascuñán et al., 2016; Fennell et al., 2019; Boyce et al., 2020).

These timing constraints indicate that the major Andean IOCG deposits formed during periods of extension or transtension up to ~15 m.y. prior to the Cretaceous major inversion event, although there may be some overlap with the initial stages of orogenesis as previously suggested by Chen et al. (2013). In conclusion, the setting and timing of the Andean IOCG deposits, as well as some manto Cu deposits, can be described as pre- to early-orogenic in their timing.

3.4 Possible hybrid settings

The setting of the Paleoprotorozoic Kiruna province and the broader region of northern Fennoscandia has been interpreted as an evolving Andean-type continental margin magmatic arc, that was subjected to a series of collision-related tectonothermal or orogenic events (as discussed by Lahtinen et al., 2015, 2018; see also references therein). Like the Cretaceous Andean setting, the Kiruna province experienced the development of large IOA deposits and probable porphyry Cu deposits (e.g. Aitik, Wanhainen & Martinsson, 2010) during arc-related magmatism (~1884-1876 Ma), with later development of IOCG and related mineralisation, commencing at ~1862 Ma (see review of geochronology, Supplementary Information and references therein). A key difference between the Kiruna and Andean IOCG settings is that in the Kiruna province the earliest IOCG deposits appear to have formed during and/or late within (rather than prior to) a major collision-related orogenic episode that post-dated arc magmatism and related IOA and porphyry Cu deposits. A second period of IOCG deposit formation at ~1782-1757 Ma or as early as ~1820 Ma (Bauer et al., 2021) also appears to have occurred during and/or late within another orogenic event affecting northern Fennoscandia (see Supplementary Information). It is notable that the Kiruna province is dominated by magmatic arc-related igneous host rocks with volumetrically minor (meta)sedimentary rocks, and although containing world-class IOA deposits the known IOCG deposits are all small. Overall, the Kiruna province can be interpreted to represent a hybrid setting where an early continental margin magmatic arc setting was overprinted by multiple orogenic events, two of which were associated with the formation of syn- to late-orogenic IOCG and related deposits.

The Paleoproterozoic Great Bear magmatic zone (GBMZ) in northwestern Canada hosts well documented but under-explored hydrothermal alteration and diverse types of mineralisation

(Cu, Au, U, Co, Mo, V, etc) including small known Au, Cu and U resources (Mumin et al., 2007, 2010; Corriveau et al., 2010a, 2010b, 2016; Montreuil et al., 2016a). Like the Andean and Kiruna settings described above, much of the igneous rocks of the GBMZ are interpreted to have formed in a continental margin magmatic arc setting (Hildebrand et al., 1987; Ootes et al., 2017). Arc magmatism, initiated at ~1876 Ma, was preceded by the short-lived Calderian orogeny. Rather than fully postdating the Calderian orogeny, as previously thought, early phases of the GBMZ magmatism (~1876-1873 Ma) are now interpreted as syn-deformational within a transpressional tectonic regime late within the Calderian orogeny, and exhibit 'syn-collisional' and 'volcanic arc' calc-alkaline geochemical signatures (Montreuil et al., 2016b; Ootes et al., 2017). The later magmatic phases (~1869-1866 Ma) have compositions indicating a transition from collisional to post-collisional and extensional settings (Montreuil et al., 2016b; Ootes et al., 2017). The overall setting therefore appears to be one where syn-orogenic magmatism was overprinted by magmas with continental arc-like character yet in an extensional, post-orogenic, setting. Accordingly, the GBMZ may share features (and represent a hybrid?) of the orogenic to post-orogenic type IOCG settings combined with an Andean type continental margin magmatic arc IOCG setting.

3.5 Synthesis: tectonic settings and geodynamic evolution of IOCG provinces

Figure 3 illustrates the three proposed regional geological and tectonic settings of different types of IOCG and related deposits in CGI mineral systems and their host provinces. The upper panel shows the setting of arc-hosted Andean-type IOCG deposits within a continental margin magmatic arc that is undergoing extension, similar to those proposed by Hitzman (2000), Sillitoe (2003) and Groves et al. (2010). The rifting arc and back-arc basinal environments host not only the IOCG deposits but also (earlier) IOA, small porphyry Cu, skarn-related and (coeval to later?) 'manto' Cu deposits. This panel also shows subduction-related metasomatism of mantle lithosphere along a continental margin or root of a lithospheric block which may have occurred in multiple episodes over 10s or 100s of millions of years. A sedimentary ± volcanic basin system is illustrated at the right side where the continental margin has undergone extension and thinning. This lithospheric and basin architecture is based partly on the Gawler Craton – Curnamona Province (Skirrow, 2010; Skirrow et al., 2018) but is herein proposed to be more generally applicable to the settings of other orogenic and post-orogenic CGI mineral systems.

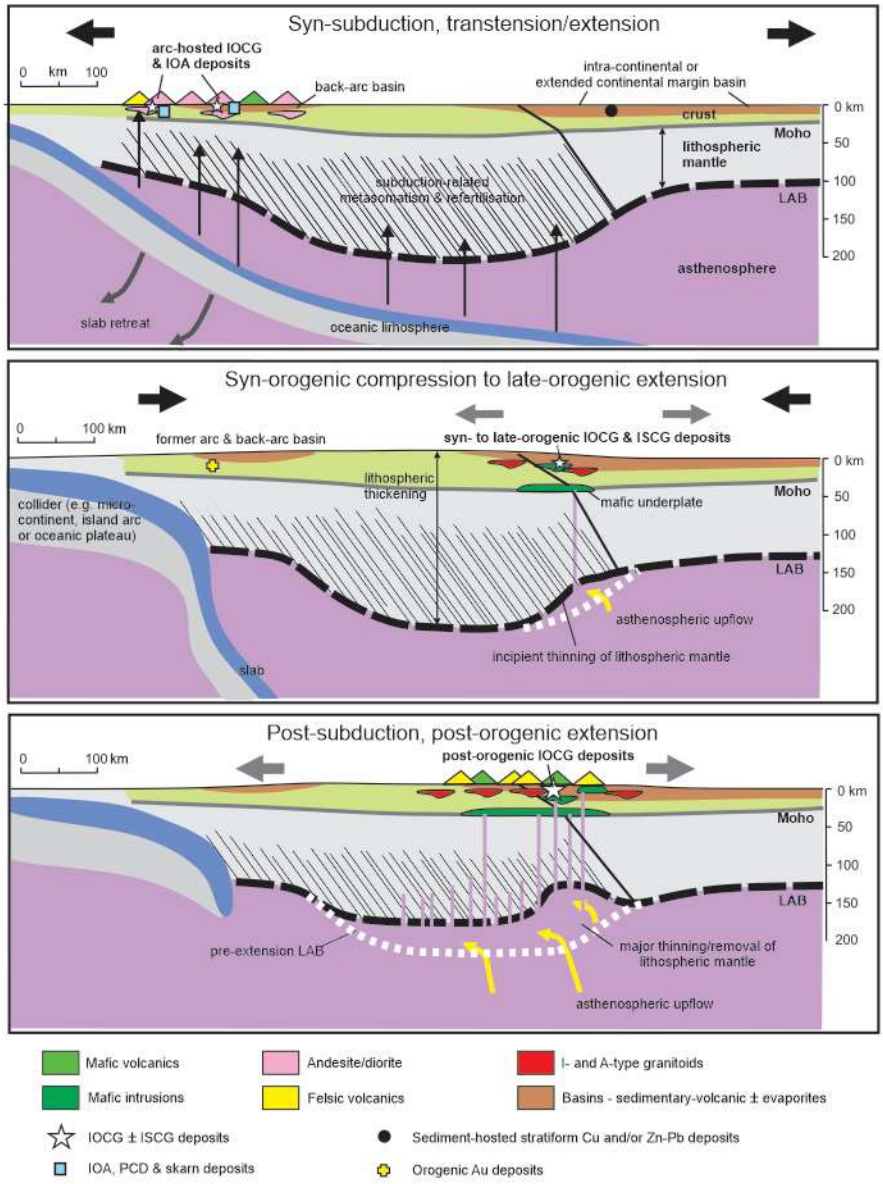

Figure 3. Schematic tectonic settings and geodynamic evolution of IOCG deposits in CGI mineral systems. Top panel: arc-hosted IOCG and IOA deposits; middle panel: orogenic IOCG and ISCG deposits; lower panel: post-orogenic IOCG deposits (see text). Other indicated deposit types may or may not be present in the IOCG provinces.

The middle panel of Figure 3 illustrates inversion of the basin and magmatic arc during an orogenic event, triggered for example by collision of an oceanic plateau, island arc or microcontinent at a plate margin relatively distal from the basin setting. Crucially for IOCG deposit formation, in this model gravitational instabilities at the LAB triggered by the collisional processes led to melting of previously metasomatized lithospheric mantle (represented by alkaline mafic igneous rocks, Groves et al., 2010; Skirrow et al., 2018) and consequent crustal melting. These occurred late within the orogenic event, during a switch from compression to transtension or extension. The juxtaposition of this mantle-derived magmatism with a pre-existing basin at an extended continental margin is the key setting for the formation of orogenic IOCG and related deposits. These syn-deformational deposits form at generally mesothermal

conditions within basinal ± igneous host rocks. The orogenic setting with a tectonic switch from compression to extension is proposed to be applicable to many of the world's major orogenic IOCG provinces.

The lower panel (Fig. 3) shows how in some cases the orogenic setting evolves from a compressional (collisional) to a fully extensional, post-orogenic, tectonic regime. This may be driven by further and major thinning of the mantle lithosphere, for example via wholesale removal or foundering of large parts of the lithospheric mantle (Skirrow et al., 2018) or via slab roll-back (Tiddy & Giles, 2020). The post-orogenic setting hosts the super-giant Olympic Dam IOCG deposit in the eastern Gawler Craton. Because the orogenic and post-orogenic settings form a continuum, earlier mesothermal orogenic IOCG deposits and/or alteration can be exhumed and overprinted by post-orogenic IOCG mineral systems in sub-volcanic to volcanic settings.

4. Hydrothermal alteration and IOCG mineralisation

Hydrothermal minerals in CGI mineral systems occur within assemblages that show a characteristic sequence through time, commonly known as a paragenetic sequence. The general features of such sequences in IOCG deposits of different types have been known for some time (since Hitzman et al., 1992), yet the interpretation of the hydrothermal mineral assemblages has not been well understood in terms of links with geotectonic settings or origins of the hydrothermal fluids. A review of published paragenetic sequences of 29 representative IOCG and ISCG deposits in 9 provinces, summarised in Figure 4, provides a framework for comparison with other deposit types and for discussion of the origins of the hydrothermal minerals. The next section focuses on hydrothermal alteration and mineralisation assemblages proximal to the deposits, and then the hydrothermal assemblages are compared with other ore deposit types, before a brief description of regional-scale alteration. The chemical/metasomatic descriptors (e.g. Na-Ca, Ca-Fe, Fe-K) generally correspond to the types previously described by Hitzman et al. (1992), Corriveau et al. (2010, 2016) and Barton (2013).

4.1 Proximal mineral assemblages and paragenetic sequences

The mineral assemblages in CGI mineral systems can be represented by their dominant chemical composition, which change systematically through paragenetic time at a given location. Although there is an influence on mineralogy by the local host rock compositions, which are highly variable in each province, the remarkably consistent mineralogy of the hydrothermal assemblages and

their sequences suggests that the hydrothermal assemblages dominantly reflect the physico-chemical characteristics of the hydrothermal fluids. This is particularly the case in the most intensely altered proximal/central parts of deposits, where it can be assumed that fluid/rock ratios were higher than in peripheral zones. The approach taken here is to identify assemblages of hydrothermal minerals that formed at broadly the same time and therefore represent possible equilibrium chemical conditions or an approach to equilibrium. This concept of an equilibrium mineral assemblage is similar to that used in metamorphic petrology. Accordingly, the focus is on the presence or absence of particular minerals during a particular paragenetic stage rather than on their relative abundance, although the modal amounts of the dominant minerals are taken into account in assigning an assemblage to particular chemical groupings and stages (i.e. Na, Na-Ca, Ca-Fe, K-Fe, etc). Published paragenetic sequences have been critically assessed and minerals assigned to stages and chemical groupings shown in Figure 4. In some cases the reported mineral assemblages do not fit neatly within the generalised sequence in Figure 4, in which cases they may be shown between stages (e.g. an assemblage with Ca-rich as well as Fe-K-rich minerals is plotted between stage 2 Ca-Fe and stage 3 Fe-K assemblages).

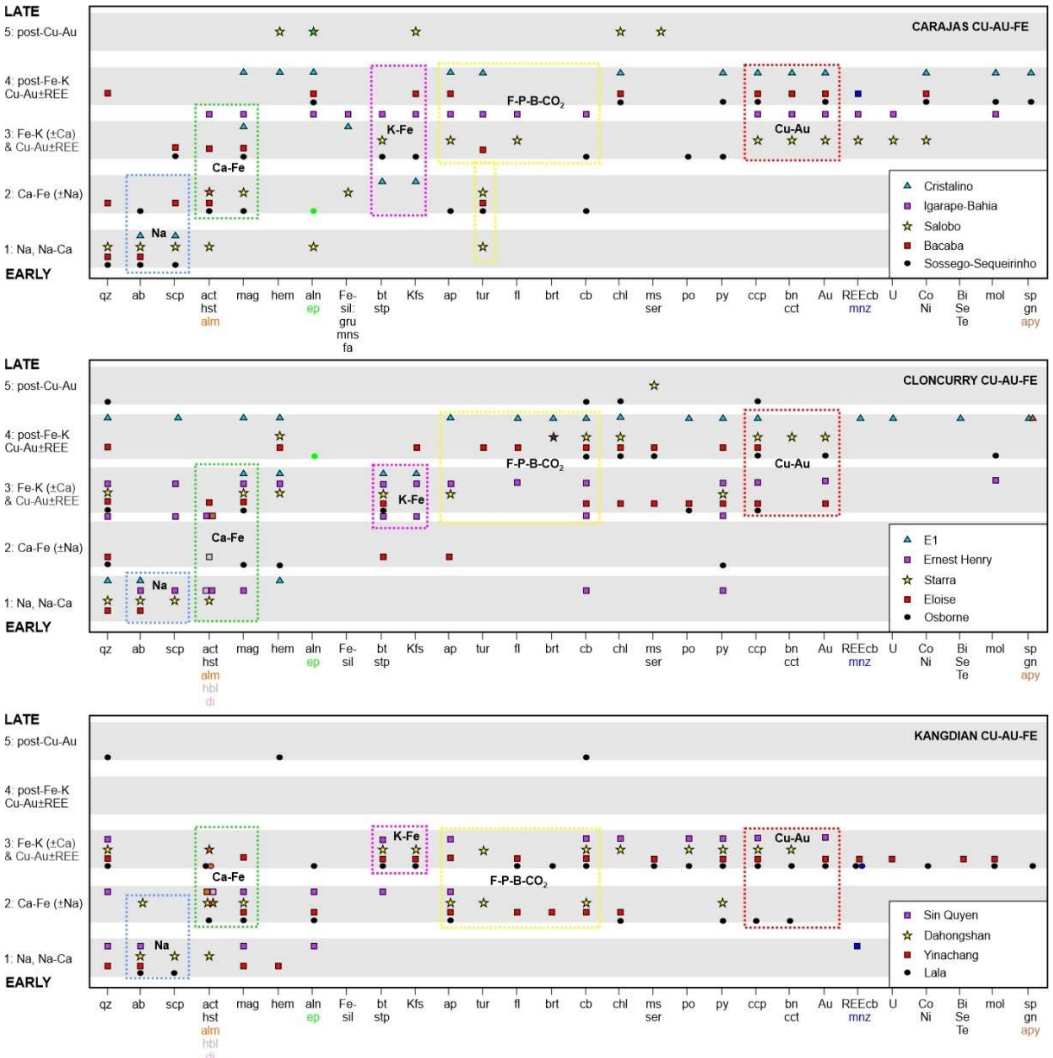

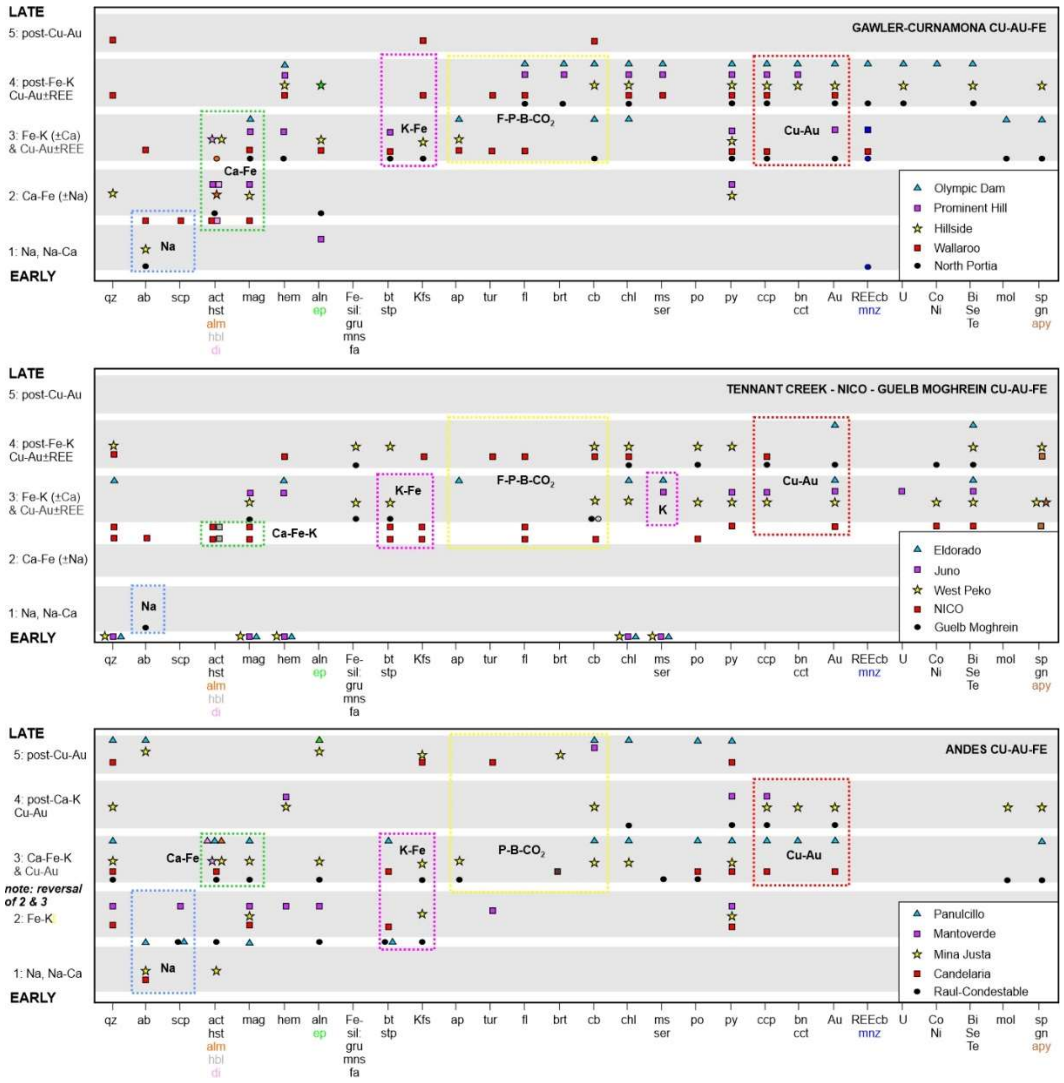

Figure 4. Paragenetic sequences of hydrothermal minerals for major and representative deposits in selected IOCG provinces. Relative timing of major stages is shown numbered on left axis from early to late. References are listed in Appendix 1. Mineral abbreviations (after Whitney & Evans, 2010): ab – albite, act – actinolite, aln – allanite, alm – almandine, anh – anhydrite, ap – apatite, apy – arsenopyrite, Au – gold, brt – barite, bn – bornite, Bi – bismuth sulfides and/or native Bi, bt – biotite, cb – carbonate, cct – chalcocite, chl – chlorite, Co – cobalt-rich sulfides, ccp – chalcopyrite, di – diopside, ep – epidote, fa – fayalite, Fe-sil – Fe-Mg-rich silicates (e.g. fayalite, greenalite, grunerite, minnesotaite), fl – fluorite, gl – galena, gru – grunerite, hbl – hornblende, hem – hematite, hst – hastingsite, Kfs – K-feldspar, mnz – monazite, mns – minnesotaite, mol – molybdenite, mag – magnetite, ms – muscovite, Ni – nickel-rich sulfides, po – pyrrhotite, py – pyrite, qz – quartz, REE – REE-rich minerals (carbonate-rich and/or P-rich including monazite and alumino-phosphate-sulfide REE minerals), scp – scapolite, Se – selenium-rich minerals, ser – sericite, sp – sphalerite, stp – stilpnomelane, Te – tellurium-rich minerals, tur – tourmaline, U – uranium-rich minerals (e.g. uraninite/pitchblende).

4.1.1 Alteration-mineralisation stages

The texturally earliest assemblages in CGI mineral systems are almost invariably of sodic character, with or without calcic minerals (Na, Na-Ca in Fig. 4) in deposits from all three of the geotectonic settings described above. Exceptions include the Tennant Creek province where no Na or Na-Ca alteration is evident at the deposits, although Na and K alteration of regional igneous

rocks has been documented in whole-rock geochemical data, albeit without isotopic age constraints (Donnellan et al., 1995). The Na and Na-Ca alteration is represented mainly by albitisation ± scapolitic alteration ± Ca-amphibole (e.g. actinolite) alteration, which are less commonly accompanied by diopside or magnetite or allanite.

In deposits in the orogenic and post-orogenic settings (i.e. all provinces in Fig. 4 except Andes) the Na and Na-Ca alteration transitions to assemblages of Ca-Fe-rich hydrothermal minerals, in some cases with continued formation of sodic minerals. The Ca-Fe assemblages (stage 2 in Fig. 4) are dominated by Fe oxides (generally magnetite) and Ca-amphiboles such as actinolite or hastingsite, and less commonly contain Ca-Fe-rich garnet such as almandine. A few deposits also contain Fe-silicates such as grunerite, minnesotaite, or fayalitic olivine that formed during the Ca-Fe stage (e.g. Guelb Moghrein; West Peko, Tennant Creek province; Salobo, Carajás province). Additionally, skarn-like Ca-Fe alteration is prominent in some orogenic and post-orogenic IOCG and related deposits, and is typically dominated by clinopyroxene or amphibole ± garnet (generally minor), with or without magnetite, scapolite and apatite. The early anhydrous skarn-like alteration is almost invariably barren of coeval Cu-Au mineralisation but may be overprinted by Cu-Au. Examples in the eastern Gawler Craton include: the Hillside deposit where early prograde magnetite-garnet skarn was overprinted by clinopyroxene-actinolite-biotite-allanite-K-feldspar and thence by hematite-chalcopyrite-chlorite-bornite-chalcocite with rare Bi, U and Pb minerals (Conor et al., 2010). A key example in the Cloncurry province is the Mt Elliott/SWAN deposit where early diopside-scapolite was overprinted by amphibole-calcite-chalcopyrite-scapolite ± magnetite, andradite, tourmaline, allanite, apatite, pyrite and pyrrhotite (Wang & Williams, 2001; Brown & Porter, 2010). Anhydrite and fluorite also have been reported from the Mt Elliott-SWAN system, which is hosted by metamorphic calcsilicate, siliciclastic (including graphitic) metasedimentary rocks and meta-mafic/intermediate igneous rocks that were Na-altered prior to skarn alteration (Brown & Porter, 2010).

The appearance of K-rich minerals marks an important chemical transition in the hydrothermal evolution, represented by K-feldspar, biotite or white mica. This K-metasomatism may commence during the Ca-Fe alteration stage or form a discrete and later Fe-K stage (stage 3 in Fig. 4) with assemblages such as magnetite-biotite or magnetite-K-feldspar. Crucially the first appearance of Cu sulfide and Au mineralisation generally overlaps with the Fe-K alteration stage, which may continue with some calcic mineral formation in a few cases. Interestingly, the available evidence for the Andean IOCG deposits shows a possible reversal of the Fe-K and Ca-Fe stages in comparison with the orogenic and post-orogenic IOCG deposits, such that the main Cu mineralisation appears with the paragenetically later Ca-Fe alteration in some Andean cases (e.g. with amphibole at Candelaria and Panulcillo; Fig. 4).

A key finding from this review of paragenetic sequences is that Cu-Au mineralisation is in every province accompanied by the deposition of volatile-rich minerals such as fluorite (F), apatite (P), carbonate (CO_2), tourmaline (B), and/or sulfates (S). The amounts and combinations of such minerals accompanying Cu-Au mineralisation are highly variable between and even within deposits. This close temporal and textural association is particularly apparent in all of the orogenic and post-orogenic provinces. The main variations to this observation are in the Carajás province where tourmaline deposition preceded and then accompanied the deposition of Cu-Au mineralisation in some deposits. Also, in some deposits of the Kangdian province and Sin Quyen deposit some of the volatile-rich minerals pre-dated as well as accompanied Cu-Au (Fig. 4). By comparison, fluorite, apatite, carbonate, tourmaline or sulfates appear to be overall less abundant with Cu-Au mineralisation in the Andean IOCG deposits.

The hematite-sericite-chlorite-carbonate assemblage is by far the most important Cu-Au-U-REE-related hydrothermal assemblage in the post-orogenic setting of the Gawler Craton CGI mineral systems. In this province only very minor Cu-Au mineralisation occurs with earlier Fe-K or Ca-Fe alteration. These stage 4 assemblages (hematite-sericite-chlorite-carbonate) are also present in many orogenic IOCG provinces in addition to stage 3 Cu-Au (Carajás, Cloncurry, Guelb Moghrein, Great Bear magmatic zone, Andean), but are generally much less developed than in the Gawler Craton. Examples include: Cristalino (with chalcopyrite) and Salobo (post-chalcopyrite) in the Carajás province; Starra, E1 and Eloise (all with chalcopyrite) in the Cloncurry province; Gecko K44 (with chalcopyrite) in the Tennant Creek province; and NICO (with chalcopyrite) in the GBMZ. The hematite-sericite-chlorite-carbonate assemblage with Cu-Au is evidently lacking in the Kangdian province and at Guelb Moghrein.

4.1.2 Uranium and REE mineral parageneses

The occurrence of REE- and U-bearing minerals varies fairly systematically between provinces, settings and deposit parageneses. The main REE-rich phases reported in the literature are allanite, REE-carbonates and monazite, whereas uraninite is the main reported U-rich phase. Certain groups of deposits and provinces have no reported or trace REE or U minerals, including many of the pyrrhotite-bearing deposits, most of the Andean deposits (although Mantoverde has anomalous REE, Rieger et al., 2010), and most Au-Cu-Bi deposits in the Tennant Creek province (except U at Juno, Large, 1975). A sub-group of deposits with magnetite-pyrite-chalcopyrite contain allanite as a REE host at various stages in the paragenetic sequences from pre-Cu-Au to syn-Cu-Au mineralisation, commonly with apatite and/or fluorite and/or carbonate. Where allanite-bearing deposits contain significant hematite, this oxide is almost always late in the paragenetic sequence and post-dates the allanite which appears to be more closely associated

with earlier magnetite and Ca-mineral formation (e.g. Gawler Craton and Curnamona deposits). Like allanite, the REE-carbonates are generally associated with apatite and/or fluorite and/or carbonate assemblages with Cu-Au mineralisation, but unlike allanite they are also associated with uraninite and do not tend to occur in pre-Cu-Au assemblages. The largest resource of REE in IOCG deposits is contained in the Olympic Dam deposit, where REE-carbonates are associated with the hematite-pyrite-chalcopyrite-bornite-chalcocite assemblages that also contain volatile-rich phases such as fluorite, carbonate and barite (Ehrig et al., 2012).

4.2 Comparison of hydrothermal assemblages in IOCG and other ore deposit types

Generalised sequences of hydrothermal mineral assemblages and major-element geochemical character for orogenic and post-orogenic IOCG deposits are compared in Figure 5 with those for Andean-type magmatic arc-hosted IOCG and selected other Fe and Cu (-Au) deposit types. First, as noted above, the relative timing of K-Fe and Ca-Fe assemblages are probably reversed in syn-syn-late-post-orogenic versus Andean-type IOCG deposits, and the relative abundances of volatile-rich minerals accompanying Cu-Au mineralisation are evidently greater in the orogenic and post-orogenic than in the Andean-type arc-hosted IOCG deposits, based on available paragenetic data.

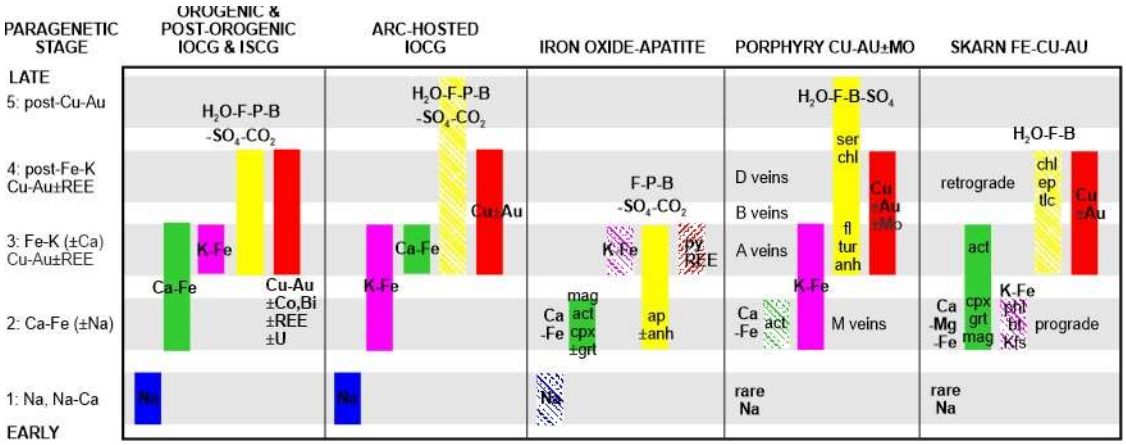

Figure 5. Generalised paragenetic sequences of hydrothermal mineral assemblages and their chemical character for orogenic and post-orogenic IOCG deposits, compared with arc-hosted IOCG, IOA, porphyry Cu-Au-Mo and skarn Fe-Cu-Au deposits. Hatchured boxes represent weakly developed assemblages compared with full-coloured boxes. Mineral abbreviations: act – actinolite, anh – anhydrite, ap – apatite, bt – biotite, chl – chlorite, cpx – clinopyroxene, fl – fluorite, grt – garnet, Kfs – K-feldspar, mag – magnetite, ms – muscovite, phl – phlogopite, py – pyrite, ser – sericite, tlc – talc, tur – tourmaline. Sources: orogenic and post-orogenic and arc-hosted IOCG deposits: this study (Fig. 4); iron oxide-apatite, porphyry Cu (-Au-Mo) and skarn Fe and Cu (-Au) deposits: Oyarzun et al. (2003); Meinert et al. (2005); Sillitoe (2010); Day et al. (2016); Li et al. (2015); Tornos et al. (2016); Rojas et al. (2018); Bonyadi & Sadeghi (2020).

Second, and with few exceptions, IOCG and related deposits in all settings contain well developed early stages of Na and/or Na-Ca alteration, whereas such alteration is rare and poorly developed in porphyry Cu and skarn Fe/Cu/Au deposits. Within proximal alteration zones at IOA deposits Na-rich alteration is generally not well developed. Interestingly, those IOA provinces with well developed and intense sodic alteration at the regional scale also contain IOCG deposits (e.g., Kiruna, Andes). In contrast, IOA provinces with poorly developed sodic alteration at any scale contain few if any significant Cu-Au deposits of IOCG type, although some contain porphyry Cu (-Au) and skarn Fe and Cu (-Au) deposits (e.g. Middle-Lower Yangtze Belt, China; Bafq region, Iran; southeast Missouri, USA).

Third, Ca-Fe alteration is well developed as an early stage in many orogenic and post-orogenic IOCG, IOA and skarn Fe/Cu/Au deposits but the accompanying mineral assemblages differ in each deposit type. In IOA deposits the magnetite-actinolite ± clinopyroxene ± garnet Ca-Fe assemblages are generally accompanied by prominent apatite and minor pyrite, and also by anhydrite in some provinces (e.g. Middle-Lower Yangtze Belt). In contrast, apatite is not a common mineral in early assemblages (Na, Na-Ca, Ca-Fe) in orogenic, post-orogenic and Andean-type IOCG deposits but forms part of later volatile-rich assemblages accompanying Cu-Au mineralisation. Nevertheless, there are examples where apatite is locally abundant with magnetite in early alteration at IOCG deposits, including the Sequeirinho orebody (Carajás province, Monteiro et al., 2008), deep parts of the Olympic Dam deposit (Ehrig et al., 2012; Apukhtina et al., 2017), the Acropolis and other magnetite-rich prospects near Olympic Dam (Bastrakov et al., 2007; Krneta et al., 2017; McPhie et al., 2020), and some magnetite-rich zones in deposits in the Kangdian province (e.g. Dahongshan deposit, Zhao et al., 2017). In the Olympic Dam district many of the sub-economic prospects with magnetite-rich and apatite-bearing alteration have assemblages including pyrite, carbonate, quartz, Ca-amphibole and K-feldspar (Bastrakov et al., 2007). Although apparently lacking amphibole, the apatite-bearing magnetite-rich veins at the Acropolis and Wirrda Well prospects are otherwise similar to those of the aforementioned occurrences, and contain variable amounts of hydrothermal K-feldspar, siderite, quartz, pyrite and biotite/phlogopite (Oreskes & Einaudi, 1992; Cross, 1993) as well as paragenetically later chalcopyrite, barite, fluorite, chlorite and sericite (Krneta et al., 2017). These magnetite-rich assemblages in the Olympic Dam district differ from the typically carbonate- and K-feldspar-biotite-poor hydrothermal assemblages in most IOA deposits. Moreover, geochronological, stable and radiogenic isotope and fluid inclusion data may indicate different timing and origins of apatite-bearing magnetite alteration in IOCG hydrothermal systems of the Gawler Craton compared to IOA deposits, as discussed further below and in the accompanying paper (Skirrow, in prep.).

Magmatic-hydrothermal skarn Fe and Cu deposits developed in carbonate-bearing host rocks generally contain garnet-rich as well as clinopyroxene- and amphibole-rich zones, whereas garnet is not abundant in most orogenic, post-orogenic and Andean-type IOCG deposits. Exceptions include several of the IOCG deposits in the Kangdian province where carbonate-rich host rocks are more abundant than in many other IOCG provinces (e.g. Dahongshan deposit, Zhao et al., 2017), and a few other deposits (e.g. Hillside, Gawler Craton, Conor et al., 2010). Moreover, one of the distinctive features of hydrothermal assemblages in IOCG deposits including those with skarn-like alteration is the generally poor development of Mg-rich alteration relative to Na, Ca, Fe and K alteration, whereas in carbonate-replacement skarn deposits Mg-rich minerals may be common, such as Mg-bearing clinopyroxenes, tremolitic amphibole, phlogopite, Mg-chlorite and talc (Meinert et al., 2005). Further differences between the orogenic + post-orogenic IOCG deposits and classic magmatic-hydrothermal skarn Fe and Cu-Au deposits are the abundances of some of the volatile-rich phases. In particular the abundances of apatite, fluorite and barite appear to be higher in orogenic + post-orogenic IOCG deposits than in skarn Fe and Cu-Fe deposits. However, there appear to be fewer differences between the Andean arc-hosted IOCG deposits and some skarn Fe-Cu deposits, in terms of settings, hydrothermal mineralogy and ore geochemistry.

Whereas many aspects of the paragenetic sequences of orogenic, post-orogenic IOCG and Andean-type arc-hosted IOCG deposits and porphyry Cu-Au deposits are superficially similar there are several important aspects of the geology and mineralogy that distinguish particularly the orogenic IOCG deposits from porphyry deposits. First, the mesothermal crustal settings of orogenic IOCG deposit formation at depths where brittle-ductile deformation is characteristic are significantly deeper than the subvolcanic settings of most porphyry deposits (Sillitoe, 2010). Second, the spatial association of Cu-Au mineralisation with coeval igneous intrusions is much weaker for the orogenic and post-orogenic IOCG deposits compared to the obvious close relationships in porphyry systems (as noted by Williams et al., 2005 and Barton, 2013 although using different classifications of IOCG deposits). Third, hydrothermal quartz is a major and almost ubiquitous phase in most subduction-related porphyry Cu-Au deposits whereas it is remarkably low in abundance in the most intensely altered and mineralised zones of most orogenic and post-orogenic IOCG deposits. However, orogenic Cu-Au deposits with little or no Fe oxide within IOCG mineral systems commonly contain minor to locally abundant hydrothermal vein quartz.

Fourth, there are differences in the extent and intensity of Na alteration as noted above, as well as differences in REE, U, Co, Ni and other minor-element abundances that will be explored further in subsequent sections. On the other hand, there appear to be many similarities between Andean-type IOCG and porphyry deposits in terms of hydrothermal mineral sequences, spatial

relationships to coeval intrusions, and geochemistry (Richards & Mumin, 2013). The key differences are the lesser development of Na alteration, higher abundance of quartz but lower magnetite, and possibly lower abundances of hydrothermal carbonate and apatite in porphyry compared to Andean-type IOCG deposits. Associated intrusions also may be somewhat more mafic at Andean-type IOCG deposits than at porphyry deposits (Sillitoe, 2003; Richards et al., 2017).

4.3 Alteration zoning – deposit scale

The sequences of hydrothermal mineral assemblages described above for IOCG deposits produce distinctive spatial patterns of alteration-mineralisation zoning which are partly controlled by the structural settings. Based on >30 deposits in 10 metallogenic province these zoning patterns have been generalised for each of the three lithostratigraphic-tectonic settings, in Figures 6A, 6B and 6C.

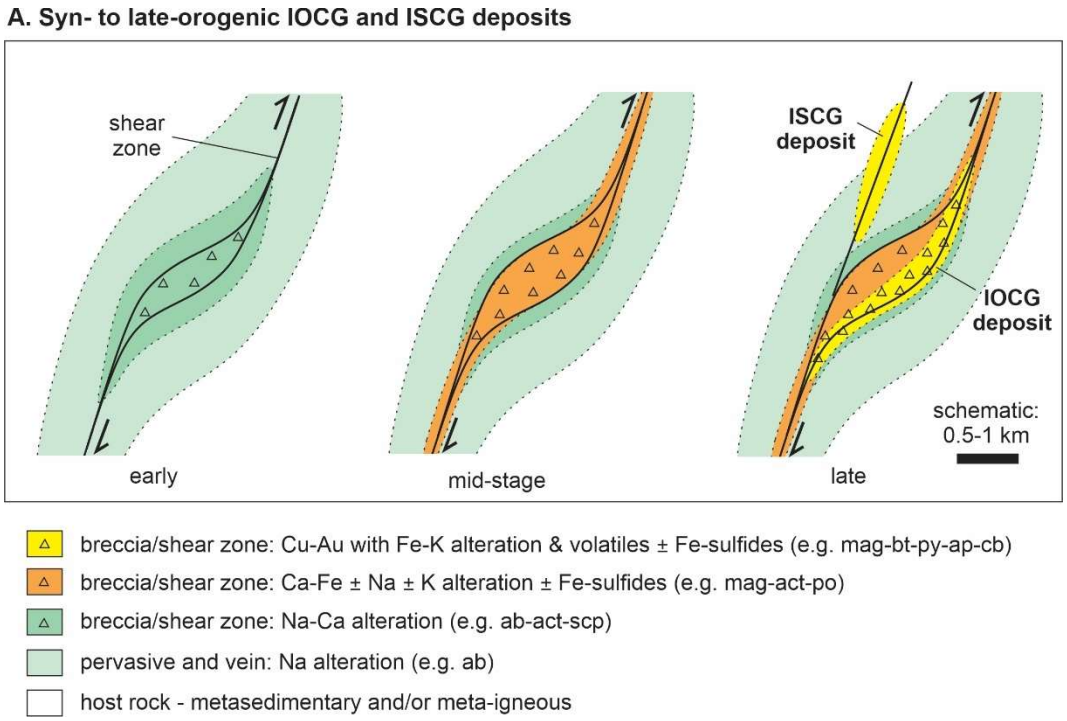

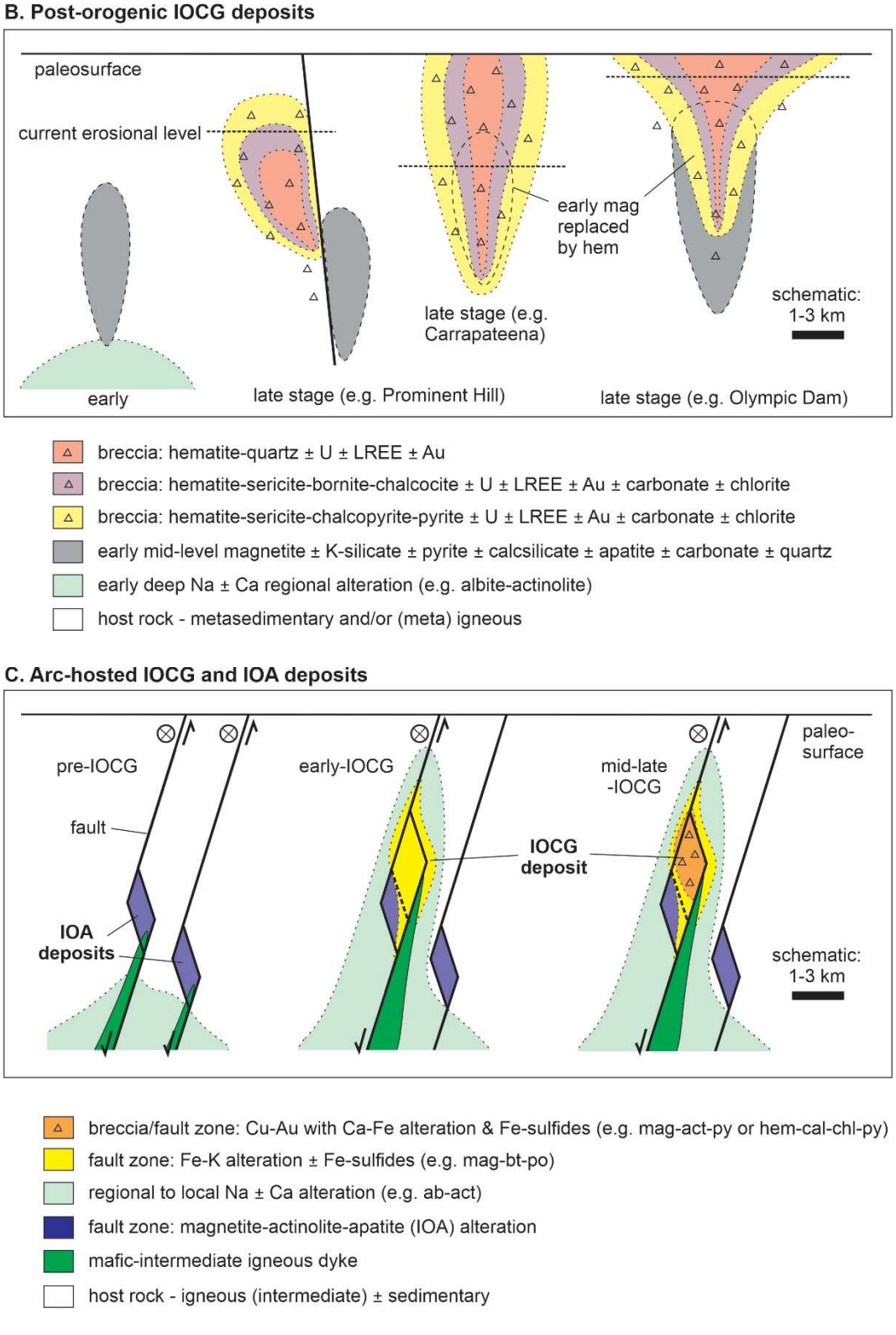

Figure 6. Schematic cross sections of deposit-scale zoning and paragenetic sequences of hydrothermal alteration-mineralisation assemblages in IOCG and related deposits in CGI mineral systems. A: orogenic settings; B: post-orogenic settings (with examples from the Gawler Craton – PH: Prominent Hill, Carr.: Carrapateena, OD: Olympic Dam Cu-Au-U-REE deposits); C: arc-hosted settings (e.g. Chilean and Peruvian Andes deposits, based on Sillitoe, 2003).

In orogenic settings structurally favourable sites along ductile to brittle-ductile shear zones (e.g. dilational jogs at rheological contrasts in local geology) commonly control the overall distribution of alteration-mineralisation. The geometric patterns of overprinting mineral assemblages vary greatly in detail between deposits (Fig. 6A). For example, the size of each zone representing a particular hydrothermal assemblage varies such that a later zone may be smaller than an earlier zone and hence it appears nested within the earlier alteration; alternatively a more extensive later zone may result in 'enclaves' of earlier alteration zones, or complete replacement of earlier by later assemblages. It should be noted that some zoning and overprinting effects may simply result from migration of alteration fronts away from fluid channelways, reflecting varying fluid:rock ratios. Also shown in Figure 6A is an ISCG deposit lacking significant Fe-oxides (at right), which is part of a CGI mineral system.

The post-orogenic setting of the Gawler Craton is typified by breccia-hosted deposits with hydrothermal mineral zoning that can be interpreted in terms of progressive migration of upward-convex shells of alteration-mineralisation towards the paleo-surface. At the Prominent Hill deposit Schlegel & Heinrich (2015) proposed a series of nested upward-convex zones resulting from upflow and migration of hydrothermal fluids, as highly simplified in Figure 6B. This concept has been extended to other zoned deposits in the eastern Gawler Craton in Figure 6B. For example at Carrapateena the sub-vertical pipe-like morphology of the hematite-rich breccia zones and Cu-Fe sulfide zones (Porter, 2010b) can be interpreted to indicate migration of alteration-mineralisation zones to a higher structural level than at Prominent Hill, with subsequent erosion to a mid or lower level in the horizontally zoned system. The flared-upward zoning of Cu-Fe sulfides and other hydrothermal assemblages at Olympic Dam (Reeve et al., 1990; Haynes et al., 1995; Ehrig et al., 2012) could represent a further progression in which the hydrothermal and breccia system breached the paleosurface to form a broad funnel-shaped body with Cu-poor hematite-quartz alteration in the upper-centre of the deposit.

Schematic zoning within CGI mineral systems in arc-hosted settings is shown in Figure 6C, based on the model of Sillitoe (2003). A possible spatial and temporal relationship between IOA deposits and IOCG deposits is also illustrated, with structural control by extensional and/or transtensional mostly brittle fault zones. Reactivation of such fault zones may result in local overprinting of IOA deposits by Cu-Au mineralisation although the two deposit types also occur independently. A close spatial relationship with mafic-intermediate magmatism is also indicated (Sillitoe, 2003), in contrast to the orogenic and post-orogenic IOCG and related deposits where magmatism is broadly coeval with, but almost invariably distal from, these deposits.

4.4 Regional alteration

Regional-scale hydrothermal alteration, characterised particularly by Na- and Na-Ca-rich mineral assemblages, is a key feature of almost all metallogenic provinces hosting CGI mineral systems and their IOCG deposits. Host rocks of widely varying composition are altered to combinations of albite, calcsilicates such as actinolitic amphibole, diopside (commonly salitic) and much less common Fe-Ca garnet, marialitic scapolite, and minor titanite. Sodic alteration with minor or no calcsilicates is commonly dominated by albite-quartz and can result in wholesale 'bleaching' of precursor rocks. Calc-silicate-rich domains range in dimensions from 100s of metres to a few centimetres, and commonly are associated with brecciation. In orogenic IOCG hydrothermal systems such breccias with Na-Ca alteration are typically syn-tectonic, forming for example along brittle-ductile shear zones and in mesoscopic fold hinges. Assemblages transitional between Na-Ca and Fe-K may include biotite or magnetite, but the timing relationships between regional Na-Ca and regional Fe-K alteration are unclear in most provinces where both types of alteration are present, generally because the two regional alteration types are not juxtaposed (e.g. Gawler Craton, Curnamona Province, and Cloncurry province). However, at deposit scales it is more evident that Fe-K overprints Na-Ca alteration, and hence we may assume this to be the case in regional alteration systems. Surprisingly, in only a few provinces have the absolute timing relationships between regional Na-Ca alteration and Cu-Au mineralisation been well constrained by geochronology (see compilation in the Supplementary Information). For example in the Cloncurry and Curnamona provinces several regional Na ± Ca alteration events have been documented, but only some were coeval with Cu-Au mineralisation events (Skirrow et al., 2000; Teale & Fanning, 2000; Duncan et al., 2011). The complex magmatic, tectonic and metallogenic-hydrothermal history of the Kiruna province (Martinsson et al., 2016) is an instructive case study where the few available U-Pb dates for prominent regional Na-Ca alteration show this metasomatism to be coeval with the first of two orogenic IOCG mineralisation events at ~1850-1865 Ma (Supplementary Information). Importantly, the dated major IOA deposits formed at ~1875-1885 Ma, significantly prior to the dated regional Na-Ca and orogenic IOCG mineralisation. More generally, the extent and intensity of regional Na-Ca alteration in provinces with IOA deposits and that lack significant orogenic, post-orogenic or arc-hosted IOCG deposits (e.g. Middle-Lower Yangtze Belt, Bafq, Southeast Missouri, Adirondacks) appears to be more limited than in the IOCG provinces.

4.5 Mineralogical classification of IOCG and related ISCG deposits

4.5.1 Redox – sulfur – iron mineralogical framework

The compilation of paragenetic sequences of hydrothermal minerals presented in section 4.1 shows that Fe-rich Cu-Au deposits contain highly variable abundances and ratios of Fe-oxide and Fe-sulfide minerals. Although highly diverse it is apparent that the characteristic Fe-oxide-sulfide mineralogies of different deposits vary systematically with the occurrences of Cu ± Fe sulfides (chalcopyrite, bornite, chalcocite), alteration minerals, and with the relative abundances of key minor elements (e.g. Co, Ni, U, REE, Ba, F, Mo). These geochemical variations are discussed in section 5. It is possible to describe the patterns of co-variation of hydrothermal minerals in terms of variations in (a) oxidation-reduction (redox) characteristics of the observed mineral assemblages, (b) the ratio of Fe-oxides to Fe-sulfides which relates mainly to the sulfur contents of the hydrothermal fluids relative to Fe, and (c) the relative timing of Fe-oxides and Cu-Fe sulfides. These three parameters are illustrated schematically in Figures 7 and 8, termed the 'IOCG-ISCG cube'. Importantly, IOCG and ISCG deposits are shown to form a continuum, with the boundary arbitrarily set where the volumetric abundance of Fe-sulfides equals that of Fe-oxides. The IOCG-ISCG cube also illustrates the hypothesised correlation between the ore-related mineralogy, minor-element geochemistry and the geological-tectonic setting for three subtypes of deposits. In Figure 7 this is shown by the three volumes outlined in red, orange and green. The three parameters (axes) of the cube and application to classification of deposit subtypes are described below.

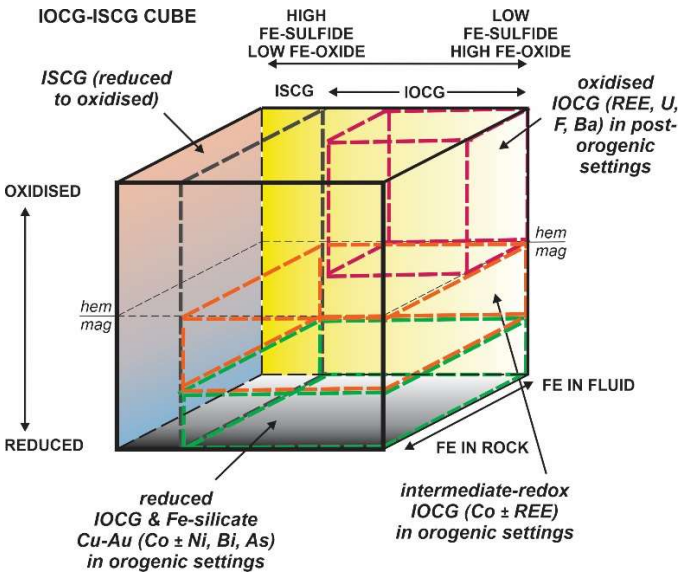

Figure 7. Three-dimensional depiction of IOCG and ISCG deposit mineralogy (the IOCG-ISCG cube), showing generalised volumes representing three mineralogical-geochemical sub-types of deposits (oxidised, intermediate-redox and reduced) in different tectonic settings. The axes are based on predominance of Fe-oxide versus Fe-sulfide minerals in Cu-Au orebodies (x-axis), interpreted redox formation conditions of key Fe-Cu-O-S minerals (y-axis), and interpreted source/timing of Fe at the ore depositional site (z-axis).

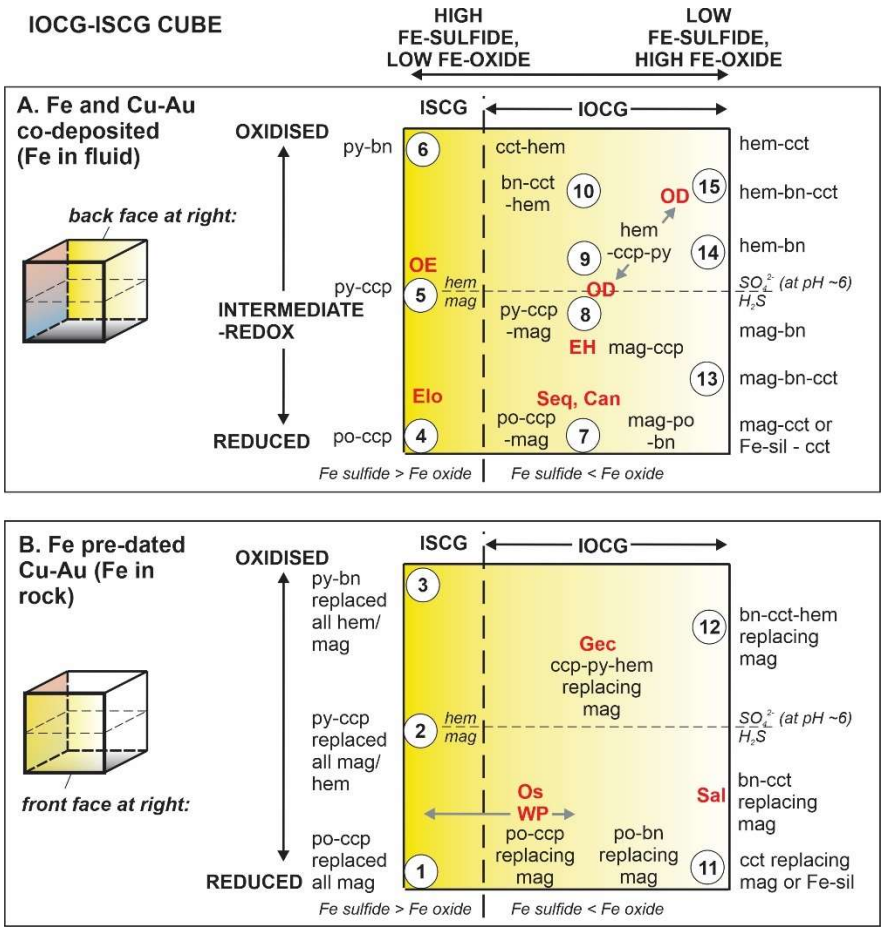

Figure 8. IOCG-ISCG cube with detail of back and front faces. Axes as in Figure 7. The back face (Fig. 8A) shows Fe-Cu-O-S mineral assemblages for deposits in which Fe-oxides and/or Fe-sulfides were broadly co-precipitated with main-stage Cu-Au ('Fe in fluid'). The front face (Fig. 8B) shows Fe-Cu-O-S mineral assemblages for deposits where most/all of the Fe-oxides pre-dated the main-stage Cu-Au, such as banded iron formation or hydrothermal ironstones ('Fe in the rock'). Stable mineral assemblages in the Fe-Cu-O-S system are based on Dick (2021), calculated at low to high values of total aqueous S and at 300°C with differing Fe:Cu ratios (courtesy E. Bastrakov and J. Dick). Numbered circles represent example deposits, as detailed in Appendix 2. Key deposits are shown in red text: Cand – Candelaria, EH – Ernest Henry, Elo – Eloise, Gec – Gecko K44 (upper), OD – Olympic Dam, OE – Orlando East, Os – Osborne, Sal – Salobo, Seq – Sequeirinho-Sossego, WP – West Peko. Mineral abbreviations as in Figure 4.

Figure 8 shows the back and front faces of the IOCG-ISCG cube in detail, where the Fe-oxide, Fe-sulfide and Cu ± Fe sulfide mineralogy of the dominant ore assemblages of individual deposits are represented by small areas of the faces (projected from small volumes within the three-dimensional space). Numbered circles represent example deposits, as detailed for some of the major IOCG provinces in Appendix 2.

The variations in observed oxide and sulfide mineralogy represented in the IOCG-ISCG cube can be understood in terms of the thermodynamic stabilities of the key Fe-oxides, Fe-sulfides and silicates, as shown in the activity diagram in Figure 9. Although depicted for specific conditions (300°C, pH = 5, etc) the topology of the stability fields of the minerals will remain roughly similar at slightly higher or lower temperatures (e.g. 250-350°C). The y-axis in Figures 7 and 8 represents the interpreted relative redox characteristics of the observed mineral assemblages, one of the

most important parameters in characterising IOCG and ISCG deposits. Oxidised assemblages are defined as those in which hematite is stable at relatively high values of logfO_2, whereas reduced assemblages are defined as those that formed at relatively low logfO_2 and where pyrrhotite and/or Fe-silicates such as grunerite or minnesotaite (boundary at ~350-370°C, Miyano & Klein, 1989) are stable, with or without magnetite and pyrite. Assemblages of intermediate redox contain magnetite and/or Fe-silicates with or without pyrite, but lack either pyrrhotite or hematite. At a fluid pH of 5 and at 300°C the hematite-magnetite boundary lies close to the predominance field boundary between oxidised sulfur (i.e. aqueous HSO_4^- or SO_4^{2-}) and reduced sulfur (i.e. aqueous H_2S or HS^-; Fig. 7); this boundary represents another useful demarcation between oxidised and reduced hydrothermal conditions (albeit pH-dependant).

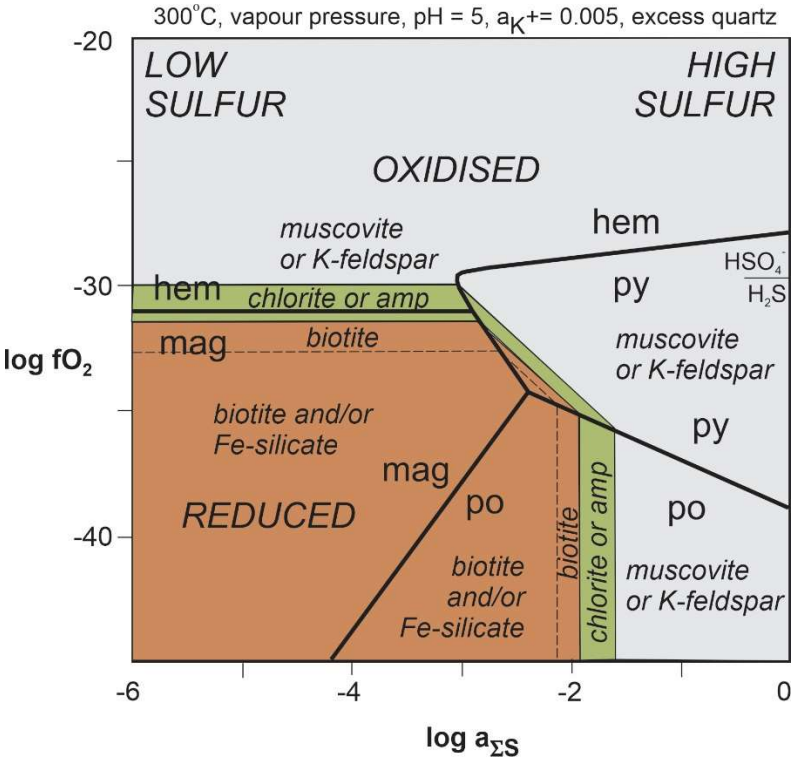

Figure 9. Activity diagram of oxygen fugacity (log fO_2) versus total aqueous sulfur activity (log $a_{\Sigma S}$) at 300°C, showing stability fields for Fe oxides and sulfides along with silicates in the system Fe-O-H-S-Si-Al-K. This diagram may be used as a 'legend' for the IOCG-ISCG cube in Figures 7 and 8. Muscovite is the stable K-silicate at pH = 5, as illustrated; K-feldspar is stable at pH > 6.5 for activity of K^+ = 0.001, or at pH > 5.5 for activity of K^+ = 0.01. At higher temperatures Fe-amphibole would occupy approximately the field of chlorite. Parts of the biotite field may be occupied by stilpnomelane and/or Fe-silicates such as minnesotaite or grunerite under certain conditions (e.g. differing activity of K^+ or temperature). Figure modified from Skirrow & Walshe (2002).

The x-axis in Figures 7 and 8 represents the observed relative abundances of Fe-sulfides and Fe-oxides in the deposits. This ratio generally reflects the concentrations of sulfur in the fluid relative to the abundances of Fe at the sites of sulfide mineral deposition, as well as redox. At the extreme left side of the IOCG-ISCG cube are ISCG deposits lacking Fe-oxides and containing abundant Fe-sulfides as well as Cu ± Fe sulfides. Examples of ISCG deposits are well known in the Cloncurry province, such as the Eloise deposit (Davidson & Large, 1994; Haynes, 2000). In the Tennant

Creek province they have been termed 'non-ironstone Cu-Au-Bi deposits' (Skirrow, 1993, 2000; Skirrow & Walshe, 2002). Indeed, many IOCG provinces contain examples of reduced to oxidised Fe-oxide-deficient Cu-Au deposits, which appear to form a continuum in terms of Fe-oxide/Fe-sulfide ratios with otherwise structurally and temporally similar Fe-oxide-bearing Cu-Au deposits (Figs. 7, 8; Appendix 2). Moreover, individual deposits may be internally zoned from massive Fe-Cu sulfide ore zones outwards through Fe-oxide-poor massive sulfide zones to outer Fe-oxide-rich sulfide-poor zones (see grey arrow at 'WP' in Fig. 8B, e.g. West Peko deposit, Tennant Creek province). At the extreme right side of the IOCG-ISCG cube (right-hand face) are Fe-oxide-rich deposits with little or no Fe-sulfide accompanying the Cu ± Fe sulfides and gold (e.g. Salobo, Carajás province, and significant parts of the Olympic Dam and Prominent Hill Cu-Au-U-REE deposits, Gawler Craton). Gold-rich or U-rich Fe oxide deposits with low Cu and minimal sulfides may be variants within CGI mineral systems, and would also occupy parts of the right-hand face of the IOCG-ISCG cube (e.g. Juno and White Devil Au deposits, Tennant Creek province; NICO Au-Co-Bi deposit, Great Bear magmatic zone; Mt Gee U-REE prospect, South Australia).

The z-axis in the IOCG-ISCG cube represents the interpreted timing of Fe-oxide deposition relative to Cu ± Fe sulfides, based on the compilation of paragenetic sequences in Figure 4 and reported geology of deposits. There are two end-member scenarios represented by the back and front faces of the cube, respectively (Figs. 8A, 8B): (1) all of the Fe-oxides were deposited contemporaneously with the Cu-Au mineralisation during evolution of an hydrothermal system, and (2) all of the Fe-oxides pre-dated Cu-Au mineralisation in separate hydrothermal or sedimentary events (e.g. sedimentary banded iron formation). Examples of scenario (2) include the 'ironstone'-hosted Au-Cu-Bi deposits of the Tennant Creek province, parts of the Osborne, Starra and Monakoff deposits (Cloncurry province), parts of the Salobo deposit (Carajás province), and the Emmie Bluff prospect (Gawler Craton). In most other IOCG deposits major proportions of the observed Fe-oxides occurring in Cu-Au ore zones were deposited directly from hydrothermal fluids either during Cu-Au mineralisation or immediately beforehand in an evolving system (scenario 1, Fig. 8A). Good examples include the Ernest Henry deposit where chalcopyrite and pyrite were deposited during the same paragenetic stage as magnetite (Mark et al., 2006), and the Prominent Hill deposit where bornite-chalcocite-chalcopyrite formed with large quantities of hematite (Schlegel & Heinrich, 2015). Cases where both 'early' Fe-oxides and syn-Cu-Au Fe-oxides occur within the same deposit (i.e. part way along the z-axis in Figs. 7 and 8) may include the Salobo deposit where banded iron formation was overprinted by hydrothermal magnetite and Cu ± Fe sulfides (de Melo et al., 2017), and in the Gawler Craton where early magnetite ± apatite ± carbonate alteration was overprinted ~4 m.y. later by Cu-Au with abundant hematite (e.g. Olympic Dam deposit and Acropolis prospect, Gawler Craton, Cherry

et al., 2018; Ehrig et al., 2012; Haynes et al., 1995; Johnson & McCulloch, 1995; McPhie et al., 2020; Oreskes & Einaudi, 1990; Reeve et al., 1990).

4.5.2 Oxidised, intermediate-redox and reduced mineralogical subtypes

As noted, both the Cu ± Fe sulfides and silicate alteration mineralogy vary systematically with the Fe-oxide and Fe-sulfide assemblages across the IOCG-ISCG cube. The IOCG and ISCG deposits can be classified into 3 mineralogical subtypes according to their dominant ore-related assemblages, which broadly correlate with the three geological-tectonic settings defined earlier (Fig. 7).

In the oxidised Fe-oxide Cu-Au (REE, U, F, Ba) subtype (red-outlined volume in Fig. 7) highly oxidised and S-poor hematite-white mica zones (top-right edge of IOCG-ISCG cube in Figs. 7 and 8, and top-left part of Fig. 9) may contain little or no sulfides or Cu but can be enriched in U and/or Au and/or REE, for example the upper and/or inner zones at Olympic Dam and Prominent Hill (Ehrig et al., 2012; Schlegel & Heinrich, 2015). These zones also may represent the most acidic conditions (e.g. Prominent Hill, Schlegel & Heinrich, 2015; Schlegel et al., 2018). Moderately oxidised hydrothermal assemblages generally contain hypogene bornite ± chalcocite with hematite ± pyrite and white mica (at low pH) or potentially K-feldspar (at high pH), as shown in Figures 8 and 9. These bornite ± chalcocite assemblages transition downwards and/or outwards into less oxidised chalcopyrite-pyrite-hematite ± magnetite assemblages where chlorite may be present with white mica (e.g. Olympic Dam, Reeve et al., 1990). Examples are present in many other IOCG-bearing provinces. These include late-stage hematite- and U-bearing chalcopyrite (-Au) mineralisation at the Sue Dianne deposit (Great Bear magmatic zone), and the paragenetically late hematite-bearing stage at Starra (Cloncurry province) where Au-rich mineralisation is associated with bornite, chalcopyrite, chalcocite, pyrite, chlorite, anhydrite, carbonate and later white mica (Rotherham et al., 1998). However, unlike the oxidised deposits of the Gawler Craton the late-stage Au-Cu at Starra is not REE-U-F-Ba-rich. This also appears to be the case in the hematite-rich examples of Au-Cu-Bi deposits in the Tennant Creek province and at the Cristalino deposit (Carajás province). Similarly, although hematite- and Cu-rich breccia at the Mantoverde deposit (Chilean Andean province) is weakly enriched in the LREE (e.g. up to 10 x local andesitic values), it contains very low U and lacks fluorite, barite, and hypogene bornite and chalcocite (Rieger et al., 2010).

A second mineralogical subtype of IOCG-ISCG deposits have intermediate-redox Cu-Au ore assemblages (green-outlined volume in Fig. 7) with variable modal proportions of magnetite, lack pyrrhotite or hematite, and contain chalcopyrite as the dominant Cu-bearing sulfide. Minor hypogene bornite is commonly present but bornite ± chalcocite dominating over chalcopyrite appears to be rare (e.g. Salobo). Many of the deposits in the Carajás, Cloncurry, Kangdian and

Tennant Creek provinces are considered here to be members of the intermediate-redox group of IOCG deposits. Silicate mineralogy in the Cu-Au ore-associated assemblages is generally dominated by Fe-K-rich phases such as biotite or rare stilpnomelane, and/or Fe-Ca-rich phases such as actinolite or garnet, and/or Fe-rich silicates such as chlorite, grunerite, and uncommon fayalite, minnesotaite or greenalite. The stability relationships of some of these minerals is shown in Figure 9 where it is clear that both the redox conditions and sulfur content of the fluids (among other parameters) are important in determining the particular oxide-sulfide-silicate assemblages at individual deposits. The intermediate-redox IOCG and ISCG deposits are highly variable in the reported occurrences of minerals hosting REE, U, Co, Ni, Bi, Mo and other ore elements, as noted above (Fig. 4). There may be a sub-set of the intermediate-redox deposits that exhibit anomalous to very high REE contents (commonly with allanite as the main REE host) and which may be transitional to the oxidised IOCG-ISCG group (e.g. Sin Quyen, SWAN, Monakoff, E1, Ernest Henry; see also Ore Geochemistry section, below).

The third mineralogical subtype of IOCG-ISCG deposits is represented by the most reduced assemblages, with pyrrhotite and/or Fe-silicates and variable modal proportions of magnetite and pyrite (blue-outlined volume, Fig. 7). Chalcopyrite is the dominant Cu sulfide with minor bornite in some deposits. Examples range from magnetite-pyrrhotite-pyrite-rich deposits (e.g. Osborne, Raúl-Condestable, Candelaria, Sin Quyen, Lala, NICO), and some with Fe-silicates such as West Peko (minnesotaite, greenalite), to pyrrhotite-rich ISCG deposits or zones lacking magnetite (e.g. Eloise, Dahongshan, Mt Elliott eastern zone) or containing only minor magnetite (e.g. Guelb Moghrein, Sequeirinho-Sossego). It is notable that reported occurrences of minor minerals in the reduced IOCG-ISCG deposit group commonly includes phases hosting Co, Ni, As and Bi but very rarely REE- or U-rich phases nor fluorite, barite or anhydrite.

5. Geochemical characterisation of IOCG and related deposits

OSNACA (Ore Samples Normalised to Average Crustal Abundances) is an open-source database of whole-rock geochemical data for ore samples from a large number of ore deposits of different types worldwide (Brauhart et al., 2017; OSNACA, 2020). Consistent analytical methods have been used for determination of 62 element abundances in all samples, with detection limits at or below average crustal abundances (OSNACA, 2020). Ore samples were assigned by Brauhart et al. (2017) into 15 deposit types or classes including IOCG plus 'other'. Of the 1165 samples accessed from OSNACA in 2020 a subset of 99 samples were classified as representing IOCG ores. Although OSNACA presently contains only a few samples for any particular deposit, the data are believed

to be representative of key ore types, and are sufficient to identify broad similarities and differences between groups and subgroups of deposits (Brauhart et al., 2017). For example, multi-dimensional scaling and principal component analysis shows that samples from IOCG deposits are geochemically distinct from all of the other ore deposit types in the data set, with closest similarities to porphyry Cu, magmatic Ni-Cu-PGE and sediment-hosted Cu deposits (Brauhart et al., 2017).

However, there are substantial variations in geochemistry within the broad group of samples attributed as IOCG ores in the OSNACA data set. Ore samples from several of the deposits attributed as IOCG type in the OSNACA data set have very different geochemistry and geology to the IOCG and ISCG deposits considered in this review. These include the Vergenoeg fluorite-magnetite deposit (South Africa), the Messina Cu deposit (South Africa), the Kurilla Cu deposit (Australia) and the Merlin Mo-Re deposit (Australia). These samples have been considered separately from the 'IOCG ores' data set in the present study, as have a few samples of hydrothermally altered rocks with low-grade mineralisation (omitted). The remaining IOCG-attributed samples have been carefully assessed against the characteristics of the IOCG and ISCG deposits as defined in this review. Samples from deposits qualifying as IOCG or related ISCG deposits have been assigned to mineralogical subtypes according to their dominant ore-related oxide-sulfide-silicate mineralogy, relative redox conditions of oxide-sulfide-silicate mineral formation, and settings, following Figures 7 and 8. A summary of deposits and subtype attribution is given in Appendix 3, which also lists the sources of additional geochemical data for several Andean IOCG deposits. This mineralogical-redox framework was then used to compare the ore geochemistry between (a) mineralogical subtypes within the family of IOCG-ISCG deposits, and (b) between IOCG-ISCG deposits and other selected ore deposit types, as described below.

5.1 Geochemical subdivision of IOCG and related ISCG deposits

Inspection of the OSNACA data for the ore samples attributed as IOCG or ISCG deposits has revealed large variations in the relative abundances of some of the chalcophile-siderophile elements (e.g. Co, Ni, Bi, Se, Te) compared to selected HFSE and LILE (e.g. U, REE, Mo). These striking variations are evident in plots of the ratio (Co+Ni+10*Bi+10*Se+50*Te)/(U+La), termed the IOCG discriminator, in which the element values are in ppm. The multipliers for Bi, Se and Te are based on an empirical comparison of their average crustal abundances with Co, Ni, U and La so that the weighted contributions of each element are similar (Fig. 10). An important and surprising finding of this study is that the widely varying values of the IOCG discriminator show a good correlation with the ore-related mineralogy and with the interpreted redox conditions of

oxide-sulfide-silicate mineral formation, from reduced to oxidised (Figs. 7, 10). As the interpreted redox conditions have been determined independently from the geochemical characterisation, the correlations in Figure 10 are considered to be a fundamental feature of the IOCG and related deposits in CGI mineral systems. Moreover, there appears to be a weak inverse correlation between the Au/Cu ratio and the IOCG discriminator index, such that the relatively oxidised ores tend to have higher Au/Cu ratios than the relatively reduced and Cu-rich ores (Fig. 10).

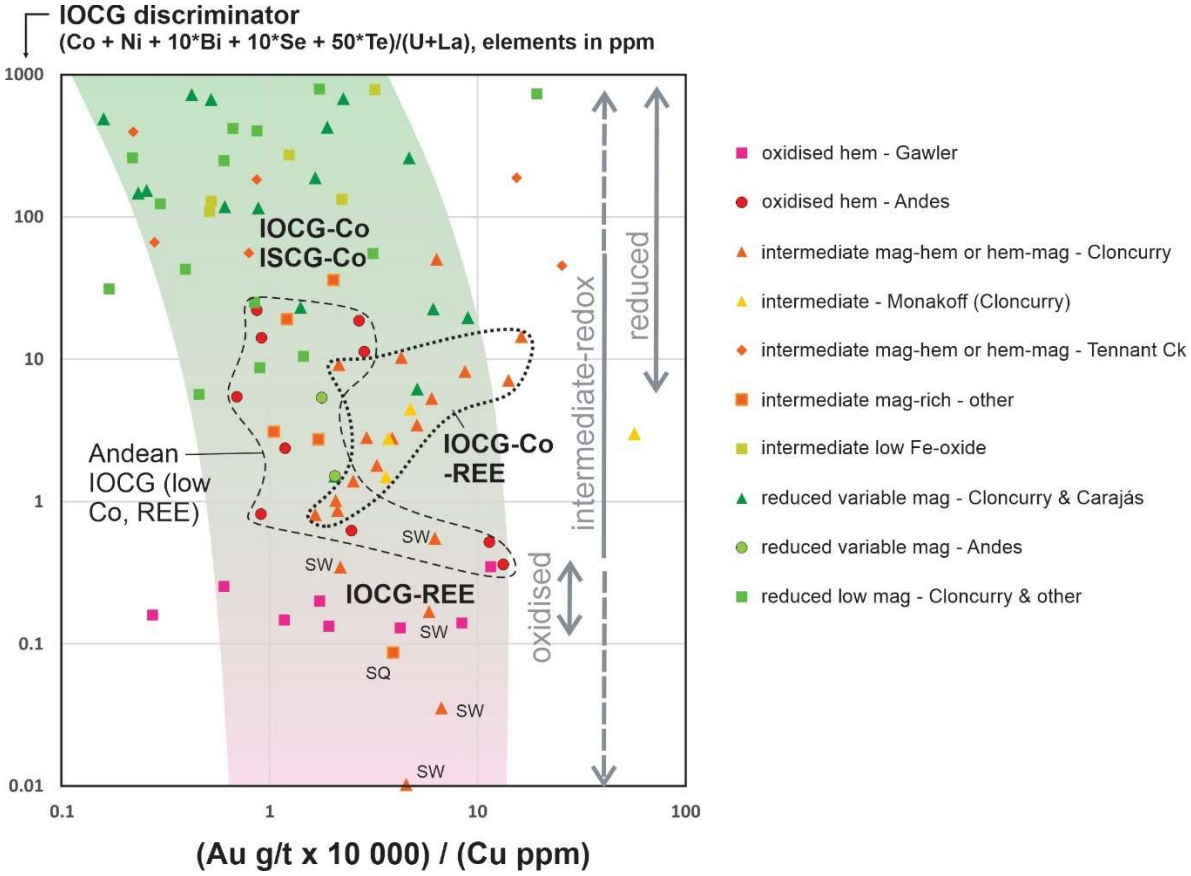

Figure 10. IOCG discrimination diagram based on whole-rock ore geochemistry, showing Au/Cu ratio versus the IOCG discriminator ratio (Co+Ni+10*Bi+10*Se+50*Te)/(U+La), with elements in ppm. The subtypes of IOCG and other deposits listed in the legend are based on independently determined mineralogical-redox subdivisions (Fig. 7); the generalised ranges of oxidised, intermediate-redox and reduced mineral assemblages are indicated with arrows. The coloured band encloses most data points. Geochemical data from the OSNACA data set (OSNACA, 2020) with additional data for Mantoverde (Chile, Rieger et al., 2010), Candelaria, Carola and Socavon Rampa (Chile, Marschik & Fontboté, 2001). Abbreviations: SQ – Sin Quyen, SW – SWAN.

The variations in key element suites are also clearly evident in plots of individual elements representing the suites, and allow discrimination of four geochemical subtypes of IOCG ores within a continuum of values of the IOCG discriminator. For example, Figure 11 shows La versus Co concentrations (with symbol size proportional to U content) and a subdivision into four subtypes demarcated by nominal boundaries at 100 ppm Co and 100 ppm La. The four geochemical subtypes are listed below, followed by detailed descriptions. The same subtypes are also labelled on Figure 10.

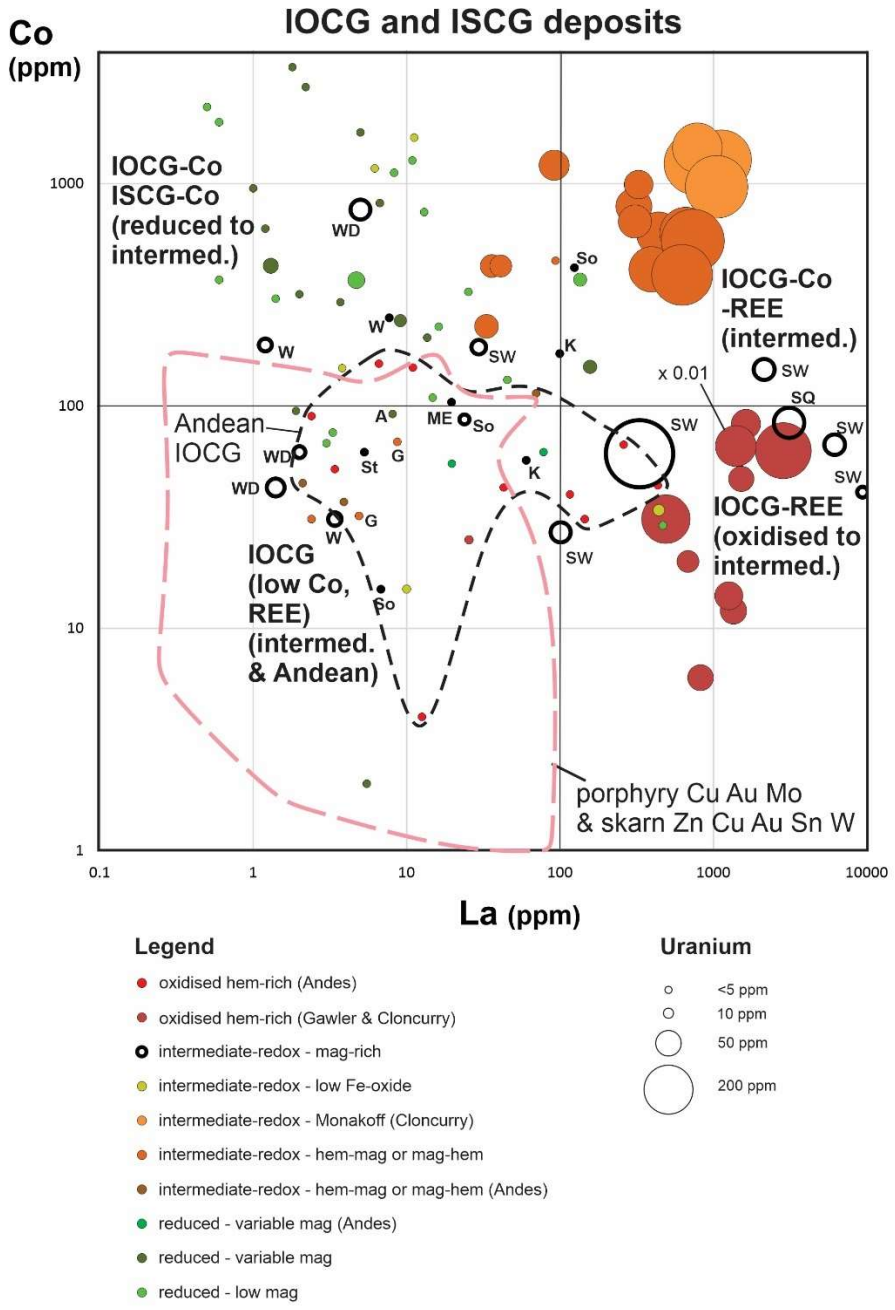

Figure 11. La (ppm) versus Co (ppm) with U (symbol size) discrimination diagram for geochemical subtypes of IOCG and ISCG deposits (IOCG-Co, IOCG-REE, etc), based on OSNACA ore geochemical data (OSNACA, 2020). Symbol colours correspond to subtypes of IOCG and ISCG deposits defined independently of the geochemical data, on the basis of mineralogy and oxidation-reduction conditions, following Figure 7. The size of the symbols is proportional to the U (ppm) values; the area of one symbol for an Olympic Dam sample is reduced by a factor of 100 for clarity (labelled x 0.01). Also shown is the field for ores from porphyry Cu-Au and Mo deposits, and various types of skarn deposits (Au, Cu, Zn, Sn, W). Abbreviations for selected deposits: W – Warrego, WD – White Devil, G – Gecko (all Tennant Creek province); SQ – Sin Quyen (Vietnam), SW – SWAN (Cloncurry province); K – Khetri (India); ME – Mount Elliott, St – Starra (Cloncurry province); So – Sossego, A - Antas (Carajás province). Additional data for Mantoverde (Chile, Rieger et al., 2010), Candelaria, Carola and Socavon Rampa (Chile, Marschik & Fontboté, 2001).

Subtype (1): 'IOCG-Co' and 'ISCG-Co' ores with moderate to high enrichments in the chalcophile and siderophile elements Co+Ni+Bi+Se+Te, and with low U and REE contents; mineralogical data indicate these deposits also lack fluorite (F) and barite (Ba) with the Cu sulfides (no Ba and F analytical data are available in OSNACA).

Subtype (2): 'IOCG-REE' ores highly enriched in selected HFSE and LILE, in particular REE and/or U, which commonly also have high Mo, F, and Ba contents, and low Co+Ni+Bi+Se+Te contents.

Subtype (3): 'IOCG-Co-REE' ores with geochemistry transitional between subtypes (1) and (2), with moderate to strong enrichments in both the Co+Ni+Bi+Se+Te and REE-U-Mo-F-Ba groups of elements.

Subtype (4): IOCG ores without strong enrichments in either the Co+Ni+Bi+Se+Te group or the REE-U-Mo-F-Ba group of elements (termed the IOCG (low Co, REE) subtype).

The IOCG-Co and related ISCG-Co ores of subtype (1) have moderate to strong enrichments in Co+Ni+Bi+Se+Te but low abundances of REE and U, and are generally characterised by variable quantities of magnetite (from very abundant in IOCG-Co to minor or absent in ISCG-Co variants) with pyrrhotite and/or pyrite, chalcopyrite ± bornite. They also may contain Fe^{2+}-rich silicates in differing combinations, such as biotite, phlogopite, actinolite, grunerite, fayalite and/or stilpnomelane. Variations in relative abundances of magnetite and sulfides may be considerable even within individual deposits in this subtype. Deposits of subtype (1) lack syn-sulfide hematite and sulfate minerals such as barite and anhydrite, as well as hypogene chalcocite. The mineral assemblages of this subtype are indicative of relatively reduced to intermediate-redox conditions during Cu-Fe sulfide ore deposition (Figs. 7, 8, 9). In the Cloncurry district where some of these reduced deposits of subtype (1) are ISCG deposits it has been suggested that local reduction of the ore fluid was effected by reductants in the host rocks such as graphite (Haynes, 2000), and with resultant suppression of magnetite formation (Williams et al., 2005). However, considered globally, almost all of the pyrrhotite-bearing ISCG and IOCG deposits occur in non-graphitic host rocks (e.g. Osborne, Cloncurry province, Adshead et al., 1998; West Peko, Tennant Creek province, Skirrow & Walshe, 2002; Guelb Moghrein, Mauritania, Kolb et al., 2010; Kolb & Petrov, 2016; Kirschbaum & Hitzman, 2016; and pyrrhotite-bearing deposits in the Carajás, Kangdian and Andean provinces). An alternative explanation is that the reduced character of the mineral assemblages is inherent to the redox properties of the ore fluid prior to ore deposition. It is also reasonable to infer that the enrichments of Co+Ni+Bi+Se+Te and low abundances of REE and U are also a fundamental feature of the hydrothermal fluids involved in the formation of the IOCG-Co and related ISCG deposits. In the special case of the Geulb Moghrein deposit graphite in the orebody is considered to be the product of breakdown of siderite to magnetite plus graphite; the host carbonate and mafic meta-igneous rock sequence is graphite-free (Kirschbaum & Hitzman, 2016). Other examples of reduced to intermediate-redox IOCG-Co and related ISCG deposits include: Eloise, Kulthor, Lorena (Cloncurry province, Australia); Antas, Sossego-Sequeirinho (Carajás province, Brazil); and Warrego (Tennant Creek province, Australia).

Ores of geochemical subtype (2), labelled 'IOCG-REE' in Figures 10 and 11, have distinctive low values of <1 for the (Co+Ni+10*Bi+10*Se+50*Te)/(U+La) discriminator, in contrast to the IOCG-Co ores of subtype (1). Although there are relatively few deposits represented in OSNACA in this subtype, the main examples are world-class hematite-rich breccia-hosted Cu-Au-U-REE deposits in the Gawler Craton, including the Olympic Dam, Prominent Hill and Carrapateena deposits. In addition to U and LREE, these deposits are also highly anomalous in Ba and F as evident from the abundances of barite and fluorite (Reeve et al., 1990; Belperio et al., 2007; Porter, 2010b; Ehrig et al., 2012). The ore-related mineral assemblages are indicative of relatively oxidised hydrothermal conditions and include hematite, barite, chalcocite and bornite (Figs. 7, 8, 9; Reeve et al., 1990; Haynes et al., 1995; Ehrig et al., 2012; Schlegel & Heinrich, 2015; Schlegel et al., 2018). The Olympic Dam deposit has a remarkably wide range of other anomalously enriched elements that in some cases are zoned across the deposit, such as deep and/or peripheral zones with anomalous Mo, W, Sb, As, Te, Ba and Sn (Ehrig et al., 2012). Minerals representing reduced conditions are absent or rare (e.g. rare pyrrhotite at Olympic Dam, Ehrig et al., 2012). Locally abundant magnetite with siderite, pyrite and chalcopyrite, in the deeper and/or peripheral zones at Olympic Dam, represent hydrothermal conditions of intermediate redox compared to relatively oxidised upper and/or inner zones (Figs. 7, 8, 9; Reeve et al., 1990; Haynes et al., 1995; Ehrig et al., 2012).

A third subtype of ores, labelled 'IOCG-Co-REE' in Figures 10 and 11, exhibit geochemical signatures that are transitional between the IOCG-Co and IOCG-REE subtypes, with strong enrichments in both REE+U and Co+Ni+Bi+Se+Te. These ores occur in relatively few deposits as presently represented in the OSNACA data set, all within the Cloncurry district (Ernest Henry, Monakoff, and E1 Group deposits). The Cu-Au ores are characterised by generally high ratios of magnetite/hematite and pyrite/pyrrhotite, and they are all relatively Fe-oxide-rich. They mostly lack minerals indicative of strongly reduced conditions (e.g. graphite, pyrrhotite, fayalite, minnesotaite, loellingite) but contain minor to locally abundant minerals representing oxidised conditions (e.g. hematite, barite; Mark et al., 2006; Williams et al., 2015). Typical assemblages with Cu-Au mineralisation include magnetite, pyrite, chalcopyrite, biotite, K-feldspar, carbonate, Ca-amphibole, chlorite and quartz. The IOCG-Co-REE ores are therefore represent intermediate-redox conditions of hydrothermal mineral formation (Figs. 10, 11).

A fourth geochemical subtype of ores is evident from Figure 11 (labelled IOCG (low Co, REE)), with low Co (<100 ppm), La (<100 ppm) and U (<5ppm). These ores have IOCG discriminator values spanning the range between the IOCG-Co and IOCG-REE subtypes (similar to the IOCG-Co-REE range) but their REE+U and Co+Ni+Bi+Se+Te contents are relatively low. Most ores in this geochemical subtype are Fe-oxide-rich and contain magnetite-pyrite-chalcopyrite ± hematite

assemblages typical of intermediate-redox formation conditions (Figs. 7, 8, 9). Importantly, most of the IOCG ores from the Andean deposits plot within this IOCG (low Co, REE) subtype, with the exception of several samples from the hematite-magnetite-rich Mantoverde deposit which contains enrichments in REE but low U (Rieger et al., 2010). It is noteworthy that this deposit also contains relatively abundant hypogene hematite with chalcopyrite (Benavides et al., 2007; Rieger et al., 2010), whereas other Andean IOCG deposits with hematite>>magnetite (Carola, Socavon Rampa, Barreal Seco) have much lower REE abundances.

The IOCG (low Co, REE) subtype also contains ore samples from parts of some Au-Cu-Bi deposits from the Tennant Creek province, although other samples from the same deposits plot within the IOCG-Co fields in Figures 10 and 11 (e.g. Warrego, White Devil). When the broader element group of Co+Ni+Bi-Se+Te is considered, most of the Cu-rich Tennant Creek Au-Cu-Bi ores plot within the same geochemical subtype as the reduced IOCG-Co ores from the Cloncurry, Carajás and Guelb Moghrein provinces (Fig. 10), including samples from the West Peko deposit (R. Skirrow, unpublished data, not in OSNACA). This suggests that at least the Cu-rich members of the Tennant Creek Au-Cu-Bi deposits are indeed geochemically very similar to other deposits in the global IOCG family of deposits (cf. Groves et al., 2010). Nevertheless, some ores with extremely high Au/Cu ratios (e.g. White Devil) plot well outside the main trend of IOCG and related ISCG deposits in Figure 10, and may represent a separate and later Au event (Huston et al., 2020; also see Tennant Creek province section of Supplementary Information).

A few deposits have mineralogical features that are inconsistent with the majority of other deposits in their geochemical subtype. For example, the SWAN Cu-Au ores in the Cloncurry province have low IOCG discriminator values and high La-Co-U contents similar to those of the oxidised IOCG-REE subtype (Figs. 10, 11), but the deposit has an intermediate-redox mineral assemblage of magnetite-amphibole-pyrite-chalcopyrite-anhydrite with albite and clinopyroxene (Brown & Porter, 2010). The Sin Quyen deposit may be another example. The origin of these mis-matches is not fully understood. Interestingly, the Mt Elliott Cu-Au deposit, which is adjacent to the SWAN deposit, is considered to be part of the same hydrothermal system as the SWAN deposit and shares similar mineralisation and alteration mineralogy including minor anhydrite, pyrrhotite, allanite, tourmaline, apatite, biotite and K-feldspar (Brown & Porter, 2010). Although few data are available in OSNACA, Mt Elliott has a higher IOCG discrimination value (16) than SWAN (0.01 to 0.55) and significantly lower REE and U contents. These relationships may indicate that fluids of similar sulfate-stable (oxidised) and LREE-rich character to those in IOCG-REE deposits were involved at both SWAN and Mt Elliott, producing local anhydrite and LREE enrichments yet without hematite development, perhaps due to high temperatures. These oxidised magnetite-anhydrite-stable fluids may have overprinted or

coexisted with a more reduced (pyrrhotite-bearing) hydrothermal environment represented at the Mt Elliott deposit. This example illustrates the complexities in the mineralogical and geochemical evolution of the IOCG and related deposits considered herein, which in places resulted in features of hybrid (e.g. multi-stage, or multi-fluid) origin.

5.2 Geochemical comparisons of IOCG deposits with other ore types

Comparison of the geochemistry of the IOCG ore samples in the OSNACA data set reveals that, for the IOCG-Co, IOCG-REE and IOCG-Co-REE subtypes, Co+Ni+Bi+Se+Te and/or U+REE are enriched relative to porphyry (Cu ± Au, Mo), skarn deposits of various types (Cu, Fe, Au, W, Sn), intrusion-related gold (IRG), granite-related greisen (Sn, W, Mo, Bi) and pegmatite (Nb, Ta, Li) deposits (Fig. 12). Although there is some overlap between these groups around y-axis values of ~100 the Telfer Au-Cu deposit in northwestern Australia stands out as an exception and has a similar Co-Ni-Bi-Se-Te compositions to those of the IOCG-ISCG deposits represented in OSNACA. The overall differences between IOCG-ISCG and these other deposit types are also clearly evident when only La and Co are plotted as key representatives of the REE and Co+Ni+Bi+Se+Te element suites (Fig. 13). The porphyry, skarn and granite-related groups of deposits, widely agreed to be of intrusion-related magmatic-hydrothermal origin, have Co+Ni+U+La (total ppm) values of generally less than 100 for samples with Cu > 1000 ppm, whereas the IOCG ores mostly have Co+Ni+U+La (total ppm) values greater than 100 for Cu > 1000 ppm (Fig. 12). In the La versus Co diagram the nominal boundaries of 100 ppm La and 100 ppm Co used for subdivision of the IOCG and related deposits appear to also effectively demarcate the fields of the porphyry and skarn deposits (Fig. 13). Notably, the low Co, La and U contents of most of the Andean IOCG ore samples (except some Mantoverde samples) match the low values of porphyry and skarn deposits, which are also mostly located within magmatic arc settings (Sillitoe, 2010). Hence this ore geochemistry is likely fundamental to the continental arc setting.

In summary, with the exception of the Andean IOCG deposits, most IOCG ores in the OSNACA data set are dissimilar to magmatic-hydrothermal deposit types, in terms of the key minor element suites Co+Ni+Bi+Se+Te and REE+U (Mo, F, Ba), but share some geochemical features of deposits formed by hydrothermal leaching of mafic and other host rocks. The possible reasons for these geochemical similarities and differences are discussed in the accompanying paper (Skirrow, in prep.), where they are suggested to relate to the relative partitioning of compatible and incompatible elements between hydrous fluids, silicate melts, and sulfide melts, and the relative stabilities of the metal complexes and mineral solubilities in hydrothermal fluids. Indeed, the elements Co, Ni, U and La have been chosen as discriminators mainly because of their contrasting

behaviours in magmatic and hydrothermal fluid-silicate-sulfide melt systems. It should be noted, however, that the inferred redox conditions (or other geochemical parameters) of the observed ore-related hydrothermal mineral assemblages do not necessarily represent the very earliest redox (or other hydrothermal) characteristics of the fluids along their flow paths to the sites of ore deposition.

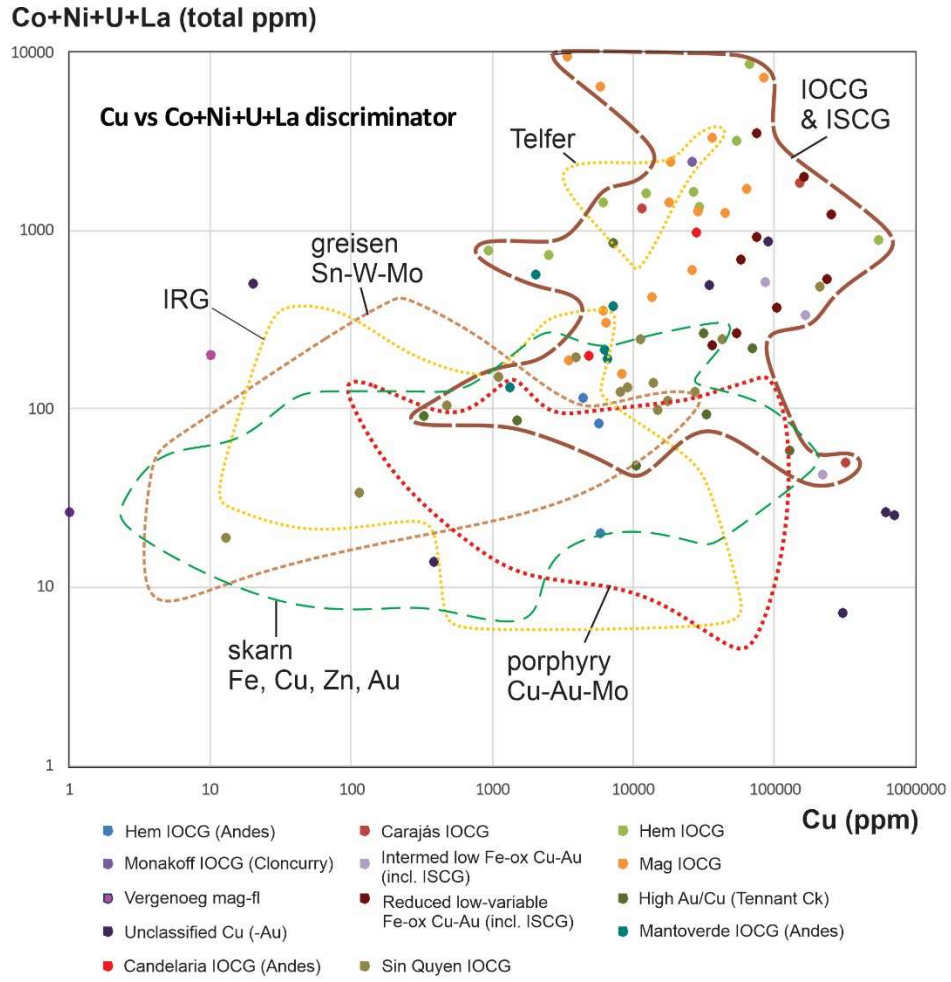

Figure 12. Copper versus Co+Ni+U+La (in ppm) discriminator diagram comparing IOCG-ISCG deposits with fields for intrusion-related magmatic-hydrothermal deposits (porphyry Cu-Au-Mo, skarn Fe Cu Zn Au, greisen Sn-W-Mo, and intrusion-related gold (IRG) deposits). The subtypes of IOCG-ISCG deposits listed in the legend are based on mineralogical subdivisions shown in Figures 7 and 8 and listed in Appendix 3. Data from the OSNACA database (OSNACA, 2020).

6. Discussion

6.1 Relationships between IOCG and IOA deposits

The relationships between IOCG and IOA deposits have been much debated since the 1980s and 1990s when the IOA deposits of Kiruna province were included by Hitzman et al. (1992) in the global family of Proterozoic iron oxide (Cu, U, Au, REE) deposits. While suggesting a genetic link and a continuum between IOA and IOCG end-members, Hitzman (2000) also noted there are fundamental differences between IOA and IOCG deposits and that they did not necessarily form coevally where they occur in the same district. Williams et al. (2005) stated that Kiruna-type iron oxide-apatite ores are not IOCG deposits and may be genetically fundamentally different and yet they may share similar geological environments and sources of some components. The different timing and tectonic settings of the Precambrian IOA and IOCG deposits was also cited by Groves et al. (2010) as evidence of distinct genesis rather than end-members in a continuum. On the other hand, Corriveau et al. (2010, 2016) proposed a generalised alteration zoning model, based on observations in the Great Bear magmatic zone and broader comparisons, in which IOA deposits formed at deeper, higher temperature and earlier stages in the same 'iron oxide-alkali alteration' systems as shallower, lower temperature and later IOCG (and albitite-hosted U and polymetallic skarn) deposits. Recent studies in the Chilean Iron Belt have also promoted a more direct genetic association between deeper IOA and shallower IOCG deposits than proposed by Sillitoe (2003), as described by Knipping et al. (2015), Reich et al. (2016), Barra et al. (2017), Simon et al. (2018) and Rodriguez-Mustafa et al. (2020).

The availability of considerable new data in recent decades brings new constraints to the issue of the relationship between IOA and IOCG deposits. First, among the world's 10 major orogenic, post-orogenic and arc-hosted IOCG provinces large IOA deposits of Kiruna type are present only in the Kiruna province itself, and in the Chilean Iron Belt, although large Fe oxide-rich apatite-poor hydrothermal bodies and/or Fe-oxide-rich alteration lacking significant Cu-Au mineralisation are present in many of the other major IOCG provinces. Available geochronological constraints for the Kiruna province and Chilean Iron Belt indicate that the formation of the large IOA deposits preceded the main IOCG mineralisation events by >10-15 m.y (see review in the Supplementary Information). Moreover, the IOA deposits in both of these provinces contain very low Cu-Au contents, although they generally contain minor pyrite and may host trace chalcopyrite. In rare cases where the IOA deposits contain small Cu (-Au) resources the textural and structural relationships indicate that the main Cu (-Au) mineralisation overprints the IOA deposit (e.g. Cerro Negro Norte, Chile, Salazar et al., 2020), consistent with the geochronological data for the Chilean Iron Belt indicating a significant time gap. Conversely, the magnetite-rich

paragenetically early stages in the main IOCG deposits in the Andean provinces (Chile and Peru) and Kiruna province are not known to be apatite-rich, nor do they contain the coarse-grained (pegmatitic) magnetite-apatite-amphibole intergrowths that are typical of parts of many IOA deposits in both regions. For example, in the Candelaria deposit the paragenetically early magnetite-rich alteration is not apatite-bearing (Marschik & Fontboté, 2001; del Real et al., 2018) despite the evidence of similar magnetite geochemical and isotopic compositions to magnetite in some IOA deposits of the Chilean Iron Belt (Rodriguez-Mustafa et al., 2020). Similarly, at the Mantoverde deposit Rieger et al. (2010) reported only minor apatite (associated with quartz, tourmaline, scapolite and white mica) within the magnetite-hematite-rich deposit, and noted the differences in alteration and magnetite geochemistry between the IOA deposits in the district and the Mantoverde deposit.

Magnetite-rich alteration with in some places local apatite is indeed present in some of the other orogenic, post-orogenic and arc-hosted IOCG provinces but, as in the Kiruna and Andean provinces, it is paragenetically earlier than, and temporally distinguishable from, the Cu-Au mineralisation where data are available. For example, in the post-orogenic Olympic Cu-Au province in the Gawler Craton magnetite-rich alteration with locally abundant apatite at the Acropolis prospect formed ~4 m.y. earlier than the major Cu-U-Au mineralisation event at the Olympic Dam deposit (based on high-precision U-Pb TIMS dating, Cherry et al., 2018; Courtney-Davies et al., 2019; McPhie et al., 2020; see also review in the Supplementary Information). Moreover, the magnetite alteration at Acropolis and elsewhere in the Olympic Dam district is associated with hydrothermal K-feldspar and carbonate as well as actinolite, pyrite and quartz (Oreskes & Einaudi, 1990, 1992; Bastrakov et al., 2007; Cherry et al., 2018). This K-CO_2-Ca-rich character is different to the typically Ca-Na-rich compositions of alteration minerals in and around most magnetite-rich IOA deposits such as those in the Kiruna district, Middle-Lower Yangtze Belt, Chilean Iron Belt, southeast Missouri (USA) and the Bafq district of Iran (Fig. 5; e.g. Oyarzun et al., 2003; Daliran et al., 2010; Zhou et al., 2013; Day et al., 2016; Martinsson et al., 2016; Bonyadi & Sadeghi, 2020). Nevertheless, potassic alteration is present in some peripheral and/or upper alteration zones of some IOA deposits, where it is generally represented by K-feldspar accompanied by hematite (e.g. Kiruna district, ; southeast Missouri, Day et al., 2016) or by phlogopite ± K-feldspar (e.g. Middle-Lower Yangtze Belt, China, Zhou et al., 2013). Neither of these assemblages have been reported in the IOCG and related deposits considered in the present review of 10 metallogenic provinces globally.

In other orogenic IOCG provinces with paragenetically early magnetite-rich alteration, apatite is either absent/not reported (Guelb Moghrein, Tennant Creek, Cloncurry, Khetri) or is only rarely and locally abundant with magnetite alteration (e.g. Sequeirinho orebody of Sossego deposit,

Carajás province, Monteiro et al., 2008). Biotite and carbonate commonly accompany the early magnetite-rich alteration in many orogenic IOCG provinces, but these minerals are rarely present in significant modal amounts in the major IOA deposits in the Kiruna, southeast Missouri, Bafq, Middle-Lower Yangtze Belt and the Chilean Iron Belt IOA provinces. A further example of large hydrothermal magnetite bodies in orogenic IOCG provinces is the Lightning Creek sill complex in the Cloncurry district. Here, the albite-magnetite-quartz ± diopside mineralogy and spherulitic textures of the magnetite-rich bodies within the monzodioritic intrusion (Perring et al., 2000) are different to the variably apatite-amphibole-albite ± K-feldspar ± pyrite-bearing mineralogy and massive to pegmatoidal textures that are typical of magnetite and/or hematite-rich Kiruna type IOA deposits.

Except for the Kiruna province and Chilean Iron Belt, other major IOA provinces including southeast Missouri, Bafq, and the Middle-Lower Yangtze Belt are not known to contain significant IOCG deposits of the types described herein (orogenic, post-orogenic and arc-hosted) but in some cases host porphyry Cu (-Au) and/or intrusion-related skarn Fe and/or Cu and/or Au deposits (e.g. Middle-Lower Yangtze Belt, Zhou et al., 2013; Sun et al., 2018). The Boss Cu deposit is the only known significant Cu resource in the southeast Missouri IOA district (40 Mt @ 0.83 % Cu), which has been described as an IOCG deposit and lacks significant apatite with the early-stage Fe-oxides (Day et al., 2016). Iron and Cu sulfides overprinted the Fe-oxides and have high $\delta^{34}S$ values indicating a sulfur source likely external to the spatially associated igneous rocks, possibly related to input of basinal brines (Johnson et al., 2016). Thus it seems likely that in this rare case of significant Cu mineralisation in an IOA province (other than Kiruna and the Chilean Iron Belt, noted above), the late introduction of Cu was not directly related to the formation of the host Fe-oxide-rich body, which is similar to other IOA deposits in the district that are generally considered to be of magmatic-hydrothermal origin (e.g. Johnson et al., 2016).

In summary, available geological and geochronological information strongly points to different timing, tectonic settings, hydrothermal evolution and probably origins of formation of the orogenic and post-orogenic IOCG deposits compared to IOA deposits. The most productive settings for orogenic and post-orogenic IOCG mineralisation appear to be those where inversion of (extended) continental margin basins occurred inboard of prior magmatic arcs, coincident with syn- to post-orogenic magmatism. In contrast, the settings of most large IOA deposits were continental margin magmatic arcs undergoing extension/transtension. Although this same broad setting was shared by the arc-hosted IOCG deposits in the Andes, available data indicate that the major IOA deposits formed >10-15 million years earlier than the IOCG deposits, and hence a direct genetic association of the two deposit types within the same hydrothermal systems is difficult to

reconcile. This does not rule out the possibility of IOCG mineralisation overprinting IOA deposits, however.

6.2 Classification of IOCG and related ISCG deposits

The results of the present review of geological and tectonic settings, alteration-mineralisation mineralogy and ore geochemistry of IOCG and related deposits in CGI mineral systems are integrated within the classification scheme shown simplified in Figures 13 and 14, and in detail in Table 2. A broader classification scheme including other types of hydrothermal Cu ± Au and/or Fe deposits is presented in Table 3. Whereas there are some similarities between this scheme and the previous classifications of Hitzman et al. (1992), Hitzman (2000), Williams et al. (2005), Williams (2010), Groves et al. (2010) and Barton (2013) there are some significant differences, as follows.

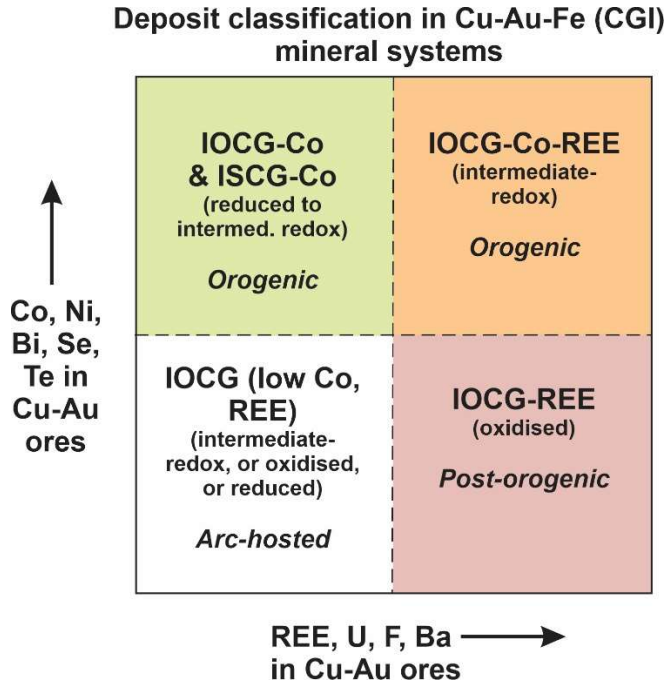

Figure 13. Classification scheme with ore geochemical axes for subtypes of deposits in the CGI mineral systems including IOCG and ISCG deposits. Note the combined use of ore geochemical, mineralogy-based redox, and geotectonic setting attributes in the proposed scheme.

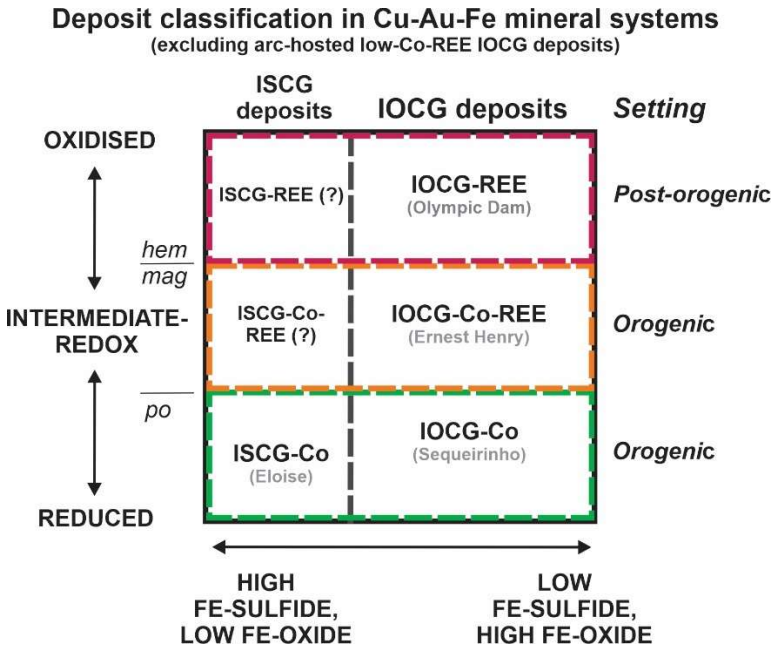

Figure 14. Classification scheme with redox and sulfide/oxide ratio axes for subtypes of deposits in CGI mineral systems including IOCG and ISCG deposits, with type examples (Olympic Dam, Ernest Henry, Sequeirinho ore body of the Sossego deposit). The boundary between IOCG and ISCG deposits is nominally set where the abundances (by volume) of oxides and Fe sulfides are equal. Some ISCG deposit types have not been documented but are predicted to exist (shown with '?').

First, this classification distinguishes three tectonic settings: orogenic, post-orogenic and arc-hosted, which only partly correlate with any previous proposals of settings. The syn-tectonic, orogenic, settings of many of the IOCG and related deposits have been especially under-emphasised previously, with far more focus on 'anorogenic' settings. In the present scheme none of the proposed three settings are 'anorogenic'; instead a post-orogenic extensional setting is proposed that is intimately linked to the preceding orogenic processes in the same terranes.

Second, this scheme distinguishes IOCG and related ISCG deposits from porphyry Cu (-Au), skarn Fe-Cu-Au, and IOA deposits, although it is recognised that some features of the geology, mineralogy and geochemistry may be shared between these deposit types. In particular, several of the previous classifications consider IOA deposits as 'end-members' within a broad family of iron oxide-associated deposits, whereas it is proposed herein that IOA deposits are of fundamentally different origin to the orogenic and post-orogenic IOCG deposits. However, they may be related to the arc-hosted Andean-type IOCG deposits in an a way that remains poorly understood.

Finally, mineralogical and geochemical subtypes of the IOCG and related ISCG deposits occurring in particular geotectonic settings are proposed in the new classification scheme – relationships that have been largely unrecognised previously. For example, deposits of the IOCG-Co subtype are characterised by correlations between reduced ore-related hydrothermal mineral

assemblages and elevated levels of Co, Ni, Bi, Se and/or Te (and low U and REE), and occur specifically within the orogenic tectonic setting (Fig. 13). Whereas the new scheme has some similarities with the mineralogy- and metal-based classification of Williams (2010) a greater focus on redox, geochemistry of minor elements, and geological setting is proposed herein. Williams (2010) included iron oxide Cu-Au ± U (IOCG) deposits within a group of 'closely affiliated deposits', along with 'low Fe-oxide Cu-Au', 'Fe oxide-U (low Cu)' and 'Co-As ± Fe-oxide ± Au (low Cu)'. Here, emphasis is placed on the IOCG and ISCG members of this family and on their membership of the newly-named CGI mineral system, while not dismissing the possible inclusion of other members of the Williams (2010) family of 'closely affiliated deposits'.

Table 2. Classification and key features of orogenic, post-orogenic and arc-hosted IOCG and related ISCG deposits, compared with IOA deposits.

Deposit type	**Deposit redox or other subtype**	**Timing, tectonic setting, deformation**	**Ore geochem. *(subtype)***	**Dominant Fe ox & Fe-Cu sulfides**	**Alteration/ metasomatism**	**Example deposits**
Orogenic IOCG & ISCG	Reduced to intermediate-redox IOCG to ISCG spectrum	orogenic, syn-tectonic, brittle-ductile	Cu, Au, Co, Ni; some have minor Zn, Pb, Bi, Se, Te, As ***(IOCG-Co) (ISCG-Co)***	mag, po, py, ccp	early Na ± Ca (ab, scp, act); mid Ca-Fe (amph, mag, di, grt, aln, ap); late Fe-K (mag, bt, Kfs) with Cu-Au & volatiles (CO_2, P, B)	IOCG: Osborne, West Peko, some Carajás (Sequeir.), some Kangdian (Dahongshan, Lala), some Khetri, some GBMZ (NICO), ISCG: Guelb Moghrein, Eloise, Greenmount, Mt Dore, parts Mt Elliott
	Intermediate-redox to oxidised IOCG to ISCG spectrum	orogenic, syn-tectonic, brittle-ductile	Cu, Au with (Co, Ni) or (Mo, F, REE, U, Ba) or both (EH, Monakoff, E1, Salobo) ***(IOCG-Co-REE)***	mag, hem, py, ccp, bn	early Na ± Ca (ab, scp, act); mid Ca-Fe (amp, mt, dp, gt, all, ap); late Fe-K (mt, bt, Kfs) with Cu-Au & volatiles (CO_2, P, F, B, SO_4) (except TCk)	IOCG: Ernest Henry; E1, Monakoff (late F, Ba, Cu?); SWAN?, Sin Quyen?, Salobo, Rakkurijarvi; some Tennant Creek; ISCG: some Kiruna CuAu; some Khetri CuAu (?SSC); Hongnipo? (Kangdian)
	Oxidised IOCG to ISCG spectrum	orogenic, syn-tectonic, brittle-ductile to brittle; some may be late-orogenic or post-orogenic(?)	Cu, Au, REE, U, F, Ba ***(some IOCG-Co-REE)***	hem, py, ccp, bn, cct	late Fe-K (hem, ms, chl) with Cu-Au & volatiles (CO_2, P, F, SO_4)	IOCG: Starra (hm-Ba-F-Au-bn zones); Gecko K44 upper, & Eldorado (but lack Co, REE, U, F or Ba)

Table 2 (continued)

Deposit type	**Deposit redox or other subtype**	**Timing, tectonic setting, deformation**	**Ore geochem. *(subtype)***	**Dominant Fe ox & Fe-Cu sulfides**	**Alteration/ metasomatism**	**Example deposits**
Post-orogenic Cu-Au-Fe (REE)	Intermediate-redox	post-orogenic, switch from compressional to extensional, brittle deformation	Minor P (ap), ± REE, ± Cu	mag, py, minor ccp	early Na ± Ca (ab, scp, act, di); mid Fe-K-Na-Ca (mag, bt, ab, act); or mid Fe-K-Ca (mag, Kfs, act, ap, cb, qz)	IOCG alteration: Acropolis, Titan, Murdie; IOCG deposits: Kalkaroo, Wallaroo
	Oxidised IOCG to ISCG spectrum	post-orogenic, switch from compressional to extensional, brittle deformation	Cu, Au, Ag, REE, U, F, Ba, ± Mo ***(IOCG-REE)***	hem, py, ccp, bn, cct; minor or no mag	mid Fe (-P-CO_2) (mag, sd, ap); late Fe-volatiles (-K) (hem, ser, chl, brt, fl, cb) with Cu-Au-REE-U	IOCG: Olympic Dam, Prominent Hill, Wirrda Well, Carrapateena, Sue Dianne?, North Portia ISCG or intrusion-related: Moonta?, White Dam Au-Mo
Magmatic arc- or back-arc-hosted IOCG	Reduced to intermediate-redox IOCG	Syn-subduction; extension before inversion, mostly brittle deformation	Cu, minor Au, (generally low P, Co, Ni, REE, U, F, Ba)	mag, po, py, ccp	early Na (ab); mid Fe-K (mag, bt, Kfs); late Ca-Fe-K (mag, amp, bt, Kfs) with Cu (-Au)	IOCG: Candelaria, Raúl-Condestable?, Marcona?
	Intermediate-redox to oxidised IOCG to ISCG spectrum	Syn-subduction; extension before inversion, mostly brittle deformation	Cu, minor Au, Ag, rare REE, U (generally low P, Co, Ni, F, Ba)	hem, mag, py, ccp, bn, cct	early-mid Fe (-Na, -K, -Ca) (mag, ab, Kfs, amp); late Fe (-CO_2) (hem, cb, chl) with Cu (-Au)	IOCG: Mantoverde, Mina Justa? ISCG?: some Chilean manto Cu-Ag±Fe (Punta del Cobre district, Mantos Blancos)
	Oxidised Cu (-Au) ± iron oxides	Syn-subduction, ?pre- or ?early-orogenic	Cu, Ag (low Au, REE, U)	ccp, bn, cct, py ± minor hem	??	ISCG?: some Chilean mantos (El Soldado)
Arc- or back-arc-hosted IOA	Fe-Ca-P	Syn-subduction, extensional / transtensional, rifted arc or back-arc	Ca, P, ± LREE, ± F, ± S	mag ± minor py, anh, (rare ccp, no Au)	Fe-Ca-P (mag, ap, amp, cpx)	Kiruna, MLYB, CIB (ER, LC, EA, EC, EL), SEM (PR, LPK), Bafq
	Fe-K	Syn-subduction, extensional / transtensional, rifted arc or back-arc	K, (low-P) ± S, ± F, ± LREE, Ba, B, ± minor Cu (lack U, Mo)	mag, hem ± minor py, anh (rare to minor Cu, no Au)	Fe-K (mag, hem, Kfs)	SEM (Boss; PR late), IM (late)) Andes (?MV (early), Marcona)

Mineral abbreviations: ab – albite, act – actinolite, aln – allanite, amp – amphibole, anh – anhydrite, ap – apatite, Au – gold, bn – bornite, brt – barite, bt – biotite, cb – carbonate, cct – chalcocite, chl – chlorite, cpy – chalcopyrite, cpx – clinopyroxene, di – diopside, fl – fluorite, hem – hematite, Kfs – K-feldspar, mag – magnetite, ms – muscovite, po – pyrrhotite, py – pyrite, qz – quartz, REE – REE-rich minerals (carbonate-rich and/or P-rich including monazite and alumino-phosphate-sulfide REE minerals), scp – scapolite, ser – sericite, U – uranium-rich minerals (e.g. uraninite/pitchblende), sd – siderite.

Abbreviations for IOA districts: CIB – Chilean Iron Belt, EA – El Algarrobo, EC – El Colorado, EL – El Laco, ER – El Romeral, IM – Iron Mountain, LC – Los Colorados, LPK – Lower Pilot Knob, MLYB – Middle-Lower Yangtze Belt, MV – Mantoverde, PR – Pea Ridge, SEM – southeast Missouri.

Table 3. Classification scheme of selected Cu- and/or Fe-rich deposit classes and types, and the place of IOCG and ISCG deposits (highlighted in yellow). Genetic class interpretations of the 'hybrid' deposit types are based on discussions in the accompanying contribution (Skirrow, in prep.); others after Meinert et al. (2005), Groves et al. (2010), Sillitoe (2003, 2010). Abbreviations: fl – fluorite, IOA – iron oxide-apatite, IR – intrusion-related, mag – magnetite, MH – magmatic-hydrothermal, MLYB – Middle-Lower Yangtze Block, SSC – sediment-hosted stratiform Cu.

Genetic class	**Cu and/or Fe deposit types**	**Timing/tectonic setting**	**Deposit subtypes**	**Example deposits and provinces**
Intrusion-related magmatic-hydrothermal (IR-MH)	Porphyry	Syn-subduction & post-collisional	Porphyry Cu Porphyry Cu-Au Porphyry Cu-Mo	Many
	Skarn	Syn-subduction	Skarn Fe, Fe-Cu Skarn Cu Skarn Au	Many Marcona Fe (-Cu)?
	Alkaline-igneous /carbonatite associated	anorogenic	Carbonatite-related Cu, REE; Alkaline-igneous-related Fe, REE, U, F	Palabora Cu Bayan Obo REE Fe Vergenoeg fl-mag
Hybrid: mainly IR-MH, minor basinal input	IOA Fe	Syn-subduction		Kiruna province SE Missouri province Adirondacks province Bafq province MLYB province
Hybrid: mainly IR-MH, minor basinal input	Arc-hosted Andean-type IOCG	Syn-subduction, pre- to early-orogenic	Reduced, intermediate-redox & oxidised IOCG & ISCG	Candelaria Mantoverde Raúl-Condestable Mina Justa
Hybrid: MH and basinal inputs	Orogenic IOCG & ISCG	Syn-late-orogenic	Reduced IOCG-Co, intermediate-redox IOCG-Co-REE & oxidised IOCG-Co-REE	Many – see *
	Post-orogenic IOCG & ISCG	Post-orogenic	Intermediate-redox IOCG-REE to oxidised IOCG-REE	Olympic Dam Prominent Hill Carrapateena Starra Eldorado Sue Dianne?
Hybrid: basinal with minor MH inputs	Manto Cu (-Ag)	Pre- or early-orogenic?		Mantos Blancos El Soldado
Basinal	Mt Isa Cu type	Orogenic/syn-tectonic		Mt Isa Cu
	SSC & redbed Cu	Diagenetic		Zambian & DRCongo Cu belt Kupferschiefer

* Obsorne, Eloise, Guelb Moghrein, NICO, West Peko, Warrego, Dahongshan, Lala, Sin Quyen, Sequeirinho, Salobo, Igarapé Bahia, SWAN/Mt Elliott, Ernest Henry, E1, Monakoff, White Devil, Juno, Gecko, Starra.

7. Summary and conclusions

Ten of the world's most important metallogenic provinces hosting IOCG and other ore deposits have been reviewed in the present contribution, including the geochronology, geological and tectonothermal evolution, alteration-mineralisation parageneses and zoning, and ore geochemistry. Key conclusions are as follows.

(1) IOCG deposits form the major part of a broader family of deposits within Cu-Au-Fe or CGI mineral systems that also includes iron sulfide Cu-Au (ISCG) deposits with little or no iron oxides.

(2) CGI mineral systems occur in three distinct tectonic settings, two of which are related to orogenic processes, and host orogenic and post-orogenic IOCG and related ISCG deposits. In the third, arc-hosted Andean-type, setting the IOCG deposits formed during extension/transtension of continental margin magmatic arcs.

(3) A common theme that links the orogenic and post-orogenic settings is a tectonic switch from compression to extension, during which the development of the CGI mineral systems occurred.

(4) Metallogenic provinces with IOCG and related deposits in all three tectonic settings are characterised by the coincidence in space and time between pre-IOCG sedimentary ± volcanic basins and syn-IOCG intrusive ± volcanic magmatism, although the compositions of the igneous rocks and relationships to deposits differs between the orogenic, post-orogenic and arc-hosted settings. As argued in the companion paper (Skirrow, in prep.), the variable inputs of basin-derived and magma-derived fluids and ore components (metals, sulfur, etc) is considered to be the main link between deposits in CGI mineral systems but also the principal cause of the observed variations in mineralogy geochemistry.

(5) In all three tectonic settings the IOCG and related deposits share several features of their alteration-mineralisation, including:

- A metal association of Cu and Au with elevated Fe, whether as low-Ti Fe oxides or Fe sulfides and/or Fe-rich silicates.
- Hydrothermal alteration that includes paragenetically early Na- ± Ca-rich minerals (generally in regional-scale alteration zones but also proximal at some deposits) followed by combinations of Fe-, Ca- and K-rich minerals that accompany or precede Cu-Au mineralisation together with volatile-bearing minerals such as carbonate (CO_2), apatite (P), fluorite (F), barite (SO_4) and tourmaline (B); however, deposits in the arc-hosted settings have less abundant volatile-rich minerals.
- A paucity of Mg-rich hydrothermal minerals and hydrothermal quartz in the IOCG members of IOCG mineral systems, but minor to abundant quartz in many of the Fe-oxide-poor ISCG members.

- A wide range of relative redox conditions of formation of ore-associated hydrothermal minerals, from reduced (e.g. pyrrhotite ± Fe-silicate-bearing) through intermediate-redox (e.g. magnetite-pyrite-bearing) to oxidised (e.g. hematite ± pyrite ± sulfate minerals). The Cu sulfide mineralogy varies systematically from chalcopyrite ± rare bornite in the relatively reduced deposits to chalcocite and bornite in the most oxidised deposits or zones within deposits.
- IOCG and related ISCG deposits are enriched in distinctive suites of minor elements (Co, Ni, Bi, Se, Te, and/or REE, U, F, Ba) compared to well known magmatic-hydrothermal deposits such as porphyry Cu (-Au), skarn Fe and Cu and granite-related greisen deposits; however, IOCG deposits in arc-hosted settings have lower levels of Co, Ni, Bi, Se, Te, REE, U, F, and Ba than IOCG deposits in orogenic and post-orogenic settings.
- Among the orogenic and post-orogenic IOCG and related ISCG deposits a correlation has been identified between (a) ore geochemical variations in the ratio (Co+Ni+10*Bi+10*Se+50*Te)/(U+La) with element values in ppm (termed the IOCG discriminator), (b) the alteration-mineralisation mineralogy, and (c) the geological-tectonic settings.

(6) IOCG and related deposits in each of the three geotectonic settings have distinctive structural, mineralogical and geochemical characteristics, as follows.

- The orogenic setting hosts IOCG and related ISCG deposits that formed during brittle-ductile to brittle deformation in mid-shallow-crustal environments, at conditions compatible with medium to low grade metamorphism. These deposits have alteration-mineralisation mineral assemblages indicating generally reduced to intermediate-redox hydrothermal conditions during Cu-Au ore formation. Sodic ± Ca regional alteration, present in all provinces except possibly Tennant Creek, is typically overprinted by proximal alteration assemblages representing Ca-Fe metasomatism and then by Fe-K alteration-metasomatism that accompanies the main Cu-Au mineralisation along with volatile-rich minerals. The reduced to intermediate-redox members of the redox spectrum of orogenic deposits form the IOCG-Co and ISCG-Co geochemical subtype. Magnetite is the dominant Fe-oxide where present, but some of the reduced deposits lack significant Fe-oxide and are dominated by Fe-sulfides (ISCG deposits). IOCG-Co-REE ores with intermediate-redox assemblages (magnetite, pyrite) constitute a separate subtype of orogenic deposits (e.g. Ernest Henry).

- The post-orogenic setting of IOCG mineral systems is apparently rare but hosts the world's largest IOCG deposit at Olympic Dam in the Gawler Craton. This setting represents the full evolution of tectonic switching from compression to extension. The Curnamona Province, Great Bear magmatic zone and Tennant Creek provinces may record similar switches in tectonic regime. Shallow-crustal to near-surface (sub-volcanic to volcanic) environments of ore formation are indicated in the Olympic Cu-Au province of the Gawler Craton. Whereas highly oxidised (hematite, barite, chalcocite, bornite) and low-pH (sericite ± pyrophyllite) conditions are evident in all of the major deposits (Olympic Dam, Prominent Hill, Carrapateena), some deposits preserve evidence of earlier and generally deeper intermediate-redox (magnetite, pyrite, siderite, chalcopyrite) chemical environments. IOCG ores in the Gawler post-orogenic setting have some of the lowest values of the IOCG discriminator (Co+Ni+10*Bi+10*Se+50*Te)/(U+La), and also contain abundant volatile-rich phases such as fluorite (F), carbonate (CO_2), barite (SO_4), and apatite (P) accompanying the Cu-Au-U-REE mineralisation.
- The third, continental margin magmatic arc-hosted, geological and tectonic setting of IOCG deposits and CGI mineral systems is mainly represented by Cretaceous deposits in the Chilean and Peruvian Andes, although hybrid settings involving Paleoproterozoic continental margin magmatic arc settings may be present in the Kiruna province and Great Bear magmatic zone. Whereas the arc-hosted IOCG deposits share some features of IOCG deposits in orogenic and post-orogenic settings, the former tend to lack abundant volatile-rich minerals coeval with the Cu-Au mineralisation, and have low Co+Ni+Bi+Se+Te+REE+U values that resemble those of most porphyry and skarn deposits. They also show a sequence of hydrothermal assemblages that may differ from those of the orogenic and post-orogenic IOCG deposits. Moreover, their close spatial and temporal association with intermediate-composition intrusions and pre- to early-orogenic timing contrasts with such relationships and igneous compositions in the orogenic and post-orogenic IOCG provinces. The arc settings also include pre-IOCG IOA, and (small) porphyry Cu (-Au) and skarn deposits of roughly similar age to the IOCG deposits. It is concluded that the arc-hosted IOCG deposits represent a sub-group of the IOCG family with different origins to the orogenic and post-orogenic IOCG deposits, and which appear to have a greater affinity with calc-alkaline arc-related magmatic-hydrothermal ore deposits that are present in the same metallogenic provinces.

Acknowledgements

This work draws upon discussions with, and support from, many colleagues over the years. In particular, the following people are thanked: Evgeniy Bastrakov, David Huston, Karol Czarnota, David Champion, Michael Doublier, Richard Blewett, Anthony Schofield, Simon van der Wielen (all Geoscience Australia), and also John Walshe, Sue Daly, Anthony Reid, Colin Conor, Martin Fairclough, Karin Barovich and Ken Cross. Additionally, David Huston and Evgeniy Bastrakov are thanked for helpful reviews of an early version of the manuscript. Carl Brauhart and Stefan Hagemann are acknowledged for the use of the OSNACA open-source ore geochemical data set. Journal reviews by Xinfu Zhou and an anonymous reviewer improved the manuscript, for which they are thanked. Editorial handling by Huayong Chen and David Lentz is gratefully acknowledged. This publication is a contribution towards the Australian Government's Exploring for the Future (EFTF) program. Published with the permission of the CEO, Geoscience Australia.

References

Acosta-Góngora, P., Gleeson, S. A., Samson, I. M., Corriveau, L., Ootes, L., Taylor, B. E., Creaser, R. A., & Muehlenbachs, K. (2015). Genesis of the Paleoproterozoic NICO iron oxide-cobalt-gold-bismuth deposit, Northwest Territories, Canada: Evidence from isotope geochemistry and fluid inclusions. *Precambrian Research*, *268*, 168–193. https://doi.org/10.1016/j.precamres.2015.06.007

Adshead, N. D., Voulgaris, P., & Muscio, V. N. (1998). Osborne copper-gold deposit. In D. A. Berkman & D. H. Mackenzie (Eds.), *Geology of Australian and Papuan New Guinean mineral deposits* (pp. 793–800). Australasian Institute of Mining and Metallurgy, Monograph 14.

Apukhtina, O. B., Kamenetsky, V. S., Ehrig, K., Kamenetsky, M. B., Maas, R., Thompson, J., McPhie, J., Ciobanu, C. L., & Cook, N. J. (2017). Early, deep magnetite-fluorapatite mineralization at the Olympic Dam Cu-U-Au-Ag deposit, South Australia. *Economic Geology*, *112*(6), 1531–1542. https://doi.org/10.5382/econgeo.2017.4520

Armistead, S. E., Betts, P. G., Ailleres, L., Armit, R. J., & Williams, H. A. (2018). Cu-Au mineralisation in the Curnamona Province, South Australia: A hybrid stratiform genetic model for Mesoproterozoic IOCG systems in Australia. *Ore Geology Reviews*, *94*(September 2017), 104–117. https://doi.org/10.1016/j.oregeorev.2018.01.024

Baker, T., & Laing, W. P. (1998). Eloise Cu-Au deposit, East Mt Isa Block: Structural environment and structural controls on ore. *Australian Journal of Earth Sciences*, *45*(3), 429–444. https://doi.org/10.1080/08120099808728402

Baker, T., Perkins, C., Blake, K. L., & Williams, P. J. (2001). Radiogenic and stable isotope constraints on the genesis of the Eloise Cu-Au deposits, Cloncurry district, Northwest Queensland. *Economic Geology*, *96*(4), 723–742. https://doi.org/10.2113/gsecongeo.96.4.723

Barra, F., Reich, M., Selby, D., Rojas, P., Simon, A., Salazar, E., & Palma, G. (2017). Unraveling the origin of the Andean IOCG clan: A Re-Os isotope approach. *Ore Geology Reviews*, *81*(October 2016), 62–78. https://doi.org/10.1016/j.oregeorev.2016.10.016

Barton, M. D. (2013). Iron Oxide(-Cu-Au-REE-P-Ag-U-Co) Systems. In *Treatise on Geochemistry: Second Edition* (Vol. 13, pp. 515–541). Elsevier Inc. https://doi.org/10.1016/B978-0-08-095975-7.01123-2

Bascuñán, S., Arriagada, C., le Roux, J., & Deckart, K. (2016). Unraveling the Peruvian Phase of the Central Andes: Stratigraphy, sedimentology and geochronology of the Salar de Atacama Basin (22°30-23°S), northern Chile. *Basin Research*, *28*(3), 365–392. https://doi.org/10.1111/bre.12114

Bastrakov, E. N., Skirrow, R. G., & Davidson, G. J. (2007). Fluid evolution and origins of iron oxide Cu-Au prospects in the Olympic Dam district, Gawler Craton, South Australia. *Economic Geology*, *102*(8). https://doi.org/10.2113/gsecongeo.102.8.1415

Bauer, T. E., Lynch, E. P., Sarlus, Z., Drejing-Carroll, D., Martinsson, O., Metzger, N., & Wanhainen, C. (2021). Structural controls on iron oxide-copper-gold mineralization and related alteration in a Paleoproterozoic supracrustal belt: Insights from the Nautanen deformation zone and surroundings, northern Sweden. *Economic Geology*, (in press).

Belperio, A., Flint, R., & Freeman, H. (2007). Prominent Hill: A hematite-dominated, iron oxide copper-gold system. *Economic Geology*, *102*(8), 1499–1510. https://doi.org/10.2113/gsecongeo.102.8.1499

Benavides, J., Kyser, T. K., Clark, A. H., Oates, C. J., Zamora, R., Tarnovschi, R., & Castillo, B. (2007). The Mantoverde iron oxide-copper-gold district, III Región, Chile: The role of regionally derived, nonmagmatic fluids in chalcopyrite mineralization. *Economic Geology*, *102*(3), 415–440. https://doi.org/10.2113/gsecongeo.102.3.415

Bierlein, F. P., Ashley, P. M., & Plimer, I. R. (1995). Sulphide mineralisation in the Olary Block, South Australia - Evidence for syn-tectonic to late-stage mobilisation. *Mineralium Deposita*, *30*(6), 424–438. https://doi.org/10.1007/BF00196402

Bonyadi, Z., & Sadeghi, R. (2020). Hydrothermal alteration associated with magnetite mineralization in the Bafq iron deposits, Iran. *Journal of Asian Earth Sciences*, *189*(February 2019), 104152. https://doi.org/10.1016/j.jseaes.2019.104152

Boric, R., Holmgren, C., Wilson, N. S. F., & Zentilli, M. (2002). The geology of the El Soldado manto type Cu (Ag) deposit, central Chile. In T. M. Porter (Ed.), *Hydrothermal iron oxide copper-gold and related deposits: A global perspective, Volume 2* (pp. 163–184). PGC Publishing.

Boyce, D., Charrier, R., & Farías, M. (2020). The First Andean Compressive Tectonic Phase: Sedimentologic and Structural Analysis of Mid-Cretaceous Deposits in the Coastal Cordillera, Central Chile (32°50′S). *Tectonics*, *39*(2), 1–24. https://doi.org/10.1029/2019TC005825

Brauhart, C. W., Grunsky, E. C., & Hagemann, S. G. (2017). Magmato-hydrothermal space: A new metric for geochemical characterisation of metallic ore deposits. *Ore Geology Reviews*, *86*, 867–895. https://doi.org/10.1016/j.oregeorev.2016.11.001

Brown, M., & Porter, T. M. (2010). The Mount Elliott IOCG system, Eastern Fold Belt, Mount Isa Inlier, northwest Queensland. In T. M. Porter (Ed.), *Hydrothermal iron oxide copper-gold and related deposits: A global perspective, Volume 3* (pp. 219–231). PGC Publishing.

Budd, A. (2006). *The Tarcoola Goldfield of the central Gawler gold province, and the Hiltaba Association Granites, Gawler craton, South Australia:* Unpublished PhD thesis, Australian National University.

Case, G. N. (2016). *Genesis of the E1 Group of iron oxide-copper-gold deposits, Cloncurry district, northwest Queensland.* Unpubl. PhD thesis, James Cook University of North Queensland.

Cave, B. W., Lilly, R., Glorie, S., & Gillespie, J. (2018). Geology, apatite geochronology, and geochemistry of the Ernest Henry inter-lens: Implications for a re-examined deposit model. *Minerals*, *8*(9). https://doi.org/10.3390/min8090405

Chen, H., Clark, A. H., Kyser, T. K., Ullrich, T. D., Baxter, R., Chen, Y., & Moody, T. C. (2010). Evolution of the giant Marcona-Mina Justa iron oxide-copper-gold district, South-Central Peru. *Economic Geology*, *105*(1), 155–185. https://doi.org/10.2113/gsecongeo.105.1.155

Chen, H., Cooke, D. R., & Baker, M. J. (2013). Mesozoic iron oxide copper-gold mineralization in the Central Andes and the Gondwana supercontinent breakup. *Economic Geology*, *108*(1), 37–44. https://doi.org/10.2113/econgeo.108.1.37

Chen, W. T., & Zhou, M. F. (2012). Paragenesis, stable isotopes, and molybdenite Re-Os isotope age of the Lala Iron-Copper deposit, Southwest China. *Economic Geology*, *107*(3), 459–480. https://doi.org/10.2113/econgeo.107.3.459

Cherry, A. R., Ehrig, K., Kamenetsky, V. S., McPhie, J., Crowley, J. L., & Kamenetsky, M. B. (2018). Precise geochronological constraints on the origin, setting and incorporation of ca. 1.59 Ga surficial facies into the Olympic Dam Breccia Complex, South Australia. *Precambrian Research*, *315*(July), 162–178. https://doi.org/10.1016/j.precamres.2018.07.012

Conor, C. H. H. (1995). Moonta-Wallaroo region - An interpretation of the geology of the Maitland and Wallaroo 1:100 000 sheet areas. *Mines and Energy South Australia, Open File Envelope 8886*.

Conor, C., Raymond, O., Baker, T., Teale, G., Say, P., & Lowe, G. (2010). Alteration and mineralisation in the Moonta-Wallaroo copper-gold mining field region, Olympic Domain, South Australia. In T. M. Porter (Ed.), *Hydrothermal iron oxide copper-gold and related deposits: A global perspective, Volume 3* (pp. 147–170). PGC Publishing.

Cook, N. D. J., & Ashley, P. M. (1992). Meta-evaporite sequence, exhalative chemical sediments and associated rocks in the Proterozoic Willyama Supergroup, South Australia: implications for metallogenesis. *Precambrian Research*, *56*(3–4), 211–226. https://doi.org/10.1016/0301-9268(92)90102-T

Corriveau, L. (2007). Iron oxide copper-gold deposits: A Canadian perspecitive. In W. D. Goodfellow (Ed.), *Mineral deposits in Canada: A synthesis of major deposit types, district metallogeny, the evolution of geological provinces and exploration methods* (pp. 307–328). Geological Association of Canada, Mineral Deposits Division, Special Publication Volume 5.

Corriveau, L., Montreuil, J. F., & Potter, E. G. (2016). Alteration facies linkages among iron oxide copper-gold, iron oxide-apatite, and affiliated deposits in the Great Bear magmatic zone,

Northwest Territories, Canada. *Economic Geology*, *111*(8), 2045–2072. https://doi.org/10.2113/econgeo.111.8.2045

Corriveau, L., Mumin, A. H., & Setterfield, T. (2010). IOCG environments in Canada: Characteristics, geological vectors to ore and challenges. In T. M. Porter (Ed.), *Hydrothermal iron oxide copper-gold and related deposits: A global perspective, Volume 4* (pp. 311–344). PGC Publishing.

Corriveau, L., Williams, P. . J., & Mumin, H. (2010a). Alteration vectors to IOCG mineralization from uncharted terranes to deposits. In *Exploring for iron oxide copper-gold deposits: Canada and global analogues* (pp. 89–110). Geological Association of Canada, Short Course Notes, Volume 20.

Corriveau, L., Williams, P. J., & Mumin, A. H. (2010b). Alteration vectors to IOCG mineralization: from uncharted terranes to deposits. In L. Corriveau & A. H. Mumin (Eds.), *Exploring for iron oxide copper-gold deposits: Canada and global analogues* (pp. 89–110). Geological Association of Canada, Short Course Notes, Volume 20.

Courtney-Davies, L., Ciobanu, C. L., Verdugo-Ihl, M. R., Dmitrijeva, M., Cook, N. J., Ehrig, K., & Wade, B. P. (2019). Hematite geochemistry and geochronology resolve genetic and temporal links among iron-oxide copper gold systems, Olympic Dam district, South Australia. *Precambrian Research*, *335*(June), 105480. https://doi.org/10.1016/j.precamres.2019.105480

Craveiro, G. S., Villas, R. N. N., & Xavier, R. P. (2020). A fluid inclusion and stable isotope (O, H, S and C) study of the Archean IOCG Cristalino deposit, Carajás Mineral Province, Brazil: Implications to ore genesis. *Ore Geology Reviews*, *127*(August), 103822. https://doi.org/10.1016/j.oregeorev.2020.103822

Cross, K. C. (1993). Acropolis and Wirrda Well prospects. In J. F. Drexel, W. v. Preiss, & A. J. Parker (Eds.), *The Geology of South Australia. Volume 1. The Precambrian* (p. 138). Geological Survey of South Australia, Bulletin 54.

Daliran, F., Stosch, H.-G., & Williams, P. J. (2010). Lower Cambrian iron oxide-apatite-REE (U) deposits of the Bafq district, east-central Iran. In L. Corriveau & H. Mumin (Eds.), *Exploring for iron oxide copper-gold deposits: Canada and global analogues* (pp. 143–155). Geological Association of Canada, Short Course Notes, Volume 20.

Davidson, G. J., & Large, R. R. (1994). Gold metallogeny and the copper-gold association of the Australian Proterozoic. *Mineralium Deposita*, *29*, 208223.

Day, W. C., Slack, J. F., Ayuso, R. A., & Seeger, C. M. (2016). Regional geologic and petrologic framework for iron oxide ± apatite ± rare earth element and iron oxide copper-gold deposits of the Mesoproterozoic St. Francois Mountains Terrane, southeast Missouri, USA. *Economic Geology*, *111*(8), 1825–1858. https://doi.org/10.2113/econgeo.111.8.1825

de Freitas Toledo, P. I., Moreto, C. P. N., Xavier, R. P., Gao, J., de Matos, J. H. da S. N., & de Melo, G. H. C. (2019). Multistage evolution of the Neoarchean (ca. 2.7 Ga) Igarapé Cinzento (GT-46) iron oxide copper-gold deposit, Cinzento Shear Zone, Carajás Province, Brazil. *Economic Geology*, *114*(1), 1–34. https://doi.org/10.5382/econgeo.2019.4617

de Haller, A., Corfu, F., Fontboté, L., Schaltegger, U., Barra, F., Chiaradia, M., Frank, M., & Alvarado, J. Z. (2006). Geology, geochronology, and Hf and Pb isotope data of the Raúl-Condestable iron oxide-copper-gold deposit, central coast of Peru. *Economic Geology*, *101*(2), 281–310. https://doi.org/10.2113/gsecongeo.101.2.281

de Melo, G. H. C., Monteiro, L. V. S., Xavier, R. P., Moreto, C. P. N., & Santiago, E. (2019). Tracing fluid sources for the Salobo and Igarapé Bahia deposits: Implications for the genesis of the iron oxide copper-gold deposits in the Carajás Province, Brazil. *Economic Geology*, *114*(4), 697–718. https://doi.org/10.5382/econgeo.4659

de Melo, G. H. C., Monteiro, L. V. S., Xavier, R. P., Moreto, C. P. N., Santiago, E. S. B., Dufrane, S. A., Aires, B., & Santos, A. F. F. (2017). Temporal evolution of the giant Salobo IOCG deposit, Carajás Province (Brazil): constraints from paragenesis of hydrothermal alteration and U-Pb geochronology. *Mineralium Deposita*, *52*(5), 709–732. https://doi.org/10.1007/s00126-016-0693-5

del Real, I., Thompson, J. F. H., & Carriedo, J. (2018). Lithological and structural controls on the genesis of the Candelaria-Punta del Cobre Iron Oxide Copper Gold district, Northern Chile. *Ore Geology Reviews*, *102*(August), 106–153. https://doi.org/10.1016/j.oregeorev.2018.08.034

Dick, J. M. (2021). Diagrams with multiple metals in CHNOSZ. *Applied Computing and Geosciences*, *10*(November 2020), 100059. https://doi.org/10.1016/j.acags.2021.100059

Donnellan, N., Hussey, K. J., & Morrison, R. S. (1995). Flynn 5759, Tennant Creek 5758: Explanatory Notes, 1:100 000 Geological Map Series. *Northern Territory Geological Survey*, 79p.

Duncan, R. J., Stein, H. J., Evans, K. A., Hitzman, M. W., Nelson, E. P., & Kirwin, D. J. (2011). A new geochronological framework for mineralization and alteration in the Selwyn-Mount Dore corridor, Eastern Fold Belt, Mount Isa Inlier, Australia: Genetic implications for iron oxide copper-gold deposits. *Economic Geology*, *106*(2), 169–192. https://doi.org/10.2113/econgeo.106.2.169

Ehrig, K. J., McPhie, J., & Kamenetsky, V. S. (2012). Geology and mineralogical zonation of the Olympic Dam iron oxide Cu-U-Au-Ag deposit, South Australia. In J. W. Hedenquist, M. Harris, & F. Camus (Eds.), *Geology and Genesis of Major Copper Deposits and Districts of the World: A Tribute to Richard H. Sillitoe. Special Publication 16* (pp. 237–267). Society of Economic Geologists. https://doi.org/10.5382/sp.17

Fairclough, M. (2005). Geological and metallogenic setting of the Carrapateena FeO-Cu-Au prospect - a PACE success story. *MESA Journal*, *38*(July), 4–7.

Fennell, L. M., Iannelli, S. B., Encinas, A., Naipauer, M., Valencia, V., & Folguera, A. S. (2019). Alternating contraction and extension in the southern central Andes (35°-37°s). *American Journal of Science*, *319*(5), 381–429. https://doi.org/10.2475/05.2019.02

Fisher, L. A., & Kendrick, M. A. (2008). Metamorphic fluid origins in the Osborne Fe oxide - Cu - Au deposit, Australia: Evidence from noble gases and halogens. *Mineralium Deposita*, *43*(5), 483–497. https://doi.org/10.1007/s00126-008-0178-2

Goad, R. E., Mumin, H., Duke, N. A., Neale, K. L., & Mulligan, D. L. (2000). Geology of the Proterozoic iron oxide-hosted, NICO cobalt-gold-bismuth, and Sue-Dianne copper-silver deposits, southern Great Bear magmatic zone, Northwest Territories, Canada. In T. M. Porter (Ed.), *Hydrothermal iron oxide copper-gold and related deposits: A global perspective, Volume 1* (pp. 249–267). Australian Mineral Foundation.

Grainger, C. J., Groves, D. I., Tallarico, F. H. B., & Fletcher, I. R. (2008). Metallogenesis of the Carajás Mineral Province, Southern Amazon Craton, Brazil: Varying styles of Archean through Paleoproterozoic to Neoproterozoic base- and precious-metal mineralisation. *Ore Geology Reviews*, *33*(3–4), 451–489. https://doi.org/10.1016/j.oregeorev.2006.10.010

Groves, D. I., Bierlein, F. P., Meinert, L. D., & Hitzman, M. W. (2010). Iron Oxide Copper-Gold (IOCG) Deposits through Earth History: Implications for Origin, Lithospheric Setting, and Distinction from Other Epigenetic Iron Oxide Deposits. *Economic Geology*, *105*, 641–654.

Haynes, D. W. (2000). Iron oxide copper (-gold) deposits: their position in the deposit spectrum and modes of origin. In *Hydrothermal iron oxide copper-gold and related deposits: A global perspective, Volume 1* (pp. 71–90). Australian Mineral Foundation.

Haynes, D. W., Cross, K. C., Bills, R. T., & Reed, M. H. (1995). Olympic Dam ore genesis: a fluid-mixing model. *Economic Geology*, *90*(2), 281–307. https://doi.org/10.2113/gsecongeo.90.2.281

Hildebrand, R. S., Hoffman, P. F., & Bowring, S. A. (1987). Tectono-magmatic evolution of the 1.9-Ga Great Bear magmatic zone, Wopmay orogen, northwestern Canada. *Journal of Volcanology and Geothermal Research*, *32*(1–3), 99–118. https://doi.org/10.1016/0377-0273(87)90039-4

Hitzman, M. W. (2000). Iron oxide-Cu-Au deposits: what, where, when and why? In T. M. Porter (Ed.), *Hydrothermal iron oxide copper-gold and related deposits: A global perspective, Volume 1* (pp. 9–25). Australian Mineral Foundation.

Hitzman, M. W., Oreskes, N., & Einaudi, M. T. (1992). Geological characteristics and tectonic setting of Proterozoic iron oxide (Cu-U-Au-REE) deposits. *Precambrian Research*, *58*, 241–287.

Hoggard, M. J., Czarnota, K., Richards, F. D., Huston, D. L., Jaques, A. L., & Ghelichkhan, S. (2020). Global distribution of sediment-hosted metals controlled by craton edge stability. *Nature Geoscience*, *13*(7), 504–510. https://doi.org/10.1038/s41561-020-0593-2

Hopper, D., & Correa, A. (2000). The Panulcillo and Teresa de Colmo copper deposits: two contrasting examples of Fe-ox Cu-Au mineralization from the Coastal Cordillera of Chile. In T. M. Porter (Ed.), *Hydrothermal iron oxide copper-gold and related deposits: A global perspective, Volume 1* (pp. 177–189). Australian Mineral Foundation.

Huang, Q., Kamenetsky, V. S., Ehrig, K., McPhie, J., Kamenetsky, M., Cross, K., Meffre, S., Agangi, A., Chambefort, I., Direen, N. G., Maas, R., & Apukhtina, O. (2016). Olivine-phyric basalt in the Mesoproterozoic Gawler silicic large igneous province, South Australia: Examples at the Olympic Dam iron oxide Cu–U–Au–Ag deposit and other localities. *Precambrian Research*, *281*, 185–199. https://doi.org/10.1016/j.precamres.2016.05.019

Huston, D., Cross, A., Skirrow, R., Champion, D., & Whelan, J. (2020). The Tennant Creek mineral field and Rover fields: Many similarities but some important differences. *AGES 2020 Conference Proceedings, Northern Territory Geological Survey*, 70–83.

Huston, D. L., Bolger, C., & Cozens, G. (1993). A comparison of mineral deposits at the Gecko and White Devil deposits: implications for ore genesis in the Tennant Creek district, Northern Territory, Australia. *Economic Geology*, *88*(5), 1198–1225. https://doi.org/10.2113/gsecongeo.88.5.1198

Ismail, R., Ciobanu, C. L., Cook, N. J., Teale, G. S., Giles, D., Mumm, A. S., & Wade, B. (2014). Rare earths and other trace elements in minerals from skarn assemblages, Hillside iron oxide-copper-gold deposit, Yorke Peninsula, South Australia. *Lithos*, *184–187*, 456–477. https://doi.org/10.1016/j.lithos.2013.07.023

Johnson, C. A., Day, W. C., & Rye, R. O. (2016). Oxygen, hydrogen, sulfur, and carbon isotopes in the Pea Ridge magnetite-apatite deposit, Southeast Missouri, and sulfur isotope comparisons to other iron deposits in the region. *Economic Geology*, *111*(8), 2017–2032. https://doi.org/10.2113/econgeo.111.8.2017

Johnson, J. P., & Cross, K. C. (1995). U-Pb geochronological constraints on the genesis of the Olympic Dam Cu-U-Au-Ag deposit, South Australia. *Economic Geology*, *90*, 1046–1063.

Johnson, J. P., & McCulloch, M. T. (1995). Sources of mineralising fluids for the Olympic Dam deposit (South Australia): Sm-Nd isotopic constraints. *Chemical Geology*, *121*(1–4), 177–199. https://doi.org/10.1016/0009-2541(94)00125-R

Kirschbaum, M. J., & Hitzman, M. W. (2016). Guelb Moghrein: an unusual, carbonate-hosted iron oxide copper-gold deposit in Mauritania, northwest Africa. *Economic Geology*, 763–770.

Knight, J., Joy, S., Lowe, J., Cameron, J., Merrillees, J., Nag, S., Shah, N., Dua, G., & Jhala, K. (2002). The Khetri copper belt, Rajasthan: iron oxide copper-gold terrane in the Proterozoic of NW India. In T. M. Porter (Ed.), *Hydrothermal iron oxide copper-gold and related deposits: A global perspective, Volume 2* (pp. 321–341). PGC Publishing.

Knipping, J. L., Bilenker, L. D., Simon, A. C., Reich, M., Barra, F., Deditius, A. P., Lundstrom, C., Bindeman, I., & Munizaga, R. (2015). Giant Kiruna-type deposits form by efficient flotation of magmatic magnetite suspensions. *Geology*, *43*(7), 591–594. https://doi.org/10.1130/G36650.1

Kolb, J., Meyer, M., Vennemann, T., Sindern, S., Prantl, S., & Bottcher, M. E. (2010). Characterisation of the hydrothermal fluids of the Guelb Moghrein iron oxide-Cu-Au-Co deposit, Mauritania: ore mineral chemistry, fluid inclusions and isotope geochemistry. In T. M. Porter (Ed.), *Hydrothermal iron oxide copper-gold and related deposits: A global perspective, Volume 4* (pp. 553–572). PGC Publishing.

Kolb, J., & Petrov, N. (2016). The Guelb Moghrein Cu–Au deposit: Neoarchaean hydrothermal sulfide mineralization in carbonate-facies iron formation. *Ore Geology Reviews*, *78*, 573–577. https://doi.org/10.1016/j.oregeorev.2015.09.003

Krneta, S., Cook, N. J., Ciobanu, C. L., Ehrig, K., & Kontonikas-Charos, A. (2017). The Wirrda Well and Acropolis prospects, Gawler Craton, South Australia: Insights into evolving fluid conditions through apatite chemistry. *Journal of Geochemical Exploration*, *181*(May), 276–291. https://doi.org/10.1016/j.gexplo.2017.08.004

Lahtinen, R., Huhma, H., Lahaye, Y., Jonsson, E., Manninen, T., Lauri, L. S., Bergman, S., Hellström, F., Niiranen, T., & Nironen, M. (2015). New geochronological and Sm-Nd constraints across the Pajala shear zone of northern Fennoscandia: Reactivation of a Paleoproterozoic suture. *Precambrian Research*, *256*, 102–119. https://doi.org/10.1016/j.precamres.2014.11.006

Lahtinen, R., Huhma, H., Sayab, M., Lauri, L. S., & Hölttä, P. (2018). Age and structural constraints on the tectonic evolution of the Paleoproterozoic Central Lapland Granitoid Complex in the Fennoscandian Shield. *Tectonophysics*, *745*(January), 305–325. https://doi.org/10.1016/j.tecto.2018.08.016

Large, R. R. (1975). Zonation of hydrothermal minerals at the Juno Mine, Tennant Creek goldfield, central Australia. *Economic Geology*, *70*, 1387–1413. https://doi.org/10.2113/gsecongeo.71.8.1615

Li, W., Audétat, A., & Zhang, J. (2015). The role of evaporites in the formation of magnetite-apatite deposits along the Middle and Lower Yangtze River, China: Evidence from LA-ICP-MS analysis of fluid inclusions. *Ore Geology Reviews*, *67*, 264–278. https://doi.org/10.1016/j.oregeorev.2014.12.003

Li, X. C., & Zhou, M. F. (2018). The nature and origin of hydrothermal REE mineralization in the Sin Quyen deposit, northwestern Vietnam. *Economic Geology*, *113*(3), 645–673. https://doi.org/10.5382/econgeo.2018.4565

Li, X. C., Zhou, M. F., Williams-Jones, A. E., Yang, Y. H., & Gao, J. F. (2019). Timing and genesis of Cu-(Au) mineralization in the Khetri Copper Belt, northwestern india: Constraints from in situ U-Pb ages and Sm-Nd isotopes of monazite-(Ce). *Mineralium Deposita*, *54*(4), 553–568. https://doi.org/10.1007/s00126-018-0823-3

Li, X., Zhao, X., Zhou, M. F., Chen, W. T., & Chu, Z. (2015). Fluid inclusion and isotopic constraints on the origin of the Paleoproterozoic Yinachang Fe-Cu-(REE) deposit, Southwest China. *Economic Geology*, *110*(5), 1339–1369. https://doi.org/10.2113/econgeo.110.5.1339

Lin, L., Chen, R., Pang, Z., Chen, H., Xue, J., & Jia, H. (2020). Sulfide Rb-Sr, Re-Os and in-situ S isotopic constraints on two mineralization events at the large Hongnipo Cu deposit, SW China. *Minerals*, *10*(5), 1–24. https://doi.org/10.3390/min10050414

Lu, C., Grand, S. P., Lai, H., & Garnero, E. J. (2019). TX2019slab: A New P and S Tomography Model Incorporating Subducting Slabs. *Journal of Geophysical Research: Solid Earth*, *124*(11), 11549–11567. https://doi.org/10.1029/2019JB017448

Maksaev, V., & Zentilli, M. (2002). Chilean strata-bound Cu- (Ag) deposits: An overview. In T. M. Porter (Ed.), *Hydrothermal iron oxide copper-gold and related deposits: A global perspective, Volume 2* (pp. 185–205). PGC Publishing.

Mark, G., Oliver, N. H. S., & Williams, P. J. (2006). Mineralogical and chemical evolution of the Ernest Henry Fe oxide-Cu-Au ore system, Cloncurry district, northwest Queensland, Australia. *Mineralium Deposita*, *40*(8), 769–801. https://doi.org/10.1007/s00126-005-0009-7

Marschik, R., & Fontboté, L. (2001). The Candelaria-Punta del Cobre iron oxide Cu-Au (-Zn-Ag) deposits, Chile. *Economic Geology*, *96*(8), 1799–1826. https://doi.org/10.2113/gsecongeo.96.8.1799

Martinsson, O., Billström, K., Broman, C., Weihed, P., & Wanhainen, C. (2016a). Metallogeny of the Northern Norrbotten Ore Province, Northern Fennoscandian Shield with emphasis on IOCG and apatite-iron ore deposits. *Ore Geology Reviews*, *78*, 447–492. https://doi.org/10.1016/j.oregeorev.2016.02.011

Martinsson, O., Billström, K., Broman, C., Weihed, P., & Wanhainen, C. (2016b). Metallogeny of the Northern Norrbotten Ore Province, Northern Fennoscandian Shield with emphasis on IOCG and apatite-iron ore deposits. *Ore Geology Reviews*, *78*, 447–492. https://doi.org/10.1016/j.oregeorev.2016.02.011

McLean, R. N. (2002). The Sin Quyen iron oxide-copper-gold-rare earth oxide mineralisation of north Vietnam. In T. M. Porter (Ed.), *Hydrothermal iron oxide copper-gold and related deposits: A global perspective, Volume 2* (pp. 293–301). PGC Publishing.

McPhie, J., Ehrig, K. J., Kamenetsky, M. B., Crowley, J. L., & Kamenetsky, V. S. (2020). Geology of the Acropolis prospect, South Australia, constrained by high-precision CA-TIMS ages. *Australian Journal of Earth Sciences*, *67*(5), 699–716. https://doi.org/10.1080/08120099.2020.1717617

Meinert, L. D., Dipple, G. M., & Nicolescu, S. (2005). World skarn deposits. In J. W. Hedenquist, J. F. H. Thompson, R. J. Goldfarb, & J. P. Richards (Eds.), *One Hundredth Anniversary Volume*. Society of Economic Geologists. https://doi.org/https://doi.org/10.5382/AV100.11

Meyer, C. (1988). Ore deposits as guides to geologic history of the Earth. In *Ann. Rev. Earth Planet. Sci* (Vol. 16). www.annualreviews.org

Miyano, T., & Klein, C. (1989). Phase equilibria in the system K_2O - FeO - MgO - Al_2O_3 - SiO_2 - H2O - CO2 and the stability limit of stilpnomelane in metamorphosed Precambrian iron-formations. *Contributions to Mineralogy and Petrology*, 478–491.

Monteiro, L. V. S., Xavier, R. P., Carvalho, E. R., Hitzman, M. W., Johnson, C. A., Souza Filho, C. R., & Torresi, I. (2008). Spatial and temporal zoning of hydrothermal alteration and mineralization in the Sossego iron oxide-copper-gold deposit, Carajás Mineral Province, Brazil: Paragenesis and stable isotope constraints. In *Mineralium Deposita* (Vol. 43, Issue 2). https://doi.org/10.1007/s00126-006-0121-3

Montreuil, J. F., Corriveau, L., & Davis, W. J. (2016). Tectonomagmatic evolution of the southern Great Bear magmatic zone (Northwest Territories, Canada): Implications for the genesis of iron oxide-alkali-altered hydrothermal systems. *Economic Geology*, *111*(8), 2111–2138. https://doi.org/10.2113/econgeo.111.8.2111

Montreuil, J. F., Corriveau, L., & Potter, E. G. (2015). Formation of albitite-hosted uranium within IOCG systems: the Southern Breccia, Great Bear magmatic zone, Northwest Territories, Canada. *Mineralium Deposita*, *50*(3), 293–325. https://doi.org/10.1007/s00126-014-0530-7

Montreuil, J. F., Corriveau, L., Potter, E. G., & de Toni, A. F. (2016). On the relationship between alteration facies and metal endowment of iron oxide-alkali-altered systems, southern Great Bear magmatic zone (Canada). *Economic Geology*, *111*(8), 2139–2168. https://doi.org/10.2113/econgeo.111.8.2139

Moreto, C. P. N., Monteiro, L. V. S., Xavier, R. P., Amaral, W. S., dos Santos, T. J. S., Juliani, C., & de Filho, C. R. S. (2011). Mesoarchean (3.0 and 2.86 Ga) host rocks of the iron oxide-Cu-Au Bacaba deposit, Carajás Mineral Province: U-Pb geochronology and metallogenetic implications. *Mineralium Deposita*, *46*(7), 789–811. https://doi.org/10.1007/s00126-011-0352-9

Mukhopadhyay, S., Kumar, V., & Sangwan, M. (2019). Sediment Hosted Stratiform Copper (SSC) Mineralization in Bhudoli-Basari Area, North Delhi Fold Belt, Mesoproterozoic Delhi Supergroup, Rajasthan. *Journal of the Geological Society of India*, *93*(6), 663–674. https://doi.org/10.1007/s12594-019-1245-2

Mumin, A. H., Corriveau, L., Somarin, A. K., & Ootes, L. (2007). Iron oxide copper-gold-type polymetallic mineralization in the Contact Lake belt, Great Bear magmatic zone, Northwest Territories, Canada. *Exploration and Mining Geology*, *16*, 187–208.

Mumin, A. H., Somarin, A. K., Jones, B., Corriveau, L., Ootes, L., & Camier, J. (2010). The IOCG-porphyry-epithermal continuum of deposit types in the Great Bear magmatic zone, Northwest Territories, Canada. In L. Corriveau & A. H. Mumin (Eds.), *Exploring for iron oxide copper-gold deposits: Canada and global analogues* (pp. 59–78). Geological Association of Canada, Short Course Notes, Volume 20.

Ootes, L., Snyder, D., Davis, W. J., Acosta-Góngora, P., Corriveau, L., Mumin, A. H., Gleeson, S. A., Samson, I. M., Montreuil, J. F., Potter, E., & Jackson, V. A. (2017). A Paleoproterozoic Andean-type iron oxide copper-gold environment, the Great Bear magmatic zone, Northwest Canada. *Ore Geology Reviews*, *81*, 123–139. https://doi.org/10.1016/j.oregeorev.2016.09.024

Oreskes, N., & Einaudi, M. T. (1990). Origin of rare earth element-enriched hematite breccias at the Olympic Dam Cu-U-Au-Ag deposit, Roxby Downs, South Australia. *Economic Geology*, *85*(1), 1–28. https://doi.org/10.2113/gsecongeo.85.1.1

Oreskes, N., & Einaudi, M. T. (1992). Origin of hydrothermal fluids at Olympic Dam: preliminary results from fluid inclusions and stable isotopes. *Economic Geology*, *87*(1), 64–90. https://doi.org/10.2113/gsecongeo.87.1.64

OSNACA (2020). *Ore samples normalised to average crustal abundance*. http://www.cet.edu.au/projects/osnaca-ore-samples-normalised-to-average-crustal-abundance

Oyarzun, R., Oyarzún, J., Ménard, J. J., & Lillo, J. (2003). The Cretaceous iron belt of northern Chile: Role of oceanic plates, a superplume event, and a major shear zone. *Mineralium Deposita*, *38*(5), 640–646. https://doi.org/10.1007/s00126-003-0359-y

Oyunjargal, L., Hayashi, K., & Teruyuki, M. (2020). Geological, mineralogical, and oxygen isotope studies of the Chandmani Uul iron oxide – copper – gold deposit in Dornogobi Province , southeastern Mongolia. *Resource Geology*, *January*, 233–253. https://doi.org/10.1111/rge.12232

Page, R. W. (1983). Chronology of magmatism, skarn formation, and uranium mineralization, Mary Kathleen, Queensland, Australia. *Economic Geology*, *78*, 838–853.

Perkins, C., & Wyborn, L. A. I. (1998). Age of Cu-Au mineralisation, Cloncurry district, eastern Mt Isa Inlier, Queensland, as determined by 40Ar/39Ar dating. *Australian Journal of Earth Sciences*, *45*(2), 233–246. https://doi.org/10.1080/08120099808728384

Perring, C. S., Pollard, P. J., Dong, G., Nunn, A. J., & Blake, K. L. (2000). The Lightning Creek Sill complex, cloncurry district, Northwest Queensland: A source of fluids for Fe Oxide Cu-Au mineralization and sodic-calcic alteration. *Economic Geology*, *95*(5), 1067–1089. https://doi.org/10.2113/gsecongeo.95.5.1067

Pestilho, A. L. S., Monteiro, L. V. S., Melo, G. H. C. de, Moreto, C. P. N., Juliani, C., Fallick, A. E., & Xavier, R. P. (2020). Stable isotopes and fluid inclusion constraints on the fluid evolution in the Bacaba and Castanha iron oxide-copper-gold deposits, Carajás Mineral Province, Brazil. *Ore Geology Reviews*, *126*(April 2019), 103738. https://doi.org/10.1016/j.oregeorev.2020.103738

Polito, P. A., Kyser, T. K., & Stanley, C. (2009). The Proterozoic, albitite-hosted, Valhalla uranium deposit, Queensland, Australia: A description of the alteration assemblage associated with uranium mineralisation in diamond drill hole V39. *Mineralium Deposita*, *44*(1), 11–40. https://doi.org/10.1007/s00126-007-0162-2

Porter, T. M. (2010a). Current understanding of iron oxide associated-alkali altered mineralised systems: Part I - An overview. In T. M. Porter (Ed.), *Hydrothermal iron oxide copper-gold and related deposits: A global perspective, Volume 3* (pp. 5–32). PGC Publishing.

Porter, T. M. (2010b). The Carrapateena iron oxide copper gold deposit, Gawler Craton, South Australia: a review. In T. M. Porter (Ed.), *Hydrothermal iron oxide copper-gold and related deposits: A global perspective, Volume 3* (pp. 191–200). PGC Publishing.

Previato, M., Monteiro, L. V. S., Bello, R. M. da S., & Gonçales, L. C. G. (2020). Evolution of brines and CO_2-rich fluids and hydrothermal overprinting in the genesis of the Borrachudo copper deposit, Carajás Province. *Ore Geology Reviews*, *121*(March), 103561. https://doi.org/10.1016/j.oregeorev.2020.103561

Sharma, P. J., Sahoo, P. R., Mahanta, H., Venkatesh, A. S., Babu, E. V. S. S. K., & John, M. M. (2020). Constraints on the genesis of the Proterozoic bornite dominated copper deposit from Nim ka Thana, western India: An IOCG perspective. *Ore Geology Reviews*, *118*(May 2019), 103338. https://doi.org/10.1016/j.oregeorev.2020.103338

Ramírez, L. E., Palacios, C., Townley, B., Parada, M. A., Sial, A. N., Fernandez-Turiel, J. L., Gimeno, D., Garcia-Valles, M., & Lehmann, B. (2006). The Mantos Blancos copper deposit: An Upper Jurassic breccia-style hydrothermal system in the Coastal Range of northern Chile. *Mineralium Deposita*, *41*(3), 246–258. https://doi.org/10.1007/s00126-006-0055-9

Reeve, J. S., Cross, K. C., Smith, R. N., & Oreskes, N. (1990). Olympic Dam copper-uranium-gold-silver deposit. In F. E. Hughes (Ed.), *Geology of the mineral deposits of Australia and Papua*

New Guinea (pp. 1009–1035). Australasian Institute of Mining and Metallurgy, Monograph 14.

Reich, M., Simon, A. C., Deditius, A., Barra, F., Chryssoulis, S., Lagas, G., Tardani, D., Knipping, J., Bilenker, L., Sánchez-alfaro, P., Roberts, M. P., & Munizaga, R. (2016). Trace element signature of pyrite from the Los Colorados iron oxide-apatite (IOA) deposit, Chile: A missing link between Andean IOA and iron oxide copper-gold systems? *Economic Geology*, *111*, 743–761.

Richards, J. P., Lopez, G. P., Zhu, J. J., Creaser, R. A., Locock, A. J., & Mumin, A. H. (2017). Contrasting tectonic settings and sulfur contents of magmas associated with Cretaceous porphyry Cu ± Mo ± Au and intrusion-related iron oxide Cu-Au deposits in northern Chile. *Economic Geology*, *112*(2), 295–318. https://doi.org/10.2113/econgeo.112.2.295

Richards, J. P., & Mumin, A. H. (2013). Magmatic-hydrothermal processes within an evolving Earth: Iron oxide-copper-gold and porphyry Cu ± Mo ± Au deposits. *Geology*, *41*(7), 767–770. https://doi.org/10.1130/G34275.1

Rieger, A. A., Marschik, R., Díaz, M., Hölzl, S., Chiaradia, M., Akker, B., & Spangenberg, J. E. (2010). The hypogene iron oxide copper-gold mineralization in the Mantoverde district, northern Chile. *Economic Geology*, *105*(7), 1271–1299. https://doi.org/10.2113/econgeo.105.7.1271

Rodriguez-Mustafa, M. A., Simon, A. C., del Real, I., Thompson, J. F. H., Bilenker, L. D., Barra, F., Bindeman, I., & Cadwell, D. (2020). A Continuum from Iron Oxide Copper-Gold to Iron Oxide-Apatite Deposits: Evidence from Fe and O Stable Isotopes and Trace Element Chemistry of Magnetite. *Economic Geology*, *115*(7), 1443–1459. https://doi.org/10.5382/econgeo.4752

Rojas, P. A., Barra, F., Deditius, A., Reich, M., Simon, A., Roberts, M., & Rojo, M. (2018). New contributions to the understanding of Kiruna-type iron oxide-apatite deposits revealed by magnetite ore and gangue mineral geochemistry at the El Romeral deposit, Chile. *Ore Geology Reviews*, *93*(January), 413–435. https://doi.org/10.1016/j.oregeorev.2018.01.003

Rotherham, J. F. (1997). A metasomatic origin for the iron-oxide Au-Cu Starra orebodies, Eastern Fold Belt, Mount Isa Inlier. *Mineralium Deposita*, *32*(3), 205–218. https://doi.org/10.1007/s001260050086

Rotherham, J. F., Blake, K. L., Cartwright, I. ., & Williams, P. J. (1998). Stable isotope evidence for the origin of the Mesoproterozoic Starra Au-Cu deposit, Cloncurry district, northwest Queensland. *Economic Geology*, *93*, 1435–1449.

Salazar, E., Barra, F., Reich, M., Simon, A., Leisen, M., Palma, G., Romero, R., & Rojo, M. (2020). Trace element geochemistry of magnetite from the Cerro Negro Norte iron oxide–apatite deposit, northern Chile. *Mineralium Deposita*, *55*(3), 409–428. https://doi.org/10.1007/s00126-019-00879-3

Sangster, D. F. (2020). Evidence that Broken Hill-type Pb-Zn deposits are metamorphosed SEDEX deposits. *Mineralium Deposita*, *55*(7), 1263–1270. https://doi.org/10.1007/s00126-020-00975-9

Schlegel, T. U., & Heinrich, C. A. (2015). Lithology and hydrothermal alteration control the distribution of copper grade in the Prominent Hill iron oxide-copper-gold deposit (Gawler Craton, South Australia). *Economic Geology*, *110*(8), 1953–1994. https://doi.org/10.2113/econgeo.110.8.1953

Schlegel, T. U., Wagner, T., Wälle, M., & Heinrich, C. A. (2018). Hematite breccia-hosted iron oxide copper-gold deposits require magmatic fluid components exposed to atmospheric oxidation: Evidence from Prominent Hill, Gawler Craton, South Australia. *Economic Geology*, *113*(3), 597–644. https://doi.org/10.5382/econgeo.2018.4564

Sillitoe, R. H. (2003). Iron oxide-copper-gold deposits: An Andean view. *Mineralium Deposita*, *38*(7), 787–812. https://doi.org/10.1007/s00126-003-0379-7

Sillitoe, R. H. (2010). Porphyry copper systems. *Economic Geology*, *105*(1), 3–41. https://doi.org/10.2113/gsecongeo.105.1.3

Sillitoe, R. H., Magaranov, G., Mladenov, V., & Creaser, R. A. (2020). Rosen, Bulgaria: A newly recognized iron oxide-copper-gold district. *Economic Geology*, *115*(3), 481–488. https://doi.org/10.5382/ECONGEO.4731

Simon, A. C., Knipping, Reich, M., Barra, F., Deditius, A. P., Bilenker, L. D., & Childress, T. (2018). Kiruna-type iron oxide-apatite (IOA) and iron oxide copper-gold (IOCG) deposits form by a combination of igneous and magmatic-hydrothermal processes: evidence from the Chilean Iron Belt. *Society of Economic Geologists Special Publication*, *No. 21*, 89–114.

Skirrow, R. G. (1993). *The genesis of gold-copper-bismuth deposits, Tennant Creek, Northern Territory.* Unpubl. PhD thesis, Australian National University.

Skirrow, R. G. (2000). Gold-copper-bismuth deposits of the Tennant Creek district, Australia: a reappraisal of diverse high-grade systems. In T. M. Porter (Ed.), *Hydrothermal iron oxide copper-gold and related deposits: A global perspective, Volume 1* (pp. 149–160). Australian Mineral Foundation.

Skirrow, R. G. (2010). "Hematite-group" IOCG±U ore systems: tectonic settings, hydrothermal characteristics, and Cu-Au and U mineralizing processes. In L. Corriveau & H. Mumin (Eds.), *Exploring for iron oxide copper-gold deposits: Canada and global analogues* (pp. 39–58). Geological Association of Canada, Short Course Notes, Volume 20.

Skirrow, R. G., Ashley, P. M., McNaughton, M. J., & Suzuki, K. (2000). Time-space framework of Cu-Au(-Mo) and regional alteration systems in the Curnamona Province. *AGSO Record 2000/10*, 83–86.

Skirrow, R. G., Bastrakov, E. N., Barovich, K., Fraser, G. L., Creaser, R. A., Fanning, C. M., Raymond, O. L., & Davidson, G. J. (2007). Timing of iron oxide Cu-Au-(U) hydrothermal activity and Nd isotope constraints on metal sources in the Gawler craton, South Australia. *Economic Geology*, *102*(8). https://doi.org/10.2113/gsecongeo.102.8.1441

Skirrow, R. G., Bastrakov, E. N., Davidson, G. J., Raymond, O. L., & Heithersay, P. (2002). The geological framework, distribution and controls of Fe-oxide Cu-Au mineralisation in the Gawler craton, South Australia: Part II - Alteration and mineralisation. In T. M. Porter (Ed.), *Hydrothermal iron oxide copper-gold and related deposits: A global perspective, Volume 2* (pp. 33–47). PGC Publishing.

Skirrow, R. G., Murr, J., Schofield, A., Huston, D. L., van der Wielen, S., Czarnota, K., Coghlan, R., Highet, L. M., Connolly, D., Doublier, M., & Duan, J. (2019). Mapping iron oxide Cu-Au (IOCG) mineral potential in Australia using a knowledge-driven mineral systems-based approach. *Ore Geology Reviews*, *113*. https://doi.org/10.1016/j.oregeorev.2019.103011

Skirrow, R. G., van der Wielen, S. E., Champion, D. C., Czarnota, K., & Thiel, S. (2018). Lithospheric Architecture and Mantle Metasomatism Linked to Iron Oxide Cu-Au Ore Formation: Multidisciplinary Evidence from the Olympic Dam Region, South Australia. *Geochemistry, Geophysics, Geosystems*, *19*(8). https://doi.org/10.1029/2018GC007561

Skirrow, R. G., & Walshe, J. L. (2002). Reduced and oxidized Au-Cu-Bi iron oxide deposits of the Tennant Creek Inlier, Australia: An integrated geologic and chemical model. *Economic Geology*, *97*(6). https://doi.org/10.2113/gsecongeo.97.6.1167

Spry, P. G., & Teale, G. S. (2021). A classification of Broken Hill-type deposits: A critical review. *Ore Geology Reviews*, *130*(January), 103935. https://doi.org/10.1016/j.oregeorev.2020.103935

Su, Z.-K., Zhao, X.-F., Li, X.-C., Zhou, M.-F., Kennedy, A. K., Zi, J.-W., Spandler, C., & Yang, Y.-H. (2021). Unraveling mineralization and multistage hydrothermal overprinting histories by integrated in-situ U-Pb and Sm-Nd isotopes in a Paleoproterozoic breccia-hosted iron oxide copper-gold deposit, SW China. *Economic Geology*, *116*(7), 1687–1710. https://doi.org/10.5382/econgeo.4840

Sun, X. J., Ni, P., Yang, Y. L., Qin, H., Chen, H., Gui, C. J., & Jing, S. (2018). Formation of the Qixiashan Pb–Zn deposit in Middle-Lower Yangtze River Valley, eastern China: Insights from fluid inclusions and in situ LA-ICP-MS sulfur isotope data. *Journal of Geochemical Exploration*, *192*(June 2017), 45–59. https://doi.org/10.1016/j.gexplo.2018.03.011

Teale, G. S., & Fanning, C. M. (2000a). The Portia - North Portia Cu-Au(-Mo) prospect, South Australia: timing of mineralisation, albitisation and origin of ore fluid. In T. M. Porter (Ed.), *Hydrothermal iron oxide copper-gold and related deposits: A global perspective, Volume 1* (pp. 137–147). Australian Mineral Foundation.

Teale, G. S., & Fanning, C. M. (2000b). The timing of Cu-Au mineralisation in the Curnamona Province. *AGSO Record 2000/10*, 98–100.

Tiddy, C. J., & Giles, D. (2020). Suprasubduction zone model for metal endowment at 1.60–1.57 Ga in eastern Australia. *Ore Geology Reviews*, *122*(March), 103483. https://doi.org/10.1016/j.oregeorev.2020.103483

Tornos, F., Velasco, F., & Hanchar, J. M. (2016). Iron-rich melts, magmatic magnetite, and superheated hydrothermal systems: The El Laco deposit, Chile. *Geology*, *44*(6), 427–430. https://doi.org/10.1130/G37705.1

Wang, S., & Williams, P. J. (2001). Geochemistry and origin of Proterozoic skarns at the Mount Elliott Cu-Au(-Co-Ni) deposit, Cloncurry district, NW Queensland, Australia. *Mineralium Deposita*, *36*(2), 109–124. https://doi.org/10.1007/s001260050292

Wanhainen, C., & Martinsson, O. (2010). The hybrid character of the Aitik deposit, Norbotten, Sweden: a porphyry Cu-Au-Ag(-Mo) system overprinted by iron-oxide Cu-Au hydrothermal fluids. In T. M. Porter (Ed.), *Hydrothermal iron oxide copper-gold and related deposits: A global perspective, Volume 4* (pp. 415–426). PGC Publishing.

Wedekind, M. R., Large, R. R., & Williams, B. T. (1989). *Controls on high-grade gold mineralization at Tennant Creek, Northern Territory, Australia* (pp. 168–179). Economic Geology, Monograph 6.

Whitney, D. L., & Evans, B. W. (2010). Abbreviations for names of rock-forming minerals. *American Mineralogist*, *95*(1), 185–187. https://doi.org/10.2138/am.2010.3371

Williams, M. R., Holwell, D. A., Lilly, R. M., Case, G. N. D., & McDonald, I. (2015). Mineralogical and fluid characteristics of the fluorite-rich Monakoff and E1 Cu-Au deposits, Cloncurry region, Queensland, Australia: Implications for regional F-Ba-rich IOCG mineralisation. *Ore Geology Reviews*, *64*(1), 103–127. https://doi.org/10.1016/j.oregeorev.2014.05.021

Williams, P. J. (2010). Classifying IOCG deposits. In L. Corriveau & H. Mumin (Eds.), *Exploring for iron oxide copper-gold deposits: Canada and global analogues* (pp. 13–21). Geological Association of Canada, Short Course Notes, Volume 20.

Williams, P. J., Barton, M. D., Johnson, D. A., Fontboté, L., de Haller, A., Mark, G., Oliver, N. H. S., & Marschik, R. (2005). Iron oxide copper-gold deposits: Geology, space-time distributions, and possible modes of origin. *Economic Geology*, *100*, 371–405.

Williams, P. J., & Skirrow, R. G. (2000). Overview of iron oxide-copper-gold deposits in the Curnamona Province and Cloncurry district (Mount Isa Block), Australia. In T. M. Porter (Ed.), *Hydrothermal iron oxide copper-gold and related deposits: A global perspective, Volume 1* (pp. 105–122). Australian Mineral Foundation.

Wilson, N. S. F., Zentilli, M., Reynolds, P. H., & Boric, R. (2003). Age of mineralization by basinal fluids at the El Soldado manto-type copper deposit, Chile: $^{40}Ar/^{39}Ar$ geochronology of K-feldspar. *Chemical Geology*, *197*(1–4), 161–176. https://doi.org/10.1016/S0009-2541(02)00350-9

Wyborn, L. A. I., Heinrich, C. A., & Jaques, A. L. (1994). Australian Proterozoic mineral systems: essential ingredients and mappable criteria. *Australasian Institute of Mining and Metallurgy Publication Series*, *5/94*, 109–115.

Zhao, X. F., & Zhou, M. F. (2011). Fe-Cu deposits in the Kangdian region, SW China: A Proterozoic IOCG (iron-oxide-copper-gold) metallogenic province. *Mineralium Deposita*, *46*(7), 731–747. https://doi.org/10.1007/s00126-011-0342-y

Zhao, X. F., Zhou, M. F., Hitzman, M. W., Li, J. W., Bennett, M., Meighan, C., & Anderson, E. (2012). Late Paleoproterozoic to early Mesoproterozoic Tangdan sedimentary rock-hosted strata-bound copper deposit, Yunnan province, southwest China. *Economic Geology*, *107*(2), 357–375. https://doi.org/10.2113/econgeo.107.2.357

Zhao, X. F., Zhou, M. F., Su, Z. K., Li, X. C., Chen, W. T., & Li, J. W. (2017). Geology, geochronology, and geochemistry of the Dahongshan Fe-Cu-(Au-Ag) deposit, southwest China: Implications for the formation of iron oxide copper-gold deposits in intracratonic rift settings. *Economic Geology*, *112*(3), 603–628. https://doi.org/10.2113/econgeo.112.3.603

Zhou, M. F., Zhao, X. F., Chen, W. T., Li, X. C., Wang, W., Yan, D. P., & Qiu, H. N. (2014). Proterozoic Fe-Cu metallogeny and supercontinental cycles of the southwestern Yangtze Block,

southern China and northern Vietnam. *Earth-Science Reviews*, *139*, 59–82. https://doi.org/10.1016/j.earscirev.2014.08.013

Zhou, T., Fan, Y., Yuan, F., Zhang, L., Qian, B., Ma, L., & Yang, X. (2013). Geology and geochronology of magnetite – apatite deposits in the Ning-Wu volcanic basin, eastern China. *Journal of Asian Earth Sciences*, *66*, 90–107. https://doi.org/10.1016/j.jseaes.2012.12.030

Appendix 1. References for Figure 4, paragenetic sequences.

Carajás province, Brazil (Cristalino, Igarapé-Bahia, Salobo, Bacaba, Sossego-Sequeirinho deposits): Monteiro et al. (2008); Moreto et al. (2011); de Melo et al. (2017); de Melo et al. (2019); Craveiro et al. (2020); Pestilho et al. (2020)

Cloncurry province, Australia (Ernest Henry, E1, Starra, Eloise, Osborne deposits):Rotherham (1997); Baker & Laing (1998); Baker et al. (2001); Mark et al. (2006); Fisher & Kendrick (2008); Williams et al. (2015); Case (2016); Cave et al. (2018)

Sin Quyen deposit, Vietnam (possible extension of Kangdian province): McLean (2002); Li & Zhou (2018)

Kangdian province, China (Dahongshan, Yinachang, Lala deposits): Chen & Zhou (2012); Li et al. (2015); Zhao et al. (2017)

Gawler Craton and Curnamona Province, Australia (Olympic Dam, Prominent Hill, Hillside, Wallaroo, North Portia deposits): Oreskes & Einaudi (1990); Reeve et al. (1990); Conor (1995); Haynes et al. (1995); Teale & Fanning (2000a); Skirrow et al. (2002); Conor et al. (2010); Ehrig et al. (2012); Ismail et al. (2014); Schlegel & Heinrich (2015)

Tennant Creek province, Australia (Eldorado, Juno, West Peko deposits): Large (1975); Skirrow & Walshe (2002)

Guelb Moghrein deposit, Mauritania: Kolb et al. (2010); Kirschbaum & Hitzman (2016); Kolb & Petrov (2016)

Great Bear magmatic zone, Canada (NICO deposit): Goad et al. (2000); Acosta-Góngora et al. (2015)

Andes province, Chile and Peru (Panulcillo, Mantoverde, Mina Justa, Candelaria, Raúl-Condestable deposits): Hopper & Correa (2000); Marschik & Fontboté (2001); de Haller et al. (2006); Benavides et al. (2007); Chen et al. (2010); Rieger et al. (2010); del Real et al. (2018)

Appendix 2. Fe-oxide and Fe-Cu sulfide mineralogical characteristics of IOCG and related ISCG deposits, listed by IOCG province.

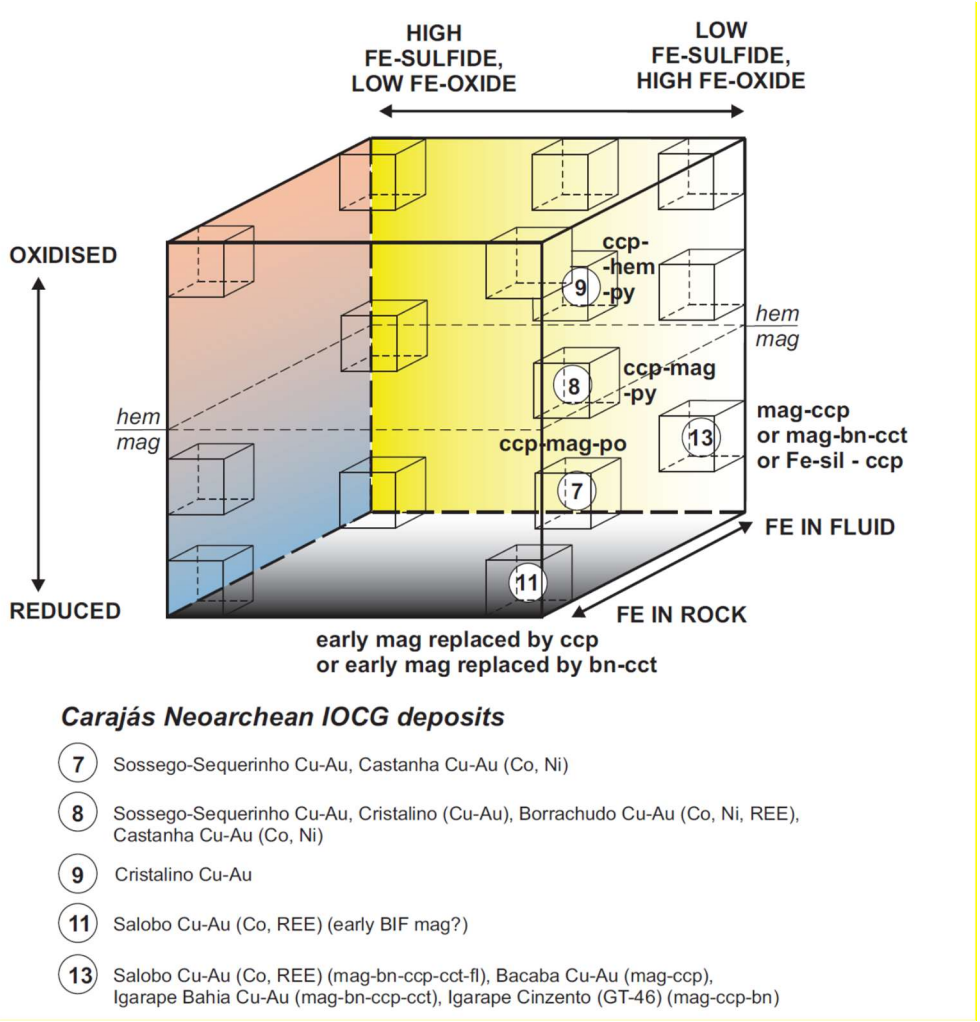

References for Carajás province:

Monteiro et al. (2008); Moreto et al. (2011); de Melo et al. (2017); de Freitas Toledo et al. (2019); de Melo et al. (2019); Craveiro et al. (2020); Pestilho et al. (2020); Previato et al. (2020)

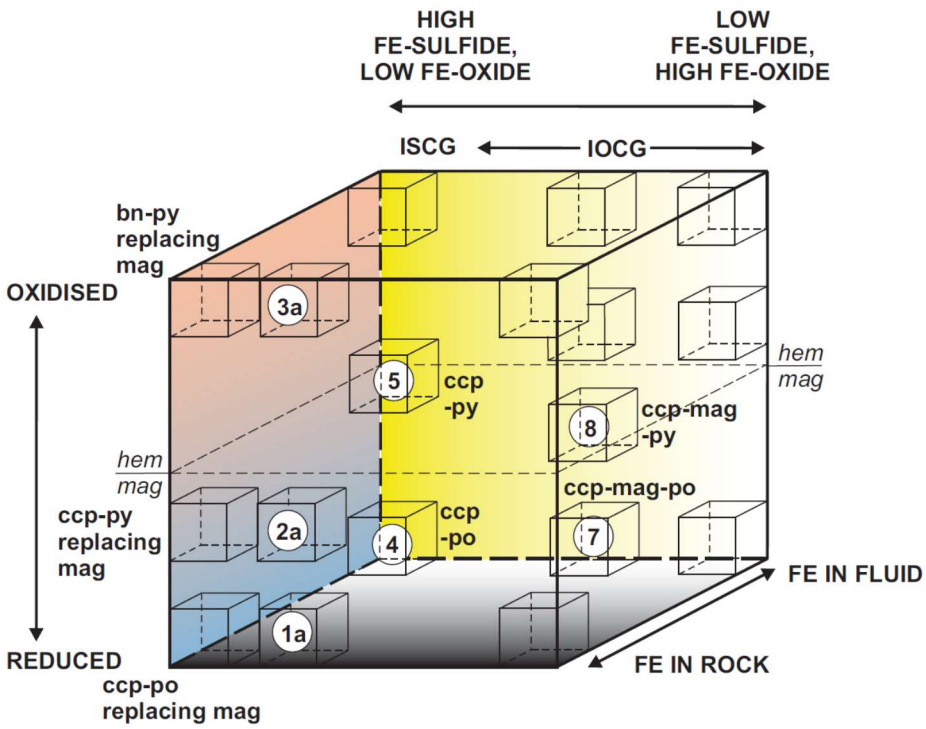

Cloncurry IOCG and ISCG deposits

- 1a Osborne Cu-Au (Co)
- 2a Osborne Cu-Au (Co), Starra Cu-Au (Co) early mag-ccp stage
- 3a Starra late Au-Cu stage
- 4 Eloise Cu-Au (Co), Mt Elliott Cu-Au (east)
- 5 Greenmount Cu-Au (Co)
- 7 Monakoff Cu-Au (Co, REE) early stage, E1N Cu-Au (REE) early stage
- 8 Ernest Henry Cu-Au (Co, REE, brt, fl), Mt Elliott (west) & SWAN Cu-Au (REE), E1N Cu-Au (REE, late brt, fl), Monakoff Cu-Au (REE, late brt, fl)

References for Cloncurry province:

Rotherham (1997); Baker & Laing (1998); Williams & Skirrow (2000); Baker et al. (2001); Mark et al. (2006); Fisher & Kendrick (2008); Brown & Porter (2010); Williams et al. (2015); Case (2016); Cave et al. (2018)

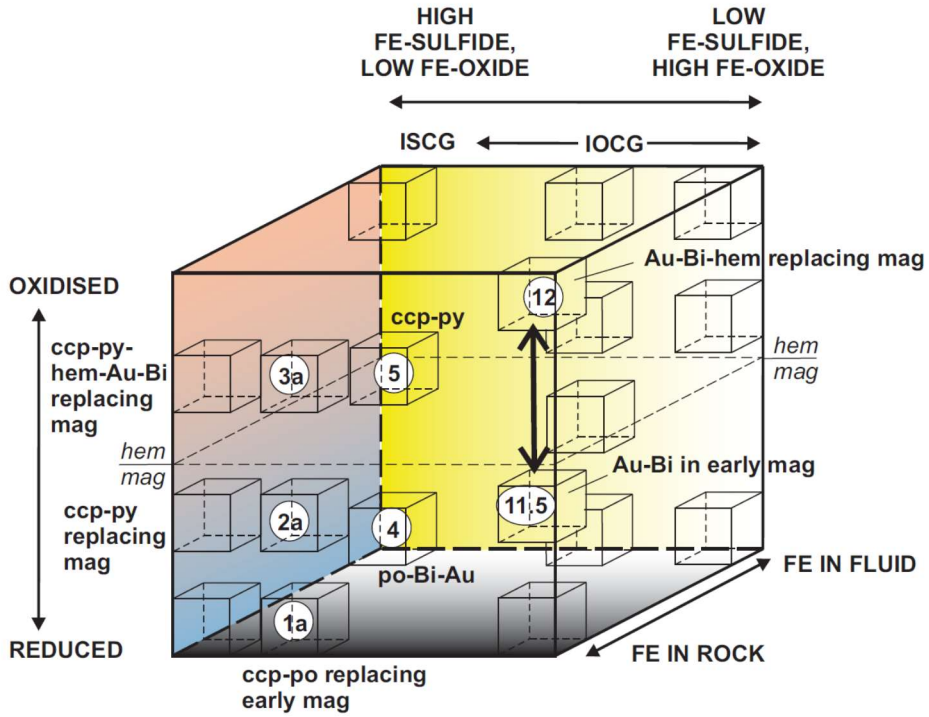

Tennant Creek Au-Cu-Bi IOCG & ISCG deposits

1a West Peko Cu-Au-Bi, Warrego Cu-Au-Bi (uncommon po)

2a Warrego Cu-Au-Bi, Gecko K44 Cu-Au-Bi (lower zone), Peko Cu-Au-Bi, Orlando Cu-Au-Bi

3a Gecko K44 Cu-Au-Bi (upper zoe)

4 West Peko shear-hosted Au-Bi outside ironstone

5 Orlando East, Gecko (Monitor, Goanna), Bishop Creek Cu-Au-Bi

12 Eldorado, Nobles Nob (?) Au (-Bi)

11.5 ↔ 12 White Devil, Juno, Argo, TC8, Chariot mag-Au-Bi (variable hem, py, Cu)

References for Tennant Creek goldfield:

Large (1975); Wedekind et al. (1989); Skirrow (1993, 2000); Huston et al. (1993); Skirrow & Walshe (2002)

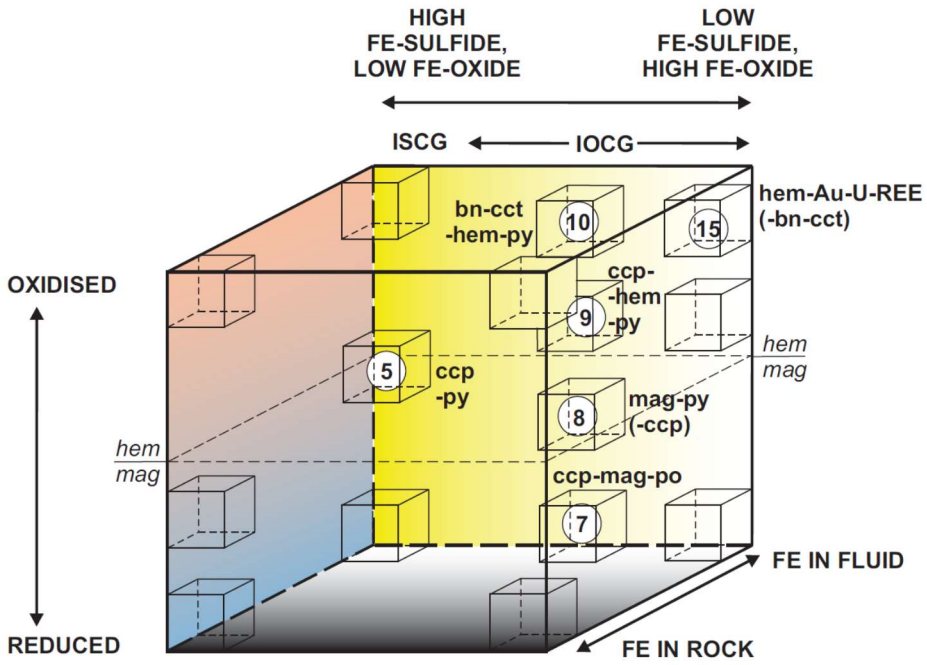

Gawler Craton IOCG and ISCG deposits

15 Olympic Dam, Prominent Hill, Carrapateena hem-qtz zones (upper / inner zones)

10 Olympic Dam, Prominent Hill, Carrapateena Cu-Au ore zones (upper / inner zones)

9 Olympic Dam, Prominent Hill, Carrapateena ore zones (lower / outer zones)

8 Olympic Dam, Prominent Hill and barren/low grade prospects (early mag-py ± ccp ± sid ± apatite)

7 Joes Dam, Manxman Cu-Au prospects

5 Moonta Cu-Au in qz-Kfs veins (ISCG or other deposit type?)

References for Gawler Craton – Olympic Cu-Au province:

Oreskes & Einaudi (1990); Reeve et al. (1990); Conor (1995); Haynes et al. (1995); Skirrow et al. (2002); Conor et al. (2010); Ehrig et al. (2012); Ismail et al. (2014); Schlegel & Heinrich (2015)

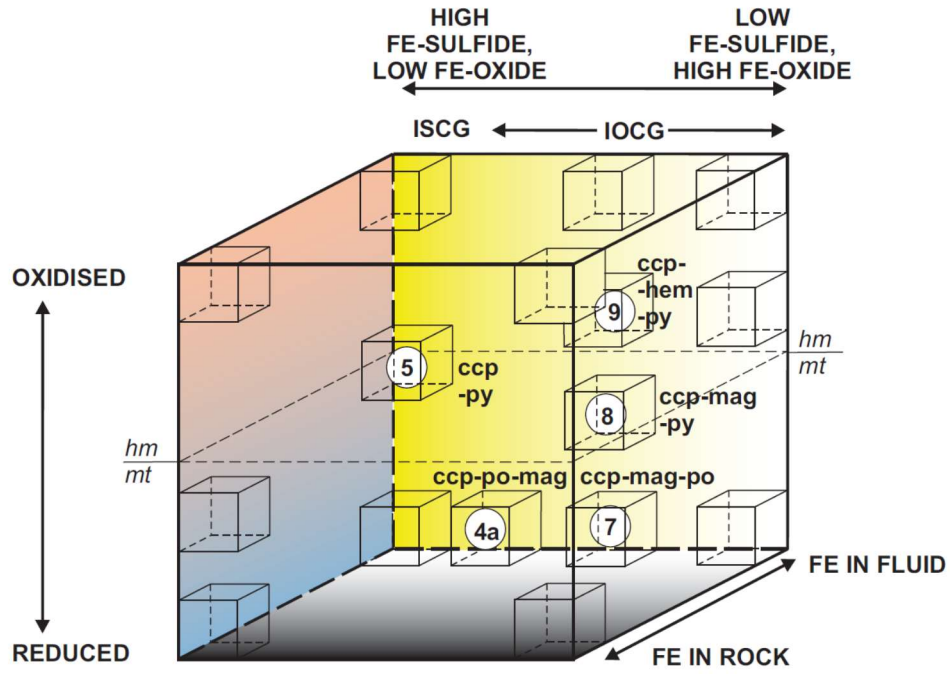

Other IOCG & ISCG deposits (Andean in bold)

7 Dahongshan Cu (-Au), Lala Cu (-Au), Sin Quyen Cu (-Au), NICO early stage Au-Co-Bi-As, **Candelaria Cu-Au, Raul-Condestable Cu-Au**

8 Dahongshan Cu (-Au), Lala Cu (-Au), Yinachang Cu (-Au), Sin Quyen Cu (-Au), **Candelaria Cu-Au, Raul-Condestable Cu-Au, Mina Justa Cu-Au**

9 Sue Dianne Cu-Au, NICO Au-Co-Bi-As (late Cu stage), **Mantoverde Cu-Au (REE, Mina Justa Cu-Au**

5 Hongnipo Cu (-Au) (Kangdian), **?manto Cu-Ag deposits (Chile)**, ?some 'SSC' Cu (-Au) deposits (Khetri)

4a Guelb Moghrein Cu-Au (Co, Ni, Bi)

References for Chilean and Peruvian Andes province:

Hopper & Correa (2000); Marschik & Fontboté (2001); Boric et al. (2002); Maksaev & Zentilli (2002); de Haller et al. (2006); Ramírez et al. (2006); Benavides et al. (2007); Chen et al. (2010); Rieger et al. (2010); del Real et al. (2018)

References for Kangdian province: Zhao & Zhou (2011); Chen & Zhou (2012); Zhou et al. (2014); Li et al. (2015); Zhao et al. (2017); Lin et al. (2020)

References for Great Bear magmatic zone: Goad et al. (2000); Acosta-Góngora et al. (2015)

References for Geulb Moghrein deposit: Kolb et al. (2010); Kirschbaum & Hitzman (2016); Kolb & Petrov (2016)

Appendix 3. Summary of deposits extracted from the OSNACA global ore geochemical data base (Brauhart et al., 2017; OSNACA, 2020) and attributed as IOCG deposits. Sub-types assigned in the present study are based on descriptions in OSNACA together with information from published literature for individual deposits, and correspond to variants in the IOCG-ISCG cube (Figs. 7, 8). Data for several additional deposits are sourced as indicated. The number of samples in OSNACA for each deposit (# samples) differs in some cases from the number of samples plotted in the figures in this contribution (# plotted) due to exclusion of samples of host rock; only ore samples have been used in this study.

OSNACA and additional ore geochemistry data set

Deposit name	Country	State	Metall. Prov.	# samples	# plotted	OSNACA class	Sub-type (this study)	Notes	Source
Kanmantoo	Australia	South Australia	Adelaide Fold Belt	2	2	IOCG	Reduced - low mt	possible ISCG?	OSNACA
Antas	Brazil	Pará	Carajás	1	1	IOCG	Reduced - variable mt		OSNACA
Sossego	Brazil	Pará	Carajás	3	3	IOCG	Intermed-redox - mt-rich		OSNACA
Barreal Seco	Chile	Atacama	Chilean Iron Belt	3	3	IOCG	Oxidised - hm-rich (Andes)		OSNACA
Candelaria	Chile	Atacama	Chilean Iron Belt	2	2	IOCG	Reduced - variable mt		Marschik & Fontboté (2001)
Carola	Chile	Atacama	Chilean Iron Belt	3	3	IOCG	Intermed-redox - hm-mt or mt-hm-rich		Marschik & Fontboté (2001)
Manto Verde	Chile	Atacama	Chilean Iron Belt	5	5	IOCG	Oxidised - hm-rich (Andes)		Rieger et al. (2010)
Socavon Rampa	Chile	Atacama	Chilean Iron Belt	2	2	IOCG	Oxidised - hm-rich (Andes)		OSNACA
Artemis	Australia	Queensland	Cloncurry	6	4	IOCG	Reduced - low mt	Zn-Pb-rich	OSNACA
Barbara	Australia	Queensland	Cloncurry	8	6	IOCG	Reduced - low mt		OSNACA
Blackard	Australia	Queensland	Cloncurry	2	1	IOCG	Cu-Au	oxidation & Fe ox unknown	OSNACA
Cameron River	Australia	Queensland	Cloncurry	9	8	IOCG	Reduced - low mt		OSNACA
Canteen	Australia	Queensland	Cloncurry	4	4	IOCG	Reduced - low mt	Fe ox unknown	OSNACA
E1	Australia	Queensland	Cloncurry	10	10	IOCG	Intermed-redox - hm-mt or mt-hm-rich		OSNACA
Eloise	Australia	Queensland	Cloncurry	7	7	IOCG	Reduced - variable mt		OSNACA
Ernest Henry	Australia	Queensland	Cloncurry	12	12	IOCG	Intermed-redox - hm-mt or mt-hm-rich		OSNACA
Great Australia	Australia	Queensland	Cloncurry	2	2	IOCG	Cu-Au	Fe ox unknown	OSNACA
Kalman	Australia	Queensland	Cloncurry	3	3	IOCG	Intermed? Cu-Au	Fe ox unknown	OSNACA
Kulthor	Australia	Queensland	Cloncurry	3	3	IOCG	Reduced - variable mt		OSNACA
Kurilla	Australia	South Australia	Cloncurry	2	2	IOCG	unknown		OSNACA
Little Eva	Australia	Queensland	Cloncurry	2	2	IOCG	Oxidised - hm-rich		OSNACA
Lorena	Australia	Queensland	Cloncurry	1	1	IOCG	Reduced - low mt		OSNACA
Merlin	Australia	Queensland	Cloncurry	4	4	IOCG		no Fe ox, not Cu-Au-Fe (Co, REE) deposit	OSNACA
Monakoff	Australia	Queensland	Cloncurry	7	7	IOCG	Intermed-redox	hybrid?	OSNACA
Mount Colin	Australia	Queensland	Cloncurry	5	3	IOCG	Cu-Au	oxidation and Fe-ox unknown	OSNACA
Mount Elliot	Australia	Queensland	Cloncurry	1	1	IOCG	Intermed-redox - mt-rich		OSNACA
Osborne	Australia	Queensland	Cloncurry	13	12	IOCG	Reduced - variable mt		OSNACA
Rocklands	Australia	Queensland	Cloncurry	3	3	IOCG	Intermed-redox - low Fe-ox		OSNACA
Starra	Australia	Queensland	Cloncurry	6	4	IOCG	Intermed-redox - hm-mt or mt-hm-rich		OSNACA
Swan	Australia	Queensland	Cloncurry	8	8	IOCG	Intermed-redox - mt-rich		OSNACA
Trekelano	Australia	Queensland	Cloncurry	2	1	IOCG	Cu-Au	oxidation and Fe-ox unknown	OSNACA
Olympic Dam	Australia	South Australia	Gawler Craton	6	6	IOCG	Oxidised - hm-rich		OSNACA
Prominent Hill	Australia	South Australia	Gawler Craton	3	3	IOCG	Oxidised - hm-rich		OSNACA
Wheal Hughes	Australia	South Australia	Gawler Craton	2	2	IOCG	Intermed-redox - low Fe-ox		OSNACA
Guelb Moghrein	Mauritania	Inchiri	Guelb Moghrein	2	2	IOCG	Reduced - low mt		OSNACA
Khetri	India	Rajasthan	Khetri	2	2	IOCG	Intermed-redox - mt-rich		OSNACA
Messina	South Afric	Limpopo	Limpopo	3	3	IOCG	unknown	not Cu-Au-Fe (Co, REE) deposit?	OSNACA
Vergenoeg	South Afric	Limpopo	Limpopo	1	1	IOCG		magnetite-fluorite, not Cu-Au-Fe (Co, REE) de	OSNACA
Sin Quyen	Vietnam	Lào Cai	Red River Fault Zone	1	1	IOCG	Intermed-redox	mag rich	OSNACA
Gecko	Australia	Northern Territory	Tennant Creek	2	2	IOCG	Intermed-redox - hm-mt or mt-hm-rich		OSNACA
Warrego	Australia	Northern Territory	Tennant Creek	3	3	IOCG	Intermed-redox - mt-rich		OSNACA
White Devil	Australia	Northern Territory	Tennant Creek	3	3	IOCG	Intermed-redox - mt-rich		OSNACA
Wernecke Mtn	Canada	Yukon	Wernecke	1	1	IOCG	Intermed-redox - low Fe-ox		OSNACA

Supplementary Information

Iron oxide copper-gold (IOCG) deposits – A review (part 1): settings, mineralogy, ore geochemistry and classification

Roger G. Skirrow

Geological settings and characteristics of provinces hosting IOCG deposits

1. Introduction

The timing of regional geological events in relation to Cu-Au-Fe mineralisation is summarised in Figure S1 for six of the world's major metallogenic provinces containing large IOCG deposits and for which comprehensive geochronological data are also available. Event time spans shown in Figure S1 represent the main bodies of available geochronological data for each event, with emphasis on ages determined with robust geochronometers such as U-Pb and U-Th-Pb isotope analyses of zircon, titanite and monazite, and Re-Os isotope analysis of molybdenite. Additional constraints from $^{40}Ar/^{39}Ar$ dating have been utilised for hydrothermal minerals in some provinces. Uncertainties on individual ages are given in the detailed descriptions below and in the accompanying figures in some cases. The timing and character of deformation/tectonism events have been largely taken from the literature, supplemented by further interpretation in some provinces as described below.

2. Carajás province, Brazil – Neoarchean IOCG and Paleoproterozoic Cu-Au deposits

The Carajás metallogenic province in the southeastern part of the Amazon Craton hosts some of the world's largest and most important iron oxide-rich Cu-Au deposits, including the Salobo, Cristalino, Sequeirinho (part of the Sossego group of deposits) and Igarapé Bahia deposits (Grainger et al., 2008; Xavier et al., 2010; Schutesky & de Oliveira, 2020; Trunfull et al., 2020). Dating of the deposits shows that Cu-Au mineralisation in the Southern Copper Belt (e.g. Cristalino, Sossego) commenced at ~2720-2680 Ma whereas in the Northern Copper Belt (including Salobo and Igarapé Bahia) the available data indicate a major Cu-Au event at ~2580-2535 Ma (Fig. S1; Re-Os molybdenite and U-Pb monazite, titanite, zircon ages – Machado et al., 1991; Requia et al., 2003; Tallarico et al., 2005; Moreto et al., 2015a, 2015b; Pollard et al., 2019). Many deposits also record younger U-Pb and ^{40}Ar-^{39}Ar ages (e.g. 2497 ± 5 Ma, U-Pb titanite age at Salobo – Machado et al., 1991), reflecting the complex and prolonged tectonothermal history of the Carajás Province. Indeed a third period of Cu-Au mineralisation is believed to have occurred at ~1900-1860 Ma in both the Southern and Northern Copper Belts (Fig. S1; e.g. Alvo 118, Estrela, Sossego-Curral, Breves, and Gameleira deposits – Tallarico et al., 2005; Moreto et al., 2015a, 2015b; Pollard et al., 2019). Although many of these relatively small Paleoproterozoic Cu-Au deposits were initially described as IOCG deposits, Pollard et al. (2019) noted their anomalous B-Be-Bi-Li-Sn-W geochemistry and distinguished these Fe-oxide-poor, quartz ± carbonate-rich deposits as separate in origin from the Neoarchean IOCG deposits and proposed a magmatic-hydrothermal derivation related to A-type granites of overlapping age. The Carajás Province is also endowed with large deposits of Fe related to banded iron formations, Mn, Cr-PGE and Ni associated with mafic intrusions (e.g. Luanga deposit), hydrothermal Au and Au-PGE deposits (e.g. Serra Pelada; Diella et al., 1995; Grainger et al., 2008; Bettencourt et al., 2016).

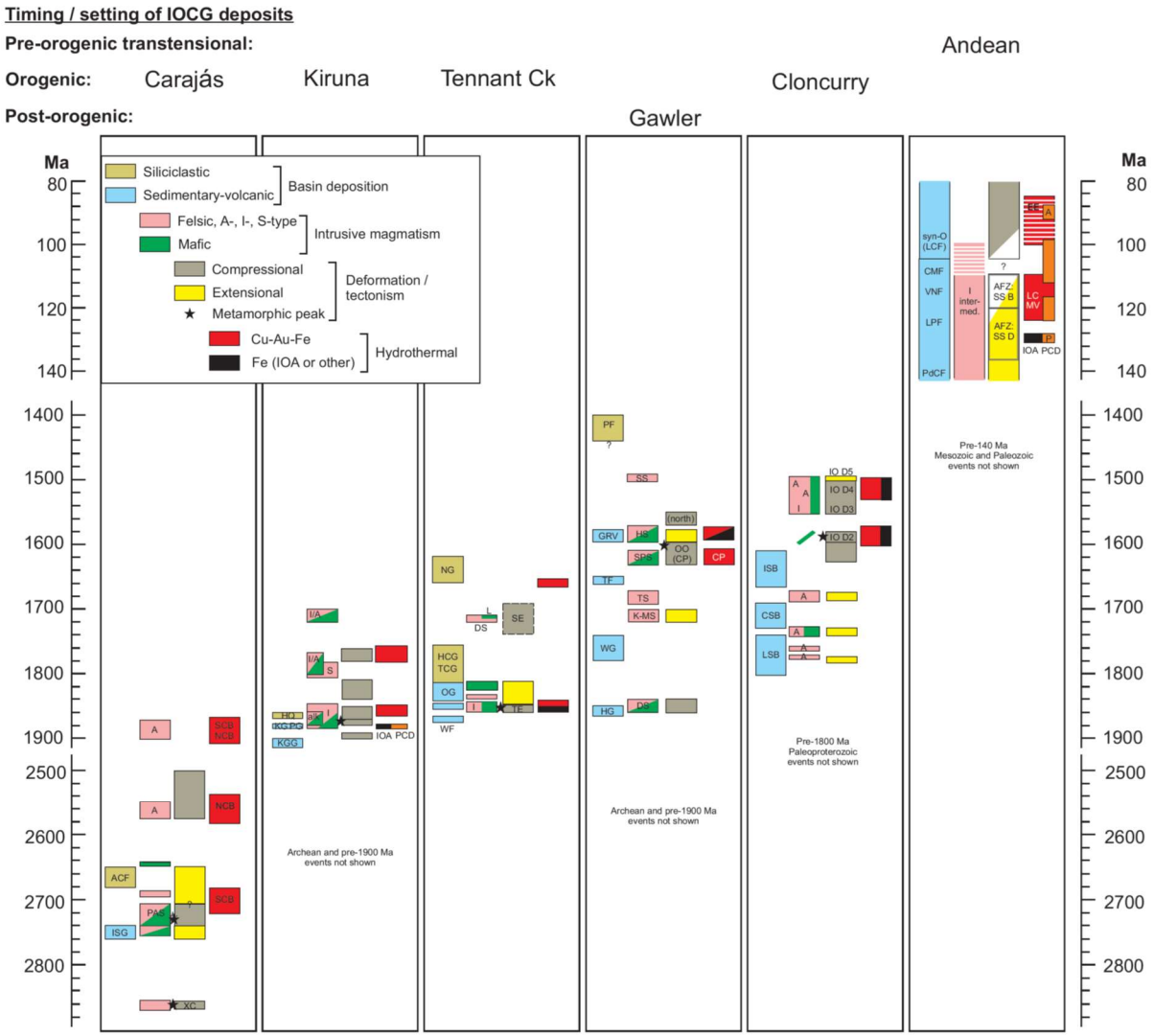

Figure S1. Synthesis of geochronological data for mineralisation, tectonic, magmatic and supracrustal depositional events in key provinces with IOCG deposits. The Kiruna and Andean provinces also contain well known IOA deposits. Note breaks in time scale. Sources of data are cited in the text of this Supplementary Information. Abbreviations for intrusive magmatism: A – A-type granites, I – I-type, S – S-type, alk – alkaline. Rock unit and other abbreviations: Carajás province, ACF – Águas Claras Formation, ISG – Itacaiunas Supergroup, NCB – Northern Copper Belt, PAS – Planalto Suite, SCB – Southern Copper Belt, XC – Xingu and Pium Complexes; HQ – Hauki Quartzite, IOA – iron oxide apatite deposits, Kiruna province, KGG – Kiruna Greenstone Group, KG – Kiirunavaara Group, PCD – porphyry Cu deposit; Tennant Creek, DS – Devils Suite, HCG – Hatches Creek Group, OG – Ooradidgee Group, NG – Namerinni Group, SE – Strangways Event, TCG – Tennant Creek Granite suite, TE – Tennant Event, WF – Warramunga Formation; Gawler Craton – CP – Curnamona Province Cu-Au deposits, DS – Donnington Suite, GRV – Gawler Range Volcanics, HG – Hutchison Group, HS – Hiltaba Suite, K-MS – Kimban-Moody Suite, OO (CP) – Olarian Orogeny in Curnamona Province, SPS – St Peter Suite, TF – Tarcoola Formation, TS- Tunkillia Suite, WG – Wallaroo Group; Cloncurry province, CSB – Calvert Superbasin, IO – Isan Orogeny, ISB – Isan Superbasin, LSB – Leichardt Superbasin; Andean province (Chile; formation names after Boyce et al., 2020), A – Carmen de Andacollo porphyry Cu deposit, AFZ – Atacama Fault Zone, CMF – Cerro Morado Formation, EE – El Espino Cu-Au-Fe deposit, IOA – iron oxide apatite deposits, LC – La Candelaria, LPF – Lo Prado Formation, MV – Mantoverde deposit, P – Productora Cu-Au deposit, PdCF – Punta del Cobre Formation, PCD – porphyry Cu deposits, SS B – strike-slip brittle, SS D – strike-slip ductile, syn-O (LCF) – syn-orogenic Las Chilcas Formation, VNF – Veta Negra Formation.

The Neoarchean IOCG and Paleoproterozoic Cu-Au deposits all occur within the Carajás Domain, which forms the northern part of the Carajás Province. The Southern Copper Belt lies along the regional shear zone system bounding the Carajás Domain with the Rio Maria Domain to the south, which is dominated by ~3066-3000 Ma basement rocks of the Xingu Complex and Pium Complex (Pidgeon et al., 2000; Moreto et al., 2011). The latter were deformed and metamorphosed at high grade at ~2860 Ma (Machado et al., 1991). Several of the Neoarchean Cu-Au deposits occur within a few kilometres of the domain boundary, hosted by the ~3.0 Ga basement and syn-orogenic ~2860 Ma granitoids (e.g., Bacuri – Moreto et al., 2011), and a few others occur within the Xingu Complex in the Northern Copper Belt (e.g. Salobo, de Melo et al., 2017). However, the majority of the Neoarchean Cu-Au deposits are hosted by the overlying ~2760-2730 Ma Itacaiúnas Supergroup which comprises lower greenschist to amphibolite facies metamorphosed mafic and felsic volcanic rocks, iron formations and clastic sedimentary rocks (Machado et al., 1991; Olszewski et al., 1989). The ~2720-2680 Ma timing of many of the major Cu-Au deposits and regional sodic alteration in the Southern Copper Belt appears to postdate regional ductile transpressional tectonism (~2780-2740 Ma) and extensive ~2740 Ma bimodal intrusive magmatism (Moreto et al., 2015b), but overlaps with the alkaline and A-type Planalto Granite Suite and possibly co-magmatic gabbros (Fig. S1; 2706 ± 5 Ma to 2754 ± 2 Ma, Feio et al., 2013). In detail, however, most of the Neoarchean Cu-Au-Fe mineralisation in the Southern Copper Belt formed during brittle-ductile and brittle deformation associated with shear zones and faults (e.g. Sequeirinho orebody - Sossego deposit; Cristalino deposit; Bacuri and Bacaba prospects; Monteiro et al., 2008; Xavier et al., 2010; Moreto et al., 2015a, 2015b; Craveiro et al., 2020; Pestilho et al., 2020). This deformation controlling IOCG mineralisation in the Southern Copper Belt may be linked to the switch from sinistral transpressional to dextral transtensional deformation that has been identified at ~2725-2700 within the Carajás and Cinzento shear zones to the north within the Carajás Domain (Xavier et al., 2010; Moreto et al., 2015b; de Melo et al., 2017; de Freitas Toledo et al., 2019). Regional transtensional deformation may have resumed in some shear zones at ~2600 Ma when there was a further period of transpression and mylonite development in the Carajás Domain (Xavier et al., 2010; Moreto et al., 2015b). Also of note is the deposition of the low metamorphic grade and siliciclastic Águas Claras Formation after ~2681 Ma (constrained by detrital zircon maximum depositional age, Trendall et al., 1998) and before intrusion of ~2645 Ma gabbro into the sequence (Fig. 1; Dias et al., 1996). This extensive basin in the Carajás Domain could be interpreted to indicate a continuation of extensional tectonism after formation of the earlier group of major Neoarchean IOCG deposits in the Southern Copper Belt but prior to the second group of major IOCG deposits in the Northern Copper Belt.

Available geochronology indicates that formation of the younger Neoarchean copper-gold deposits in the Northern Copper Belt at ~2580-2535 Ma (Fig. S1) could have been coeval with emplacement of uncommon A-type felsic intrusions of similar age such as the Old Salobo Granite (2573 ± 2 Ma, Machado et al., 1991; ~2550 Ma, de Melo et al., 2017), as proposed by Tallarico et al. (2005). In any case, Cu-Au mineralisation at the Salobo deposit appears to have been synchronous with ductile and/or brittle-ductile deformation at medium to low grade metamorphic conditions (~650°C to <350°C) within the multiply-reactivated Cinzento Shear Zone (Souza & Vieira, 2000; de Melo et al., 2017). To the west of Salobo along the Cinzento Shear Zone, a syn-deformational setting also has been reported for the Igarapé Cinzento (Alvo GT46) IOCG deposit, although here breccia-hosted mineralisation is controlled by brittle-ductile faults cross-cutting the Cinzento Shear Zone (Xavier et al., 2010; de Freitas Toledo et al., 2019). Breccias also host the Igarapé Bahia (including Alemão) IOCG deposit near the Carajás Fault ~25 km south of the Salobo deposit, where breccia fragments and Cu-sulfidic matrix in some cases exhibit a tectonic foliation (Ronzê et al., 2000). The Gameleira Cu-Au deposit, ~30 km southeast of Salobo along the Cinzento Shear Zone, is a possible example of Neoarchean IOCG mineralisation overprinted by Paleoproterozoic Cu-Au ore. Texturally early banded quartz-grunerite-magnetite rock with Cu sulfides (2614 ± 14 Ma, Re-Os molybdenite age, Marschik et al., 2005) is cut by vein

networks of quartz, biotite, Cu-sulfides, and minor REE, F, Co, Ni, and B minerals dated at 1908 ± 7 Ma (^{40}Ar-^{39}Ar biotite, Pollard et al., 2019). Another example is the Sossego-Curral orebody (1879 ± 4 to 1904 ± 5 Ma, U-Pb monazite, Moreto et al., 2015a) which lies <1 km east of the Neoarchean Fe-oxide-rich Sequeirinho IOCG orebody of the Sossego deposit. Similar Paleoproterozoic ages have been reported for other Cu-Au vein-type and breccia-hosted deposits lacking significant iron oxides in the Carajás Domain, including Alvo 118 (1869 ± 7 Ma, U-Pb xenotime, Tallarico, 2003; 1885 ± 4 Ma, ^{40}Ar-^{39}Ar biotite, Pollard et al., 2019), Breves (1886 ± 5 Ma, ^{40}Ar-^{39}Ar biotite, Pollard et al., 2019), and Estrela (1896 ± 7 Ma, ^{40}Ar-^{39}Ar biotite, Pollard et al., 2019). These ages overlap with the ~1880 Ma ages of several A-type granites identified in the Carajás Domain (Machado et al., 1991; Moreto et al., 2015b), although a close spatial association (e.g. <2 km) with the ~1900-1860 Ma Cu-Au deposits is only apparent at Gameleira (cf. Pollard et al., 2019) and possibly at the Sossego-Curral orebody which is situated >4 km from a large ~1880 Ma granite (Moreto et al., 2015a).

In summary, Neoarchean IOCG deposits of the Carajás province formed during two episodes of regional tectonothermal activity, at ~2720-2680 Ma and ~2580-2535 Ma. The first event was post-peak metamorphic with shear-hosted and other syn-tectonic mineralisation forming during a possible switch from transpressional to transtensional tectonism. This IOCG deposit formation overlapped temporally with the felsic A-type Planalto Suite and likely coeval mafic intrusive magmatism. Deposits in the second Neoarchean IOCG event were also shear-hosted and syn-tectonic, and were roughly coeval with another period of A-type felsic magmatism.

3. Guelb Moghrein Cu-Au deposit, Mauritania – Neoarchean/Paleoproterozoic

The Guelb Moghrein Cu-Au deposit (57.7 Mt of sulfide ore @ 1.15 % Cu, 0.69 g/t Au plus 9.6 Mt of oxide ore) is hosted mainly by metacarbonate rocks within a package of dominantly meta-mafic igneous rocks, metacarbonate, banded iron formation and felsic meta-volcanic rocks (Kolb et al., 2010; Kirschbaum & Hitzman, 2016; Kolb & Petrov, 2016). Although no geochronology is available for the host rocks, and syn-mineralisation proximal igneous intrusive rocks are not evident at the Guelb Moghrein deposit (Kolb et al., 2010), some of the coarse grained amphibolites have been interpreted as meta-gabbros. A volcanic arc setting of magmatism was proposed by Kolb et al. (2008). Early sodic and distal biotite alteration of amphibolites within and adjacent to shear zones, and siderite development, were succeeded by grunerite-cummingtonite-magnetite-graphite alteration and then Cu-Fe sulfide and Au mineralisation (Kolb et al., 2010; Kirschbaum & Hitzman, 2016; Kolb & Petrov, 2016). An age of 2492 ± 9 Ma has been reported for hydrothermal monazite and xenotime associated with chalcopyrite and pyrrhotite (Meyer et al., 2006). Much of the Cu-Au mineralisation is hosted by breccias attributed to a regional D2 thrusting and shearing event at upper greenschist facies conditions, which overprinted an earlier thrusting event at amphibolite facies conditions (Kolb et al., 2010). Alteration and Cu-Au mineralisation therefore can be described as post-peak metamorphic, syn-tectonic, and synchronous with compressional deformational. A later hydrothermal event at lower greenschist facies conditions resulted in magnesian metasomatism (chlorite, anthophyllite, talc) and has been dated at 1742 ± 12 Ma (Meyer et al., 2006).

4. Kiruna province, Sweden – Paleoproterozoic IOA, IOCG and other Cu-Au deposits

The Archean to Paleoproterozoic northern Fennoscandian shield in northern Sweden, Finland and Russia hosts a range of mainly Paleoproterozoic Fe, Cu, Au, Ni and Zn deposits (Billström et al., 2010; Martinsson et al., 2016). Best known for its large Fe deposits such as the Kiirunavaara iron oxide-apatite (IOA) deposit at Kiruna township, the Norbotten region of northern Sweden also contains the large porphyry style Aitik Cu-Au-Ag (-Mo) deposit (500 Mt @ 0.4% Cu, 0.2 g/t

Au, Wanhainen et al., 2005; Wanhainen & Martinsson, 2010), several small Cu-Au-Fe deposits described as IOCG deposits, skarn-related Fe deposits, and stratabound to stratiform Cu-Zn-Pb volcanic-hosted deposits such as the Viscaria Cu-Zn deposit (Weihed et al., 2005; Billström et al., 2010; Martinsson et al., 2016). There are also a diverse range of 'epigenetic Au and Cu-Au' deposits including orogenic Au deposits that extend across northern Fennoscandia from the Norbotten region to the Central Lapland region of Finland (Billström et al., 2010). The metallogenic province of the Norbotten region is referred to as the Kiruna province in the present study.

The northern Fennoscandian shield is an important example of a metallogenic province with both IOA and Cu-Au-Fe deposits including IOCG deposits, and where sufficient new geochronology data are available to constrain their relative timing. Five key events can be recognised during the period ~1890 Ma to ~1750 Ma (Fig. S2, right side, E1-E5), representing early magmatism and IOA and porphyry-style Cu-Au (-Mo) mineralisation, a regional tectonothermal event, a period of initial IOCG mineralisation, further tectonism and magmatism, and a second period of IOCG mineralisation. While many of these events have been previously recognised (e.g. Bergman et al., 2001; Billström et al., 2010; Martinsson et al., 2016), the recent new geochronological data allows some further refinement of the metallogenic evolution. The following descriptions summarise the geological setting and key metallogenic features of each event.

Archean basement is overlain by 2.50-1.96 Ga supracrustal rocks and mafic-ultramafic intrusions mainly in Finland and also in the Kiruna district where they are known as the Kovo Group and Kiruna Greenstone Group. These predominantly mafic-ultramafic to intermediate volcanic sequences with lesser mafic tuff, black schist and minor carbonate units are unconformably overlain by volcanic and sedimentary rocks of the Kurravaara Conglomerate, Porphyrite Group (mainly calc-alkaline mafic-intermediate volcanic rocks) and the Kiirunavaara Group (mainly alkaline intermediate to felsic volcanic rocks; Billström et al., 2010; Martinsson et al., 2016. Earlier and recently available high quality zircon U-Pb geochronology indicates deposition of these supracrustal rocks mainly at ~1884-1878 Ma (Fig. S2; Welin, 1987; Edfelt et al., 2006; Westhues et al., 2016; Billström et al., 2019). The unconformably overlying Hauki and Maatavaara quartzites in the Norbotten region are stratigraphically equivalent to the epiclastic-dominated Kumpu Group in Finland (Billström et al., 2010) which has a maximum depositional age of ~1870 Ma (Fig. S2; Köykkä et al., 2019). Calc-alkaline felsic and mafic intrusions of the Haparanda suite were emplaced from ~1886 Ma to ~1872 Ma with a possible later phase at ~1856-1846 Ma (Fig. S2); the initial phases may be co-magmatic with the Porphyrite Group volcanics (Martinsson et al., 2016). The temporally overlapping but partly later and compositionally separate Perthite-Monzonite suite (1882-1860 Ma, Fig. S2; Bergman et al., 2001; Westhues et al., 2016; Sarlus et al., 2018) may be co-magmatic with the alkaline Kiirunavaara Group volcanics (Martinsson et al., 2016).

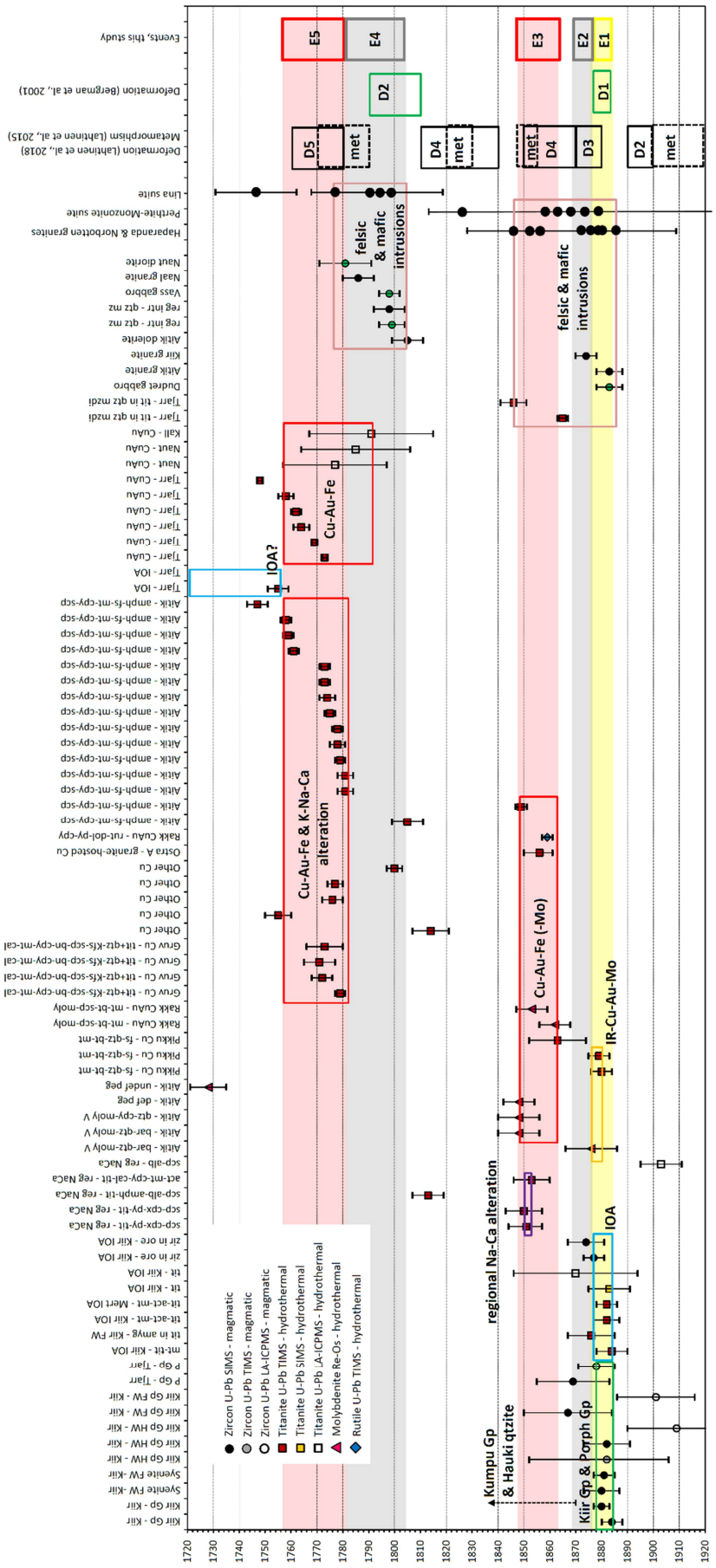

Figure S2. Synthesis of geochronology for mineralisation, tectonic, magmatic and supracrustal depositional events for the Kiruna-Norbotten region, northern Sweden.

Previous workers recognised a major metallogenic event at ~1920-1870 Ma (Billström et al., 2010) or 1890-1880 Ma (Martinsson et al., 2016) when major IOA deposits together with porphyry style Cu-Au (-Mo) and IOCG deposits formed coevally with calc-alkaline and/or alkaline volcanic and intrusive magmatism. A second epigenetic Cu-Au event was also recognised at 1850-1790 Ma (Billström et al., 2010) or ~1780 Ma (Martinsson et al., 2016). Building on this broad temporal framework, the currently available geochronological data are interpreted here as indicating a first event at ~1884-1876 Ma, labelled E1 in Figure S2. This event involved formation of major IOA deposits and porphyry-style Cu-Au (-Mo) deposits contemporaneously with the Porphyry Group and Kiirunavaara Group volcanic and associated syenitic subvolcanic intrusions (Romer et al., 1994; Martinsson et al., 2016; Westhues et al., 2016; Billström et al., 2019). The porphyry-style deposits evidently are uncommon yet include the large Aitik Cu-Au-Ag (Mo) deposit.

Previous workers have proposed a major regional deformation and metamorphic event, the Svecofennian orogeny, at ~1880 Ma (Bergman et al., 2001). According to Martinsson et al. (2016) this event occurred between volcanism of the Porphyrite and Kiirunavaara groups. However, Lahtinen et al. (2018) proposed a regional compressive tectonic event (D3) at ~1880-1870 Ma across northern Fennoscandia, which would largely postdate volcanism of the Porphyrite and Kiirunavaara groups as well as IOA and porphyry-style Cu-Au mineralisation. This reasonable geological scenario is consistent with the documented geology and geochronology for the Norbotten region. Accordingly, it is tentatively proposed herein that this D3 'Svecofennian' tectonothermal event of Lahtinen et al. (2018) occurred at ~1876-1870 Ma in the Norbotten region, and postdated volcanism, IOA and porphyry Cu-Au formation (Fig. S2, event E2).

The oldest dated Cu-Au deposit with abundant co-genetic iron oxides and other typical features of IOCG deposits is the Rakkurijarvi deposit, where Re-Os ages of 1862 ± 6 Ma and 1853 ± 6 Ma have been reported for molybdenite associated with magnetite (Smith et al., 2007, 2010). These ages are well supported by a U-Pb age of 1859 ± 2 Ma for hydrothermal rutile in chalcopyrite-carbonate-bearing veins (Martinsson et al., 2016). Similar ages have been published for Cu-bearing mineralisation and alteration at several other deposits including Aitik, Pikkujärvi and Östra Aijäjärvi, as well as for regional Na-Ca alteration (Wanhainen et al., 2005; Martinsson et al., 2016). At Rakkurijarvi breccia-hosted magnetite-rich Cu-Au mineralisation is partly hosted by a regional shear zone, with evidence of post-brecciation shear deformation (Smith et al., 2010). Although it is unclear whether initial Cu-Au mineralisation at Rakkurivarvi formed pre- or syn-shearing, the proposed timing of event E3 is consistent with the ~1870-1850 Ma regional D4 tectonothermal event described by Lahtinen et al. (2018) and with ductile deformation and metamorphism at ~1860-1850 Ma in the northern Norbotten region and Central Lapland to the east (Bergman et al., 2006; Lahtinen et al., 2015). A few data also indicate that felsic intrusions were emplaced regionally during the E3 event (Fig. S2; e.g. molybdenite-bearing pegmatite at Aitik, Wanhainen et al., 2005; and latest phases of the Haparanda and Perthite-Monzonite suites in northern Norbotten, Bergman et al., 2001, 2006; and the Aalinstunturi suite in Central Lapland, Lahtinen et al., 2018).

Widespread emplacement of the S-type granitic Lina suite occurred across northern Fennoscandia during ~1810-1770 Ma, as well as the first phase of the A- and I-type felsic intrusions of the Trans-scandinavian igneous belt (TIB) at ~1800 Ma (Fig. S2; Bergman et al., 2001). Recent work in the Norbotten region has also identified significant mafic intrusive activity around this period (Sarlus et al., 2018). Although a regional deformation event was previously recognised at ~1810-1790 Ma (D2 of Bergman et al., 2001) more recent work has refined the temporal framework so that the D5 event of Lahtinen et al. (2018) postdates the Lina Suite and early TIB magmatism (Fig. S2). This deformation was mainly partitioned into shear zones (Bergman et al., 2006). Timing constraints from U-Pb dating of monazite and zircon overgrowths near the Pajala Shear Zone in northern Norbotten indicate metamorphism at medium to high grades during possibly two stages at ~1830-1820 Ma and ~1790-1770 Ma (Fig. S2; Lahtinen et

al., 2015). Based on these observations a thermal event E4 at ~1805-1782 Ma is suggested in the present review, comprising regional felsic and mafic magmatism and commencement of metamorphism (Fig. S2).

A large number of U-Pb ages for hydrothermal titanite within Na-, Ca-, K- and Fe-rich alteration assemblages and Cu-Au mineralisation have been reported for the period ~1800-1750 Ma, defining a previously well recognised metallogenic event (e.g. Billström et al., 2010; Martinsson et al., 2016). The data compiled in Figure S2 shows that the titanite ages commence during the latest stages of the regional S-, A- and I-type bimodal magmatism and metamorphism (Bergman et al., 2006; R. Lahtinen et al., 2015), continue through the metamorphic event, and cover a period of regional deformation as documented in the Pajala Shear Zone (D5 of Bergman et al., 2006; Lahtinen et al., 2015, 2018). Accordingly, the timing of this metallogenic event has been refined herein to the period ~1782-1757 Ma (event E5, Fig. S2). Given the locally high grade metamorphic conditions (e.g. Bergman et al., 2006) it is unclear whether these titanite ages represent cooling ages, reset ages, and/or formation ages of hydrothermal titanite. The E5 metallogenic event includes relatively small iron oxide-bearing Cu-Au deposits such as Tjårrojåkka Cu-Au (Edfelt, 2007), Gruvberget Cu-Au and Nautanen Cu-Au (Martinsson et al., 2016). There are also alteration features of similar age at the Aitik Cu-Au (-Mo) deposit (Wanhainen et al., 2005). A somewhat older age range of ~1820-1790 Ma was proposed by Bauer et al. (2021) for their D2 regional deformation event, during which syn-deformational IOCG mineralisation was suggested to have formed within the Nautanen deformation zone. An overall 'post-orogenic collapse' tectonic environment was suggested for their D2 event.

The significance of two titanite U-Pb ages (1755 ± 4 Ma, 1694 ± 2 Ma) from the Tjårrojåkka IOA deposit, which is located ~500 m southeast of the Tjårrojåkka Cu deposit (Edfelt, 2007), is unclear. They may record a second relatively minor stage of IOA formation (Edfelt, 2007; Billström et al., 2010), or alternatively may be a consequence of resetting or new titanite growth overprinting an earlier-formed IOA deposit. Given the lack of other supporting ages for a second stage of IOA formation in the region, together with the fact that metamorphic conditions would have been capable of disturbing titanite U-Pb isotopic systems (e.g. 550-660°C, 1.5-1.8 kb in the Nautanen area, Sarlus et al., 2018), and also the widely reported textural relationships of Cu-Au mineralisation overprinting rather than co-precipitating with IOA mineral assemblages in the Norbotten region (e.g. Billström et al., 2010; Martinsson et al., 2016), a second stage of IOA formation seems unlikely and requires further testing.

In summary, the sequence of events described above for northern Fennoscandia has been explained within the geodynamic context of an evolving continental margin, as recently discussed by Lahtinen et al. (2015, 2018) and Lahtinen & Huhma (2019). Rifting and crustal attenuation of the Karelia continent between 2.44 Ga and 1.98 Ga led to passive margin sedimentation including siliclastics, carbonate rocks, iron formations and local evaporites, as well as rift-related (mainly mafic) magmatism (Billstrom et al., 2010). Subduction along the western margin resulted in a series of magmatic arcs and collisions between ~1920 Ma and ~1750 Ma. Subduction-generated calc-alkaline igneous rocks of the Porphyrite Group and Haparanda Suite granitoids and then alkaline igneous rocks of the Kiirunavaara Group and Perthite-Monzonite Suite, together with IOA and porphyry-style Cu-Au deposits (Fig. S2, E1) were subjected to compressional tectonics during collision of a crustal block from the southwest (Fig. S2, event E2, and D3 of Lahtinen et al., 2018). A change in plate motion direction resulted in north-northwest-directed shortening and orocline development across northern Fennoscandia during the D4 event of Lahtinen et al. (2018), broadly coeval with metamorphism and formation of the first major IOCG deposits such as Rakkurijarvi at ~1864-1848 Ma (Fig. S2, E3). This early Cu-Au-Fe hydrothermal activity, including regional Na-Ca alteration, therefore appears to have occurred post-subduction in a syn-orogenic setting distal from the continental margin, perhaps associated with a switch in plate motion direction. Interestingly, Lahtinen et al. (2018) described some extensional domains within the Central Lapland region during their D4 event. The second major Cu-Au-Fe event (Fig. S2, E5, ~1782-1757

Ma) also appears to have been closely related to preceding orogenic events, perhaps in a post-orogenic extensional setting (Bauer et al., 2021) and distal from new arc magmatism along the continental margin well to the west (Lahtinen et al., 2018).

5. Great Bear magmatic zone, Canada – Paleoproterozoic Au-Co-Bi, Cu and U deposits

The Paleoproterozoic Great Bear magmatic zone (GBMZ) in northwestern Canada hosts well documented hydrothermal alteration and diverse types of mineralisation (Cu, Au, U, Co, Mo, V, etc) including small Au, Cu and U resources that have been described within the context of 'iron oxide and alkali-altered systems' (Gandhi & Bell, 1989; Corriveau, 2007; Mumin et al., 2007, 2010; Corriveau et al., 2010, 2016). Igneous rocks of the GBMZ are interpreted to have formed in a continental margin magmatic arc setting above an easterly-dipping subducting slab (Hildebrand et al., 1987; Ootes et al., 2017). Arc magmatism, initiated at ~1876 Ma, was preceded by the short-lived Calderian orogeny which was caused by collision of an island arc (Hildebrand et al., 2010) or accretion of a previously rifted arc (Hottah terrane) with the western margin of the Slave Craton (Ootes et al., 2017). Rather than fully postdating the Calderian orogeny, as previously thought, early phases of the GBMZ magmatism (~1876-1873 Ma) are now interpreted as syn-deformational within a transpressional regime late within the Calderian orogeny, and exhibit 'syn-collisional' and 'volcanic arc' calc-alkaline geochemical signatures (Montreuil et al., 2016; Ootes et al., 2017). The later magmatic phases (~1869-1866 Ma) show greater components of 'within-plate' and 'transitional' signatures and some units have shoshonitic compositions indicating a transition from collisional to a post-collisional and extensional setting (Montreuil et al., 2016; Ootes et al., 2017). The final stages of magmatism at ~1860-1850 Ma comprise extensive and mainly A-type granites. Deformation style also transitioned from dominantly ductile and brittle-ductile up to ~1871-1869 Ma to brittle deformation (Montreuil et al., 2016). Supracrustal rocks are areally subordinate to intrusive rocks in the GBMZ, and comprise small inliers of ~1880 Ma metasedimentary rocks of the Treasure Lake Group and older rocks of the Hottah terrane, together with somewhat larger areas of mainly andesitic and felsic volcanic rocks forming part of the ~1876-1860 Ma Great Bear magmatism (see summaries by Slack et al., 2016; Ootes et al., 2017).

Iron oxide and alkali alteration such as sodic, sodic-calcic, Fe skarn and high-temperature Ca-Fe±K alteration commenced during the earlier stages of magmatism within a regime of ductile to brittle-ductile deformation (Corriveau et al., 2010; Montreuil et al., 2016). Syn- to pre-deformational Mo-Cu-U mineralisation associated with magnetite-K-feldspar ± biotite alteration at the Nori prospect has yielded a molybdenite Re-Os age of 1877 ± 8 Ma (Acosta-Góngora et al., 2015; Montreuil et al., 2016), and deformed Mo-U-bearing veins with biotite, tourmaline and minor magnetite and chalcopyrite in the Southern Breccia Zone have a molybdenite Re-Os age of 1873 ± 6 Ma (Ootes et al., 2010). Magnetite-biotite-amphibole-K-feldspar alteration and Au-Co-Bi-As mineralisation at the NICO deposit (33 Mt @ 1.0 g/t Au, 0.11 % Co, 0.14 % Bi, 0.04% Cu, Acosta-Góngora et al., 2015) appear to have formed during the waning stages of brittle-ductile deformation, inferred at ~1870 Ma (Acosta-Góngora et al., 2015; Montreuil et al., 2016) which is within error of an age of 1865 ± 9 Ma for deformed molybdenite interpreted to have formed during an early hydrothermal stage (Acosta-Góngora et al., 2015). A later retrograde stage with minor Cu, Bi, hematite and chlorite at NICO was related to brittle deformation-controlled IOCG style alteration-mineralisation, according to Montreuil et al. (2016). An undeformed ~1868 Ma dyke cuts the Au-Co-Bi ore zone and therefore sets a minimum age for such ore at NICO (Acosta-Góngora et al., 2015) but not necessarily for the overprinting Cu-hematite-chlorite assemblage. Montreuil et al. (2016) further described IOCG and albitite-hosted U mineralisation associated with brittle deformation features such as brittle fractures and breccias, although no radiometric ages of such hydrothermal assemblages have been reported. An end to Na-Fe-Ca-K alteration and related hydrothermal activity by ~1866 Ma has been suggested, as unaltered plutons of this age

cut the alteration. Similarly, Cu-U-V mineralisation at the FAB prospect associated with K-feldspar – amphibole – magnetite/hematite – biotite veins and breccias has been constrained to the period ~1870-1867 Ma using zircon U-Pb ages of pre- and post-mineralisation intrusions (Montreuil et al., 2016). No radiometric age constraints are available for the small magnetite-hematite-fluorite-rich breccia-hosted Sue Dianne Cu (-Au) deposit (resource of 8.4 Mt @ 0.8 % Cu, 0.07 g/t Au, Hennessey & Puritch, 2008 reported in Corriveau et al., 2010).

Overall, the GBMZ transitioned from a late-orogenic phase of mainly intermediate-composition arc magmatism, brittle-ductile compressive deformation and early magnetite-rich K-Ca-Na alteration with relatively small Au-Co-Bi and Mo ± U deposits, to a later phase of post-orogenic K-rich arc-related magmatism, extensional and brittle deformation, and hematite-magnetite-rich K-Ca-Na alteration with currently known small resources of Fe-oxide-associated Cu ± U mineralisation. The timing of the later stage of Cu mineralisation has yet to be directly dated although it seems likely this was prior to 1865 Ma (Montreuil et al., 2016).

Apatite-bearing magnetite-actinolite alteration and deposits of modest size also have been described in the GBMZ, and have been likened to Kiruna type IOA deposits (Hildebrand, 1986). They are recognised as forming the core parts of zoned hydrothermal IOAA systems with inner sodic and high-temperature Ca-Fe ± Mg zones (± skarn) grading outwards and upwards to high-temperature K-Fe, low-temperature K-Fe-H-CO_2 and finally Si zones in distal and/or shallow zones or alteration facies (Corriveau et al., 2010a, 2010b, 2016; Mumin et al., 2010). These systems along with associated Au, Co, Bi, Cu and U mineralisation are interpreted to be spatially, temporally and genetically associated with GBMZ magmatism (Mumin et al., 2007, Corriveau et al., 2010a, 2010b, 2016; Acosta-Góngora et al., 2015; Montreuil et al., 2016; Ootes et al., 2017).

6. Tennant Creek goldfield, Australia – Paleoproterozoic Au-Cu-Bi-Fe deposits

High-grade Au-Cu-Bi deposits in the Tennant Creek goldfield are hosted by epigenetic magnetite- and/or hematite-rich bodies, locally known as ironstones, within a dominantly siliciclastic sedimentary Paleoproterozoic basin in the North Australian Craton. Of the >500 known ironstones only several dozen contain economic grades of Au and/or Cu and/or Bi, the vast majority being barren of such metals (Wedekind et al., 1989). Ironstones appear to be confined to the Warramunga Formation, a sequence of low metamorphic grade turbiditic greywackes, siltstones and shales with distinctive yet volumetrically minor intervals of 'hematitic shales' and several felsic tuff units. The Warramunga Formation was deposited at ~1865-1860 Ma (Fig. S3; Compston, 1995; Smith, 2001; Donnellan, 2013; Maidment et al., 2013). Disseminated magnetite is relatively abundant (up to several volume percent) in lower parts of the sequence, whereas the hematitic shales and most ironstones appear to be most common in upper parts of the Warramunga Formation. No carbonaceous units are known in the Tennant Creek goldfield, but minor carbonate-rich rock occurs within some hematitic shale intervals.

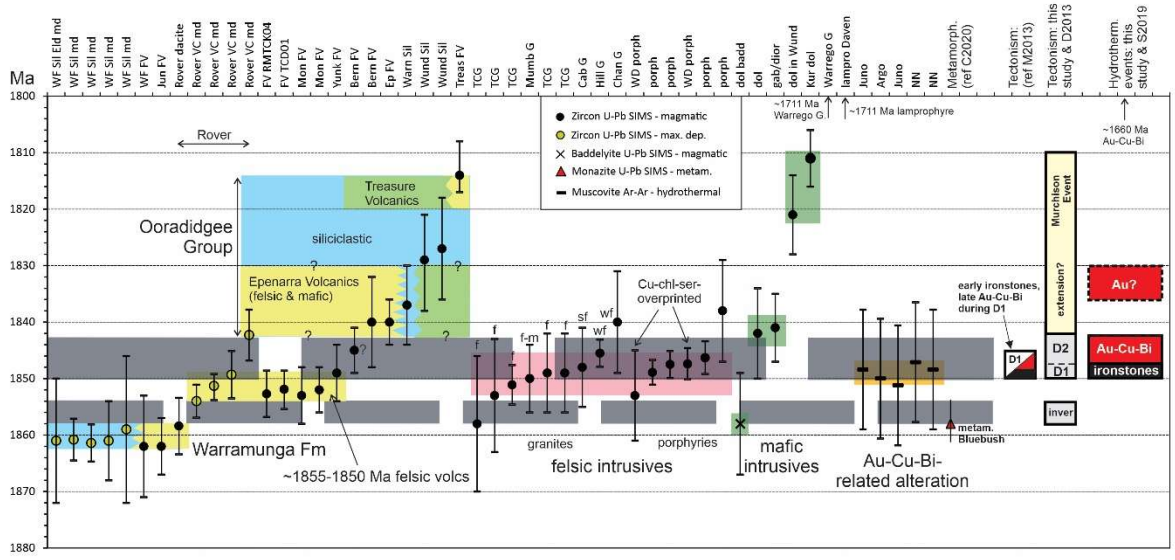

Figure S3. Synthesis of geochronology for mineralisation, tectonic, magmatic and supracrustal depositional events for the Tennant Creek goldfield and Rover field, northern Australia, from 1800 Ma to 1880 Ma. Abbreviations for granite samples: f – foliated, f-m – foliated to massive, sf – strongly foliated, wf – weakly foliated; abbreviations for rock units: WF – Warramunga Formation, Jun – Junalki Formation, VC – volcaniclastic, FV – felsic volcanic, Mon – Monument Formation, Bern – Bernborough Formation, Ep – Epennara Volcanics, Warn – Warnbro Siltstone, Wund – Wundirgi Formation, Treas – Treasure Volcanics, Mumb G – Mumbilla Granite, TCG – Tennant Creek Granite, Cab G – Cabbage Gum Granite, Hill G – Hill of Leaders Granite, Chan G – Channingum Granite, WD porph – White Devil porphyry, dol – dolerite, gab/dior – gabbro/diorite, Kur dol – Kurinelli dolerite, lampro Daven – lamprophyre, Davenport region, NN – Nobles Nob deposit. References: Compston (1995), Smith (2001), Claoué-Long et al. (2008a, 2008b), Fraser et al. (2008), Donnellan (2013), Maidment et al. (2013), Skirrow et al. (2019), Cross et al. (2020), Huston et al. (2020).

The Warramunga Formation is intruded by widespread I-type granites and felsic porphyries of the Tennant Suite dated between ~1854 Ma and ~1846 Ma (Fig. S3; Compston, 1995; Smith, 2001; Donnellan et al., 1995; Donnellan, 2013; Maidment et al., 2013). This magmatism accompanied the D1 tectonothermal event, initially correlated with the Barramundi Orogeny of northern Australia (Compston, 1995) and then named the Tennant Event which was constrained by Maidment et al. (2013) to the period ~1850-1845 Ma. The Ooradidgee Group, a sequence of bimodal felsic and mafic volcanic and siliciclastic sedimentary rocks, was emplaced unconformably upon older units including the Warramunga Formation (Fig. S3; Donnellan et al., 1995; Donnellan, 2013). The Ooradidgee Group includes the Epenarra Volcanics near its base and the Treasure Volcanics near its top (1840 ± 4 Ma, and 1814 +3/-6 Ma, respectively; Claoué-Long et al., 2008a). This sequence is overlain by siliciclastic and bimodal volcanic rocks of the layer-cake-like Hatches Creek Group, deposited from 1814 ± 3 Ma to ~1800 Ma (Claoué-Long et al., 2008a). Constraining the timing of earliest Ooradidgee Group deposition has been problematic, yet it is important in understanding the tectonic and metallogenic evolution. Earlier studies placed several ~1855-1850 Ma felsic volcanic units (e.g. Monument Formation, Yunkulungu Formation) at the base of the Ooradidgee Group (Donnellan et al., 1995; Smith, 2001; Donnellan, 2013; Maidment et al., 2013). confirmed the presence of ~1855-1850 Ma felsic volcanic units in several additional locations, peripheral to the exposed Tennant Creek inlier, and also included these units within the Ooradidgee Group. However, there are reasons to believe that the ~1855-1850 Ma volcanic rocks may constitute a package that is stratigraphically separate from both the Ooradidgee Group and the Warramunga Formation, as discussed further below.

The latest major magmatic event in the Tennant Creek region includes S-type granites of the Devils Suite, with zircon U-Pb ages around 1710-1715 Ma (Wyborn et al., 1998; Donnellan, 2013). The Warrego Granite forms a large intrusion in the northwest part of the Tennant Creek province, and recently has been confirmed to be the same age as the Devils Suite (1711 ± 10 Ma, Huston et al., 2020). Finally, the timing of volumetrically minor lamprophyre dykes in the Tennant Creek region is best constrained by a U-Pb zircon age of 1711 ± 3 Ma (Claoué-Long et al., 2008b) indicating they may be broadly coeval with the Devils Suite magmatism.

The timing of deformation and metamorphic events has been only partly resolved in the Tennant Creek province. Deformation of the Warramunga Formation is characterised by tight, upright, folding and brittle-ductile shearing at low metamorphic grade (Rattenbury, 1994), and occurred during the regional D1 compressional Tennant Event (Wedekind et al., 1989; Compston, 1995; Donnellan et al., 1995; Donnellan, 2013; Maidment et al., 2013). This deformation also affected many of the Tennant Suite felsic intrusive rocks, with earlier intrusions exhibiting strong foliation and later phases tending to have weak or no tectonic foliation (Fig. S3). A second regional deformation event (D2, or D1a of Donnellan, 2013) also has been recognised which resulted in a locally well developed second tectonic foliation, brittle-ductile shearing, and other related deformation features (Nguyen et al., 1989; Skirrow, 1993, 2000; Donnellan et al., 1995; Skirrow & Walshe, 2002; Donnellan, 2013). Broad open folding of the Hatches Creek Group and older units to the south of Tennant Creek represents the D3 regional deformation event (Donnellan, 2013), which also may have affected the Tennant Creek province.

Although the timing of metamorphism is not well constrained in the vicinity of the Au-Cu-Bi deposits, metamorphic monazite in deformed amphibolite facies rocks at the southwest margin of the Tennant Creek goldfield (Bluebush area) records a metamorphic age of ~1858 Ma (Cross et al., 2020). This age appears at odds with the ~1850-1845 Ma timing of the D1 event proposed by Maidment et al. (2013). Also problematic is the overlapping ages of the earliest Ooradidgee Group volcanism, if this stratigraphic sequence commenced deposition at ~1855-1850 Ma as previously proposed, with the ~1850-1845 Ma age of D1 inferred by Maidment et al. (2013). It seems unlikely that such volcanism could have occurred at the same structural level in the same areas as D1 tight folding, brittle-ductile shearing, and low grade metamorphism. Furthermore, at least parts of the Ooradidgee Group have been affected only by open folding during D3, whereas the Warramunga Formation was tightly folded (e.g. Smith, 2001). Finally, the presence of minor ironstones within the 'Ooradidgee Group', and intrusion of Tennant Suite granites into lower parts of the 'Ooradidgee Group' (Smith, 2001), are difficult to explain if the Ooradidgee Group deposition commenced at ~1855 Ma and continued through the Tennant Event at ~1850-1845 Ma as previously proposed.

These relationships and inconsistencies may be reconciled in a revised event sequence as shown in Figure S3. This involves: (a) deposition of the ~1855-1850 Ma felsic volcanic rocks as a separate unit unconformably and/or disconformably upon the Warramunga Formation and prior to the ~1840 Ma Epenarra Volcanics of the Ooradidgee Group, (b) deposition of this volcanic unit during and/or after ~1858 Ma exhumation of the latter formation, which coincided with amphibolite facies metamorphism at depth at ~1858 Ma in the Bluebush area, and which also records the initial inversion of the Warramunga Formation, (c) continued deformation of the Warramunga Formation and ~1855-1850 Ma volcanic sequence within a fold and thrust belt (Rattenbury, 1992, 1994) during the low metamorphic grade Tennant Event at ~1850-1845 Ma in what has been termed the D1 deformation event, (d) a progressive rotation of stress axes resulting in the D1a event of Donnellan (2013) (termed the D2 deformation herein), (e) post-D2 deposition of the ~1840-1814 Ma Ooradidgee Group. There are implications of this revised model for the numbers of tectonic foliations in units of different age, which would provide a test of the proposed event sequence, and also for presence/absence of hydrothermal systems, as explained below.

Hydrothermal activity was closely linked to the regional tectonothermal evolution. Structural relationships indicate that the massive to banded magnetite-hematite-quartz-chlorite ironstones formed epigenetically during D1 tight folding, as generally steeply dipping lens-shaped and irregular bodies that cut stratigraphy at commonly high angles and occur within shear and fault zones with minor offsets (Wedekind et al., 1989; Rattenbury, 1992, 1994). Some ironstones have outer zones rich in Ca-Mg carbonates and/or talc (Wedekind et al., 1989). Whereas chloritic alteration with minor muscovite is ubiquitous, biotite alteration is uncommon (e.g. Navigator 6; West Peko), as are Fe silicates such as stilpnomelane, minnesotaite and greenalite (West Peko deposit; Skirrow, 1993, 2000; Skirrow & Walshe, 2002).

The timing of Au-Cu-Bi mineralisation also has been problematic. Ore deposits in the goldfield range from Cu-Au-Bi-rich magnetite-pyrrhotite-pyrite styles to Au-Bi-rich magnetite- and/or hematite-rich styles (Wedekind et al., 1989; Huston et al., 1993; Skirrow, 2000; Skirrow & Walshe, 2002). The vast bulk, if not all, of the sulfides and Au overprinted the magnetite ± hematite-rich ironstones, and occur in syn-deformational brittle-ductile to brittle style veins, replacements and breccias cutting the ironstones and also occurring outside the ironstones in fault and shear zones (Wedekind et al., 1989; Huston et al., 1993; Skirrow, 2000; Skirrow & Walshe, 2002; Cuison et al., 2014). Early dating studies of hydrothermal muscovite associated with Au mineralisation indicated an ^{40}Ar-^{39}Ar age of ~1820-1830 Ma, interpreted as a minimum age of ore formation (Compston & McDougall, 1994). This age, during the Ooradidgee Group volcanism, was apparently inconsistent with the syn-deformational timing of mineralisation and with known (earlier) tectonothermal and magmatic events (Fraser et al., 2008). Re-calibration of the ^{40}Ar-^{39}Ar ages based on revised decay constants and standards led Fraser et al. (2008) to revise the ^{40}Ar-^{39}Ar ages to ~1850 Ma, in close alignment with the Tennant Event of Maidment et al. (2013), although the uncertainties are ca. ± 10 million years (Fig. S3).

It has been previously proposed that the main Au-Cu-Bi mineralisation occurred during D2 (Nguyen et al., 1989; Skirrow, 1993; Skirrow & Walshe, 2002) rather than during D1 as suggested by some other workers (e.g. Maidment et al., 2013). The absolute timing of the D2 event has not been determined directly. However, the 1847 ± 3 Ma age of a felsic porphyry intrusion at the White Devil deposit, which was overprinted by Au-Cu-Bi-related hydrothermal alteration, provides a maximum age of Au-Cu-Bi mineralisation at this site (Huston & Cozens, 1994; Maidment et al., 2013). There are no robust isotopic minimum age constraints on Au-Cu-Bi ore formation other than the ^{40}Ar-^{39}Ar ages which have uncertainties ranging to as young as ~1840-1836 Ma (Fig. S3; Fraser et al., 2008). Therefore, on balance, the most likely timing of the syn-D2 major Au-Cu-Bi mineralisation is inferred to have been between ~1847 Ma and ~1842 Ma, prior to emplacement of the Ooradidgee Group but after at least some of the felsic porphyries. Although the suggested timing of Au-Cu-Bi overlaps with that proposed by Maidment et al. (2013) a syn-D2 rather than syn-D1 timing is suggested here, extending to as young as ~1842 Ma.

Several lines of evidence suggest there was more than one base-precious metal mineralisation event in the Tennant Creek goldfield. First, Pb isotope data for Pb-rich minerals (mostly galena) indicates differences in composition between less radiogenic Cu-rich Au-Bi mineralisation in the Tennant Creek goldfield and more radiogenic Cu- and Au-rich mineralisation (Huston et al., 2020). The difference may be explained either by a ~10-15 m.y. age difference, and/or by different sources of lead (Huston et al., 2020). Conceivably, if the less radiogenic Cu-Au-Bi mineralisation formed at ~1847-1843 Ma as suggested above, then the more radiogenic Cu- and Au-rich mineralisation could have formed as late as ~1830 Ma if its different isotopic composition is due to its younger age rather than a different Pb source (Fig. S3). A second, late-stage, Au event is also supported by the presence of texturally late high grade Au with hematite in breccias at the Eldorado deposit, representing a brittle deformation style that is rare in Au-Cu-Bi deposits of the Tennant Creek goldfield (Skirrow & Walshe, 2002). Moreover, high grade Au mineralisation in 'pods' at the Warrego deposit paragenetically overprints Cu-Au-Bi mineralisation (Wedekind et al., 1989).

An even later style of Au-Cu-Bi mineralisation in shear zones outside ironstones may have formed at ~1660 Ma, possibly via re-distribution of earlier-formed mineralisation (Skirrow et al., 2019). This hydrothermal activity and other thermal events around the age of the Devils Suite magmatism (~1710 Ma) may be the cause of the disturbance reported in K-Ar, Ar-Ar (e.g. Compston & McDougall, 1994) and perhaps Re-Os isotopic data (e.g. McInnes et al., 2008).

Implications of these interpretations are (1) ironstones and syn-D2 Au-Cu-Bi mineralisation may not be restricted to the Warramunga Formation but also could exist within the ~1855-1845 Ma felsic volcanic sequence, (2) Cu and Au mineralisation with or without hematite hosted by brittle deformation features may be present within the older parts of the Ooradidgee Group and any older units.

In summary, Au-Cu-Bi mineralisation in the Tennant Creek province can be described as syn-orogenic as it formed syn-deformationally at initially brittle-ductile and low metamorphic grade conditions. Mineralisation post-dated the early stages of magmatism of the Tennant Suite and associated porphyries, and was coeval with the latest stages of this magmatism. Donnellan (2013) suggested that the D1 event was compressional whereas the D1a (equivalent to D2 herein) event may have been transpressional, in response to a rotation of stress fields. Given that the Ooradidgee Group contains bimodal volcanics, possibly indicating an extensional tectonic regime, it is inferred that Cu-Au-Bi mineralisation in the Tennant Creek goldfield formed during a switch from compressional (D1) to transpressional (D1a) tectonics prior to major regional extension (syn-Ooradidgee Group). Further work is required to test the proposed revised temporal and tectonic framework.

7. Gawler Craton and Curnamona Province - Mesoproterozoic IOCG (-U-REE) deposits

7.1 Overview of deposit types

The Gawler Craton is a Mesoarchean to Mesoproterozoic crustal element in south-central Australia hosting the Olympic Dam Cu-U-Au deposit, the world's largest IOCG deposit and largest uranium resource (10.73 Bt @ 0.72 % Cu, 0.30 g/t Au, 0.23 kg/t U_3O_8, 1.28 g/t Ag, measured + indicated + inferred resource, BHP, 2018, www.bhp.com). The Olympic Cu-Au province forms a >500 km length belt along the eastern margin of the Gawler Craton with major IOCG deposits in three districts that developed between ~1600 Ma and ~1575 Ma (Skirrow et al., 2002, 2007). In addition to Olympic Dam, this metallogenic province contains large Cu-Au resources at the Prominent Hill deposit (160 Mt @ 1.0 % Cu, 0.7 g/t Au, 3 g/t Ag, measured + indicated resources, OZ Minerals 2017, www.ozminerals.com) adjacent to the Mount Woods Inlier in the north, the Carrapateena and nearby Fremantle Doctor deposits (Carrapateena: 130 Mt @ 1.5 % Cu, 0.6 g/t Au, 7 g/t Ag, measured + indicated + inferred resources, OZ Minerals 2017; Fremantle Doctor: inferred resource of 104 Mt @ 0.7 % Cu, 0.5 g/t Au and 3 g/t Ag, OZ Minerals 2018, www.ozminerals.com) in the Olympic Dam district, and the Hillside deposit (337 Mt @ 0.60 % Cu, 0.14 g/t Au, measured + indicated + inferred resources, Rex Minerals 2013, www.rexminerals.com.au) in the Moonta-Wallaroo district in the south. Many other smaller Cu-Au deposits and prospects are known in the Olympic Cu-Au province, with or without significant iron oxides, along with regional-scale hydrothermal alteration. Small quartz-vein style copper deposits and greisen-hosted Mo-bearing mineralisation in the Moonta district are examples without significant iron oxides (Conor et al., 2010). West of the Olympic Cu-Au province, the Central Gawler gold province contains several small Au-only deposits characterised by quartz veinlet and disseminated mineralisation styles hosted by brittle-ductile shear zones (Ferris & Schwarz, 2003; Budd & Fraser, 2004; Budd & Skirrow, 2007; Fraser et al., 2007). A number of epithermal style hydrothermal systems with local Ag and Pb-Zn enrichments and advanced argillic alteration have also been described in the south-central part of the Gawler Craton (Nicolson et al., 2017).

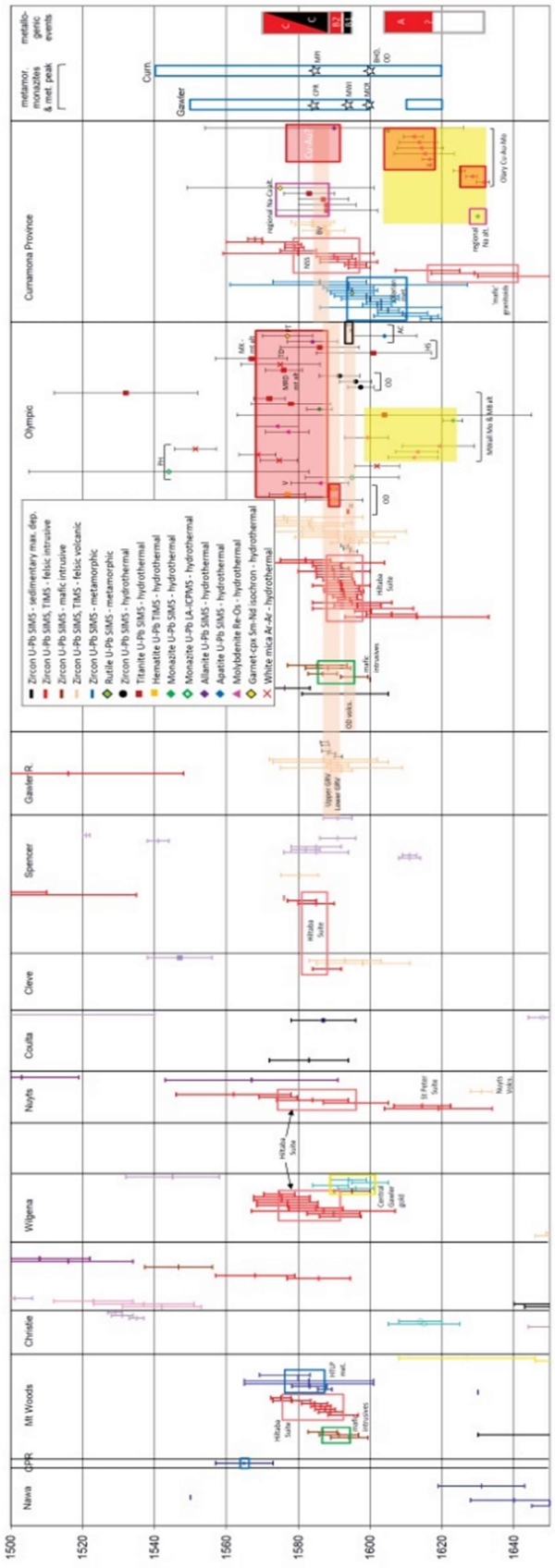

Figure S4. Synthesis of geochronology for mineralisation, tectonic, magmatic and supracrustal depositional events for the Gawler Craton and Curnamona Province, southern Australia. Names of lithostratigraphic names are listed along the top of the diagram (see Ferris et al., 2002) for locations and descriptions).

The Paleoproterozoic-Mesoproterozoic Curnamona Province lies ~150-200 km to the east of the Gawler Craton, separated by Neoproterozoic to Cambrian rocks of the Adelaide Fold Belt. Although differing in much of its pre-1750 Ma geology, the Curnamona Province shares many features of the Gawler Craton after this time. In particular, the distinctive igneous rocks of the early Mesoproterozoic Hiltaba Suite and Gawler Range Volcanics (GRV) in the Gawler Craton have equivalents in the Curnamona Province (Jagodzinski & Fricke, 2010; Schofield, 2010; Wade et al., 2012; Jagodzinski et al., 2016). The southwestern and central-western parts of the Curnamona Province, known as the Olary Domain, also contains several relatively small Cu-Au-Mo deposits and hydrothermal alteration that resemble aspects of the early Mesoproterozoic hydrothermal IOCG systems in the Gawler Craton. For these reasons the geological and metallogenic evolution of both crustal elements are described sequentially in each sub-section, below (Fig. S4).

7.2 Host rocks

Iron oxide-rich to iron oxide-poor Cu-Au deposits and related alteration in the Olympic Cu-Au province of the Gawler Craton are hosted by ~1850 Ma to ~1585 Ma rocks including felsic and mafic intrusions of the ~1850 Ma syn-orogenic Donington Suite (Hand et al., 2007; Reid, 2019), metasedimentary rocks of the ~1760-1740 Ma Wallaroo Group (Hand et al., 2007; Cowley, 2008), and felsic and mafic igneous rocks of the ~1600 Ma to ~1580 Hiltaba Suite and GRV. Although Meso- to Neoarchean rocks of generally medium-high grade metamorphic are widespread in basement to the west of the Olympic Cu-Au province, Archean rocks are also known within the province, represented by the low metamorphic grade Devils Playground mafic volcanics between the Olympic Dam and Prominent Hill deposits (Reid et al., 2009). A key host rock for IOCG and related mineralisation in the metallogenic province is the volcano-sedimentary Wallaroo Group and equivalents (Hand et al., 2007) which is dominated by siltstone and fine-grained psammite, with lesser calcsilicates, quartzites, iron-rich sediments, graphitic schists and thinly bedded sodium-rich calc-albitite sediments locally rich in scapolite. The latter sodic lithologies are taken as evidence of former evaporitic minerals or rocks (Conor, 1995; Skirrow et al., 2007; Conor et al., 2010). The volcanic component is bimodal with A-type felsic units which, together with the evaporitic and Fe-rich nature of the sediments, has led to the suggestion of an extensional setting such as a rift along the eastern margin of the Gawler Craton (Hand et al., 2007; Conor et al., 2010). The timing of upper greenschist to lower amphibolite facies metamorphism, cleavage development, folding and shearing of the Wallaroo Group (Conor et al., 2010) has not been tightly constrained but this unit appears to have been unaffected by the medium to high grade metamorphism during the ~1730-1690 Ma Kimban orogeny that was prevalent in the Gawler Craton to the west of the Olympic Cu-Au province (Reid & Fabris, 2015). More broadly, however, there is clear evidence of deformation associated with the ~1595-1575 Ma Hiltaba Suite in the Gawler Craton (Hand et al., 2007), as described further below.

The ~1730-1690 Ma Kimban orogeny and associated felsic intrusive magmatism in the Gawler Craton temporally overlaps with the ages of supracrustal rocks identified in the Curnamona Province, the Willyama Supergroup, where the oldest maximum depositional ages are ~1730-1720 Ma and the youngest are ~1640 Ma (Page et al., 2005; Conor & Preiss, 2008). Extensive quartz-albite rocks in the lower parts of the Willyama Supergroup (Thackaringa Group in the Broken Hill Domain and Curnamona Group in the Olary Domain) are interpreted as sodic-altered psammopelitic sedimentary rocks associated with evaporitic environments (Cook & Ashley, 1992). Minor iron formations are also present in the lower Willyama Supergroup. A-type felsic magmatism accompanied deposition of the Thackaringa and Curnamona groups which are unconformably overlain by the Upper Willyama Supergroup (Ashley et al., 1996; Fanning et al., 1998). This volcanic-sedimentary package is interpreted to have formed within a continental rift environment, with early crustal extension followed by sag-phase sedimentation (Willis et al., 1983; Conor & Preiss, 2008).

7.3 Metallogenic events in the Gawler Craton and Curnamona Province

Metallogenic event A: Hydrothermal activity in the late Paleoproterozoic in the Gawler Craton commenced at ~1620 Ma with Mo-bearing and greisen style mineralisation in the Moonta-Wallaroo district of the southern Olympic Cu-Au province (Fig. S4; Skirrow and Creaser, molybdenite Re-Os unpublished geochronological data). The timing of this early hydrothermal activity is supported by sparse dates from hydrothermal and/or metamorphic monazite and titanite in syn-deformational magnetite-biotite-albite and magnetite-amphibole-albite alteration of the Wallaroo Group, which record ages from 1623 ± 3 Ma to 1578 ± 11 Ma (Fig. S4; Conor, 1995; Raymond et al., 2002; Skirrow et al., 2002, 2007; Conor et al., 2010; Skirrow, 2010). Although magmatism of the ~1633-1608 Ma syn-tectonic and arc-related St Peter Suite (Swain et al., 2008; Reid et al., 2019) is known in the Gawler Craton only from far to the west of the Moonta-Wallaroo district, it temporally overlaps the period of metallogenic event A.

Metallogenic event A is also represented in the Curnamona Province. Several styles of Cu, Au, Mo and other mineralisation are known from the Olary Domain. Anomalous concentrations of Cu, Zn, Pb, As and Co occur in stratabound zones within the calc-silicate- and pelite-pyrrhotite-bearing Bimba Formation, immediately above the unconformity between the lower and upper parts of the Willyama Supergroup. This style of mineralisation, which lacks significant Fe-oxides, has been likened to 'redbed' or stratiform sedimentary Cu (-Co) deposits such as those in the Zambian copper belt and the Kupferschiefer in Europe (Cook & Ashley, 1992). Among the wide range of epigenetic sulfide deposits and occurrences in the Olary Domain (Bierlein et al., 1995) the White Dam Au (-Mo) deposit is distinctive in its lack of iron oxides, syn-deformational quartz-K-feldspar-plagioclase-biotite vein style, high Au:Cu ratio, and lower stratigraphic position within medium grade metamorphic host rocks, compared to the main Cu-Au-Mo deposits (Williams & Skirrow, 2000). Molybdenite has yielded Re-Os ages of ~1631 Ma, ~1616 Ma and ~1612 Ma for the White Dam deposit (Fig. S4; Skirrow et al., 2000). In contrast, the Kalkaroo, North Portia and Waukaloo Cu-Au-Mo deposits to the north of White Dam are hosted by lower metamorphic grade (upper greenschist facies) mainly albite ± magnetite-rich metasedimentary rocks, and exhibit evidence of both stratabound (Armistead et al., 2018) and transgressive vein and related replacement styles (Skirrow et al., 2000; Teale & Fanning, 2000; Williams & Skirrow, 2000). Although magnetite is common in bedding-transgressive quartz ± K-feldspar ± amphibole ± biotite veins with Cu-Au-Mo mineralisation much of the Cu-Au-Mo mineralisation occurs in stratabound replacements and discordant veins with little or no iron oxides (Williams and Skirrow, 2000; Teale and Fanning, 2000). Such mineralisation is therefore not strictly of IOCG style but can be likened to ISCG deposits and is broadly associated with magnetite-rich Cu-Au-Mo mineralisation in other parts of the same deposits (e.g. Kalkaroo). Dating of molybdenite has yielded ages of ~1628-1625 Ma at Kalkaroo and ~1615-1613 Ma at North Portia and Waukaloo (Fig. S4; Skirrow et al., 2000; Skirrow & Suzuki, unpublished data). Re-analysis of a Waukaloo sample returned a molybdenite Re-Os age of ~1605 Ma (Skirrow and Creaser, upublished data), in good agreement with the U-Pb SIMS age of ~1605 Ma for hydrothermal monazite associated with Cu-Au-Mo mineralisation at the North Portia deposit (Teale & Fanning, 2000).

Regionally extensive and stratabound sodic alteration in the Curnamona Province has been constrained by few isotope dates, the oldest of which is ~1630 Ma for monazite associated with albitisation near the North Portia Cu-Au-Mo deposit (Teale & Fanning, 2000). However, it is possible that some regional sodic alteration occurred much earlier, during and/or soon after deposition of the host sequences in the rift basin. Accordingly, it is suggested that earliest Mo (± Au) mineralisation may have commenced at ~1630-1620 Ma, with a possibly main period of Cu-Au-Mo mineralisation at ~1610-1605 Ma in the Curnamona Province. The earlier part of this broad metallogenic event A (Fig. S4) may predate the peak of the Olarian Orogeny at ~1600 Ma as recorded by U-Pb ages of metamorphic zircon overgrowths and monazite (Page et al., 2005; Forbes et al., 2007), and therefore could represent pre-orogenic mineralisation (Armistead et al., 2018). However, the later and arguably most important Cu-Au mineralisation within metallogenic

event A at ~1605 Ma in the Curnamona Province appears to temporally overlap with the earliest stages of the Olarian Orogeny, and hence can be considered early-orogenic. Whether this phase of mineralisation represents remobilisation of earlier-formed mineralisation during deformation (Armistead et al., 2018) or a separate syn-deformational Cu-Au-Fe (-Mo) mineralising event, as preferred herein, remains to be confirmed. The timing of Cu-Au-Mo mineralisation also overlaps (within uncertainties) with the ages of several I-type granitoid intrusions dated at 1641 ± 11 Ma to 1616 ± 9 Ma in the Olary Domain (Cook et al., 1994; Ashley et al., 1997; Fanning et al., 1998), but the spatial and genetic relationships between the Cu-Au-Mo and the intrusions remain unclear.

In conclusion, it is tentatively proposed that the ~1630-1605 Ma metallogenic event A affected both the Curnamona Province and parts of the southeastern Gawler Craton, and resulted in pre- to early-orogenic Mo (± Au) and Cu-Au-Fe (Mo) mineralisation.

Metallogenic events B and C (Fig. S4): The major period of Cu-Au-Fe including IOCG mineralisation in the Gawler Craton occurred during 1600-1575 (Fig. S4, right side, events B and C), broadly coeval with granitic and mafic intrusions of the Hiltaba Suite and the mafic to felsic Gawler Range Volcanics. Earliest phases of the high-temperature A- and I-type Hiltaba Suite granitoids at ~1600-1595 Ma were syntectonic (Daly et al., 1998; Ferris et al., 2002; Budd, 2006; Hand et al., 2007; Conor et al., 2010), and some of the earlier GRV units are folded (e.g. Daly et al., 1998). Although later intrusive phases and younger GRV units are generally undeformed there is geochronological evidence of deformation and metamorphism along several major shear/fault zones in the southern and central Gawler Craton between ~1611 Ma and ~1580 Ma (Hand et al., 2007). Similar to the temporally overlapping Olarian Orogeny in the Curnamona Province, this tectonothermal activity was interpreted by Hand et al. (2007) to have occurred in an overall compressive regime, with northwest-southeast shortening. However, at least local and transient extensional conditions also appear to have existed when much of the GRV and equivalents in the Curnamona Province with associated sedimentary rocks were deposited, as implied in many earlier models of an intracontinental tectonic setting during the Hiltaba-GRV event (e.g. Daly et al., 1998; Giles, 1988). As noted by Skirrow (2010) extension is supported by the geochemistry of compositionally bimodal mafic to felsic magmatism, seismic reflection data showing GRV-filled half-graben (Carr et al., 2010), and sedimentary basinal deposition coeval with the GRV (Curtis et al., 2018). Recent high-precision U-Pb zircon dating by TIMS has revealed that GRV felsic volcanic rocks were deposited in two discrete stages: at ~1595-1593 Ma in the Olympic Dam district, and at ~1591-1587 Ma in the central Gawler Craton (lower and upper GRV) and northwestern Curnamona Province (Jagodzinski et al., 2016; McPhie et al., 2020).

Importantly, magnetite-rich veins with local pyrite and apatite but lacking significant copper mineralisation at the Acropolis prospect are inferred to have formed at ~1594 Ma, with a maximum age constrained by the early felsic volcanism (1594.03 ± 0.68 Ma) and a minimum age constrained by the age of felsic dykes that lack magnetite veins, with an age of 1593.88 ± 0.56 Ma (McPhie et al., 2020). The ages of Hiltaba Suite granite host rocks at both Olympic Dam and Acropolis (1593.87 ± 0.21 Ma and 1594.88 ± 0.50; Cherry et al., 2018; McPhie et al., 2020) are very similar and provide maximum ages of Cu-U-Au mineralisation at these locations. An age of ~1590 Ma was determined for Cu-U-Au mineralisation at the Olympic Dam deposit by Johnson & Cross (1995); this timing has been confirmed and refined by dating of hydrothermal hematite associated with Cu-U-Au, with ages of 1590 ± 8 Ma (^{207}Pb-^{206}Pb LA-ICPMS age, Ciobanu et al., 2013) and more precisely at 1589.91 ± 0.91 Ma (^{207}Pb-^{206}Pb TIMS age, Courtney-Davies et al., 2019). A zircon age of 1590.97 ± 0.58 Ma from blocks of altered bedded volcaniclastic rocks in the mineralised Olympic Dam Breccia Complex (Cherry et al., 2018) provides a further maximum age constraint on the timing of hydrothermal activity at Olympic Dam. Therefore, the high-precision dating permits the conclusion that the magnetite-apatite veining at ~1594 Ma at

Acropolis occurred about 4 million years prior to the main Cu-U-Au ore-forming event at Olympic Dam.

Younger ages recorded in hematite at Olympic Dam (1577 ± 5 Ma, Ciobanu et al., 2013), and in hydrothermal molybdenite, titanite, monazite, apatite and white mica through to ~1570 Ma in the Olympic Cu-Au province indicate that Cu-Au-Fe hydrothermal activity continued over a period of at least ~20-25 m.y., possibly in several stages (Fig. S4, event C; Skirrow et al., 2007; Conor et al., 2010; Gregory et al., 2011; Reid et al., 2013; Bowden et al., 2017; Cherry et al., 2018). The Kararan orogeny (~1570-1550 Ma, Hand et al., 2007) is characterised by medium-high grade metamorphism and is apparently confined to the northern Gawler Craton (e.g. Mt Woods Inlier, Mabel Creek Ridge, Coober Pedy Ridge; Fig. S4; Hand et al., 2007). Although all of the known major Cu-Au-Fe deposits occur to the south of these Kararan medium-high grade terranes, the Mt Woods Inlier contains several small magnetite-rich deposits with low grade Cu (e.g. Cairn Hill, Freeman & Tomkinson, 2010). Their affinity to Kiruna type IOA or to Cu-Au-Fe deposits is unclear.

Several later (hydro)thermal events of generally minor significance in terms of metal accumulation subsequently affected the eastern Gawler Craton and caused resetting of ages and/or remobilisation of various minerals (e.g. Davidson et al., 2007; Conor et al., 2010; Cherry et al., 2018). However, recent dating work at Olympic Dam indicates that major introduction of U as well as redistribution of metals in the deposit occurred at ~700-500 Ma (Ehrig et al., 2021).

In the Curnamona Province, there are no reported radiometric ages for Cu-Au mineralisation during metallogenic events B and C. However, the timing of syn-deformational (syn-D3), transgressive and in-part shear-related sodic and sodic-calcic alteration, has been constrained to ~1588-1583 Ma by U-Pb SIMS dating of hydrothermal titanite (Fig. S4; Skirrow et al., 2000; Skirrow and Fletcher, unpublished data). There is also evidence for base metal leaching and redistribution within the widespread Na and Na-Ca alteration zones (e.g. Clark et al., 2005; Skirrow & Ashley, unpublished data). These observations could indicate significant potential for as-yet undiscovered Cu-Au mineralisation of similar age to events B and C in the western Curnamona Province.

7.4 Summary and tectonic settings – Gawler Craton and Curnamona Province

In summary, small deposits of epigenetic Cu, Mo and Au ± magnetite formed at ~1630-1605 Ma prior to and during the early stages of the Olarian orogeny, a compressional event that inverted ~1760-1640 Ma rift basins in both the Gawler Craton and Curnamona Province and resulted in a metamorphic peak at ~1600 Ma in the latter region (Page et al., 2005; Forbes et al., 2007). Syn-deformational Na-Ca and Fe-K-Ca-Na magnetite-biotite-bearing alteration commenced in the Moonta-Wallaroo and possibly in the Mt Woods Inlier late within the Olarian orogeny as bimodal magmatism flared up. Mineralogically and structurally distinct from these biotite-albite-bearing assemblages, apatite-bearing magnetite-K-feldspar-actinolite-carbonate ± pyrite veins in the Olympic Dam district formed during brittle deformation at ~1594 Ma. Crucially, precise dating has shown that this essentially Cu-barren magnetite-apatite-bearing alteration predated the formation of the principal Cu-U-Au mineralisation at Olympic Dam by ~4 m.y., whereas Cu-Au mineralisation at the Prominent Hill and Hillside deposits may have formed up to ~20 m.y. later than the initial magnetite-apatite alteration. Overall, the major Cu-Au-Fe ore-forming systems in the Gawler Craton are considered to have formed in a broadly late-orogenic to post-orogenic tectonic setting, during a switch from compressional to extensional tectonism.

Various geodynamic scenarios have been proposed for the Gawler Craton and Curnamona Province during the early Mesoproterozoic, with earlier models emphasising intracontinental 'anorogenic' settings (e.g. Daly et al., 1998; Giles, 1988) which were incorporated into some models of global IOCG deposits (e.g. Hitzman, 2000; Groves et al., 2010). However, the recognition of syn-orogenic as well as cryptic subduction-related features in the late Paleoproterozoic to early

Mesoproterozoic geology of the region (e.g. Hand et al., 2007) has led to several alternative geodynamic proposals. Most place the Olympic Cu-Au province in an upper plate distal from subduction at a continental margin, and account for the Olarian orogeny via arc/continent collision or oceanic plateau subduction. However, there is debate on the geodynamic mechanisms of heating that produced the Hiltaba Suite, GRV and temporally associated Cu-Au-Fe mineralisation (e.g. Ferris et al., 2002; Betts et al., 2009; Skirrow et al., 2018; Tiddy & Giles, 2020).

8. Cloncurry province, Australia - Mesoproterozoic IOCG and ISCG deposits

The Cloncurry district of the eastern Mt Isa Inlier, Queensland, hosts numerous Mesoproterozoic Cu-Au-Fe deposits of diverse character including large magnetite-rich Cu-Au deposits such as Ernest Henry (grade, tonnage) and Mt Elliott, pyrrhotite- and/or pyrite-rich Cu-Au deposits with variable amounts of magnetite (e.g. Eloise, Osborne), and hematite-rich deposits with high Au:Cu ratios (e.g. Starra; Williams, 1998; Haynes, 2000; Williams et al., 2005). Most of the iron oxide-rich Cu-Au deposits have been described as IOCG deposits (Williams et al., 2005) whereas the iron oxide-poor members, or iron sulfide Cu-Au (ISCG) deposits, have been considered to be variants of IOCG deposits (Haynes, 2000). The giant Mt Isa Cu deposit, which lacks significant Fe oxides and Au, was also included in the latter group by Haynes (2000). The Cloncurry district also hosts the giant Paleoproterozoic Cannington Ag-Pb-Zn deposit (Walters & Bailey, 1998) and the high-grade Mo-Re but Fe-oxide- and Cu-Au-poor Merlin deposit (Babo et al., 2017).

Copper-Au-Fe deposits of the Cloncurry district are hosted by metamorphosed sedimentary, volcanic and intrusive rocks that form parts of three superbasins deposited as rift-sag sequences between ~1790 Ma and ~1575 Ma across the Mt Isa Inlier (Blake, 1987; Southgate et al., 2000, 2013). Back-arc, intracontinental, and/or extended continental (passive) margin depositional settings have been proposed for the superbasins (e.g. Scott et al., 2000; Southgate et al., 2000, 2013; Giles et al., 2002; Gibson et al., 2016). In the Cloncurry District (part of the Eastern Succession of the Mt Isa Inlier) the lower sequences comprise bimodal volcanic rocks and overlying siliciclastic and calcareous sedimentary rocks (now calcsilicate- and scapolite-bearing, including the Corella Formation and Doherty Formation) of the Leichardt Superbasin, and upper sequences of siliciclastic, carbonaceous pelitic and mafic volcanic rocks (e.g. Soldiers Cap Group, Young Australia Group) which are part of the Isa Supergroup (Blake, 1987; Scott et al., 2000; Foster & Austin, 2008; Southgate et al., 2013). In broad terms the lower sequence is relatively oxidised, as it contains sulfate-bearing scapolite (Morrissey & Tomkins, 2020) and lacks abundant carbonaceous units, whereas the upper sequence is relatively reduced as indicated by the presence of carbonaceous units (e.g. Answer Slate, Marrimo Slate) and mafic volcanics (e.g. Toole Creek Formation) and lack of ex-evaporitic rocks. The youngest units in the Cloncurry district were deposited at or after ~1618-1610 Ma (Tommy Creek Formation and upper Marimo Slate, Foster & Austin, 2008). Extensive Fe-rich tholeiitic dolerite/gabbro/trondhjemite dykes and sills were emplaced within the Soldiers Cap Group and elsewhere in the Eastern Succession, and are believed to be related to the voluminous mafic Toole Creek Volcanics (1658 ± 8 Ma; Foster & Austin, 2008; Oliver et al., 2008) and/or earlier events (e.g. 1686 ± 6 Ma sills, Rubenach et al., 2008). An early stage of localised sodic (albitic) alteration and Cu-Au leaching from the mafic rocks and local re-precipitation may have occurred in association with these mafic intrusions (Oliver et al., 2008; Rubenach et al., 2008). The three basin supersequences and related felsic and mafic intrusions were subjected to the first phase of the compressional Isan Orogeny at ~1595-1580 Ma, when peak metamorphic conditions in the amphibolite facies were attained in the Cloncurry district (syn-D2; Foster and Austin, 2008; Foster & Austin, 2008; Tiddy & Giles, 2020). The earliest stages of this heating event may have commenced by ~1640 Ma (Oliver et al., 2008; Rubenach et al., 2008). Whereas only minor magmatism (e.g. pegmatites and mafic dykes, Oliver et al., 2008) accompanied this first phase of the Isan Orogeny there is field evidence for syn-D2 regional-scale sodic alteration and locally associated K-Fe (e.g. biotite) alteration (Rubenach & Lewthwaite, 2002). Titanite associated with albite, magnetite and biotite alteration at the Starra

deposit records a U-Pb age of ~1595 Ma, described by Duncan et al. (2011) as representing Na-Ca alteration but perhaps also recording the timing of magnetite-biotite-albite (Fe-K-Na) alteration. Iron leaching and redeposition during this and/or later deformational events may have produced some of the large hydrothermal 'ironstones' in the Cloncurry district (Williams, 1994).

The earliest major Cu-Au-Fe deposits in the Cloncurry district formed during this first phase of the Isan Orogeny, as recorded by molybdenite Re-Os, titanite U-Pb and amphibole ^{40}Ar-^{39}Ar ages at the Osborne Cu-Au deposit (~1600-1595 Ma; Perkins & Wyborn, 1998; Gauthier et al., 2001; Duncan et al., 2011). Oliver et al. (2008) proposed that some Fe±Cu sulfides and magnetite in banded rocks at the Osborne, Eloise, and Starra deposits may have formed prior to the D2 metamorphic peak of the early Isan Orogeny, consistent with the ~1600-1595 Ma ages for hydrothermal minerals at Osborne. Some Fe and Cu were then redistributed during the early phase of the Isan Orogeny (Oliver et al., 2008). A Re-Os age of ~1567 Ma for molybdenite associated with Cu-Au mineralisation at the Starra deposit may indicate introduction of Cu-Au-Mo during post-peak stages of the early phase of the Isan Orogeny (Duncan et al., 2011).

The second, post-peak-metamorphic, phase of the Isan Orogeny occurred between ~1550 Ma and ~1500 Ma, during which several deformation stages have been identified (e.g. D3 shortening at ~1550 Ma, D4 transpression at ~1530 Ma, Rubenach et al., 2008; D5 extension at ≤1500 Ma, Austin & Blenkinsop, 2010). Felsic intrusions of the Williams and Naraku batholiths were initially emplaced at ~1550 Ma early in this second phase of the Isan Orogeny, with large volumes intruded during ~1530-1500 Ma and continuing to ~1490 Ma (see geochronology summary in Duncan et al., 2011 and references therein). Compositions range from early tonalite-trondhjemite (~1550 Ma) to later K-rich A-type monzodiorite, monzonite and monzogranite (Mark, 2001), with evidence of mixing/mingling between felsic and mafic magmas (Rubenach et al., 2008). Renewed and widespread Na (-Ca) alteration occurred along major fault/shear zone corridors at ~1550-1520 Ma, based on sparse titanite U-Pb dates; at least some Na-Ca alteration also was spatially and temporally associated with Williams-Naraku plutons (Mark et al., 2004; Oliver et al., 2004). Several large magnetite bodies also formed within or in close proximity to felsic intrusions of the Williams-Naraku batholiths, such as the magnetite-feldspar-quartz accumulations within the Lightning Creek sill complex (Perring et al., 2000).

Many of the major Cu-Au-Fe deposits in the Cloncurry district record hydrothermal mineral ages between ~1530 Ma and ~1500 Ma (e.g. molybdenite Re-Os, titanite U-Pb, amphibole and biotite Ar-Ar ages; Perkins & Wyborn, 1998; Gauthier et al., 2001; Duncan et al., 2011). This timing overlaps with the felsic (-mafic) magmatism of the Williams-Naraku batholiths as well as with regional Na-Ca alteration and the D3 deformation event within the later phase of the Isan Orogeny. Consistent with a syn-deformational and syn- or late-orogenic timing, many of the ~1530-1500 Ma IOCG and ISCG deposits are hosted by structures such as brittle-ductile shear zones and faults (e.g. Ernest Henry – Mark et al., 2006; Starra – Rotherham, 1997; Eloise – Baker & Laing, 1998; Mt Elliott – Brown & Porter, 2010). The unusual Merlin Mo-Re deposit, which lacks iron oxides and has low Cu and Au contents, formed over several stages commencing at 1535 Ma and with later stages at ~1520 Ma and ~1500 Ma (Duncan et al., 2011; Babo et al., 2017). Significantly, many of the Cu-Au-Fe deposits with reduced assemblages (e.g. pyrrhotite-pyrite-biotite-rich), with or without magnetite (e.g. Osborne, Eloise, Greenmount), are hosted by the upper, relatively reduced, metasedimentary-metavolcanic rock package (e.g. Soldiers Cap Group, Young Australia Group). Conversely, deposits containing relatively oxidised hydrothermal assemblages (e.g. lacking pyrrhotite but containing magnetite, hematite, K-feldspar and/or sulfates) appear to be mostly hosted by rocks of the lower sequence which is of broadly intermediate to oxidised redox character (e.g. Ernest Henry, E1), or occur close to the contact between the upper and lower sequences (e.g. Monakoff, Starra). The Mt Elliott-SWAN deposit straddles this boundary and exhibits a broad zoning from anhydrite-magnetite-pyrite-bearing assemblages in the SWAN deposit (hosted by the Stavely Formation) to more reduced pyrrhotite-

magnetite-bearing assemblages in the Mt Elliott deposit hosted by the upper sequence (Brown & Porter, 2010). The issue of local-scale host rock control on such mineralogy (e.g. Haynes, 2000) versus broader scale controls on fluid composition are discussed in the accompanying contribution (Skirrow, in prep.).

In summary, both of the two main stages of Cu-Au-Fe mineralisation in the Cloncurry district were broadly syn-orogenic, with the earlier stages coeval with the first phase of the Isan Orogeny (with early-, syn- and late-orogenic timing), and the second during the syn-D4 to syn-D5 events of the later phase of the Isan Orogeny. Interestingly, this latter and major Cu-Au-Fe event along with separate and rare high-grade Mo-Re mineralisation appear to have occurred across a period when tectonism switched from compression (D3) to transpression (D4) to at least local extension (D5; Austin & Blenkinsop, 2010). The two phases of the Isan Orogeny have been attributed to plate convergence and terrane accretion distal from the Mt Isa Inlier, initially to the south commencing at ~1640 Ma and then to the east (Scott et al., 2000; Southgate et al., 2000, 2013; Giles et al., 2002; Gibson et al., 2016).

9. Kangdian province (China)and Sin Quyen Cu-Au deposit (Vietnam) – Paleo- to Neoproterozoic Cu-Au and Fe deposits

The ~300 km long Kangdian metallogenic province in the southwestern Yangtze block of China contains several large Cu-Au deposits associated with iron oxides as well as separate Fe-oxide and stratabound Cu deposits known locally as stratiform sedimentary copper or SSC deposits (e.g. Zhao & Zhou, 2011; Zhou et al., 2014; Zhu et al., 2019; Lin et al., 2020 Zhao and Zhou, 2011; Zhou et al., 2014; Zhu et el., 2019; Lin et al., 2020). The province is important not only economically but also on account of the range of Cu and Fe deposits, the presence of gabbro/dolerite intrusions near the Cu-Au-Fe deposits, carbonate-rich basinal host rocks, and apparent absence or presence of only minor felsic intrusive rocks in the Cu-Au-Fe districts. Although the stratigraphy is relatively well understood, constraining the timing of deformation, metamorphic and mineralisation events has proved problematic in the Kangdian Cu province, probably due to multiple overprinting events. The major Cu and Fe deposits are hosted by Paleoproterozoic supracrustal rocks with maximum ages of ~1742-1681 Ma and which comprise metamorphosed siliciclastic rocks (mica schists, meta-conglomerate), meta-carbonates, amphibolite, and minor carbonaceous schist and felsic meta-volcanic rocks which were extensively albitised (Zhao & Zhou, 2011; Zhou et al., 2014). Zircon dating of gabbro and dolerite bodies within a few kilometres of the Fe and Cu deposits indicate intrusive ages mostly in the range ~1720-1659 Ma and ~1490 Ma (Li et al., 2015). The oldest ages of hydrothermal minerals in the Fe and Cu deposits are molybdenite and chalcopyrite Re-Os ages of ~1660 Ma at the Yinachang Fe-Cu deposit (Zhao et al., 2013) and an age of 1653 ± 18 Ma for hydrothermal zircon with chalcopyrite and albite inclusions from Cu mineralisation at the Dahongshan Fe-Cu deposit, which is within error of the age of dolerites at the deposit (Zhao et al., 2017). Massive and banded magnetite-rich bodies with spatially associated albitisation, likened to Kiruna type IOA deposits, occur spatially separately from the Cu orebodies at this deposit and have been inferred to be temporally, spatially and genetically related to the ~1660 Ma dolerites (Zhao et al., 2017). The Cu-Au mineralisation at Dahongshan is mostly of banded style with sulfides and associated biotite ± garnet alteration along a strong tectonic foliation and, where magnetite is present, the Cu-Fe sulfides postdate this oxide (Zhao et al., 2017). Overall, the first Fe and Cu event(s) at ~1660 Ma in the Kangdian Cu province appear to have occurred not long after deposition of the sedimentary and volcanic host rocks. The geochemical compositions of the volcanic and mafic intrusive rocks have been interpreted to indicate an intracontinental extensional setting of basin formation (Zhao & Zhou, 2011; Zhou et al., 2014).

A large number of ages younger than 1660 Ma have been reported for other Fe and Cu deposits in the Kangdian Cu province, for example at ~1450 Ma, ~1050-1070 Ma and ~880-850 Ma (Chen & Zhou, 2014; Zhou et al., 2014; see also summaries in Zeng et al., 2018 and Lin et al., 2020). Of particular note are ^{40}Ar-^{39}Ar ages of ~851 Ma to ~817 Ma for biotite and amphibole within several of the Fe-Cu deposits which are interpreted as recording a major regional Neoproterozoic tectonothermal event (Zhou et al., 2014). These align roughly with the ~880-850 Ma ages of some allanite at the Lala deposit (Chen & Zhou, 2014) and molybdenite with chalcopyrite in the Dahongshan deposit (833 ± 9 Ma to 799 ± 13 Ma, Zhao et al., 2017). Indeed, descriptions of the Fe-Cu ores indicate intense ductile to brittle-ductile deformation features in the Cu-sulfide ores of many of the Kangdian deposits. Interestingly, the period 860-740 Ma was also marked by arc granites, adakitic rocks, and subduction-related mafic-ultramafic rocks (Zhou et al., 2002, 2014).

Less published information is available for the SSC deposits than for the Fe-Cu deposits in the Kangdian Cu province (Zhao et al., 2012, 2013), and the relationships between the SSC and Fe-Cu deposits remain unclear. At the Yinmin SSC deposit an age of Cu mineralisation has been constrained between 1742 ± 13 Ma (the age of the host strata) and 1701 ± 28 Ma (the age of a dolerite dyke cutting the Cu mineralisation; Zhao et al., 2012, 2013). Allanite intergrown with hydrothermal magnetite alteration at the Lanniping Fe-Cu and REE-bearing deposit in the same district as the Yunmin SSC deposit has yielded a U-Pb ion probe age of 1728 ± 20 Ma. Later generations of allanite yielded ages of 1015 ± 33 Ma and 800 ± 16 Ma which may post-date chalcopyrite (Su et al., 2021), but the reported textures do not rule out chalcopyrite growth during or after the ~800 Ma allanite event. These timing constraints and uncertainties allow for the alternative possibilities of (1) SSC mineralisation overprinting earlier-formed magnetite alteration to form hybrid IOCG-like mineralisation, and (2) syn-deformational IOCG- or ISCG-style Cu mineralisation forming during or after ~800 Ma in the district of the Yinmin and Lanniping deposits.

Additionally, the province contains other Cu deposits that lack significant modal amounts of iron oxides, such as the large Hongnipo deposit (4.3 Bt @ 1.42 % Cu) located 5-10 km southwest of the Lala IOCG deposit (Lin et al., 2020). The Hongnipo deposit contains Cu mineralisation of both stratiform appearance and transgressive vein styles; the latter hosts most of the Cu mineralisation (Lin et al., 2020). In the lower grade stratiform ores pyrite and minor to scarce chalcopyrite, pyrrhotite, arsenopyrite and sphalerite occur along a tectonic foliation (sub)parallel to compositional layering (see Fig. 4 of Lin et al., 2020), similar to the form of banded Cu-Au mineralisation in some of the Fe-Cu deposits such as Dahongshan and Lala. Vein-type ore comprises pyrite and chalcopyrite with calcite and quartz and minor pyrrhotite, magnetite, bornite and hematite. Geochronological data indicate an initial sulfide-forming event at 1552 ± 80 Ma (stratiform pyrite Rb-Sr isochron age) followed by transgressive Cu mineralisation at 795 ± 8 Ma (chalcopyrite Re-Os isochron age, Lin et al., 2020). A volcanic massive sulfide origin of the stratiform ores was suggested by Lin et al. (2020), overprinted by Neoproterozoic epigenetic vein-type Cu mineralisation. However, both the foliation-parallel and the vein-type Cu mineralisation at Hongnipo bear similarities to low-Fe-oxide ISCG variants of the Cu-Au-Fe global deposit family as described in this review. Given that Fe-oxide-rich Cu-Au-Fe (i.e. IOCG) deposits with Neoproterozoic ages occur in the same district (at Lala) it seems likely that both ISCG and IOCG variants of orogenic Cu-Au-Fe deposits are present in the Kangdian Cu province.

Recent models of IOCG ore genesis for the Kangdian Cu province favour an early (~1720-1650 Ma) stage of Fe-oxide and at least some Cu hydrothermal activity genetically linked to emplacement of mafic intrusions within an extensional basinal setting and involving both magmatic-hydrothermal and basin-derived fluids (e.g. Zhao et al., 2017; Su et al., 2021). Later, syn-metamorphic and syn-deformational features of the ores have been interpreted to represent overprinting and remobilisation of earlier Cu-Au ores, with or without new introduction of Cu (-Au) during superimposed tectonothermal events (e.g. Zhao et al., 2017; Su et al., 2021). However, detailed structural study of the Lala deposit has correlated gabbro intrusion and the formation of

most magnetite and albitisation with the regional extension-related ~1660 Ma events, whereas the main Cu-Fe sulfide mineralisation and additional magnetite was correlated with compressional deformation during the Sabie orogeny at ~1050 Ma (Zeng et al., 2018). Later biotite-sulfide veins cutting banded Cu-Fe ore were interpreted as syn-extensional at ~851-817 Ma (Zeng et al., 2018).

In summary, the available data for the Kangdian Cu province seem permissive of not only remobilisation of ~1720-1650 Ma Cu and REE-bearing mineralisation but also of introduction of significant new Cu-Au-Fe mineralisation during either or both of the ~1050 Ma and ~851-817 Ma tectonothermal (orogenic?) events affecting the metallogenic province. It is presently unclear whether the latter tectonothermal event was pre-, syn- or post-arc magmatism, and whether it was extensional or compressional. Further work could examine whether an as-yet unidentified tectonothermal event accompanied the ~1720-1650 Ma Cu-Au event, as would be consistent with the reported textures and tectonic fabrics.

The Sin Quyen Fe-Cu-Au-REE deposit in northern Vietnam (52.8 Mt @ 0.91 % Cu, 0.41 g/t Au and 0.7 % combined Ce, La, Pr and Nd) is situated within the Red River fault zone to the south of the Yangtze craton (McLean, 2002). Earlier work proposed that the host metamorphic sequences could be correlated with the sequence hosting Fe-Cu deposits in the Kangdian Cu province, with lateral displacement of the Sin Quyen area along the Red River fault zone (Zhou et al., 2014). Host rocks are highly deformed amphibolite facies gneisses and schists including a lower, graphitic, unit and an upper unit of felsic and mafic orthogneisses which hosts most of the Cu-Au-REE mineralisation and related alteration. Recent geochronology has shown that the host sequence is in fact younger than the Fe-Cu-hosting <1742-1681 Ma sequence in the Kangdian province, with depositional ages of 870-830 Ma for this part of the Sin Quyen Formation (Liu & Chen, 2019). Other parts of the host rock sequence, however, are of similar Paleoproterozoic age to those in the Kangdian Cu provinces (Liu & Chen, 2019). Iron-potassic-calcic alteration and some sulfide mineralisation are distributed along a strong tectonic foliation, and comprise an early stage of magnetite with amphiboles, hedenbergite and allanite, and a later stage with initial chalcopyrite-pyrrhotite-pyrite along the foliation and a latest, volumetrically dominant, and undeformed chalcopyrite-pyrrhotite assemblage (McLean, 2002; Li & Zhou, 2018; Liu & Chen, 2019). Dating of hydrothermal zircon and monazite from the early magnetite-allanite hydrothermal stage has yielded ages of 841 ± 12 Ma and 836 ± 18 Ma (Li et al., 2018), similar to the timing of tectonothermal and arc-related igneous activity regionally within and near the Kangdian Cu province (Zhou et al., 2014). However, U-Pb dating of allanite from the early magnetite-allanite (Ca-REE) hydrothermal stage yielded ages of ~880 Ma whereas allanite associated with the later magnetite-chalcopyrite-forming (Fe-Ca-Na-K-Cu-REE) stage yielded ages of ~840 Ma (Ngo et al., 2020). The allanite results were interpreted by Ngo et al. (2020) as indicating a different, possibly back-arc, tectonic setting for the Sin Quyen deposit at ~880-840 Ma compared to the ~1660 Ma phase of IOCG mineralisation in the Kangdian Cu province. Nevertheless, as noted above, ~880-800 Ma hydrothermal and metamorphic mineral ages in IOCG deposits are widespread in the Kangdian Cu province, where they represent either remobilisation of earlier IOCG mineralisation and/or introduction of new Cu-Au mineralisation coincidentally with that at Sin Quyen.

10. Khetri province, India – Neoproterozoic IOCG deposits

The Khetri copper province in Rajasthan is situated within the northwestern part of the Aravalli-Delhi Orogenic Belt, a Proterozoic deformed sedimentary-volcanic sequence along and overlying the western margin of the Archean-Proterozoic Bundelkund craton (Knight et al., 2002). Significant resources of Cu-Au are present in the Khetri area in Fe-oxide-rich IOCG deposits, for example 30 Mt @ 1.7 % Cu, 0.3-1.3 g/t Au at the Banwas deposit, 66 Mt @ 1.12-1.71 % Cu and 0.2-2 g/t Au at the Madan-Kudan deposit, and 40 Mt @ 1.14-1.62% Cu and 0.2 g/t Au at the Kolihan and Chandmari deposits (Knight et al., 2002; Bhardwaj et al., 2014 cited in Li et al., 2019).

Additionally, the region contains several groups of sedimentary stratiform Cu (or SSC) deposits that are zoned from pyrite-chalcopyrite to bornite and chalcocite and have been likened to 'redbed' Cu deposits in the Central African Copper Belt (e.g. Mukhopadhyay et al., 2019) or have affinities with IOCG deposits (Sharma et al., 2020).

Host rocks of both the IOCG and SSC type deposits are the Delhi Supergroup, which in the Khetri-Alwar region comprise a 1.7-1.5 Ga dominantly siliciclastic sequence with minor carbonate and mafic volcanic rocks (Kaur et al., 2017). This sequence is age-equivalent to parts of the Aravalli Supergroup in the southern part of the Aravalli-Delhi Orogenic Belt, which also hosts Au (-Cu-Fe) mineralisation in albitite-carbonate rocks in the Bhukia district (Fareeduddin et al., 2012; Mukherjee et al., 2019). An environment of deposition along an active Andean-type convergent margin has been suggested for the Aravalli Supergroup and equivalents in the Delhi Supergroup (McKenzie et al., 2013). Although the Delhi Supergroup was multiply deformed and metamorphosed there are few high-precision geochronological constraints on tectonothermal activity. The youngest tectonothermal event reported by Ozha et al. (2016) based on monazite U-Pb EPMA dating is ~1.05-0.99 Ga which these authors related to the amalgamation of Rodinia. However, the extensive suite of felsic intrusions of the ~870-800 Ma Erinpura Suite along the western margin of the Aravalli-Delhi Orogenic Belt is highly tectonised and migmatised in places (Just et al., 2011). Whereas the Erinpura Suite was previously interpreted to be syn-tectonic, which is supported by dating work reported in several studies (e.g. see Kaur et al., 2017), Just et al. (2011) proposed that the tectonothermal overprint occurred significantly later, at ~780-736 Ma and was partly coeval with emplacement of the bimodal Malani Suite intrusions and related volcanic rocks.

In this context, the recently determined ages for hydrothermal monazite in Cu-Au-Fe deposits in the Khetri Cu province (833 ± 5 Ma to 840 ± 6 Ma, U-Pb LA-ICPMS dates) overlap with the ages of the syn- or pre-tectonic Erinpura Suite (Li et al., 2019). It is also evident that regional-scale sodic alteration in the Khetri Cu province also developed at a similar time (~847-831 Ma) to the Cu-Au-Fe mineralisation, based on a titanite U-Pb SIMS dating and a Sm-Nd isochron age for scapolite-altered pyroxenite (Knight et al., 2002; Kaur et al., 2013). The timing of this sodic metasomatism and Cu-Au-Fe mineralisation in relation to metamorphism remains unclear, although a post-peak timing seems probable (Knight et al., 2002). The significance of EPMA (chemical) ages of ~1300-1100 Ma for uraninite in several of the Cu-Au-Fe deposits, reported by Baidya and Pal (2020), is unclear at present. Regardless, chalcopyrite-pyrrhotite-pyrite-magnetite mineralisation and associated amphibole-biotite-albite-garnet-carbonate-bearing alteration exhibit strong structural controls such as fault-controlled *en echelon* ore shoots, sulfidic bands along the tectonic foliation, and later sulfidic veins that cut this foliation (Knight et al., 2002). The author's observations at several of the deposits supports the proposal that some mineralisation postdates deformation fabrics (Knight et al., 2002) but there are significant proportions of the mineralisation that either were synchronous with, or predated, the brittle-ductile deformation that produced the main tectonic foliation. Overall, the available limited data are permissive of either syn- or pre-orogenic timing of Neoproerozoic IOCG mineralisation in the Khetri Cu province.

11. Chilean and Peruvian Andes – IOCG and IOA deposits

Iron oxide-rich Cu-Au deposits of Cretaceous age are distributed in two principal belts in the Andes, one in northern Chile hosting the large Candelaria, Mantoverde and other Cu-Au deposits and a second, less endowed, belt in southern Peru hosting the Raúl-Condestable and Mina Justa Cu-Au deposits. Whereas many of these deposits have been classified as members of the IOCG family (e.g. (Sillitoe, 2003; Williams et al., 2005; Groves et al., 2010; Barton, 2013; Chen et al., 2013), the two belts of iron oxide-rich Cu-Au deposits also contain, or lie adjacent to, groups of other Cretaceous deposit types including IOA, porphyry Cu-Au (-Mo), skarn Fe ± Cu-Au and 'manto' Cu (-Ag) deposits. The large Fe resources in northern Chile define the Chilean Iron Belt

(CIB; Oyarzun et al., 2003). These relatively well preserved Andean metallogenic provinces are important not only economically but also are useful in understanding the genetic relationships between the differing types of Fe and Cu-Au deposits. The timing and regional geological settings of the deposits is crucial in deciphering such relationships, which has been aided by the availability of considerable new data in recent years. Here, the focus is on timing constraints determined from the more robust geochronometers such as zircon U-Pb dating of igneous rocks, and U-Pb, Re-Os and Ar-Ar dating of selected hydrothermal minerals with higher closure temperatures such as titanite, apatite, molybdenite, amphibole and biotite. Less emphasis is placed on some of the earlier geochronology using K-Ar and Rb-Sr methods on whole-rock, K-feldspar and sericite/clay samples which can be highly vulnerable to fluid-induced disturbance and thermal resetting.

The broad setting for the Cretaceous Fe and IOCG deposits or northern Chile and southern Peru is a convergent margin situated over a long-lived and still-active subduction system (Sillitoe, 2003; Chen et al., 2013). A major transition occurred during the Late Cretaceous when Jurassic magmatic arc and sedimentary back-arc basin rocks that formed within an extensional tectonic setting were subjected to inversion. This transition to a compressive setting has been the subject of many studies and is now thought to have been diachronous from south to north and may have commenced as early as 130-122 Ma at latitudes of 40°-46° S (Gianni et al., 2020). However at the latitudes of the CIB and partly co-located IOCG deposits (e.g. 20°-33° S) the onset of inversion of the Jurassic arc and basin system has been refined to the period ~107-105 Ma with a main phase of compression at ~100-95 Ma (Bascuñán et al., 2016; Fennell et al., 2017; Boyce et al., 2020). This tectonic switch was also preceded by a major decrease in the flux of arc magmas from ~140 Ma to ~100 Ma and a change from dominantly intermediate-composition dioritic/andesitic igneous rocks to tonalitic and dioritic/andesitic compositions at ~100 Ma (Fig. S1, Girardi, 2014). Strike-slip movement along the arc-parallel Atacama Fault System (AFS), which accommodated northwest to southeast directed plate convergence, was initially ductile at ~135-120 Ma at depths of ~5-7 km where movement was facilitated by thermal weakening, and then transitioned to brittle behaviour until ~110 Ma (latitudes 24°-28° S, Seymour et al., 2020).

The metallogenic evolution appears to have evolved in parallel with these tectonic and magmatic transitions. An early stage of large iron oxide (not necessarily IOA) deposits formed in Peru along with stratabound epigenetic 'manto' Cu (-Ag) deposits in Chile in the Jurassic rocks around 164-155 Ma (e.g. Marcona: Hawkes et al., 2002; Chen et al., 2010a, 2010b; 2013; Mantos Blancos and Michilli manto district: Maksaev & Zentilli, 2002; Tristá-Aguilera et al., 2006; Oliveros et al., 2008). The main stage of large IOA deposits of the CIB, together with IOCG deposits and a second manto Cu-forming event, occurred in the Late Cretaceous between ~130 Ma and ~85 Ma. The few available dates for Cretaceous manto Cu (-Ag) deposits indicate alteration at ~106-101 Ma, based on K-feldspar ^{40}Ar-^{39}Ar dating (El Soldado deposit, Wilson et al., 2003). Despite the paucity of high-precision ages using robust geochronometers for the Fe and Cu-Au deposits, the available data show a possible sequence from IOA to IOCG and finally to manto Cu (-Ag) deposits, and with small porphyry Cu deposits sporadically throughout the ~130-85 Ma period (Fig. S1). The few high-precision age constraints for IOA deposits include the Carmen and nearby IOA deposits (131.0 ± 1.0 Ma, apatite-magnetite U-Pb age; 126.8 ± 1.9 Ma, actinolite alteration, ^{40}Ar-^{39}Ar plateau age; Gelcich et al., 2005), the El Romeral deposit (127.7 ± 1.5 Ma, amphibole alteration, ^{40}Ar-^{39}Ar plateau age; Rojas et al., 2018), and a minimum age of 127.1 ± 0.7 Ma for the Dominga IOA deposit constrained by a Re-Os age for molybdenite in allanite-chalcopyrite-bearing breccia cutting the IOA deposit (Veloso et al., 2017). The age of IOA formation at the Dominga deposit is supported by an imprecise apatite U-Pb age of 127 ± 15 Ma (Veloso et al., 2017). These ~131-127 Ma ages are within error of the ages of abundant dioritic intrusions in the CIB which in many cases are proximal to the IOA deposits (e.g. Rojas et al., 2018; Seymour et al., 2020). Control of the sites of the large IOA deposits by sinistral strike-slip movement on regional shear zones linked to the AFS (e.g. Bookstrom, 1977) appears to be consistent with recently proposed timing constraints on ductile and then brittle movement on the AFS during the period ~135-120 Ma

(Seymour et al., 2020). This would place such IOA deposit formation well within the extension/transtension stage of Cretaceous Andean evolution rather than during the later compressional/transpressional regime, although local zones of transpression also may have controlled IOA formation along parts of the AFS (Oyarzun et al., 2003). The significance of a possible younger phase of IOA formation, recorded by a Pb-Th age of 116 ± 4 Ma for titanite associated with Na-Ca alteration at the Cerro Negro Norte magnetite (-apatite) deposit (Raab, 2001), has yet to be determined. Other mineralisation that formed at ~130 Ma includes small-medium sized porphyry Cu-Au-Mo deposits such as Productora, which was recently re-categorised from the IOCG class (Ray & Dick, 2002; Richards et al., 2017) to the porphyry copper class (130.1 ± 0.6 Ma, molybdenite Re-Os age, Escolme et al., 2020).

Many of the large IOA deposits in the CIB contain minor pyrite and in places minor chalcopyrite, and there has been much debate on the timing, origin and significance of such sulfides in relation to IOCG deposit formation (e.g. Sillitoe, 2003; Knipping et al., 2015; Reich et al., 2016; Simon et al., 2018; Childress et al., 2020 Sillitoe, 2003; Knipping et al., 2015; Simon et al., 2018; Childress et al., 2020). Unfortunately there appears to be a lack of geochronological data that relate clearly to the formation of the minor copper sulfides in IOA deposits in the CIB. Texturally, copper sulfides are almost invariably described as 'late' with respect to magnetite (-apatite) formation, and are commonly associated with very different mineral assemblages to those associated with massive and vein style magnetite (-apatite). For example at the Cerro Negro Norte IOA deposit small Cu-Au resources (e.g. 0.55 Mt @ 0.24 % Cu and 1.4 g/t Au) are associated with pyrite-chalcopyrite-bearing quartz-feldspar-tourmaline veins that cross-cut magnetite-actinolite-scapolite-titanite-apatite assemblages (Raab, 2001). Moreover, copper mineralisation is also present separately from IOA deposits in the Cerro Negro Norte district, within a broad zone of tourmaline-quartz alteration (Raab, 2001). More broadly, Sillitoe (2003) noted that nowhere in the CIB are complete transitions observable from IOA to IOCG deposits even though Cu is present at low levels in some IOA deposits. Whether the paragenetically early magnetite that is present in many of the IOCG deposits is of IOA origin, or is not directly related to IOA deposits, is an unresolved question in the CIB that requires more and better geochronology among other data.

The earliest examples of Cu ± Au mineralisation that formed coevally with abundant iron oxides are several 'IOCG veins' where associated actinolite alteration ^{40}Ar-^{39}Ar ages of ~120 Ma have been reported (e.g. 117.8 ± 1.9 Ma, Todos Los Santos prospect, Gelcich et al., 2005; and 121.9 ± 1.5 Ma and 119.8 ± 1.6 Ma, El Trapiche prospect, Creixell et al., 2009). This timing is consistent with K-Ar ages of hydrothermal sericite alteration at the large Mantoverde IOCG deposit (117 ± 3 Ma and 121 ± 3 Ma, Vila et al., 1996), and a two-point Re-Os isochron possible age of ~116 Ma for this deposit (Mathur, 2002). The best available age constraints for IOCG deposits are molybdenite Re-Os and amphibole and biotite ^{40}Ar-^{39}Ar ages from the large Candelaria IOCG deposit, which cluster around 116-114 Ma and 112-110 Ma (Marschik & Fontboté, 2001; Mathur et al., 2002). The timing of alteration at the Raúl-Condestable Cu-Au deposit in Peru is also tightly constrained by a titanite U-Pb age of 115.2 ± 0.3 Ma, which is the same age (within error) of subjacent tonalitic intrusions (de Haller et al., 2006). These ages place the formation of the earliest 'IOCG' veins and the major IOCG deposits at Candelaria and possibly Mantoverde towards the end of the extensional phase of Andean Jurassic-Cretaceous evolution (Sillitoe, 2003), coincident with thermally-enhanced major sinistral strike-slip movement on the AFS (Seymour et al., 2020). Indeed, syn-extensional timing of mineralisation has been proposed for the Candelaria deposit by Oyarzun et al. (2003) and Arévalo et al. (2006).

Several iron oxide-rich Cu-Au deposits in Chile and Peru record ages in the range ~110-84 Ma (Richards et al., 2017), but the significance of many of these reported 'young' ages is unclear. For example, whereas at Mina Justa (Peru) ~111-110 Ma ^{40}Ar-^{39}Ar ages for actinolite are likely a robust record of the timing of magnetite alteration because of the relatively high closure temperature for actinolite, ^{40}Ar-^{39}Ar ages of ~104-95 Ma from adularia associated with copper mineralisation (Chen et al., 2010a) may represent cooling ages rather than the timing of copper

introduction, on account of the relatively low closure temperatures for adularia. Adding to the uncertainty in the significance of the ~110-84 Ma ages of some Cu-Au-Fe deposits, copper deposits of undoubted porphyry Cu (-Au-Mo) affiliation with broadly similar ages to both the iron oxide-rich Cu-Au and IOA deposits (Richards et al., 2017) are also present within and adjacent to the CIB (Sillitoe, 2003; Richards et al., 2017). For example, the Tropezón Cu-Mo (-Au) deposit has been included within the IOCG family (e.g. Richards et al., 2017) yet was considered by Tornos et al. (2010) as transitional between an IOCG and a porphyry Cu deposit. The age of the host quartz diorite to tonalite stock (110.0 ± 2.1 Ma) therefore may be close to either the timing of iron oxide-rich porphyry style mineralisation or the timing of a hybrid style of IOCG deposit. A third case is the El Espino Cu-Au deposit which has been described as an IOCG deposit, and has been dated at ~88-86 Ma (actinolite, sericite and K-feldspar ^{40}Ar-^{39}Ar ages, Lopez et al., 2014). If this deposit is of IOCG affinity, its age would imply the presence of a significantly younger IOCG event than that forming the Candelaria deposit.

In summary, variably apatite-rich magnetite IOA deposits without significant Cu-Au formed at ~130 Ma, prior to commencement of the main stage of IOCG mineralisation at ~120-110 Ma. Relatively small porphyry Cu-Au-Mo deposits also formed across this ~130-110 Ma metallogenic period, which occurred within an overall extensional to transtensional tectonic regime mostly prior to, but also perhaps overlapping with (Chen et al., 2013), the onset of inversion tectonism at ~107-100 Ma regime in northern Chile when arc-related magmatism was waning. Strike-slip brittle-ductile to brittle deformation on the Atacama Fault System, enhanced by intrusion-induced thermal softening, appears to have partly controlled the locations of some of the larger IOA as well as IOCG deposits. Although minor IOCG deposit formation may have continued during the early stages of inversion it appears that manto Cu (-Ag) and small porphyry Cu and affiliated deposits were the dominant types of mineralisation during the compressional regime in the Late Cretaceous. Hybrid mineralisation styles hypothetically could have developed where later hydrothermal systems (e.g. porphyry, skarn, manto) overprinted earlier mineralisation (e.g. IOCG, IOA).

12. Other possible IOCG provinces

Singhbhum Shear Zone, India

The Singhbhum Shear Zone (SSZ) is located in eastern part of the Indian Precambrian Shield, ~200 km west of Kolkata. It separates an Archean craton to the south from the Proterozoic North Singhbhum Mobile Belt to the north. The arcuate SSZ hosts numerous economic deposits of Cu and U and is also known for its apatite-magnetite deposits (Bhattachuryya, 1992). Pal et al. (2010) and Chowdhury et al. (2020) have drawn attention to the similarities between Fe-oxide-bearing Cu and U mineralisation in the SSZ and IOCG deposits, including the association of Fe oxides with Cu and U, presence of Na-altered rocks in the SSZ, lack of significant Zn in the Cu and U deposits, hypersaline fluid inclusions, boron isotope compositions of hydrothermal tourmaline, and trace element compositions of pyrite. However, there are few published comprehensive geological descriptions of the Cu and U deposits and their host geological settings and alteration, making it difficult to fully assess the affinity of these deposits with the IOCG and ISCG deposits in CGI mineral systems discussed in the present review.

Wernecke Mountains, Canada

Copper-Au ± U ± Co mineralisation and hydrothermal alteration with similarities to those in IOCG deposits and CGI mineral systems has been described from the Wernecke Mountains in the Yukon Territory of Canada (Hitzman et al., 1992; Hunt et al., 2005). To date, only prospects have been discovered in this region; it is unclear whether the lack of known major deposits is due to the limited exploration or whether a crucial 'ingredient' is missing in the mineral systems.

Lufilian Belt, southern-central Africa

Although the Zambian Copperbelt of south-central Africa is well known for its sediment-hosted stratiform and stratabound Cu (-Co) deposits there are also strong indications of the presence of IOCG mineralisation (Nisbet et al., 2002). Iron-rich Cu-Co-U mineralisation has been described in association with the Cambrian Hook Granitoid, an A-type suite associated with syn- to late-stages of the Lufilian Orogeny (Nisbet et al., 2002; Simusokwe et al., 2021).

References (for Supplementary Information)

Acosta-Góngora, P., Gleeson, S. A., Samson, I. M., Corriveau, L., Ootes, L., Taylor, B. E., Creaser, R. A., & Muehlenbachs, K. (2015). Genesis of the Paleoproterozoic NICO iron oxide-cobalt-gold-bismuth deposit, Northwest Territories, Canada: Evidence from isotope geochemistry and fluid inclusions. *Precambrian Research*, *268*, 168–193. https://doi.org/10.1016/j.precamres.2015.06.007

Arévalo, C., Grocott, J., Martin, W., Pringle, M., & Taylor, G. (2006). Structural setting of the Candelaria Fe oxide Cu-Au deposit, Chilean Andes (27°30′ S). *Economic Geology*, *101*(4), 819–841. https://doi.org/10.2113/gsecongeo.101.4.819

Armistead, S. E., Betts, P. G., Ailleres, L., Armit, R. J., & Williams, H. A. (2018). Cu-Au mineralisation in the Curnamona Province, South Australia: A hybrid stratiform genetic model for Mesoproterozoic IOCG systems in Australia. *Ore Geology Reviews*, *94*(September 2017), 104–117. https://doi.org/10.1016/j.oregeorev.2018.01.024

Ashley, P. M., Cook, N. D. J., & Fanning, C. M. (1996). Geochemistry and age of metamorphosed felsic igneous rocks with A-type affinities in the Willyama Supergroup, Olary Block, South Australia, and implications for mineral exploration. *Lithos*, *38*(3–4), 167–184. https://doi.org/10.1016/0024-4937(96)00011-4

Ashley, P. M., Lawie, D. C., Conor, C. H. H., & Plimer, I. R. (1997). *Geology of the Olary Domain, Curnamona Province, South Australia and field guide to 1997 excursion stops*. *Report Book*.

Austin, J. R., & Blenkinsop, T. G. (2010). Cloncurry fault zone: Strain partitioning and reactivation in a crustal-scale deformation zone, mt isa inlier. *Australian Journal of Earth Sciences*, *57*(1), 1–21. https://doi.org/10.1080/08120090903416187

Babo, J., Spandler, C., Oliver, N. H. S., Brown, M., Rubenach, M. J., & Creaser, R. A. (2017). The high-grade mo-Re Merlin deposit, Cloncurry district, Australia: Paragenesis and geochronology of hydrothermal alteration and ore formation. *Economic Geology*, *112*(2), 397–422. https://doi.org/10.2113/econgeo.112.2.397

Baidya, A. S., & Pal, D. C. (2020). Geochemical evolution and timing of uranium mineralization in the Khetri Copper Belt, western India. *Ore Geology Reviews*, *127*(January 2019), 103794. https://doi.org/10.1016/j.oregeorev.2020.103794

Baker, T., & Laing, W. P. (1998). Eloise Cu-Au deposit, East Mt Isa Block: Structural environment and structural controls on ore. *Australian Journal of Earth Sciences*, *45*(3), 429–444. https://doi.org/10.1080/08120099808728402

Barton, M. D. (2013). Iron Oxide(-Cu-Au-REE-P-Ag-U-Co) Systems. In *Treatise on Geochemistry: Second Edition* (Vol. 13, pp. 515–541). Elsevier Inc. https://doi.org/10.1016/B978-0-08-095975-7.01123-2

Bascuñán, S., Arriagada, C., le Roux, J., & Deckart, K. (2016). Unraveling the Peruvian Phase of the Central Andes: Stratigraphy, sedimentology and geochronology of the Salar de Atacama Basin (22°30-23°S), northern Chile. *Basin Research*, *28*(3), 365–392. https://doi.org/10.1111/bre.12114

Bauer, T. E., Lynch, E. P., Sarlus, Z., Drejing-Carroll, D., Martinsson, O., Metzger, N., & Wanhainen, C. (2021). Structural controls on iron oxide-copper-gold mineralization and related alteration in a Paleoproterozoic supracrustal belt: Insights from the Nautanen deformation zone and surroundings, northern Sweden. *Economic Geology*, (in press).

Bergman, S., Billström, K., Persson, P. O., Skiöld, T., & Evins, P. (2006). U-pb age evidence for repeated palaeoproterozoic metamorphism and deformation near the pajala shear zone in the northern fennoscandian shield. *Gff*, *128*(1), 7–20. https://doi.org/10.1080/11035890601281007

Bergman, S., Kübler, L., & Martinsson, O. (2001). *Description of regional geological and geophysical maps of northern Norrbotten County (east of the Caledonian orogen)*.

Bettencourt, J. S., Juliani, C., Xavier, R. P., Monteiro, L. V. S., Bastos Neto, A. C., Klein, E. L., Assis, R. R., Leite, W. B., Moreto, C. P. N., Fernandes, C. M. D., & Pereira, V. P. (2016). Metallogenetic

systems associated with granitoid magmatism in the Amazonian Craton: An overview of the present level of understanding and exploration significance. *Journal of South American Earth Sciences*, *68*(May), 22–49. https://doi.org/10.1016/j.jsames.2015.11.014

Betts, P. G., Giles, D., Foden, J., Schaefer, B. F., Mark, G., Pankhurst, M. J., Forbes, C. J., Williams, H. A., Chalmers, N. C., & Hills, Q. (2009). Mesoproterozoic plume-modified orogenesis in eastern Precambrian Australia. *Tectonics*, *28*(3), 1–28. https://doi.org/10.1029/2008TC002325

Bhattacharyya, D. S. (1992). Early proterozoic metallogeny, tectonics and geochronology of the singhbhum CuU belt, eastern India. *Precambrian Research*, *58*(1–4), 71–83. https://doi.org/10.1016/0301-9268(92)90113-3

Bierlein, F. P., Ashley, P. M., & Plimer, I. R. (1995). Sulphide mineralisation in the Olary Block, South Australia - Evidence for syn-tectonic to late-stage mobilisation. *Mineralium Deposita*, *30*(6), 424–438. https://doi.org/10.1007/BF00196402

Billström, K., Evins, P., Martinsson, O., Jeon, H., & Weihed, P. (2019). Conflicting zircon vs. titanite U-Pb age systematics and the deposition of the host volcanic sequence to Kiruna-type and IOCG deposits in northern Sweden, Fennoscandian shield. *Precambrian Research*, *321*(December 2018), 123–133. https://doi.org/10.1016/j.precamres.2018.12.003

Billström, Kjell, Eilu, P., Martinsson, O., Niiranen, T., Broman, C., Weihed, P., & Wanhainen, C. (2010). IOCG and related mineral deposits of the northern Fennoscandian Shield. In T. M. Porter (Ed.), *Hydrothermal iron oxide copper-gold and related deposits: A global perspective, Volume 4* (pp. 381–414). PGC Publishing.

Blake, D. H. (1987). *Geology of the Mount Isa Inlier and environs, Queensland and Northern Territory*. Bureau of Mineral Resources Bulletin 225.

Bookstrom, A. A. (1977). The magnetite deposits of El Romeral, Chile. *Economic Geology*, *72*(6), 1101–1130. https://doi.org/10.2113/gsecongeo.72.6.1101

Bowden, B., Fraser, G., Davidson, G. J., Meffre, S., Skirrow, R., Bull, S., & Thompson, J. (2017). Age constraints on the hydrothermal history of the Prominent Hill iron oxide copper-gold deposit, South Australia. *Mineralium Deposita*, *52*(6), 863–881. https://doi.org/10.1007/s00126-016-0689-1

Boyce, D., Charrier, R., & Farías, M. (2020). The First Andean Compressive Tectonic Phase: Sedimentologic and Structural Analysis of Mid-Cretaceous Deposits in the Coastal Cordillera, Central Chile (32°50′S). *Tectonics*, *39*(2), 1–24. https://doi.org/10.1029/2019TC005825

Brown, M., & Porter, T. M. (2010). The Mount Elliott IOCG system, Eastern Fold Belt, Mount Isa Inlier, northwest Queensland. In T. M. Porter (Ed.), *Hydrothermal iron oxide copper-gold and related deposits: A global perspective, Volume 3* (pp. 219–231). PGC Publishing.

Budd, A. (2006). *The Tarcoola Goldfeld of the central Gawler gold province, and the Hiltaba Association Granites, Gawler craton, South Australia: Unpublished PhD thesis*, Australian National University.

Budd, A. R., & Fraser, G. L. (2004). Geological relationships and 40Ar/39Ar age constraints on gold mineralisation at Tarcoola, central Gawler gold province, South Australia. *Australian Journal of Earth Sciences*, *51*(5), 685–699. https://doi.org/10.1111/j.1400-0952.2004.01084.x

Budd, A. R., & Skirrow, R. G. (2007). The nature and origin of gold deposits of the Tarcoola Goldfield and implications for the central Gawler Gold Province, South Australia. *Economic Geology*, *102*(8). https://doi.org/10.2113/gsecongeo.102.8.1541

Carr, L. K., Korsch, R. J., Holzschuh, J., Costelloe, R. D., Meixner, A. J., Matthews, C., & Godsmark, B. (2010). Geological interpretation of seismic reflection lines 08GA-C1 and 09TE-01: Arrowie Basin, South Australia. In R. J. Korsch & N. Kositcin (Eds.), *South Australian Seismic and MT Workshop 2010, Extended Abstracts, Record 2010/10* (pp. 54–65). Geoscience Australia.

Chowdhury, S., Pal, D. C., Papineau, D., & Lentz, D. R. (2020). Major and trace element and multiple sulfur isotope composition of sulfides from the Paleoproterozoic Surda copper deposit, Singhbhum shear Zone, India: Implications for the mineralization processes. *Ore Geology Reviews*, *120*(February), 103396. https://doi.org/10.1016/j.oregeorev.2020.103396

Chen, H., Clark, A. H., & Kyser, T. K. (2010). The Marcona magnetite deposit, Ica, south-central Peru: A product of hydrous, iron oxide-rich melts? *Economic Geology*, *105*(8), 1441–1456. https://doi.org/10.2113/econgeo.105.8.1441

Chen, H., Clark, A. H., Kyser, T. K., Ullrich, T. D., Baxter, R., Chen, Y., & Moody, T. C. (2010). Evolution of the giant Marcona-Mina Justa iron oxide-copper-gold district, South-Central Peru. *Economic Geology*, *105*(1), 155–185. https://doi.org/10.2113/gsecongeo.105.1.155

Chen, H., Cooke, D. R., & Baker, M. J. (2013). Mesozoic iron oxide copper-gold mineralization in the Central Andes and the Gondwana supercontinent breakup. *Economic Geology*, *108*(1), 37–44. https://doi.org/10.2113/econgeo.108.1.37

Chen, W. T., & Zhou, M. F. (2014). Ages and compositions of primary and secondary allanite from the Lala Fe-Cu deposit, SW China: Implications for multiple episodes of hydrothermal events. *Contributions to Mineralogy and Petrology*, *168*(2), 1–20. https://doi.org/10.1007/s00410-014-1043-1

Cherry, A. R., Ehrig, K., Kamenetsky, V. S., McPhie, J., Crowley, J. L., & Kamenetsky, M. B. (2018). Precise geochronological constraints on the origin, setting and incorporation of ca. 1.59 Ga surficial facies into the Olympic Dam Breccia Complex, South Australia. *Precambrian Research*, *315*(July), 162–178. https://doi.org/10.1016/j.precamres.2018.07.012

Childress, T. M., Simon, A. C., Reich, M., Barra, F., Arce, M., Lundstrom, C. C., & Bindeman, I. N. (2020). Formation of the Mantoverde iron oxide-copper-gold (IOCG) deposit, Chile: insights from Fe and O stable isotopes and comparisons with iron oxide-apatite (IOA) deposits. *Mineralium Deposita*, *55*(7), 1489–1504. https://doi.org/10.1007/s00126-019-00936-x

Ciobanu, C. L., Wade, B. P., Cook, N. J., Schmidt Mumm, A., & Giles, D. (2013). Uranium-bearing hematite from the Olympic Dam Cu-U-Au deposit, South Australia: A geochemical tracer and reconnaissance Pb-Pb geochronometer. *Precambrian Research*, *238*, 129–147. https://doi.org/10.1016/j.precamres.2013.10.007

Claoué-Long, J., Maidment, D., & Donnellan, N. (2008). Stratigraphic timing constraints in the Davenport Province, central Australia: A basis for Palaeoproterozoic correlations. *Precambrian Research*, *166*, 204–218. https://doi.org/10.1016/j.precamres.2007.06.021

Claoué-Long, J., Maidment, D., Hussey, K., & Huston, D. (2008). The duration of the Strangways Event in central Australia: Evidence for prolonged deep crust processes. *Precambrian Research*, *166*(1–4), 246–262. https://doi.org/10.1016/j.precamres.2007.06.023

Clark, C., Schmidt Mumm, A., & Faure, K. (2005). Timing and nature of fluid flow and alteration during Mesoproterozoic shear zone formation, Olary domain, South Australia. *Journal of Metamorphic Geology*, *23*(3), 147–164. https://doi.org/10.1111/j.1525-1314.2005.00568.x

Compston, D. M. (1995). Time constraints on the evolution of the Tennant Creek Block, northern Australia. *Precambrian Research*, *71*(1–4), 107–129. https://doi.org/10.1016/0301-9268(94)00058-Y

Compston, D. M., & McDougall, I. (1994). 40Ar-39Ar and K-Ar Age Constraints on the Early Proterozoic Tennant Creek Block, Northern Australia, and the Age of Its Gold Deposits. *Australian Journal of Earth Sciences*, *41*(6), 609–616. https://doi.org/10.1080/08120099408728171

Conor, C. H. H. (1995). *Moonta-Wallaroo region - An interpretation of the geology of the Maitland and Wallaroo 1:100 000 sheet areas*. Geological Survey of South Australia.

Conor, C., Raymond, O., Baker, T., Teale, G., Say, P., & Lowe, G. (2010). Alteration and mineralisation in the Moonta-Wallaroo copper-gold mining field region, Olympic Domain, South Australia. In T. M. Porter (Ed.), *Hydrothermal iron oxide copper-gold and related deposits: A global perspective, Volume 3* (pp. 147–170). PGC Publishing.

Conor, Colin H.H., & Preiss, W. v. (2008). Understanding the 1720-1640 Ma Palaeoproterozoic Willyama Supergroup, Curnamona Province, Southeastern Australia: Implications for tectonics, basin evolution and ore genesis. *Precambrian Research*, *166*(1–4), 297–317. https://doi.org/10.1016/j.precamres.2007.08.020

Conor, Colin, Raymond, O., Baker, T., Teale, G., Say, P., & Lowe, G. (2010). *Alteration and Mineralisation in the Moonta-Wallaroo Cu-Au Mining Field Region, Olympic Domain, South Australia*. 147–170.

Cook, N. D. J., & Ashley, P. M. (1992). Meta-evaporite sequence, exhalative chemical sediments and associated rocks in the Proterozoic Willyama Supergroup, South Australia: implications for metallogenesis. *Precambrian Research*, *56*(3–4), 211–226. https://doi.org/10.1016/0301-9268(92)90102-T

Cook, N. D. J., Fanning, C. M., & Ashley, P. M. (1994). New geochronological results from the Willyama Supergroup, Olary Block, South Australia. *Australian Research on Ore Genesis Symposium, Adelaide, South Australia, December 12-14 1994*.

Corriveau, L., Montreuil, J. F., & Potter, E. G. (2016). Alteration facies linkages among iron oxide copper-gold, iron oxide-apatite, and affiliated deposits in the Great Bear magmatic zone, Northwest Territories, Canada. *Economic Geology*, *111*(8), 2045–2072. https://doi.org/10.2113/econgeo.111.8.2045

Corriveau, L., Williams, P. . J., & Mumin, H. (2010). Alteration vectors to IOCG mineralization from uncharted terranes to deposits. In *Exploring for iron oxide copper-gold deposits: Canada and global analogues* (pp. 89–110). Geological Association of Canada, Short Course Notes, Volume 20.

Corriveau, Louise. (2007). Iron oxide copper-gold deposits: A Canadian perspective. In W. Goodfellow (Ed.), *Mineral deposits in Canada: A synthesis of major deposit types, district metallogeny, the evolution of geological provinces and exploration methods* (pp. 307–328). Geological Association of Canada, Mineral Deposits Division, Special Publication Volume 5.

Corriveau, Louise, Mumin, A. H., & Setterfield, T. (2010). IOCG environments in Canada: Characteristics, geological vectors to ore and challenges. In T. M. Porter (Ed.), *Hydrothermal iron oxide copper-gold and related deposits: A global perspective, Volume 4* (pp. 311–344). PGC Publishing.

Courtney-Davies, L., Ciobanu, C. L., Verdugo-Ihl, M. R., Dmitrijeva, M., Cook, N. J., Ehrig, K., & Wade, B. P. (2019). Hematite geochemistry and geochronology resolve genetic and temporal links among iron-oxide copper gold systems, Olympic Dam district, South Australia. *Precambrian Research*, *335*(June), 105480. https://doi.org/10.1016/j.precamres.2019.105480

Cowley, W. M. (compiler). (2008). *Solid geology of South Australia: Archaean to Early Mesoproterozoic time slice map*. Geological Survey of South Australia. https://sarigbasis.pir.sa.gov.au/WebtopEw/ws/samref/sarig1/wcir/Record?r=0&m=1&w=catno=2038279

Craveiro, G. S., Villas, R. N. N., & Xavier, R. P. (2020). A fluid inclusion and stable isotope (O, H, S and C) study of the Archean IOCG Cristalino deposit, Carajás Mineral Province, Brazil: Implications to ore genesis. *Ore Geology Reviews*, *127*(August), 103822. https://doi.org/10.1016/j.oregeorev.2020.103822

Creixell, C., Arévalo, C., & Fanning, C. M. (2009). Geochronology of the cretaceous magmatism from the Coastal Cordillera of north-central Chile (29°15' to 29°30' S): metallogenic implications. *XII Congreso Geológico Chileno, Santiago, 22-26 Noviembre, 2009*, 3 p.

Cross, A. J., Clark, A. D., Schofield, A., Kositcin, N., Creek, T., Isa, M., & Supersuite, T. (2020). New SHRIMP U-Pb zircon and monazite geochronology of the East Tennant region: a possible undercover extension of the Warramunga Province, Tennant Creek. *Geoscience Australia, Exploring for the Future, Extended Abstract Volume*, 1–4. https://doi.org/http://dx.doi.org/10.11636/132771

Cuison, A. G., Osborne, G. A., Russell, S. C., & Bills, R. T. (2014). An integrated geological model for the Tennant Creek style Au-Bi-Cu mineralization - Evolution of the Gecko corridor, Tennant Creek Goldfield. *Northern Territory Geological Survey, Annual Geoscience Exploration Seminar (AGES), Record of Abstracts*, *Record 56*.

Curtis, S., Wade, C., & Reid, A. (2018). Sedimentary basin formation associated with a silicic large igneous province: stratigraphy and provenance of the Mesoproterozoic Roopena Basin, Gawler Range Volcanics. *Australian Journal of Earth Sciences*, *65*(4), 447–463. https://doi.org/10.1080/08120099.2018.1460398

Daly, S. J., Fanning, C. M., & Fairclough, M. C. (1998). Tectonic evolution and exploration potential of the Gawler craton. *AGSO Journal of Australian Geology and Geophysics*, *17*, 145–168.

Davidson, G. J., Paterson, H., Meffre, S., & Berry, R. F. (2007). Characteristics and origin of the oak dam East Breccia-Hosted, iron oxide Cu-U-(Au) Deposit: Olympic Dam region, Gawler Craton, South Australia. *Economic Geology*, *102*(8), 1471–1498. https://doi.org/10.2113/gsecongeo.102.8.1471

de Freitas Toledo, P. I., Moreto, C. P. N., Xavier, R. P., Gao, J., de Matos, J. H. da S. N., & de Melo, G. H. C. (2019). Multistage evolution of the Neoarchean (ca. 2.7 Ga) Igarapé Cinzento (GT-46) iron oxide copper-gold deposit, Cinzento Shear Zone, Carajás Province, Brazil. *Economic Geology*, *114*(1), 1–34. https://doi.org/10.5382/econgeo.2019.4617

de Haller, A., Corfu, F., Fontboté, L., Schaltegger, U., Barra, F., Chiaradia, M., Frank, M., & Alvarado, J. Z. (2006). Geology, geochronology, and Hf and Pb isotope data of the Raúl-Condestable iron oxide-copper-gold deposit, central coast of Peru. *Economic Geology*, *101*(2), 281–310. https://doi.org/10.2113/gsecongeo.101.2.281

de Melo, G. H. C., Monteiro, L. V. S., Xavier, R. P., Moreto, C. P. N., Santiago, E. S. B., Dufrane, S. A., Aires, B., & Santos, A. F. F. (2017). Temporal evolution of the giant Salobo IOCG deposit, Carajás Province (Brazil): constraints from paragenesis of hydrothermal alteration and U-Pb geochronology. *Mineralium Deposita*, *52*(5), 709–732. https://doi.org/10.1007/s00126-016-0693-5

Dias, G. S., Macambira, M. B. Dall'Agnol, R., Soares, A. D. v., & Barros, C. E. M. (1996). Datações de zircões de sill de metagabro: comprovação de idade arqueana da Formação Águas Claras, Carajás, Pará. *Simpósio de Geologia Da Amazônia, 5th: Belém*, 376–378.

Diella, V., Ferrario, A., & Girardi, V. A. V. (1995). PGE and PGM in the Luanga mafic-ultramafic intrusion in Serra dos Carajás (Pará State, Brazil). *Ore Geology Reviews*, *9*(6), 445–453. https://doi.org/10.1016/0169-1368(95)00002-J

Donnellan, N. (2013). Chapter 9: Warramunga Province. In M. Ahmad & T. J. Munson (Eds.), *Geology and mineral resources of the Northern Territory* (pp. 9:1-9:61). Northern Territory Geological Survey, Special Publication.

Donnellan, N., Hussey, K. J., & Morrison, R. S. (1995). *Flynn 5759, Tennant Creek 5758: Explanatory Notes, 1:100 000 Geological Map Series*.

Duncan, R. J., Stein, H. J., Evans, K. A., Hitzman, M. W., Nelson, E. P., & Kirwin, D. J. (2011). A new geochronological framework for mineralization and alteration in the Selwyn-Mount Dore corridor, Eastern Fold Belt, Mount Isa Inlier, Australia: Genetic implications for iron oxide copper-gold deposits. *Economic Geology*, *106*(2), 169–192. https://doi.org/10.2113/econgeo.106.2.169

Edfelt, Å. (2007). *The Tjårrojåkka Apatite-Iron and Cu (-Au) - Products of One Ore Forming Event*. Unpublished PhD thesis, Luleä University, Sweden.

Edfelt, Å., Sandrin, A., Evins, P., Jeffries, T., Storey, C., Elming, S. Å., & Martinsson, O. (2006). Stratigraphy and tectonic setting of the host rocks to the Tjårrojåkka Fe-oxide Cu-Au deposits, Kiruna area, northern Sweden. *Gff*, *128*(3), 221–232. https://doi.org/10.1080/11035890601283221

Ehrig, K., Kamenetsky, V. S., McPhie, J., Macmillan, E., Thompson, J., Kamenetsky, M., & Maas, R. (2021). Staged formation of the supergiant Olympic Dam uranium deposit, Australia. *Geology*, *XX*(Xx), 1–5. https://doi.org/10.1130/g48930.1

Escolme, A., Cooke, D. R., Hunt, J., Berry, R. F., Maas, R., & Creaser, R. A. (2020). The Productora Cu-Au-Mo Deposit, Chile: A Mesozoic Magmatic-Hydrothermal Breccia Complex with Both Porphyry and Iron Oxide Cu-Au Affinities. *Economic Geology*, *115*(3), 543–580. https://doi.org/10.5382/ECONGEO.4718

Fanning, C. M., Ashley, P. M., Cook, N. D. J., Teale, G. S., & Conor, C. C. H. (1998). A geochronological perspective of crustal evolution in the Curnamona Province. In G. M. Gibson (Ed.), *Broken Hill Exploration Initiative, Record 1998/25* (pp. 30–37). Australian Geological Survey Organisation.

Fareeduddin, G. S., Kirmani, I. R., & Suresh, C. (2012). Petrology, geochemistry and fluid inclusion studies of Cu-Au mineralization in Paleoproterozoic Salumbar-Ghatol Belt, Aravalli Supergroup, Rajasthan. *Journal of the Geological Society of India*, *80*(July), 5–38.

Feio, G. R. L., Dall'Agnol, R., Dantas, E. L., Macambira, M. J. B., Santos, J. O. S., Althoff, F. J., & Soares, J. E. B. (2013). Archean granitoid magmatism in the Canaã dos Carajás area: Implications for crustal evolution of the Carajás province, Amazonian craton, Brazil. *Precambrian Research*, *227*, 157–185. https://doi.org/10.1016/j.precamres.2012.04.007

Fennell, L. M., Folguera, A., Naipauer, M., Gianni, G., Rojas Vera, E. A., Bottesi, G., & Ramos, V. A. (2017). Cretaceous deformation of the southern Central Andes: synorogenic growth strata in the Neuquén Group (35° 30′–37° S). *Basin Research*, *29*, 51–72. https://doi.org/10.1111/bre.12135

Ferris, G. M., Schwarz, M. P., & Heithersay, P. (2002). The geological framework, distribution and controls of Fe-oxide Cu-Au deposits in the Gawler craton. Part I. Geological and tectonic framework. In T. M. Porter (Ed.), *Hydrothermal iron oxide copper-gold and related deposits: A global perspective, Volume 2* (pp. 9–31).

Ferris, G., & Schwarz, M. (2003). Proterozoic gold province of the central Gawler Craton. *MESA Journal*, *30*(July), 4–12.

Forbes, C. J., Giles, D., Betts, P. G., Weinberg, R., & Kinny, P. D. (2007). Dating prograde amphibolite and granulite facies metamorphism using in situ monazite U-Pb SHRIMP analysis. *Journal of Geology*, *115*(6), 691–705. https://doi.org/10.1086/521611

Foster, D. R. W., & Austin, J. R. (2008). The 1800-1610 Ma stratigraphic and magmatic history of the Eastern Succession, Mount Isa Inlier, and correlations with adjacent Paleoproterozoic terranes. *Precambrian Research*, *163*(1–2), 7–30. https://doi.org/10.1016/j.precamres.2007.08.010

Fraser, G. L., Hussey, K., & Compston, D. M. (2008). Timing of Palaeoproterozoic Au-Cu-Bi and W-mineralization in the Tennant Creek region, northern Australia: Improved constraints via intercalibration of 40Ar/39Ar and U-Pb ages. *Precambrian Research*, *164*(1–2), 50–65. https://doi.org/10.1016/j.precamres.2008.03.005

Fraser, G. L., Skirrow, R. G., Schmidt-Mumm, A., & Holm, O. (2007). Mesoproterozoic gold in the central Gawler craton, South Australia: Geology, alteration, fluids, and timing. *Economic Geology*, *102*(8). https://doi.org/10.2113/gsecongeo.102.8.1511

Freeman, H., & Tomkinson, M. (2010). Geological setting of iron oxide related mineralisation in the southern Mount Woods Domain, South Australia. In T. M. Porter (Ed.), *Hydrothermal iron oxide copper-gold and related deposits: A global perspective, Volume 3* (pp. 171–190). PGC Publishing.

Gandhi, S. S., & Bell, R. T. (1989). Potential for Olympic Dam-type Cu-Au-U-Fe deposits in the Great Bear magmatic zone. In *Exploration Overview 1989, Northwest Territories, Part 2, Preliminary reports on geological work in N.W.T.* (pp. 32–33). Geological Mapping Division, Indian Affairs and Northern Development, Canada.

Gauthier, L., Hall, G., Stein, H. J., & Schaltegger, U. (2001). The Osborne deposit, Cloncurry district: A 1595 Ma Cu-Au skarn deposit. *Contributions of the Economic Geology Research Unit, James Cook University*, *59*, 58–59.

Gelcich, S., Davis, D. W., & Spooner, E. T. C. (2005). Testing the apatite-magnetite geochronometer: U-Pb and 40Ar/ 39Ar geochronology of plutonic rocks, massive magnetite-apatite tabular bodies, and IOCG mineralization in Northern Chile. *Geochimica et Cosmochimica Acta*, *69*(13), 3367–3384. https://doi.org/10.1016/j.gca.2004.12.020

Gianni, G. M., Navarrete, C., Echaurren, A., Díaz, M., Butler, K. L., Horton, B. K., Encinas, A., & Folguera, A. (2020). Northward propagation of Andean genesis: Insights from Early Cretaceous synorogenic deposits in the Aysén-Río Mayo basin. *Gondwana Research*, *77*, 238–259. https://doi.org/10.1016/j.gr.2019.07.014

Gibson, G. M., Meixner, A. J., Withnall, I. W., Korsch, R. J., Hutton, L. J., Jones, L. E. A., Holzschuh, J., Costelloe, R. D., Henson, P. A., & Saygin, E. (2016). Basin architecture and evolution in the Mount Isa mineral province, northern Australia: Constraints from deep seismic reflection

profiling and implications for ore genesis. *Ore Geology Reviews*, *76*, 414–441. https://doi.org/10.1016/j.oregeorev.2015.07.013

Giles, C. W. (1988). Petrogenesis of the Proterozoic Gawler Range Volcanics, South Australia. *Precambrian Research*, *40–41*(C), 407–427. https://doi.org/10.1016/0301-9268(88)90078-2

Giles, D., Betts, P., & Lister, G. (2002). northeastern Australia. *Geological Society of America*, *30*(9), 823–826.

Girardi, J. D. (2014). *Comparison of Mesozoic magmatic evolution and iron oxide (-copper-gold) ('IOCG') mineralization, central Andes and western North America*. Unpublished MSc thesis, The University of Arizona.

Grainger, C. J., Groves, D. I., Tallarico, F. H. B., & Fletcher, I. R. (2008). Metallogenesis of the Carajás Mineral Province, Southern Amazon Craton, Brazil: Varying styles of Archean through Paleoproterozoic to Neoproterozoic base- and precious-metal mineralisation. *Ore Geology Reviews*, *33*(3–4), 451–489. https://doi.org/10.1016/j.oregeorev.2006.10.010

Gregory, C. J., Reid, A. J., Say, P., & Teale, G. S. (2011). U–Pb geochronology of hydrothermal allanite and titanite and magmatic zircon from the Hillside Cu–Au deposit, Yorke Peninsula. In A.J. Reid & E. A. Jagodzinski (Eds.), *PACE geochronology: results of collaborative geochronology projects 2009–10 South Australia, Report Book 2011/00003* (pp. 95–126). Department of Primary Industries and Resources.

Groves, D. I., Bierlein, F. P., Meinert, L. D., & Hitzman, M. W. (2010). Iron Oxide Copper-Gold (IOCG) Deposits through Earth History: Implications for Origin, Lithospheric Setting, and Distinction from Other Epigenetic Iron Oxide Deposits. *Economic Geology*, *105*, 641–654.

Hand, M., Reid, A., & Jagodzinski, L. (2007). Tectonic framework and evolution of the Gawler craton, Southern Australia. *Economic Geology*, *102*(8), 1377–1395. https://doi.org/10.2113/gsecongeo.102.8.1377

Hawkes, N., Clark, A. H., & Moody, T. C. (2002). Marcona and Pampa de Pongo: Giant Mesozoic Fe-(Cu, Au) deposits in the Peruvian Coastal Belt. In T. M. Porter (Ed.), *Hydrothermal iron oxide copper-gold and related deposits: A global perspective, Volume 2* (pp. 115–130). PGC Publishing.

Haynes, D. W. (2000). Iron oxide copper (-gold) deposits: their position in the deposit spectrum and modes of origin. In *Hydrothermal iron oxide copper-gold and related deposits: A global perspective, Volume 1* (pp. 71–90). Australian Mineral Foundation.

Hennessey, B. T., & Puritch, E. (2008). *A technical report on a mineral resource estimate for the Sue-Dianne deposit, Mazenod Lake area, Northwest Territories, Canada*. www.sedar.com

Hildebrand, R. S. (1986). Kiruna-type deposits: their origin and relationship to intermediate subvolcanic plutons in the Great Bear magmatic zone, northwest Canada. *Economic Geology*, *81*(3), 640–659. https://doi.org/10.2113/gsecongeo.81.3.640

Hildebrand, Robert S., Hoffman, P. F., & Bowring, S. A. (1987). Tectono-magmatic evolution of the 1.9-Ga Great Bear magmatic zone, Wopmay orogen, northwestern Canada. *Journal of Volcanology and Geothermal Research*, *32*(1–3), 99–118. https://doi.org/10.1016/0377-0273(87)90039-4

Hildebrand, Robert S., Hoffman, P. F., & Bowring, S. A. (2010). The Calderian orogeny in Wopmay orogen (1.9 Ga), northwestern Canadian Shield. *Bulletin of the Geological Society of America*, *122*(5–6), 794–814. https://doi.org/10.1130/B26521.1

Hitzman, M. W. (2000). Iron oxide-Cu-Au deposits: what, where, when and why? In T. M. Porter (Ed.), *Hydrothermal iron oxide copper-gold and related deposits: A global perspective, Volume 1* (pp. 9–25). Australian Mineral Foundation.

Hitzman, M. W., Oreskes, N., & Einaudi, M. T. (1992). Geological characteristics and tectonic setting of Proterozoic iron oxide (Cu-U-Au-REE) deposits. *Precambrian Research*, *58*, 241–287.

Hunt, J., Baker, T., & Thorkelson, D. (2005). Regional-scale Proterozoic IOCG-mineralized breccia systems: Examples from the Wernecke Mountains, Yukon, Canada. *Mineralium Deposita*, *40*(5), 492–514. https://doi.org/10.1007/s00126-005-0019-5

Huston, D., Cross, A., Skirrow, R., Champion, D., & Whelan, J. (2020). *The Tennant Creek mineral field and Rover fields : Many similarities but some important differences*.

Huston, D. L., Bolger, C., & Cozens, G. (1993). A comparison of mineral deposits at the Gecko and White Devil deposits: implications for ore genesis in the Tennant Creek district, Northern Territory, Australia. *Economic Geology*, *88*(5), 1198–1225. https://doi.org/10.2113/gsecongeo.88.5.1198

Huston, D. L., & Cozens, G. J. (1994). The geochemistry and alteration of the White Devil porphyry: implications to intrusion timing. *Mineralium Deposita*, *29*(3), 275–287. https://doi.org/10.1007/BF00206871

Jagodzinski, E. A., Reid, A., Crowley, J., McAvaney, S., & Wade, C. (2016). Precise zircon U-Pb dating of Mesoproterozoic silicic large igneous province: the Gawler Range Volcanics and Benagerie Volcanic Suite, South Australia. *Australian Earth Science Convention, Abstracts*.

Jagodzinski, L., & Fricke, C. E. (2010). Compilation of new SHRIMP U-Pb geochronological data for the Southern Curnamona Province, South Australia. *South Australia. Department of Primary Industries and Resources*, *Report Boo*.

Johnson, J. P., & Cross, K. C. (1995). U-Pb geochronological constraints on the genesis of the Olympic Dam Cu-U-Au-Ag deposit, South Australia. *Economic Geology*, *90*, 1046–1063.

Just, J., Schulz, B., de Wall, H., Jourdan, F., & Pandit, M. K. (2011). Monazite CHIME/EPMA dating of Erinpura granitoid deformation: Implications for Neoproterozoic tectono-thermal evolution of NW India. *Gondwana Research*, *19*(2), 402–412. https://doi.org/10.1016/j.gr.2010.08.002

Kaur, P., Chaudhri, N., Hofmann, A. W., Raczek, I., & Okrusch, M. (2013). Geochemistry and Sm-Nd geochronology of the metasomatised mafic rocks in the Khetri complex, Rajasthan, NW India: Evidence of an Early Cryogenian metasomatic event in the northern Aravalli orogen. *Journal of Asian Earth Sciences*, *62*, 401–413. https://doi.org/10.1016/j.jseaes.2012.10.023

Kaur, P., Zeh, A., & Chaudhri, N. (2017). Palaeoproterozoic continental arc magmatism, and Neoproterozoic metamorphism in the Aravalli-Delhi orogenic belt, NW India: New constraints from in situ zircon U-Pb-Hf isotope systematics, monazite dating and whole-rock geochemistry. *Journal of Asian Earth Sciences*, *136*, 68–88. https://doi.org/10.1016/j.jseaes.2017.01.024

Kirschbaum, M. J., & Hitzman, M. W. (2016). Guelb Moghrein: an unusual, carbonate-hosted iron oxide copper-gold deposit in Mauritania, northwest Africa. *Economic Geology*, 763–770.

Knight, J., Joy, S., Lowe, J., Cameron, J., Merrillees, J., Nag, S., Shah, N., Dua, G., & Jhala, K. (2002). The Khetri copper belt, Rajasthan: iron oxide copper-gold terrane in the Proterozoic of NW India. In T. M. Porter (Ed.), *Hydrothermal iron oxide copper-gold and related deposits: A global perspective, Volume 2* (pp. 321–341). PGC Publishing.

Knipping, J. L., Bilenker, L. D., Simon, A. C., Reich, M., Barra, F., Deditius, A. P., Lundstrom, C., Bindeman, I., & Munizaga, R. (2015). Giant Kiruna-type deposits form by efficient flotation of magmatic magnetite suspensions. *Geology*, *43*(7), 591–594. https://doi.org/10.1130/G36650.1

Kolb, J., Meyer, F. M., Vennemann, T. W., Hoffbauer, R., Gerdes, A., & Sakellaris, G. A. (2008). Geologic setting of the Guelb Moghrein Fe oxide-Cu-Au-Co mineralisation,Akjoujt area, Mauritania. In N. Ennih & J.-P. Liégeois (Eds.), *The boundaries of the West African craton* (pp. 53–75). Geological Society of London, Special Publication.

Kolb, J., Meyer, M., Vennemann, T., Sindern, S., Prantl, S., & Bottcher, M. E. (2010). Characterisation of the hydrothermal fluids of the Guelb Moghrein iron oxide-Cu-Au-Co deposit, Mauritania: ore mineral chemistry, fluid inclusions and isotope geochemistry. In T. M. Porter (Ed.), *Hydrothermal iron oxide copper-gold and related deposits: A global perspective, Volume 4* (pp. 553–572). PGC Publishing.

Kolb, J., & Petrov, N. (2016). The Guelb Moghrein Cu–Au deposit: Neoarchaean hydrothermal sulfide mineralization in carbonate-facies iron formation. *Ore Geology Reviews*, *78*, 573–577. https://doi.org/10.1016/j.oregeorev.2015.09.003

Köykkä, J., Lahtinen, R., & Huhma, H. (2019). Provenance evolution of the Paleoproterozoic metasedimentary cover sequences in northern Fennoscandia: Age distribution,

geochemistry, and zircon morphology. *Precambrian Research*, *331*(March), 105364. https://doi.org/10.1016/j.precamres.2019.105364

Lahtinen, R., Huhma, H., Lahaye, Y., Jonsson, E., Manninen, T., Lauri, L. S., Bergman, S., Hellström, F., Niiranen, T., & Nironen, M. (2015). New geochronological and Sm-Nd constraints across the Pajala shear zone of northern Fennoscandia: Reactivation of a Paleoproterozoic suture. *Precambrian Research*, *256*, 102–119. https://doi.org/10.1016/j.precamres.2014.11.006

Lahtinen, Raimo, & Huhma, H. (2019). A revised geodynamic model for the Lapland-Kola Orogen. *Precambrian Research*, *330*(April), 1–19. https://doi.org/10.1016/j.precamres.2019.04.022

Lahtinen, Raimo, Huhma, H., Sayab, M., Lauri, L. S., & Hölttä, P. (2018). Age and structural constraints on the tectonic evolution of the Paleoproterozoic Central Lapland Granitoid Complex in the Fennoscandian Shield. *Tectonophysics*, *745*(January), 305–325. https://doi.org/10.1016/j.tecto.2018.08.016

Li, X. C., & Zhou, M. F. (2018). The nature and origin of hydrothermal REE mineralization in the Sin Quyen deposit, northwestern Vietnam. *Economic Geology*, *113*(3), 645–673. https://doi.org/10.5382/econgeo.2018.4565

Li, X. C., Zhou, M. F., Chen, W. T., Zhao, X. F., & Tran, M. D. (2018). Uranium-lead dating of hydrothermal zircon and monazite from the Sin Quyen Fe-Cu-REE-Au-(U) deposit, northwestern Vietnam. *Mineralium Deposita*, *53*(3), 399–416. https://doi.org/10.1007/s00126-017-0746-4

Li, X. C., Zhou, M. F., Williams-Jones, A. E., Yang, Y. H., & Gao, J. F. (2019). Timing and genesis of Cu-(Au) mineralization in the Khetri Copper Belt, northwestern india: Constraints from in situ U-Pb ages and Sm-Nd isotopes of monazite-(Ce). *Mineralium Deposita*, *54*(4), 553–568. https://doi.org/10.1007/s00126-018-0823-3

Li, X., Zhao, X., Zhou, M. F., Chen, W. T., & Chu, Z. (2015). Fluid inclusion and isotopic constraints on the origin of the Paleoproterozoic Yinachang Fe-Cu-(REE) deposit, Southwest China. *Economic Geology*, *110*(5), 1339–1369. https://doi.org/10.2113/econgeo.110.5.1339

Lin, L., Chen, R., Pang, Z., Chen, H., Xue, J., & Jia, H. (2020). Sulfide Rb-Sr, Re-Os and in-situ S isotopic constraints on two mineralization events at the large Hongnipo Cu deposit, SW China. *Minerals*, *10*(5), 1–24. https://doi.org/10.3390/min10050414

Liu, L., & Terry Chen, W. (2019). Geology, mineralization styles and age of ore-hosting rocks of the Proterozoic Longbohe–Sin Quyen Fe-Cu belt: Implications for regional metallogeny. *Ore Geology Reviews*, *111*(July), 103013. https://doi.org/10.1016/j.oregeorev.2019.103013

Lopez, G. P., Hitzman, M. W., & Nelson, E. P. (2014). Alteration patterns and structural controls of the El Espino IOCG mining district, Chile. *Mineralium Deposita*, *49*(2), 235–259. https://doi.org/10.1007/s00126-013-0485-0

Machado, N., Lindenmayer, Z., Krogh, T. E., & Lindenmayer, D. (1991). U-Pb geochronology of Archean magmatism and basement reactivation in the Carajás area, Amazon shield, Brazil. *Precambrian Research*, *49*(3–4), 329–354. https://doi.org/10.1016/0301-9268(91)90040-H

Maidment, D. W., Huston, D. L., Donnellan, N., & Lambeck, A. (2013). Constraints on the timing of the Tennant Event and associated Au – Cu – Bi mineralisation in the Tennant Region , Northern Territory. *Precambrian Research*, *237*, 51–63. https://doi.org/10.1016/j.precamres.2013.07.020

Maksaev, V., & Zentilli, M. (2002). Chilean strata-bound Cu- (Ag) deposits: An overview. In T. M. Porter (Ed.), *Hydrothermal iron oxide copper-gold and related deposits: A global perspective, Volume 2* (pp. 185–205). PGC Publishing.

Mark, G. (2001). Nd isotope and petrogenetic constraints for the origin of the Mount Angelay igneous complex: Implications for the origin of intrusions in the Cloncurry district, NE Australia. *Precambrian Research*, *105*(1), 17–35. https://doi.org/10.1016/S0301-9268(00)00101-7

Mark, Geordie, Foster, D. R. W., Pollard, P. J., Williams, P. J., Tolman, J., Darvall, M., & Blake, K. L. (2004). *Stable isotope evidence for magmatic fluid input during large-scale Na – Ca alteration in the Cloncurry Fe oxide Cu – Au district , NW Queensland , Australia*. https://doi.org/10.1111/j.1365-3121.2004.00527.x

Mark, Geordie, Oliver, N. H. S., & Williams, P. J. (2006). Mineralogical and chemical evolution of the Ernest Henry Fe oxide-Cu-Au ore system, Cloncurry district, northwest Queensland, Australia. *Mineralium Deposita*, *40*(8), 769–801. https://doi.org/10.1007/s00126-005-0009-7

Marschik, R., & Fontboté, L. (2001). The Candelaria-Punta del Cobre iron oxide Cu-Au (-Zn-Ag) deposits, Chile. *Economic Geology*, *96*(8), 1799–1826. https://doi.org/10.2113/gsecongeo.96.8.1799

Marschik, R., Mathur, R., Ruiz, J., Leveille, R. A., & de Almeida, A. J. (2005). Late Archean Cu-Au-Mo mineralization at Gameleira and Serra Verde, Carajàs Mineral Province, Brazil: Constraints from Re-Os molybdenite ages. *Mineralium Deposita*, *39*(8), 983–991. https://doi.org/10.1007/s00126-004-0450-z

Martinsson, O., Billström, K., Broman, C., Weihed, P., & Wanhainen, C. (2016a). Metallogeny of the Northern Norrbotten Ore Province, Northern Fennoscandian Shield with emphasis on IOCG and apatite-iron ore deposits. *Ore Geology Reviews*, *78*, 447–492. https://doi.org/10.1016/j.oregeorev.2016.02.011

Martinsson, O., Billström, K., Broman, C., Weihed, P., & Wanhainen, C. (2016b). Metallogeny of the Northern Norrbotten Ore Province, Northern Fennoscandian Shield with emphasis on IOCG and apatite-iron ore deposits. *Ore Geology Reviews*, *78*, 447–492. https://doi.org/10.1016/j.oregeorev.2016.02.011

Mathur, R., Marschik, R., Ruiz, J., Munizaga, F., Leveille, R. A., & Martin, W. (2002). Age of mineralization of the Candelaria Fe oxide Cu-Au deposit and the origin of the Chilean Iron Belt, based on Re-Os isotopes. *Economic Geology*, *97*, 59–71.

McInnes, B. I. A., Keays, R. R., Lambert, D. D., Hellstrom, J., & Allwood, J. S. (2008). Re-Os geochronology and isotope systematics of the Tanami, Tennant Creek and Olympic Dam Cu-Au deposits. *Australian Journal of Earth Sciences*, *55*(6–7), 967–981. https://doi.org/10.1080/08120090802097443

McKenzie, N. R., Hughes, N. C., Myrow, P. M., Banerjee, D. M., Deb, M., & Planavsky, N. J. (2013). New age constraints for the Proterozoic Aravalli-Delhi successions of India and their implications. *Precambrian Research*, *238*, 120–128. https://doi.org/10.1016/j.precamres.2013.10.006

McLean, R. N. (2002). The Sin Quyen iron oxide-copper-gold-rare earth oxide mineralisation of north Vietnam. In T. M. Porter (Ed.), *Hydrothermal iron oxide copper-gold and related deposits: A global perspective, Volume 2* (pp. 293–301). PGC Publishing.

McPhie, J., Ehrig, K. J., Kamenetsky, M. B., Crowley, J. L., & Kamenetsky, V. S. (2020). Geology of the Acropolis prospect, South Australia, constrained by high-precision CA-TIMS ages. *Australian Journal of Earth Sciences*, *67*(5), 699–716. https://doi.org/10.1080/08120099.2020.1717617

Meyer, M. F., Kolb, J., Sakellaris, G. A., & Gerdes, A. (2006). New ages from the Mauritanides Belt: Recognition of Archean IOCG mineralization at Guelb Moghrein, Mauritania. *Terra Nova*, *18*(5), 345–352. https://doi.org/10.1111/j.1365-3121.2006.00698.x

Monteiro, L. V. S., Xavier, R. P., Carvalho, E. R., Hitzman, M. W., Johnson, C. A., Souza Filho, C. R., & Torresi, I. (2008). Spatial and temporal zoning of hydrothermal alteration and mineralization in the Sossego iron oxide-copper-gold deposit, Carajás Mineral Province, Brazil: Paragenesis and stable isotope constraints. In *Mineralium Deposita* (Vol. 43, Issue 2). https://doi.org/10.1007/s00126-006-0121-3

Montreuil, J. F., Corriveau, L., & Davis, W. J. (2016). Tectonomagmatic evolution of the southern Great Bear magmatic zone (Northwest Territories, Canada): Implications for the genesis of iron oxide-alkali-altered hydrothermal systems. *Economic Geology*, *111*(8), 2111–2138. https://doi.org/10.2113/econgeo.111.8.2111

Moreto, C. P.N., Monteiro, L. V. S., Xavier, R. P., Creaser, R. A., DuFrane, S. A., Tassinari, C. C. G., Sato, K., Kemp, A. I. S., & Amaral, W. S. (2015). Neoarchean and paleoproterozoic iron oxide-copper-gold events at the sossego deposit, Carajás Province, Brazil: Re-Os and U-Pb geochronological evidence. *Economic Geology*, *110*(3), 809–835. https://doi.org/10.2113/econgeo.110.3.809

Moreto, Carolina Penteado Natividade, Monteiro, L. V. S., Xavier, R. P., Amaral, W. S., dos Santos, T. J. S., Juliani, C., & de Filho, C. R. S. (2011). Mesoarchean (3.0 and 2.86 Ga) host rocks of the iron oxide-Cu-Au Bacaba deposit, Carajás Mineral Province: U-Pb geochronology and metallogenetic implications. *Mineralium Deposita*, *46*(7), 789–811. https://doi.org/10.1007/s00126-011-0352-9

Moreto, Carolina P.N., Monteiro, L. V. S., Xavier, R. P., Creaser, R. A., DuFrane, S. A., Melo, G. H. C., Delinardo da Silva, M. A., Tassinari, C. C. G., & Sato, K. (2015). Timing of multiple hydrothermal events in the iron oxide–copper–gold deposits of the Southern Copper Belt, Carajás Province, Brazil. *Mineralium Deposita*, *50*(5), 517–546. https://doi.org/10.1007/s00126-014-0549-9

Morrissey, L. J., & Tomkins, A. G. (2020). Evaporite-bearing orogenic belts produce ligand-rich and diverse metamorphic fluids. *Geochimica et Cosmochimica Acta*, *275*, 163–187. https://doi.org/10.1016/j.gca.2020.02.017

Mukherjee, R., Venkatesh, A. S., & Fareeduddin, G. S. (2019). Geochemical characterization of mineralized albitite from Paleoproterozoic Bhukia IOCG - IOA deposit of Aravalli - Delhi Fold Belt , Rajasthan , western India : Genetic linkage to the gold (± Cu ± U) mineralization. *Geological Journal*, *October 2018*, 4203–4225. https://doi.org/10.1002/gj.3669

Mukhopadhyay, S., Kumar, V., & Sangwan, M. (2019). Sediment Hosted Stratiform Copper (SSC) Mineralization in Bhudoli-Basari Area, North Delhi Fold Belt, Mesoproterozoic Delhi Supergroup, Rajasthan. *Journal of the Geological Society of India*, *93*(6), 663–674. https://doi.org/10.1007/s12594-019-1245-2

Mumin, A. H., Corriveau, L., Somarin, A. K., & Ootes, L. (2007). Iron oxide copper-gold-type polymetallic mineralization in the Contact Lake belt, Great Bear magmatic zone, Northwest Territories, Canada. *Exploration and Mining Geology*, *16*, 187–208.

Mumin, A. H., Somarin, A. K., Jones, B., Corriveau, L., Ootes, L., & Camier, J. (2010). The IOCG-porphyry-epithermal continuum of deposit types in the Great Bear magmatic zone, Northwest Territories, Canada. In Louise Corriveau & A. H. Mumin (Eds.), *Exploring for iron oxide copper-gold deposits: Canada and global analogues* (pp. 59–78). Geological Association of Canada, Short Course Notes, Volume 20.

Ngo, X. D., Zhao, X. F., Tran, T. H., Deng, X. D., & Li, J. W. (2020). Two episodes of REEs mineralization at the Sin Quyen IOCG deposit, NW Vietnam. *Ore Geology Reviews*, *125*(June), 103676. https://doi.org/10.1016/j.oregeorev.2020.103676

Nguyen, P. T., Booth, S. A., Both, R. A., & James, P. R. (1989). The White Devil gold deposit, Tennant Creek, Northern Territory, Australia. *Economic Geology Monograph*, *6*, 180–192.

Nicolson, B., Reid, A., McAvaney, S., Keeling, J., Fraser, G., Vasconcelos, P., & Department of State Development. (2017). *A Mesoproterozoic advanced argillic alteration system: 40Ar/39Ar thermochronology from Nankivel Hill, Gawler Craton*. *Report Book 2017/00011*, 39.

Nisbet, B., Cooke, J., Richards, M., & Williams, C. (2000). Exploration for iron oxide copper gold deposits in Zambia and Sweden: comparison with the Australian experience. In T. M. Porter (Ed.), *Hydrothermal iron oxide copper-gold and related deposits: A global perspective, Volume 1* (pp. 297–308). PGC Publishing.

Oliver, N. H. S., Butera, K. M., Rubenach, M. J., Marshall, L. J., Cleverley, J. S., Mark, G., Tullemans, F., & Esser, D. (2008). The protracted hydrothermal evolution of the Mount Isa Eastern Succession: A review and tectonic implications. *Precambrian Research*, *163*(1–2), 108–130. https://doi.org/10.1016/j.precamres.2007.08.019

Oliver, N. H. S., Cleverley, J. S., Mark, G., Pollard, P. J., Fu, B., Marshall, L. J., Rubenach, M. J., Williams, P. J., & Baker, T. (2004). Modeling the role of sodic alteration in the genesis of iron oxide-copper-gold deposits, Eastern Mount Isa Block, Australia. *Economic Geology*, *99*(6), 1145–1176. https://doi.org/10.2113/gsecongeo.99.6.1145

Oliveros, V., Tristá-Aguilera, D., Féraud, G., Morata, D., Aguirre, L., Kojima, S., & Ferraris, F. (2008). Time relationships between volcanism-plutonism-alteration-mineralization in Cu-stratabound ore deposits from the Michilla mining district, northern Chile: A 40Ar/39Ar geochronological approach. *Mineralium Deposita*, *43*(1), 61–78. https://doi.org/10.1007/s00126-007-0147-1

Olszewski, W. J., Wirth, K. R., Gibbs, A. K., & Gaudette, H. E. (1989). The age, origin, and tectonics of the Grão Pará Group and associated rocks, Serra dos Carajás, Brazil: Archean continental volcanism and rifting. *Precambrian Research*, *42*(3–4), 229–254. https://doi.org/10.1016/0301-9268(89)90013-2

Ootes, L., Goff, S., Jackson, V. A., Gleeson, S. A., Creaser, R. A., Samson, I. M., Evensen, N., Corriveau, L., & Mumin, A. H. (2010). Timing and thermochemical constraints on multi-element mineralisation at the Nori/RA Cu-Mo-U prospect, Great Bear magmatic zone, Northwest Territories, Canada. *Mineralium Deposita*, *45*(6), 549–566. https://doi.org/10.1007/s00126-010-0291-x

Ootes, L., Snyder, D., Davis, W. J., Acosta-Góngora, P., Corriveau, L., Mumin, A. H., Gleeson, S. A., Samson, I. M., Montreuil, J. F., Potter, E., & Jackson, V. A. (2017). A Paleoproterozoic Andean-type iron oxide copper-gold environment, the Great Bear magmatic zone, Northwest Canada. *Ore Geology Reviews*, *81*, 123–139. https://doi.org/10.1016/j.oregeorev.2016.09.024

Oyarzun, R., Rodríguez, M., Pincheira, M., Doblas, M., & Helle, S. (1999). The Candelaria (Cu-Fe-Au) and Punta del Cobre (Cu-Fe) deposits (Copiapo, Chile): A case for extension-related granitoid emplacement and mineralization processes? *Mineralium Deposita*, *34*(8), 799–801. https://doi.org/10.1007/s001260050241

Oyarzun, Roberto, Oyarzún, J., Ménard, J. J., & Lillo, J. (2003). The Cretaceous iron belt of northern Chile: Role of oceanic plates, a superplume event, and a major shear zone. *Mineralium Deposita*, *38*(5), 640–646. https://doi.org/10.1007/s00126-003-0359-y

Ozha, M. K., Mishra, B., Hazarika, P., Jeyagopal, A. v., & Yadav, G. S. (2016). EPMA monazite geochronology of the basement and supracrustal rocks within the Pur-Banera basin , Rajasthan: Evidence of Columbia breakup in Northwestern India. *JOURNAL OF ASIAN EARTH SCIENCES*, *117*, 284–303. https://doi.org/10.1016/j.jseaes.2015.12.016

Pal, D. C., Trumbull, R. B., & Wiedenbeck, M. (2010). Chemical and boron isotope compositions of tourmaline from the Jaduguda U (-Cu-Fe) deposit, Singhbhum shear zone, India: Implications for the sources and evolution of mineralizing fluids. *Chemical Geology*, *277*(3–4), 245–260. https://doi.org/10.1016/j.chemgeo.2010.08.008

Page, R. W., Stevens, B. P. J., & Gibson, G. M. (2005). Geochronology of the sequence hosting the Broken Hill Pb-Zn-Ag orebody, Australia. *Economic Geology*, *100*(4), 633–661. https://doi.org/10.2113/gsecongeo.100.4.633

Perkins, C., & Wyborn, L. A. I. (1998). Age of Cu-Au mineralisation, Cloncurry district, eastern Mt Isa Inlier, Queensland, as determined by 40Ar/39Ar dating. *Australian Journal of Earth Sciences*, *45*(2), 233–246. https://doi.org/10.1080/08120099808728384

Perring, C. S., Pollard, P. J., Dong, G., Nunn, A. J., & Blake, K. L. (2000). The Lightning Creek Sill complex, cloncurry district, Northwest Queensland: A source of fluids for Fe Oxide Cu-Au mineralization and sodic-calcic alteration. *Economic Geology*, *95*(5), 1067–1089. https://doi.org/10.2113/gsecongeo.95.5.1067

Pestilho, A. L. S., Monteiro, L. V. S., Melo, G. H. C. de, Moreto, C. P. N., Juliani, C., Fallick, A. E., & Xavier, R. P. (2020). Stable isotopes and fluid inclusion constraints on the fluid evolution in the Bacaba and Castanha iron oxide-copper-gold deposits, Carajás Mineral Province, Brazil. *Ore Geology Reviews*, *126*(April 2019), 103738. https://doi.org/10.1016/j.oregeorev.2020.103738

Pidgeon, R. T., MacAmbira, M. J. B., & Lafon, J. M. (2000). Th-U-Pb isotopic systems and internal structures of complex zircons from an enderbite from the Pium Complex, Carajas Province, Brazil: Evidence for the ages of granulite facies metamorphism and the protolith of the enderbite. *Chemical Geology*, *166*(1–2), 159–171. https://doi.org/10.1016/S0009-2541(99)00190-4

Pollard, P. J., Taylor, R. G., Peters, L., Matos, F., Freitas, C., Saboia, L., & Huhn, S. (2019). 40 Ar- 39 Ar dating of Archean iron oxide Cu-Au and Paleoproterozoic granite-related Cu-Au deposits in the Carajás Mineral Province, Brazil: implications for genetic models. *Mineralium Deposita*, *54*(3), 329–346. https://doi.org/10.1007/s00126-018-0809-1

Priyam Sharma, J., Ranjan Sahoo, P., Mahanta, H., Venkatesh, A. S., Babu, E. V. S. S. K., & John, M. M. (2020). Constraints on the genesis of the Proterozoic bornite dominated copper deposit

from Nim ka Thana, western India: An IOCG perspective. *Ore Geology Reviews*, *118*(May 2019), 103338. https://doi.org/10.1016/j.oregeorev.2020.103338

Raab, A. K. (2001). *Geology of the Cerro Negro Norte Fe-oxide (Cu-Au) district, Coastal Cordillera, northern Chile*.

Rattenbury, M. S. (1992). Stratigraphic and structural controls on ironstone mineralization in the Tennant Creek goldfield, Northern Territory, Australia. *Australian Journal of Earth Sciences*, *39*(5), 591–602. https://doi.org/10.1080/08120099208728052

Rattenbury, M. S. (1994). A linked fold-thrust model for the deformation of the Tennant Creek goldfield, northern Australia. *Mineralium Deposita*, *29*(3), 301–308. https://doi.org/10.1007/BF00206873

Ray, G. E., & Dick, L. A. (2002). The Productora prospect in north-central Chile: An example of an intrusion-related, Candelaria type Fe-Cu-Au hydrothermal system. In T. M. Porter (Ed.), *Hydrothermal iron oxide copper-gold and related deposits: A global perspective, Volume 2* (pp. 131–151). PGC Publishing.

Raymond, O. L., Fletcher, I., & McNaughton, N. J. (2002). Copper-gold mineral systems in the south-east Gawler Craton - Another Mt Isa Eastern Succession? *16th Australian Geological Convention, Abstracts*.

Reich, M., Simon, A. C., Deditius, A., Barra, F., Chryssoulis, S., Lagas, G., Tardani, D., Knipping, J., Bilenker, L., Sánchez-alfaro, P., Roberts, M. P., & Munizaga, R. (2016). *Scientific Communications*, 743–761.

Reid, A. J., Fricke, C., & Cowley, W. M. (2009). Extent of the low-grade Archaean Devils Playground Volcanics in the north-eastern Gawler Craton: Evidence from recent PACE drilling. *MESA Journal*, *54*, 9–19.

Reid, A., Smith, R. N., Baker, T., Jagodzinski, E. A., Selby, D., Gregory, C. J., & Skirrow, R. G. (2013). Re-Os dating of molybdenite within hematite breccias from the vulcan Cu-Au prospect, olympic Cu-Au province, South Australia. *Economic Geology*, *108*(4). https://doi.org/10.2113/econgeo.108.4.883

Reid, Anthony J. (2019). The Olympic Cu-Au Province , Gawler Craton: A review of the lithospheric architecture, alteration systems, cover successions and prospectivity. *Minerals*, 1–37.

Reid, Anthony J., & Fabris, A. (2015). Influence of preexisting low metamorphic grade sedimentary successions on the distribution of iron oxide copper-gold mineralization in the Olympic Cu-Au Province, Gawler Craton. *Economic Geology*, *110*(8), 2147–2157. https://doi.org/10.2113/econgeo.110.8.2147

Requia, K., Stein, H., Fontboté, L., & Chiaradia, M. (2003). Re-Os and Pb-Pb geochronology of the Archean Salobo iron oxide copper-gold deposit, Carajás mineral province, northern Brazil. *Mineralium Deposita*, *38*(6), 727–738. https://doi.org/10.1007/s00126-003-0364-1

Richards, J. P., Lopez, G. P., Zhu, J. J., Creaser, R. A., Locock, A. J., & Mumin, A. H. (2017). Contrasting tectonic settings and sulfur contents of magmas associated with cretaceous porphyry Cu ± Mo ± Au and intrusion-related iron oxide Cu-Au deposits in northern Chile. *Economic Geology*, *112*(2), 295–318. https://doi.org/10.2113/econgeo.112.2.295

Rojas, P. A., Barra, F., Reich, M., Deditius, A., Simon, A., Uribe, F., Romero, R., & Rojo, M. (2018a). A genetic link between magnetite mineralization and diorite intrusion at the El Romeral iron oxide-apatite deposit, northern Chile. *Mineralium Deposita*, *53*(7), 947–966. https://doi.org/10.1007/s00126-017-0777-x

Rojas, P. A., Barra, F., Reich, M., Deditius, A., Simon, A., Uribe, F., Romero, R., & Rojo, M. (2018b). A genetic link between magnetite mineralization and diorite intrusion at the El Romeral iron oxide-apatite deposit, northern Chile. *Mineralium Deposita*, *53*(7), 947–966. https://doi.org/10.1007/s00126-017-0777-x

Romer, R. L., Martinsson, O., & Perdahl, J.-A. (1994). Geochronology of the Kiruna iron ores and hydrothermal alterations. *Economic Geology*, *89*, 1249–1261.

Ronzê, P. C., Soares, A. D. v., dos Santos, M. G. S., & Barreira, C. F. (2000). Alemão copper-gold (U-REE) deposit, Carajás, Brazil. In T. M. Porter (Ed.), *Hydrothermal iron oxide copper-gold and*

related deposits: A global perspective, Volume 1 (pp. 191–202). Australian Mineral Foundation.

Rotherham, J. F. (1997). A metasomatic origin for the iron-oxide Au-Cu Starra orebodies, Eastern Fold Belt, Mount Isa Inlier. *Mineralium Deposita*, *32*(3), 205–218. https://doi.org/10.1007/s001260050086

Rubenach, M. J., Foster, D. R. W., Evins, P. M., Blake, K. L., & Fanning, C. M. (2008). Age constraints on the tectonothermal evolution of the Selwyn Zone, Eastern Fold Belt, Mount Isa Inlier. *Precambrian Research*, *163*(1–2), 81–107. https://doi.org/10.1016/j.precamres.2007.08.014

Rubenach, M. J., & Lewthwaite, K. A. (2002). Metasomatic albitites and related biotite-rich schists from a low-pressure polymetamorphic terrane, Snake Creek Anticline, Mount Isa Inlier, North-Eastern Australia: Microstructures and P-T-d paths. *Journal of Metamorphic Geology*, *20*(1), 191–202. https://doi.org/10.1046/j.0263-4929.2001.00348.x

Sarlus, Z., Andersson, U. B., Bauer, T. E., Wanhainen, C., Martinsson, O., Nordin, R., & Andersson, J. B. H. (2018). Timing of plutonism in the Gällivare area: Implications for Proterozoic crustal development in the northern Norrbotten ore district, Sweden. *Geological Magazine*, *155*(6), 1351–1376. https://doi.org/10.1017/S0016756817000280

Schofield, A. (2010). Investigation of drill holes in the vicinity of the 08GA-C1 seismic line in the Curnamona Province , South Australia Investigation of drill holes in the vicinity of the 08GA-C1 seismic line in the Curnamona Province , South Australia. *Geoscience Australia*, *Record 201*.

Schutesky, M. E., & de Oliveira, C. G. (2020). From the roots to the roof: An integrated model for the Neoarchean Carajás IOCG System, Brazil. *Ore Geology Reviews*, *127*(October), 103833. https://doi.org/10.1016/j.oregeorev.2020.103833

Scott, D. L., Rawlings, D. J., Page, R. W., Tarlowski, C. Z., Idnurm, M., Jackson, M. J., & Southgate, P. N. (2000). Basement framework and geodynamic evolution of the Palaeoproterozoic superbasins of north-central Australia: An integrated review of geochemical, geochronological and geophysical data. *Australian Journal of Earth Sciences*, *47*(3), 341–380. https://doi.org/10.1046/j.1440-0952.2000.00793.x

Seymour, N. M., Singleton, J. S., Mavor, S. P., Gomila, R., Stockli, D. F., Heuser, G., & Arancibia, G. (2020). The Relationship Between Magmatism and Deformation Along the Intra-arc Strike-Slip Atacama Fault System, Northern Chile. *Tectonics*, *39*(3). https://doi.org/10.1029/2019TC005702

Sillitoe, R. H. (2003). Iron oxide-copper-gold deposits: An Andean view. *Mineralium Deposita*, *38*(7), 787–812. https://doi.org/10.1007/s00126-003-0379-7

Simon, A. C., Knipping, Reich, M., Barra, F., Deditius, A. P., Bilenker, L. D., & Childress, T. (2018). Kiruna-type iron oxide-apatite (IOA) and iron oxide copper-gold (IOCG) deposits form by a combination of igneous and magmatic-hydrothermal processes: evidence from the Chilean Iron Belt. *Society of Economic Geologists Special Publication*, *No. 21*, 89–114.

Simusokwe, M., Watanabe, Y., & Echigo, T. (2021). Hydrothermal alteration and Cu–Co mineralization at the peripheral zone (Target H) of the Kitumba iron–oxide copper–gold system, Mumbwa District, Zambia. *Resource Geology*, *71*, 409–435. https://doi.org/https://doi-org.virtual.anu.edu.au/10.1111/rge.12274

Skirrow, R. G. (1993). *The genesis of gold-copper-bismuth deposits, Tennant Creek, Northern Territory*. Unpublished PhD thesis, Australian National University.

Skirrow, R. G. (2000). Gold-copper-bismuth deposits of the Tennant Creek district, Australia: a reappraisal of diverse high-grade systems. In T. M. Porter (Ed.), *Hydrothermal iron oxide copper-gold and related deposits: A global perspective, Volume 1* (pp. 149–160). Australian Mineral Foundation.

Skirrow, R. G. (2010). "Hematite-group" IOCG±U ore systems: tectonic settings, hydrothermal characteristics, and Cu-Au and U mineralizing processes. In L. Corriveau & H. Mumin (Eds.), *Exploring for iron oxide copper-gold deposits: Canada and global analogues* (pp. 39–58). Geological Association of Canada, Short Course Notes, Volume 20.

Skirrow, R. G., Ashley, P. M., McNaughton, M. J., & Suzuki, K. (2000). Time-space framework of Cu-Au(-Mo) and regional alteration systems in the Curnamona Province. *AGSO Record 2000/10*, 83–86.

Skirrow, R. G., Bastrakov, E. N., Barovich, K., Fraser, G. L., Creaser, R. A., Fanning, C. M., Raymond, O. L., & Davidson, G. J. (2007). Timing of iron oxide Cu-Au-(U) hydrothermal activity and Nd isotope constraints on metal sources in the Gawler craton, South Australia. *Economic Geology*, *102*(8). https://doi.org/10.2113/gsecongeo.102.8.1441

Skirrow, R. G., Bastrakov, E. N., Davidson, G. J., Raymond, O. L., & Heithersay, P. (2002). The geological framework, distribution and controls of Fe-oxide Cu-Au mineralisation in the Gawler craton, South Australia: Part II - Alteration and mineralisation. In T. M. Porter (Ed.), *Hydrothermal iron oxide copper-gold and related deposits: A global perspective, Volume 2* (pp. 33–47). PGC Publishing.

Skirrow, R. G., Cross, A. J., Lecomte, A., & Mercadier, J. (2019). A shear-hosted Au-Cu-Bi metallogenic event at ~1660 Ma in the Tennant Creek goldfield (northern Australia) defined by in-situ monazite U-Pb-Th dating. *Precambrian Research*, *332*. https://doi.org/10.1016/j.precamres.2019.105402

Skirrow, R. G., van der Wielen, S. E., Champion, D. C., Czarnota, K., & Thiel, S. (2018). Lithospheric Architecture and Mantle Metasomatism Linked to Iron Oxide Cu-Au Ore Formation: Multidisciplinary Evidence from the Olympic Dam Region, South Australia. *Geochemistry, Geophysics, Geosystems*, *19*(8). https://doi.org/10.1029/2018GC007561

Skirrow, R. G., & Walshe, J. L. (2002). Reduced and oxidized Au-Cu-Bi iron oxide deposits of the Tennant Creek Inlier, Australia: An integrated geologic and chemical model. *Economic Geology*, *97*(6). https://doi.org/10.2113/gsecongeo.97.6.1167

Slack, J. F., Corriveau, L., & Hitzman, M. W. (2016). A special issue devoted to proterozoic iron oxide-apatite (±REE) and iron oxide copper-gold and affiliated deposits of Southeast Missouri, USA, and the great bear Magmatic Zone, Northwest Territories, Canada. *Economic Geology*, *111*(8), 1803–1814. https://doi.org/10.2113/econgeo.111.8.1803

Smith, J. (2001). Summary of Results Joint NTGS – AGSO Age Determination Program. *Darwin*, *November*.

Smith, M., Coppard, J., Herrington, R., & Stein, H. (2007). The geology of the Rakkurijärvi Cu-(Au) prospect, Norrbotten: A new iron oxide-copper-gold deposit in north Sweden. *Economic Geology*, *102*(3), 393–414. https://doi.org/10.2113/gsecongeo.102.3.393

Smith, M. P., Coppard, J., & Herrington, R. (2010). The geology of the Rakurijarvi copper-prospect, Norbotten County, Sweden. In T. M. Porter (Ed.), *Hydrothermal iron oxide copper-gold and related deposits: A global perspective, Volume 4* (pp. 427–440). PGC Publishing.

Southgate, P. N., Bradshaw, B. E., Domagala, J., Jackson, M. J., Idnurm, M., Krassay, A. A., Page, R. W., Sami, T. T., Scott, D. L., Lindsay, J. F., McConachy, B. A., & Tarlowski, C. (2000). Chronostratigraphic basin framework for Palaeoproterozoic rocks (1730–1575 Ma) in northern Australia and implications for base-metal mineralisation. *Australian Journal of Earth Sciences*, *47*, 461–483.

Southgate, P. N., Neumann, N. L., & Gibson, G. M. (2013). Depositional systems in the Mt Isa Inlier from 1800 Ma to 1640 Ma: Implications for Zn-Pb-Ag mineralisation. *Australian Journal of Earth Sciences*, *60*(2), 157–173. https://doi.org/10.1080/08120099.2013.758176

Souza, L. H., & Vieira, E. A. P. (2000). Salobo 3 Alpha deposit: geology and mineralisation. In T. M. Porter (Ed.), *Hydrothermal iron oxide copper-gold and related deposits: A global perspective, Volume 1* (pp. 213–224). Australian Mineral Foundation.

Tallarico, F. H. B. (2003). *O cinturão cupro-aurifero de Carajas, Brasil*. Unpublished PhD thesis, Universidade Estadual de Campinas.

Tallarico, Fernando H.B., Figueiredo, B. R., Groves, D. I., Kositcin, N., McNaughton, N. J., Fletcher, I. R., & Rego, J. L. (2005). Geology and SHRIMP U-Pb geochronology of the Igarapé Bahia deposit, Carajás copper-gold belt, Brazil: An Archean (2.57 Ga) example of Iron-Oxide Cu-Au-(U-REE) mineralization. *Economic Geology*, *100*(1), 7–28. https://doi.org/10.2113/100.1.0007

Tallarico, Fernando Henrique Bucco, McNaughton, N. J., Groves, D. I., Fletcher, I. R., Figueiredo, B. R., Carvalho, J. B., Rego, J. L., & Nunes, A. R. (2004). Geological and SHRIMP II U-Pb constraints on the age and origin of the Breves Cu-Au-(W-Bi-Sn) deposit, Carajás, Brazil. *Mineralium Deposita*, *39*(1), 68–86. https://doi.org/10.1007/s00126-003-0383-y

Teale, G. S., & Fanning, C. M. (2000). The timing of Cu-Au mineralisation in the Curnamona Province. *AGSO Record 2000/10*, 98–100.

Tiddy, C. J., & Giles, D. (2020). Suprasubduction zone model for metal endowment at 1.60–1.57 Ga in eastern Australia. *Ore Geology Reviews*, *122*(March), 103483. https://doi.org/10.1016/j.oregeorev.2020.103483

Tornos, F., Velasco, F., Barra, F., & Morata, D. (2010). The Tropezón Cu–Mo–(Au) deposit, Northern Chile: the missing link between IOCG and porphyry copper systems? *Mineralium Deposita*, *45*, 313–321. https://doi.org/DOI 10.1007/s00126-010-0277-8

Trendall, A. F., Basei, M. A. S., de Laeter, J. R., & Nelson, D. R. (1998). SHRIMP zircon U-Pb constraints on the age of the Carajas formation, Grao Para Group, Amazon Craton. *Journal of South American Earth Sciences*, *11*(3), 265–277. https://doi.org/10.1016/S0895-9811(98)00015-7

Tristá-Aguilera, D., Barra, F., Ruiz, J., Morata, D., Talavera-Mendoza, O., Kojima, S., & Ferraris, F. (2006). Re-Os isotope systematics for the Lince-Estefanía deposit: Constraints on the timing and source of copper mineralization in a stratabound copper deposit, Coastal Cordillera of Northern Chile. *Mineralium Deposita*, *41*(1), 99–105. https://doi.org/10.1007/s00126-006-0048-8

Trunfull, E. F., Hagemann, S. G., Xavier, R. P., & Moreto, C. P. N. (2020). Critical assessment of geochronological data from the Carajás Mineral Province, Brazil: Implications for metallogeny and tectonic evolution. *Ore Geology Reviews*, *121*(March), 103556. https://doi.org/10.1016/j.oregeorev.2020.103556

Veloso, E., Cembrano, J., Arancibia, G., Heuser, G., Neira, S., Siña, A., Garrido, I., Vermeesch, P., & Selby, D. (2017). Tectono-metallogenetic evolution of the Fe–Cu deposit of Dominga, northern Chile. *Mineralium Deposita*, *52*(4), 595–620. https://doi.org/10.1007/s00126-016-0682-8

Vila, T., Lindsay, N., & Zamora, R. (1996). Geology of the Mantoverde copper deposit, northern Chile: A specularite-rich hydrothermal-tectonic breccia related to the Atacama fault zone. *Economic Geology Special Publication 5*, 157–170.

Wade, C. E., Reid, A. J., Wingate, M. T. D., Jagodzinski, E. A., & Barovich, K. (2012). Geochemistry and geochronology of the c. 1585Ma Benagerie Volcanic Suite, southern Australia: Relationship to the Gawler Range Volcanics and implications for the petrogenesis of a Mesoproterozoic silicic large igneous province. *Precambrian Research*, *206–207*, 17–35. https://doi.org/10.1016/j.precamres.2012.02.020

Walters, S., & Bailey, A. (1998). Geology and mineralization of the Cannington Ag-Pb-Zn deposit: An example of Broken Hill-type mineralization in the Eastern Succession, Mount Isa Inlier, Australia. *Economic Geology*, *93*, 1307–1329.

Wanhainen, C., Billström, K., Martinsson, O., Stein, H., & Nordin, R. (2005). 160 Ma of magmatic/hydrothermal and metamorphic activity in the Gällivare area: Re-Os dating of molybdenite and U-Pb dating of titanite from the Aitik Cu-Au-Ag deposit, northern Sweden. *Mineralium Deposita*, *40*(4), 435–447. https://doi.org/10.1007/s00126-005-0006-x

Wanhainen, C., & Martinsson, O. (2010). The hybrid character of the Aitik deposit, Norbotten, Sweden: a porphyry Cu-Au-Ag(-Mo) system overprinted by iron-oxide Cu-Au hydrothermal fluids. In T. M. Porter (Ed.), *Hydrothermal iron oxide copper-gold and related deposits: A global perspective, Volume 4* (pp. 415–426). PGC Publishing.

Wedekind, M. R., Large, R. R., & Williams, B. T. (1989). *Controls on high-grade gold mineralization at Tennant Creek, Northern Territory, Australia* (pp. 168–179). Economic Geology, Monograph 6.

Weihed, P., Arndt, N., Billström, K., Duchesne, J. C., Eilu, P., Martinsson, O., Papunen, H., & Lahtinen, R. (2005). 8: Precambrian geodynamics and ore formation: The Fennoscandian

Shield. *Ore Geology Reviews*, *27*(1–4), 273–322. https://doi.org/10.1016/j.oregeorev.2005.07.008

Welin, E. (1987). The depositional evolution of the Sveccofennian supracrustal sequence in Finland and Sweden. *Precambrian Research*, *35*, 95–113.

Westhues, A., Hanchar, J. M., Whitehouse, M. J., & Martinsson, O. (2016). New constraints on the timing of host-rock emplacement, hydrothermal alteration, and iron oxide-apatite mineralization in the Kiruna District, Norrbotten, Sweden. *Economic Geology*, *111*(7), 1595–1618. https://doi.org/10.2113/econgeo.111.7.1595

Williams, P. J. (1994). Iron mobility during synmetamorphic alteration in the Selwyn Range area, NW Queensland: implications for the origin of ironstone-hosted Au-Cu deposits. *Mineralium Deposita*, *29*(3), 250–260. https://doi.org/10.1007/BF00206868

Williams, P J, Barton, M. D., Johnson, D. A., Fontboté, L., de Haller, A., Mark, G., Oliver, N. H. S., & Marschik, R. (2005). Iron oxide copper-gold deposits: Geology, space-time distributions, and possible modes of origin. *Economic Geology*, *100*, 371–405.

Williams, P. J., & Skirrow, R. G. (2000). Overview of iron oxide-copper-gold deposits in the Curnamona Province and Cloncurry district (Mount Isa Block), Australia. In T. M. Porter (Ed.), *Hydrothermal iron oxide copper-gold and related deposits: A global perspective, Volume 1* (pp. 105–122). Australian Mineral Foundation.

Williams, Patrick J. (1998). Metalliferous economic geology of the Mt Isa Eastern Succession, northwest Queensla. *Australian Journal of Earth Sciences*, *45*, 329–341.

Willis, I. L., Brown, R. E., Stroud, W. J., & Stevens, B. P. J. (1983). The Early Proterozoic Willyama Supergroup: Stratigraphic subdividion and interpretation of high- to low-grade grade metamorphic rocks in the Broken Hill block, New South Wales. *Geological Society of Australia Journal*, *30*, 195–224.

Wilson, N. S. F., Zentilli, M., Reynolds, P. H., & Boric, R. (2003). Age of mineralization by basinal fluids at the El Soldado manto-type copper deposit, Chile: 40Ar/39Ar geochronology of K-feldspar. *Chemical Geology*, *197*(1–4), 161–176. https://doi.org/10.1016/S0009-2541(02)00350-9

Wyborn, L. A. I., Budd, A. R., & Bastrakova, I. v. (1998). Metallogenic potential of felsic igneous rocks of the Tennant Creek and Davenport Provinces, Northern Territory. *AGSO Research Newsletter*, *29*, 26–28.

Xavier, R. P., Monteiro, L. V. S., Souza Filho, C. R., Torresi, I., Carvalho, E. R., Dreher, A. M., Wiedenbeck, M., Trumbull, R. B., Pestilho, A. L. S., & Moreto, C. P. N. (2010). The iron oxide copper-gold deposits of the Carajás mineral province, Brazil: An updated and critical review. In T. M. Porter (Ed.), *Hydrothermal iron oxide copper-gold and related deposits: A global perspective, Volume 3* (pp. 285–306). PGC Publishing.

Zeng, M., Zhang, D., Zhang, Z., Li, T., Li, C., & Wei, C. (2018). Structural controls on the Lala iron-copper deposit of the Kangdian metallogenic province, southwestern China: Tectonic and metallogenic implications. *Ore Geology Reviews*, *97*(July 2017), 35–54. https://doi.org/10.1016/j.oregeorev.2018.04.028

Zhao, X. F., & Zhou, M. F. (2011). Fe-Cu deposits in the Kangdian region, SW China: A Proterozoic IOCG (iron-oxide-copper-gold) metallogenic province. *Mineralium Deposita*, *46*(7), 731–747. https://doi.org/10.1007/s00126-011-0342-y

Zhao, X. F., Zhou, M. F., Hitzman, M. W., Li, J. W., Bennett, M., Meighan, C., & Anderson, E. (2012). Late Paleoproterozoic to early Mesoproterozoic Tangdan sedimentary rock-hosted strata-bound copper deposit, Yunnan province, southwest China. *Economic Geology*, *107*(2), 357–375. https://doi.org/10.2113/econgeo.107.2.357

Zhao, X. F., Zhou, M. F., Li, J. W., & Qi, L. (2013). Late Paleoproterozoic sedimentary rock-hosted stratiform copper deposits in South China: Their possible link to the supercontinent cycle. *Mineralium Deposita*, *48*(1), 129–136. https://doi.org/10.1007/s00126-012-0445-0

Zhao, X. F., Zhou, M. F., Li, J. W., Selby, D., Li, X. H., & Qi, L. (2013). Sulfide Re-Os and Rb-Sr isotope dating of the Kangdian IOCG metallogenic province, southwest China: Implications for regional metallogenesis. *Economic Geology*, *108*(6), 1489–1498. https://doi.org/10.2113/econgeo.108.6.1489

Zhao, X. F., Zhou, M. F., Su, Z. K., Li, X. C., Chen, W. T., & Li, J. W. (2017). Geology, geochronology, and geochemistry of the Dahongshan Fe-Cu-(Au-Ag) deposit, southwest China: Implications for the formation of iron oxide copper-gold deposits in intracratonic rift settings. *Economic Geology*, *112*(3), 603–628. https://doi.org/10.2113/econgeo.112.3.603

Zhou, M. F., Yan, D. P., Kennedy, A. K., Li, Y., & Ding, J. (2002). SHRIMP U-Pb zircon geochronological and geochemical evidence for Neoproterozoic arc-magmatism along the western margin of the Yangtze Block, South China. *Earth and Planetary Science Letters*, *196*(1–2), 51–67. https://doi.org/10.1016/S0012-821X(01)00595-7

Zhou, M. F., Zhao, X. F., Chen, W. T., Li, X. C., Wang, W., Yan, D. P., & Qiu, H. N. (2014). Proterozoic Fe-Cu metallogeny and supercontinental cycles of the southwestern Yangtze Block, southern China and northern Vietnam. *Earth-Science Reviews*, *139*, 59–82. https://doi.org/10.1016/j.earscirev.2014.08.013

Zhu, L., Liu, J., Bagas, L., Carranza, E. J. M., Zhai, D., Meng, G., Wang, J., Wang, Y., Zhang, F., & Liu, Z. (2019). The Yinachang Fe-Cu-Au-U-REE deposit and its relationship with intermediate to mafic intrusions, SW China: Implications for ore genesis and geodynamic setting. *Ore Geology Reviews*, *104*(November 2018), 190–207. https://doi.org/10.1016/j.oregeorev.2018.11.005